14th International Workshop on
Physical Processes in Natural Waters

Reykjavík, Iceland, June 28 to July 1, 2010

Conference Proceedings

Editor: Hrund Ólöf Andradóttir

UNIVERSITY OF ICELAND
SCHOOL OF ENGINEERING AND
NATURAL SCIENCES

14th International Workshop on Physical Processes in Natural Waters Reykjavík, Iceland, June 28 to July 1, 2010

Conference Proceedings

Editor: Hrund Ólöf Andradóttir

Faculty of Civil and Environmental Engineering
School of Engineering and Natural Sciences
University of Iceland, June 2010

14th International Workshop on
Physical Processes in Natural Waters
Reykjavík, Iceland, June 28 to July 1, 2010

Editor: Hrund Ólöf Andradóttir

Faculty of Environmental Engineering
School of Engineering and Natural Sciences
University of Iceland
Hjarðarhagi 2-6
107, Reykjavik
Iceland

Telephone: 525 4000

Bibliographic information: H. O. Andradottir (Ed.), *Proceedings of the 14th International Workshop on Physical Processes in Natural Waters*, June 28 - July 1, Reykjavík, Iceland, pp. 166.

ISBN 978-9979-9812-9-9

About the Physical Processes in Natural Waters (PPNW) Workshops

The focus of the PPNW international workshops is the physics of inland and coastal water bodies, and their interactions with the physical and biogeochemical processes that control water quality, ecosystem function, and the services such systems provide. The workshops traditionally cover a broad spectrum of scientific topics. Besides general topics, the 14th workshop held in June 2010 in Reykjavík, Iceland, paid a special attention to water bodies in cold climate and lake response to climate change.

PPNW is an open workshop, actively seeking to expand contacts with neighboring fields such as physical oceanography, the atmospheric sciences, and engineering. With 40-60 participants and a small number of invited speakers, the PPNW meetings are characterized by their active workshop atmosphere and a comfortable time frame for presentations and discussion.

The participants in the PPNW Reykjavík workshop were asked to submit either a 2 page extended abstract or a full paper (max. 8 pages). These contributions are published in this proceedings book.

PPNW International Steering Committee:

- Adolf Stips, adolf.stips@jrc.it
- Andrew Folkard, a.folkard@lancaster.ac.uk
- Alfred Wuest, wuest@eawag.ch
- Arkady Terzhevik, ark@nwpi.krc.karelia.ru
- Bertram Boehrer, bertram.boehrer@ufz.de
- Francisco Rueda, fjrueda@ugr.es
- Geoffrey Schladow, gschladow@ucdavis.edu
- Guiseppe Ciraolo, giuseppe.ciraolo@unipa.it
- Hrund Andradóttir, hrund@hi.is
- Lars Bengtsson, Lars.Bengtsson@tvrl.lth.se
- Lars Umlauf, lars.umlauf@io-warnemuende.de
- Madis-Jaak Lilover, madis@phys.sea.ee
- Nikolai Filatov, nfilatov@nwpi.krc.karelia.ru
- Xavier Castamitjana, xavier.casamitjana@udg.es

Local partners in PPNW Reykjavík 2010

- Icelandic Meteorological Office
- Icelandic Hydrological Committee
- Reykjavík Energy
- Landsvirkjun

Icelandic Met Office ÍSLENSKA VATNAFRÆÐINEFNDIN Reykjavik Energy Landsvirkjun

TABLE OF CONTENTS

Session 1

p. 1	**Impact of climate change on aquatic systems** T. Blenckner
p. 3	**Comparing the lake thermal regime in different northern climates - a climate change analysis** L. Bengtsson
p. 4	**Evidence of warming in two aquatic systems in the northeast of Spain** T. Serra, J. Pascual, J. Torcque, J. Colomer, X. Casamitjana, M. Soler and J. Calbó
p. 6	**Headwater lakes of the Chilean Patagonia: A laboratory for studying the impacts of global and local stressors** S. G. Schladow, M. Winder, R. Urrutia, A. Araneda, A. Stehr and B. Reid
p. 8	**On the spatially water temperature and heat flux variability over a tropical hydroelectric reservoir** E.H. Alcântara, J.L. Stech, X. Casamitjana, M.P. Bonnet, J.A. Lorenzzetti and E.M.L.M. Novo
p. 16	**Impact of a Hydroelectric Power Station on Water Mixing Processes within a Stratified Lake** C. Lemckert, Gibbes, B.R., J. Zier and J. Udy

Session 2

p. 18	**Modeling circulation in Lake Huron** D. Beletsky, D. Schwab, E. Anderson and G. Lang
p. 20	**Process oriented modeling of Lake Ontario hydrodynamics** L. Boegman and Y.R. Rao
p. 22	**Density of water from partial molal volumes** B. Boehrer, P. Herzsprung, M. Schultze and F. J. Millero
p. 25	**Combined use of the conservative tracers ^{18}O and SF_6 to detect groundwater inflow in the monimolimnion of a meromictic mining lake** J. Ilmberger and C. von Rohden
p. 27	**Factors influencing the currents over the shallow bank in the Gulf of Finland** M.-J. Lilover, J. Pavelson and T. Kõuts
p. 29	**Wind-driven ocean upper layer model** A. Toompuu and J. Heinloo
p. 31	**Can we simulate the hydrodynamics of the European Shelf Sea by using a shallow water model?** A. Stips, E. Garcia-Gorriz, S. Miladinova and R. Perez

Session 3

p. 32	**The Ecodynamics of Lake Myvatn** Á. Einarsson
p. 34	**Climate change and its effects on lakes in SW−Iceland** H.J. Malmquist, F. Ingimarsson, H.R. Ingvason and S.M. Stefánsson
p. 36	**The significance of accurate hydrological modeling for long-term lake water quality predictions in volcanic zones** S.O. Palmarsson, E.M. Myer, H. Sigurjonsson and S.L. Holm
p. 38	**Internal waves in weakly stratified Lake Lagarfljót** H.Ó. Andradóttir
p. 40	**Modelling of physical processes in a large deep polar lake** Y.R. Rao, A. Huang, W. M. Schertzer and N. Bussières
p. 42	**Internal seiching in ice covered lakes** G. Kirillin, C. Engelhardt, S. Golosov, M. Leppäranta, N. Palshin, A. Terzhevik, G. Zdorovennova, R. Zdorovennov

Session 4

p. 51	**Temperature driven flows in natural lakes** M.G. Wells, M. Colman and P. Pernica
p. 53	**Internal wave-induced flow in shallow, stratified waters** M. Carr and P.A. Davies
p. 55	**Spatial and temporal variability of turbulent hot spots in a large stratified lake** D. Bouffard, L. Boegman1 and R.R. Yerubandi
p. 57	**Vertical structure of the ex-fjord Powell Lake in British Columbia** A. Wüest, Roger Pieters and R. Pawlowicz
p. 59	**Variability in the circulation in Kalbaksfjord, Faroe Islands** K. Simonsen, G. á Norði and E. Gaard

Session 5

p. 61	**Effect of submerged aquatic vegetation on turbulence induced by an oscillating grid: Application of a k-ε model** D. Pujol, J. Colomer, T. Serra and X. Casamitjana
p. 69	**Modeling mean flow and turbulence in aquatic vegetation** A.T. King
p. 71	**Velocity variations in a patterned wetland from lattice-Boltzmann flow modeling** E.A. Variano, M.C. Sukop, D.T. Ho, S. Anwar, and V. C. Engel
p. 73	**A new model for mixing in turbulent open channel flows** J. Atkinson, S. Bennett and H. Rubin
p. 81	**Effects of lock operation and shipping on hydrodynamic conditions and geochemical fluxes in a heavily impounded river** A. Mäck, C. Noss, H. Fischer and A. Lorke

Poster session

p. 83	**Seiche-induced heat and mass exchange between the sediments and the near-bottom waters** J. Bernhardt, K. Frindte, S. Jordan, M. Hupfer, H.-P. Grossart, C. Engelhardt and G. Kirillin
p. 86	**Cross wavelet, coherence and phase between water surface temperature and heat flux in a tropical hydroelectric reservoir** E.H. Alcântara, J.L. Stech, J.A. Lorenzzetti and E.M.L.M. Novo
p. 94	**The impacts of the cold fronts on thermal stratification and water quality in a tropical reservoir (Brazil)** J.L. Stech, E.H. Alcântara, J.A. Lorenzzetti, E.M.L.M. Novo, A.T. Assireu
p. 102	**Modelling the diurnal migration of Microcystis in a stratified reservoir with a particle trajectory approach** Y.C. Chien and S.C. Wu
p. 110	**Scaling plankton persistence in complex flow networks** J.G.P. Gamarra, E.A. Variano and M.B. Bain
p. 112	**Using hyperspectral optical methods to examine the effect of turbulent mixing on ecosystem functioning in a coastal lagoon** O.N. Ross, J. Piera, E. Torrecilla, M. Lara and E. Berdalet
p. 114	**Benthic imagery survey of Asian clam in Lake Tahoe** A.L. Forrest, M. Wittmann, B. Allen, V. Schmidt, N.A. Raineault, W. Pike, A. Hamilton, L.P. Kost, B.E. Laval, A.C. Trembanis and G. Schladow
p. 116	**The net water budget of a lake without surface in- and outflow: a non-stationary approach** G. Kirillin, W. Philipp , G. Nützmann and C. Engelhardt
p. 125	**Temperature in Hálslón reservoir** V.K. Helgason and A. Gunnarsson
p. 126	**Modelling the thermal behaviour of subarctic water system during ice free conditions** M. Priet-Mahéo and H.Ó. Andradóttir
p. 128	**Modeling underflows in Lake Thingvallavatn in varying surface shear conditions** A.L. Forrest, H. Andradottir, B.E. Laval
p. 130	**Turbulence modulation by suspended sediment in a zero-shear geophysical flow** S.J. Bennett, J.F. Atkinson, and M.J. Fay
p. 138	**Hydrophysical processes in the Gulf of Finland inferred from bottom-mounted ADCP Measurements** L. Talsepp, J. Elken, T. Kõuts, M.-J.Lilover, I.Suhova
p. 140	**Dissolved oxygen dynamics in a shallow ice-covered lake** A. Terzhevik, G. Kirillin, C. Engelhardt, S. Golosov, M. Leppäranta, N. Palshin, R. Zdorovennov, G. Zdorovennova

Session 6

p. 141	**Littoral zones as source of methane in lakes: Dynamics and distribution** H. Hofmann, C. Seibt and F. Peeters
p. 143	**Extreme methane emissions from a temperate reservoir: The importance of ebullition** T. DelSontro, D.F. McGinnis, S. Sobek, I. Ostrovsky, W. Eugster, and B. Wehrli
p. 145	**Physical characterization of oxygen fluxes across the water column in the central North Sea** L. Rovelli, M. Dengler, J. Schafstall, M. Schmidt, S. Sommer, P. Linke and D. F. McGinnis
p. 147	**Using the source as the solution: oxygenation effects on Mn cycling and water quality** L.D. Bryant, P.A. Gantzer and J.C. Little
p. 155	**Sampling strategies for multi-scale characterisation of biological and hydrodynamic interactions: the role of lothir observatories** J. Piera, O.N. Ross, E. Torrecilla, S. Pons, I. F. Aymerich, J. J. Dañobeitia, R. Quesada, M. L. Artigas and E. Berdalet

Session 7

p. 158	**Mixing and secondary circulation in stratified oscillating boundary layers near sloping topography** L. Umlauf and H. Burchard
p. 159	**Seasonal variation of mechanisms governing sediment dynamics in South San Francisco Bay** A. Brand, J. Lacy, K. Hsu, D. Hoover, S. Gladding, and M. Stacey
p. 161	**The dynamics of benthic boundary layer in Lake Biwa** M. Kumagai, D. Nover, S.G. Schladow and C.R. Goldman
p. 163	**Instrument comparison: Laser diffraction, microscopy and flow cytometry for assessing fine particle concentration and size distribution** D.M. Nover, S. Andrews, T. Schuler, M. Winder, D. Hunter, J.E. Reuter and S.G. Schladow
p. 165	**In-situ optical observations of particulates in Lake Tahoe** S. Andrews, D.M. Nover, S.G. Schladow and J.E. Reuter

Scientific Program

Monday June 28th

8:00-8:25 Registration in Room 101 in Háskólatorg, University of Iceland

8:25-8:30 Welcome by Dr. Sigurður Magnús Garðarsson, Head of the Faculty of Civil and Environmental Engineering, University of Iceland

Session 1

8:30-9:30	**Keynote: Impact of climate change on aquatic systems** Thorsten Blenckner, Stockholm Resilience Center, Stockholm University
9:30-10:00	**Comparing the lake thermal regime in different northern climates - a climate change analysis** Lars Bengtsson, Water Resources Engineering, Lund University
10:00-10:30	**Evidence of warming in two aquatic systems in the northeast of Spain** Teresa Serra, Department of Physics, University of Girona
10:30-10:50	*Coffee*
10:50-11:20	**Headwater lakes of the Chilean Patagonia: A laboratory for studying the impacts of global and local stressors** Geoffrey Schladow, University of California, Davis
11:20-11:50	**On the spatially water temperature and heat flux variability over a tropical hydroelectric reservoir** Enner Alcântara, National Institute for Space Research, Brazil
11:50-12:20	**Impact of a Hydroelectric Power Station on Water Mixing Processes within a Stratified Lake** Charles Lemckert, Griffith School of Engineering
12:20-13:00	*Lunch*

Session 2

13:00-13:30	**Modeling circulation in Lake Huron** Dmitry Beletsky, University of Michigan, Ann Arbor
13:30-14:00	**Process oriented modeling of Lake Ontario hydrodynamics** Leon Boegman, Dept. of Civil Engineering, Queen's University, Kingston
14:00-14:30	**Density of water from partial molal volumes** Bertram Boehrer, Helmholtz-Centre for Environmental Research - UFZ, Magdeburg
14:30-15:00	**Combined use of the conservative tracers ^{18}O and SF_6 to detect groundwater inflow in the monimolimnion of a meromictic mining lake** Johann Ilmberger, Institute of Environmental Physics, Univ. of Heidelberg
15:00-15:20	*Coffee*

Session 2 (cont)

15:20-15:50	**Factors influencing the currents over the shallow bank in the Gulf of Finland** Madis-Jaak Lilover, Marine Systems Institute, Tallinn Univ. of Technology
15:50-16:20	**Wind-driven ocean upper layer model** Aleksander Toompuu, Marine Systems Institute, Tallinn Univ. of Technology
16:20-17:00	**Can we simulate the hydrodynamics of the European Shelf Sea by using a shallow water model?** Adolf Stips, CEC Joint Research Centre, Global Environment Monitoring Unit

Tuesday June 29th

8:00 Meeting for bus in front of VRII, University of Iceland

8:00-11:00 Travel to Hotel Geysir, with a stop at Lake Þingvallavatn

Session 3

11:00-12:00	**Keynote: The Ecodynamics of Lake Myvatn** Árni Einarsson, Mývatn Research Station
12:00-12:30	**Climate change and its effects on lakes in SW−Iceland** Hilmar Malmquist, Natural History Museum of Kópavogur
12:30-13:30	*Lunch*
13:30-14:00	**The significance of accurate hydrological modeling for long-term lake water quality predictions in volcanic zones** Sveinn Óli Pálmarsson, Vatnaskil Consulting Engineers
14:00-14:30	**Internal waves in weakly stratified Lake Lagarfljót** Hrund Andradóttir, Faculty of Civil and Env. Engineering, Univ. of Iceland
14:30-15:00	**Modelling of physical processes in a large deep polar lake** Ram Yerubandi, National Water Research Institute, Environment Canada
15:00-15:30	**Internal seiching in ice covered lakes** Georgiy Kirillin, Leibniz-Institute of Freshwater Ecology, Berlin
15:30-16:00	*Coffee*

16:00-18:30 Travel to Reykjavík, with a stop at Gullfoss

Wednesday June 30th

Conducted in Room 101 in Háskólatorg, University of Iceland

Session 4

8:30-9:30	**Keynote: Temperature driven flows in natural lakes** Matthew Wells, Dept. of Physical and Environmental Sciences. Univ. Toronto
9:30-10:00	**Internal wave-induced flow in shallow, stratified waters** Peter Davies, Department of Civil Engineering, University of Dundee
10:00-10:30	**Spatial and temporal variability of turbulent hot spots in a large stratified lake** Damien Bouffard, Dept. of Civil Engineering, Queen's University, Kingston
10:30-10:50	*Coffee*
10:50-11:20	**Vertical structure of the ex-fjord Powell Lake in British Columbia** Alfred Wüest, Eawag, Kastanienbaum
11:20-11:50	**Variability in the circulation in Kalbaksfjord, Faroe Islands** Knud Simonsen, The University of the Faroe Islands
11:50-12:30	*Lunch*

Session 5

12:30-13:00	**Effect of submerged aquatic vegetation on turbulence induced by an oscillating grid: Application of a k-ε model** Xavier Casamitjana, Department of Physics. University of Girona
13:00-13:30	**Modeling mean flow and turbulence in aquatic vegetation** Alexandra King, DeFrees Hydraulics Laboratory, Cornell University
13:30-14:00	**Velocity variations in a patterned wetland from lattice-Boltzmann flow modeling** Evan Variano, Civil and Environmental Engineerinng, Univ. of California, Berkeley
14:00-15:30	*Poster session and coffee*
15:30-16:00	**A new model for mixing in turbulent open channel flows** Joseph Atkinson, Dept. of Civil, Structural and Environmental Engineering, University at Buffalo, Buffalo
16:00-16:30	**Effects of lock operation and shipping on hydrodynamic conditions and geochemical fluxes in a heavily impounded river** Andreas Mäck, Institute for Environmental Science, Univ. of Koblenz-Landau

18:00 Meeting for bus in front of VRII, University of Iceland. **Conference dinner**

Poster session (Wednesday afternoon)

1	**Seiche-induced heat and mass exchange between the sediments and the near-bottom waters** Juliane Bernhardt, Leibniz-Institute of Freshwater Ecology and Inland Fisheries
2	**Cross wavelet, coherence and phase between water surface temperature and heat flux in a tropical hydroelectric reservoir** Enner Alcântara, National Institute for Space Research, Brazil
3	**The impacts of the cold fronts on thermal stratification and water quality in a tropical reservoir (Brazil)** José Stech, National Institute for Space Research, Brazil
4	**Modelling the diurnal migration of Microcystis in a stratified reservoir with a particle trajectory approach** Yu-ching Chien, Graduate Institute of Environmental Engineering, National Taiwan University
5	**Scaling plankton persistence in complex flow networks** Evan Variano, Civil and Environmental Engineerinng, Univ. of California, Berkeley
6	**Using hyperspectral optical methods to examine the effect of turbulent mixing on ecosystem functioning in a coastal lagoon** Oliver Ross, Marine Technology Unit (UTM)., Mediterranean Centre for Marine and Environmental Research (CMIMA, CSIC), Barcelona
7	**Benthic imagery survey of Asian clam in Lake Tahoe** Geoffrey Schladow, University of California, Davis
8	**The net water budget of a lake without surface in- and outflow: a non-stationary approach** Christof Engelhardt, Leibniz-Institute of Freshwater Ecology and Inland Fisheries
9	**Temperature in Hálslón reservoir** Victor Helgason, Landsvirkjun, Research and Planning
10	**Modelling the thermal behaviour of subarctic water system during ice free conditions** Morgane Priet-Mateo, Faculty of Civil and Env. Engineering, Univ. of Iceland
11	**Modeling underflows in Lake Thingvallavatn in varying surface shear conditions** Hrund Andradóttir, Faculty of Civil and Env. Engineering, Univ. of Iceland
12	**Turbulence modulation by suspended sediment in a zero-shear geophysical flow** Joseph Atkinson, Dept. of Civil, Structural and Environmental Engineering, University at Buffalo, Buffalo
13	**Hydrophysical processes in the Gulf of Finland inferred from bottom-mounted ADCP Measurements** Madis-Jaak Lilover, Marine Systems Institute, Tallinn Univ. of Technology
14	**Dissolved oxygen dynamics in a shallow ice-covered lake** Georgiy Kirillin, Leibniz-Institute of Freshwater Ecology, Berlin

Thursday July 1st

8:00 Meeting for bus in front of VRII, University of Iceland

8:00-8:50 Travel to Blue Lagoon

Session 6

9:00-9:30	**Littoral zones as source of methane in lakes: Dynamics and distribution** Hilmar Hofmann, Limnological Institute, University of Konstanz
9:30-10:00	**Extreme methane emissions from a temperate reservoir: The importance of ebullition** Tonya Delsontro, Eawag, Kastanienbaum
10:00-10:30	**Physical characterization of oxygen fluxes across the water column in the central North Sea** Lorenzo Rovelli, IFM-GEOMAR, Leibniz Institute of Marine Sciences, University of Kiel
10:30-10:50	*Coffee*
10:50-11:20	**Using the source as the solution: oxygenation effects on Mn cycling and water quality** Lee Bryant, Civil and Environmental Engineering Dept., Virginia Tech
11:20-11:50	**Sampling strategies for multi-scale characterisation of biological and hydrodynamic interactions: the role of lothir observatories** Jaume Piera, Marine Technology Unit (UTM)., Mediterranean Centre for Marine and Environmental Research (CMIMA, CSIC), Barcelona
11:50-12:40	*Lunch*

Session 7

12:40-13:10	**Mixing and secondary circulation in stratified oscillating boundary layers near sloping topography** Lars Umlauf, Leibniz-Institute for Baltic Sea Research, Warnemünde
13:10-13:40	**Seasonal variation of mechanisms governing sediment dynamics in South San Francisco Bay** Andreas Brand, Dept. of Civil and Environmental Engineering, Univ. of California, Berkeley
13:40-14:10	**The dynamics of benthic boundary layer in Lake Biwa** Michio Kumagai, Lake Biwa Environmental Research Institute
14:10-14:30	*Coffee*
14:30-15:00	**Instrument comparison: Laser diffraction, microscopy and flow cytometry for assessing fine particle concentration and size distribution** Daniel Nover, Tahoe Environmental Research Center, Univ. of Calif., Davis
15:00-15:30	**In-situ optical observations of particulates in Lake Tahoe** Stephen Andrews, Tahoe Environmental Research Center, Univ. of California, Davis

16:00-17:30 Optional swimming in Blue Lagoon

17:30-18:20 Travel to Reykjavík

Impact of climate change on aquatic systems

Thorsten Blenckner

Baltic Nest Institute, Stockholm Resilience Centre, Stockholm University, Sweden

e-mail tblen@mbox.su.se

KEYWORDS
Modelling, time-series analysis, biogeochemical models, biological models, CLIME

EXTENDED ABSTRACT

INTRODUCTION

While in the 1960s and 70s, the main point of interest in water quality management focused on predictive schemes to assess the quantitative consequences of nutrient transfer from the catchment to the lake, the apparent simplicity of these relationships does not consider a number of complex interactions within the ecosystem and its surrounding catchment that have to be understood in order to manage water resources in an efficient and sustainable way.

In recent years, it has become clear that interannual changes in climate influence to a large extent the water quality of freshwater resources by affecting these interactions. Long-term assessments (over a period of 20-30 years) have shown that many water quality problems that were once considered as local phenomena are affected by changes in weather and climate that operate on a regional or even global scale. These include changes in total precipitation, precipitation frequency, winter air temperature etc.

Consequently, any research of climate effects on water resources can only be done successfully when concentrating on integrated catchment-lake-ocean processes and any assessment requires a study of long-term variation and change on several different sites using time-series analysis and applying biogeochemical and biological models to study the processes and feedbacks behind water quality changes.

Here I will present first some general changes in climate and the effects on lake ecosystems. Then, the experiences from the large European project “Climate and Lakes Impacts in Europe” will be shown. In addition, new state-of-the-art modelling exercise from the Baltic Nest Institute and its decision support system will be presented.

RESULTS & DISCUSSIONS

The CLIME project focused on the analysis of long-term time-series from many European lakes and on the linkage of regional climate models and weather generators with biogeochemical catchment and lake models. The models that formed the core of the project have been designed to bridge the gap between the empirical models widely used by environmental managers and the complex process-based models favoured by research scientists. The main results were integrated in a decision support system (see Fig. 1) and in a book published recently (edited by George 2010).

Further, the different combination of models used by the Baltic Nest Institute, will be presented in order to show the potential linkages of biogeochemical and food-web models model in relation to climate change models. Finally, the research gaps and challenges will be mentioned.

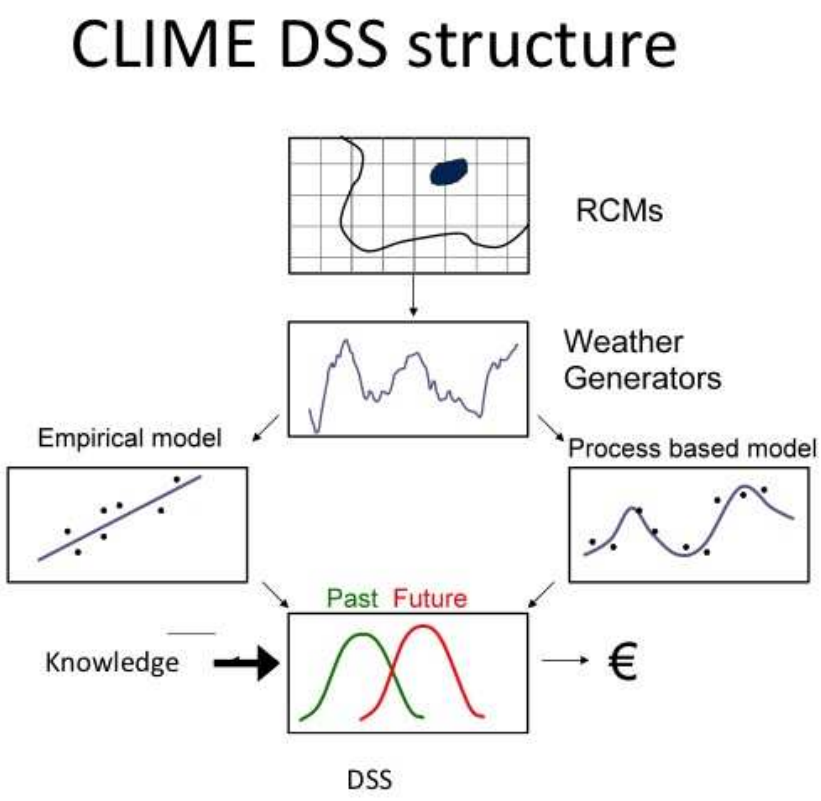

Fig. 1. Showing the information and data flow of the CLIME Decision Support System (DSS)

REFERENCE

George, G. (2010) The impact of climate change on European lakes. Aquatic Ecology Series, Springer, 507pp

Comparing the lake thermal regime in different northern climates - a climate change analysis

Lars Bengtsson

Water Resources Engineering, Lund University, Sweden

e-mail lars.bengtsson@TVRL.LTH.se

KEYWORDS
Thermal stratification, lake ice-cover, climate change.

ABSTRACT

A future warmer climate will change the thermal regime of lakes. The ice conditions will change and the water temperature. Since the solar radiation remains the same in a new climate, it is relevant to compare the lake conditions in years when the air temperature has been rather different but the solar rdiation almost the same. This has been done for Lake Velen in Sweden. Ice conditions, lake surface temperature and thermal stratification have also been determined for different hypothetical lakes using simple models varying the climatic conditions and the lake parameters. In general it is found that the ice conditions do not influence the thermal stratification during summer. The surface temperature during summer increases somewhat less than the air temperature increase. The stratification is mainly determined by wind conditions and how fast the solar radiation is attenuated with depth. A warmer winter means a shorter duration of the ice cover but not much reduction of the ice thickness and rather colder than warmer water temperature during winter.

Evidence of warming in two aquatic systems in the northeast of Spain

T. Serra[1]*, J. Pascual[2], J. Torcque[1], J. Colomer[1], X. Casamitjana[1], M. Soler[1] and J. Calbó[1]

[1] *Department of Physics, University of Girona, Campus Montilivi, 17071-Girona, Spain*
[2] *Observatori de l'Estartit. 17258-L'Estarti, Girona, Spain*

**Corresponding author, e-mail teresa.serra@udg.edu*

KEYWORDS
Lake warming; climatic change; air temperature; Mediterranean.

EXTENDED ABSTRACT

Both large scale variability and climate change are recognized as the key factors controlling the thermal structure of aquatic systems (Arhonditsis et al., 2004; Coats et al. 2006, Verburg et al., 2003; Vollmer et al., 2005). Some studies show a greater warming of the surface layer compared with a minor increase in the deeper layer (Verburg et al., 2003; Coats et al. 2006), which will result in a sharper temperature gradient. A stronger temperature gradient also means an increase in the stability of the water column, reducing or inhibiting the mixing processes and the oxygenation of the system. All of the above mentioned processes may have a large impact on the ecology and the water quality of the aquatic media, as found in lake Tanganyika (Verburg et al., 2003). Other aquatic systems, as in lake Malawi, deeper layers show a warming trend while surface layers remain at the same temperature (Vollmer et al., 2005). Therefore, this lake presents a tendency towards a state more prone to the mixing events. The tendency observed for lake Malawi has been mainly attributed to the milder winters observed during the last 70 years of observations. The above mentioned examples demonstrate that climate change and variability will have chemical, physical and ecological impacts on lakes and also that these effects will vary depending on the particular region of the world and the specific dynamics of each lake. As a result, local effects may not correspond exactly to what we might expect from global warming trends addressed by the IPCC (Intergovernmental Panel on Climate Change) scenarios (Danis et al., 1994). In this work, data on water and air temperature from 1969 until 2008 for two aquatic systems situated in the Northeast of Spain has been analyzed. The analysis was done in order to find long term trends in the temporal evolution of the temperature records and also in order to determine if there is any warming evidence during this period. One of the data records correspond to the water column of Lake Banyoles, which has been largely studied before for its interest because it is the second largest lake in Spain. The second data record corresponds to the temperature of the water column of the northwest coast of the Mediterranean, in front of l'Estartit (Northeast of Spain).

The study was performed at two different times of the year: one corresponding to the period of stratification of the water column (May-August) and the other for the period of mixing (December-February). Two depths of the water column were selected for the analysis. One at the upper part of the water column (at z=-5m), which will give us the information of the thermal evolution of the mixed layer. The second depth considered in the study will be at z=-

15 m, for lake Banyoles, and z=-50 m for the sea water. These temperature records will give us the thermal evolution of the deep layer in these systems. In lake Banyoles, all the measurements were done in the central part of the lake that has a maximum depth of 40 m. In the station situated at l'Estartit coast, the maximum depth was 90 m. A reversing thermometer was used from 1969 until 1990 for measuring the temperature at different water depths. However, from 1990 a CTD was used in order to have a better vertical resolution of the temperature profiles. From 1990 on both the CTD and the reversing thermometer were periodically used together in order to find differences between instruments and make appropriate calibrations when necessary.

For the stratified period, both systems show a warming of the surface layer, 0.99ºC decade^{-1} for lake Banyoles and 0.39ºC decade^{-1} for l'Estartit coastal sea water. During this period, the deep waters of l'Estartit warm up significantly, at a rate of 0.58ºC decade^{-1}, while the deep waters of lake Banyoles do not show any significant trend. The increase in the surface water temperature coincides with an even greater increase in the air temperature for the same period (May-August, from 1969 until 2008). In Banyoles, the air temperature was found to increase at a rate of 1.13ºC decade^{-1} and in l'Estartit station the rate was 0.78ºC decade^{-1}. Therefore, a tendency to harsh summers may explain the warming of the surface water layer. During the mixed period, the surface waters of lake Banyoles do not show any significant trend like what was found for the air temperature evolution. In contrast, for l'Estartit station, the surface water temperature was found to increase at a rate of 0.21ºC decade^{-1}, coinciding with a warming of the air of 0.31ºC decade^{-1}. These results show that the water column of lake Banyoles will present a sharper stratification during the summer period, whereas the stratification of the sea water, at least in the region studied, will weaken. These results might represent important changes in the ecosystem and might determine the fate of all the organisms inhabiting there.

REFERENCES

Arhonditsis, B.B., Brett, T., DeGasperi, C.L. & Schindler, D.E. (2004), Effects of climatic variability on the thermal properties of Lake Washington. *Limnol. Oceanogr.*, 49. 256-270.

Coats, R., Perez-Losada, J., Schladow, G., Richards, R. & Goldman, C. (2006), The warming of lake Tahoe. Climatic Change, 76. 121-148.

Danis, P.A., Grafenstein, U., Masson-Delmonte, V., Planton, S., Gerdeaux, D. & Moisselin, J.M. (2004), Vulnerability of two European lakes in response to future climatic changes, Geophys. Res. Let., doi: 10.1029/2004GL020833.

Verburg, P., Hecky, R.E. & Kling H. (2003), Ecological consequences of a century of warming in lake Tanganyika, Science, 301. 505-507.

Vollmer, M.K., Bootsma, H.A., Hecky, R.E., Patterson, G., Halfman, J.D., Edmond, J.M., Eccles, D.H. & Weiss, R.F. (2005), Deep-water warming trend in lake Malawi, East Africa, Limnol. Oceanogr., 50. 727-732.

Headwater lakes of the Chilean Patagonia: A laboratory for studying the impacts of global and local stressors

S. G. Schladow[1]*, M. Winder[1], R. Urrutia[2], A. Araneda[2], A. Stehr[2] and B. Reid[3]

[1] *Tahoe Environmental Research Center, University of California, Davis, CA 95616, USA*
[2] *Centro de Ciencias Ambientales EULA-CHILE, Universidad de Concepcion, Concepcion, Chile.*
[3] *Centro de Investigacion en Ecosistemas de la Patagonia (CIEP), Coyhaique, Chile.*

**Corresponding author, e-mail gschladow@ucdavis.edu*

KEYWORDS
Patagonia, lakes, GLOF, anthropogenic change, climate change, Baker River watershed

EXTENDED ABSTRACT

INTRODUCTION
The Chilean Patagonia represents a unique region where the principal anthropogenic stress on inland waters is the result of atmospheric deposition of global contaminants, and climate change. This makes the region important on a global scale for studying these impacts, free of the confounding local effects that dominate water resources in most countries. The impacts of climate change may already be evident, with GLOF (Glacial Lake Outflow Flood) events increasing in frequency in recent years. There is particular urgency to addressing these issues as a new anthropogenic stress, hydroelectric development, may soon start having an impact on lakes in Patagonia. This in itself presents an additional opportunity – the possibility of studying the evolution of undisturbed lakes in response to both climate change and hydroelectric development over the coming decades. This paper describes the first results in a collaboration between the University of California (Davis) and the University of Concepcion on the interdisciplinary study of the Baker River watershed. This watershed encompasses the full range of land form, land use and geographic features that characterize Patagonia. It includes the largest river (the Baker River) and lake (General Carrera Lake) in Chile, while at the same time includes numerous smaller streams, lakes wetlands and glaciers.

METHODS
The sampling was concentrated on L. Bertrand (max. depth 220 m), L. Cochrane-Chica (max. depth 43 m), and L. Negro (max. depth 150 m). These are headwater lakes of the Rio Baker and differ widely in their physical and morphological characteristics. The watersheds differ widely and range from glacial-dominated runoff (L. Bertrand) to forested and non-forested vegetation. L. Bertrand is characterized by high concentration of glacial flour and low light transparency. In contrast, visibility of the other two lakes is high, indicative of low primary productivity and absence of glacial flour.

Thermistor chains were installed in all three lakes. Profiles of temperature, conductivity, chlorophyll-a, dissolved oxygen and pH were measured with a Hydrolab. In addition, water samples for chemical analysis (phosphorus, nitrogen, silica) and chlorophyll a concentration were collected at three depths in the epilimnion and two depths in the hypolimnion.

RESULTS AND DISCUSSION
Hydrolab profiles for temperature, chlorophyll-a, dissolved oxygen and pH are shown in Figure 1. The panels are (A) Lago Bertrand, (B) Lago Cochrane-Chica, and (C) Lago Negro,

and were taken on December 16, 17 and 18 in 2008, respectively. The different characteristics of the 3 lakes are evident in all measured parameters. Secchi depths were 2.5 m, 18 m and 15.5 m respectively.

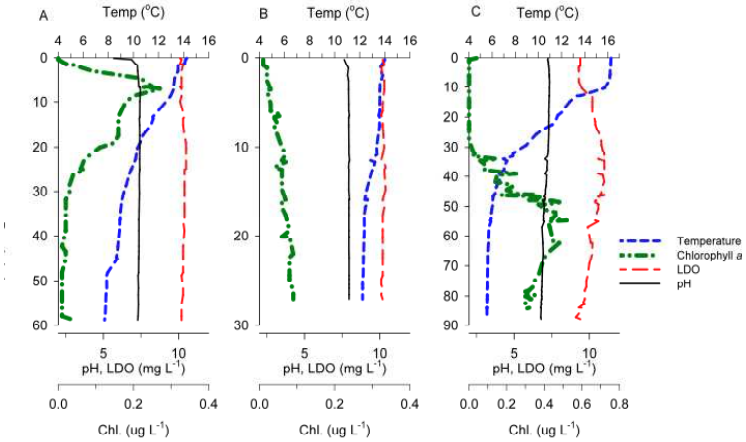

Figure 1. Hydrolab profiles from three lakes

Figure 2 shows part of the thermistor chain record for Lago Cochrane-Chica for the month of September 2009. The most noticeable feature is the sudden increase in temperature in thermistors 2nd, 3rd and 4th from the bottom on September 16 and the abrupt temperature change in the bottom thermistor on September 20. This is believed to be the result of a wave initiated by a GLOF (Glacial Lake Outburst Flood) in the Colonia River, a **downstream** tributary of the Baker River. The outburst event was estimated to produce a flow of approximately 2500 m^3s^{-1}, five times the typical flow in the Baker River in September.

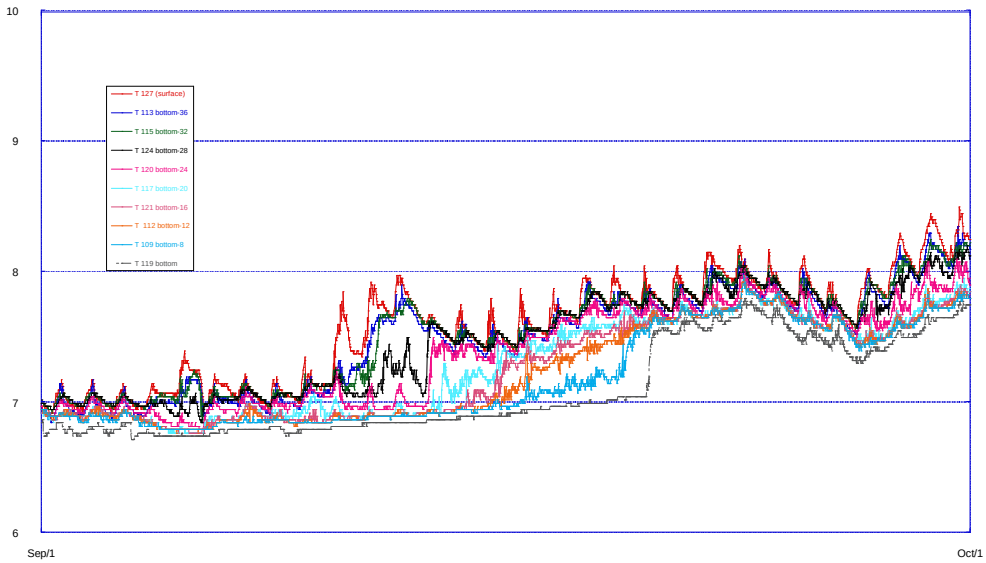

Figure 2. Thermistor chain from Lago Cochrane-Chica

REFERENCES

Dussaillant, A., Benito, G., Buytaert, W., Carling, P., Meier, C. and Espinoza, F. (2009). Repeated glacial-lake outburst floods in Patagonia: an increasing hazard? Nat Hazards, DOI 10.1007/s11069-009-9479-8.

On the spatially water surface temperature and heat flux variability over a tropical hydroelectric reservoir

E.H. Alcântara[1*], J.L. Stech[1], X. Casamitjana[2], M.P. Bonnet[3], J.A. Lorenzzetti[1], E.M.L.M. Novo[1]

[1]*National Institute for Space Research, Remote Sensing Division, Brazil.*
[2]*Environmental Physics Group, Physics Department, University of Girona, Spain*
[3]*Institut de Recherche pour le Développement, France*

**Corresponding author, e-mail enner@dsr.inpe.br*

ABSTRACT

Water temperature plays an important role in ecological functioning and in controlling the biogeochemical processes of a water body. Conventional water quality monitoring is expensive and time consuming. It is particularly problematic if the water bodies to be examined are large. Conventional techniques also bring about a high probability of undersampling. Conversely, remote sensing is a powerful tool to assess aquatic systems. The objective of this study was to map the surface water temperature and improve understanding of spatiotemporal variations in a hydroelectric reservoir. In this work, MODIS land-surface temperature (LST) level 2, 1-km nominal resolution data (MOD11L2, version 5) were used. All available clear-sky MODIS/Terra images from 2003 to 2008 were used, resulting in a total of 786 daytime and 473 nighttime images. Descriptive statistics (mean, maximum and minimum) were computed for the historical images to build a time series of daytime and nighttime monthly mean temperatures. The thermal amplitude and anomaly were also computed. In-situ meteorological variables were used from 2003 to 2008 to help understand the spatiotemporal variability of the surface water temperature. The surface energy budget and the depth at which the wind can distribute the heat input of a given surface were also measured. A correlation between daytime and nighttime surface water temperatures and the computed heat fluxes were made. These relationships and the causes of the water surface temperature variability are discussed.

Keywords: Remote sensing**;** water surface temperature; heat flux; mixed depth layer; thermal amplitude; MODIS.

INTRODUCTION

In accordance with Kimmel et al. (1990), water temperature distribution is fundamental to understanding the performance and functioning of reservoir ecosystems. Surface water temperature is a key parameter in the physics of aquatic system processes since it accounts for the water-atmosphere interactions and energy fluxes between the atmosphere and the water surface. Because it influences the water's chemistry, it also affects its biological processes (Lerman, Imboden and Gat, 1995). Moreover, temperature differences between the water and air moisture control the heat exchange in the air/water boundary layer, and as a consequence, they are crucial to understanding the hydrological cycle.

Thermal infrared remote sensing applied to freshwater ecosystems has aimed to map surface temperatures (Oesch et al., 2008; Reinart and Reinhold, 2008; Crosman and Horel, 2009), bulk temperatures (Thiemann and Schiller, 2003), circulation patterns (Schladow et al., 2004)

and to characterize upwelling events (Steissberg et al., 2005). However, the application of thermal infrared images to the study of surface water temperatures in hydroelectric reservoirs is scarce and, in Brazil, is being attempt for the first time.

The objectives of this paper are to map the spatial variability of the water surface temperature (WST) of a tropical hydroelectric reservoir using daytime and nighttime satellite images. Through the WST maps, the heat flux budget will be calculated and used to explain the observed patterns in the WST by the physical forcing related to the geomorphological, meteorological and hydrological context.

STUDY AREA

The Itumbiara hydroelectric reservoir (18°25'S, 49°06'W) is located in a region stretched between Minas Gerais and Goiás States (Central Brazil) that was originally covered by tropical grassland savanna. The damming of the Parnaiba River flooded its main tributaries: the Araguari and Corumbá rivers. The basin's geomorphology resulted in a lake with a dendritic pattern covering an area of approximately 814 km² and a volume of 17.03 billion m³ (Figure 1).

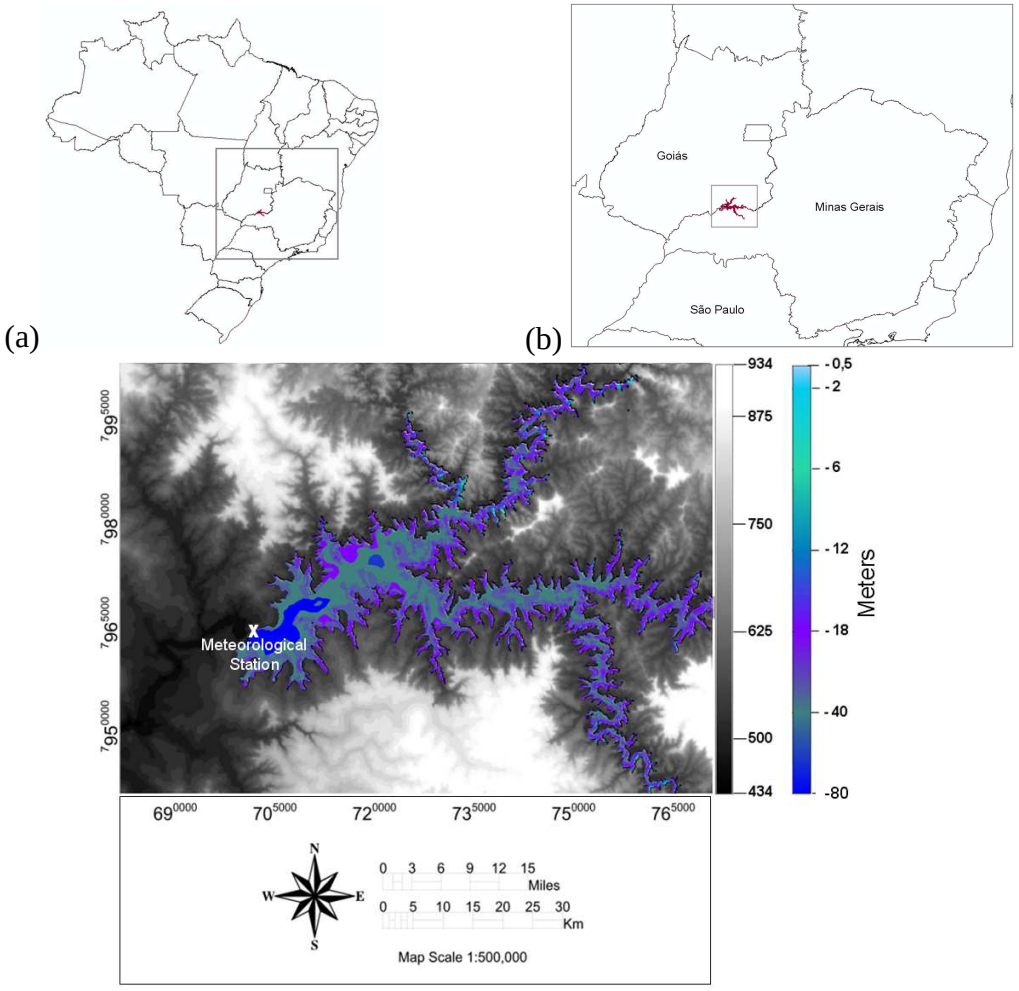

Figure 1: Localization of Itumbiara hydroelectric reservoir in Brazil's central area (a), at the state scale (b) and at the regional scale (c) with the bathymetric map. On a regional scale, the flooded area is shown over an SRTM (Shuttle Radar Topography Mission) image.

METHODOLOGICAL APPROACH

The methodological approach was developed using the concept of disturbing influences that reservoirs are exposed to. These are described by Fischer et al. (1979) as: (1) meteorological variables, such as wind velocity, and short and long wave radiation in the area, which determine the strength of any energy transfers across the air-water interface; (2) water from the inflowing streams, which may impart kinetic and potential energy; and (3) turbulent mixing generated close to outflows, which can make some of the energy of the outflowing water transform into kinetic energy of the reservoir water. We hypothesize, then, that the heat fluxes, which are a function of the meteorological variable, could explain the spatial-temporal water surface temperature variation in the Itumbiara reservoir.

Hydrometeorological data

The daily mean air temperature (ºC), relative humidity (%), wind intensity (ms^{-1}) and precipitation (mm) from 2003 to 2008 were used for the study. These data were obtained from a meteorological station (see Figure 1 for location) near the dam. The daily mean of each variable was converted into monthly means to adequate it to the time scale of the satellite data.

Satellite data

MODIS water surface temperature (WST) level 2, 1-km nominal resolution data (MOD11L2, version 5) were obtained from the National Aeronautics and Space Administration Land Processes Distributed Active Archive Center (Wan, 2008). All available clear-sky MODIS Terra imagery between 2003 and 2008 were selected by visual inspection, resulting in a total of 786 daytime images and 473 nighttime images (Figure 2). A shoreline mask to isolate land from water was built using the TM/Landsat-5 image in order to isolate some anomalously cold or warm pixels remaining at some locations near the shoreline of the reservoir.

The WST-MODIS data were extensively validated for inland waters and were considered accurate (Oesch et al., 2005; Oesch et al., 2008; Reinart and Reinhold, 2008; Crosman and Horel, 2009).

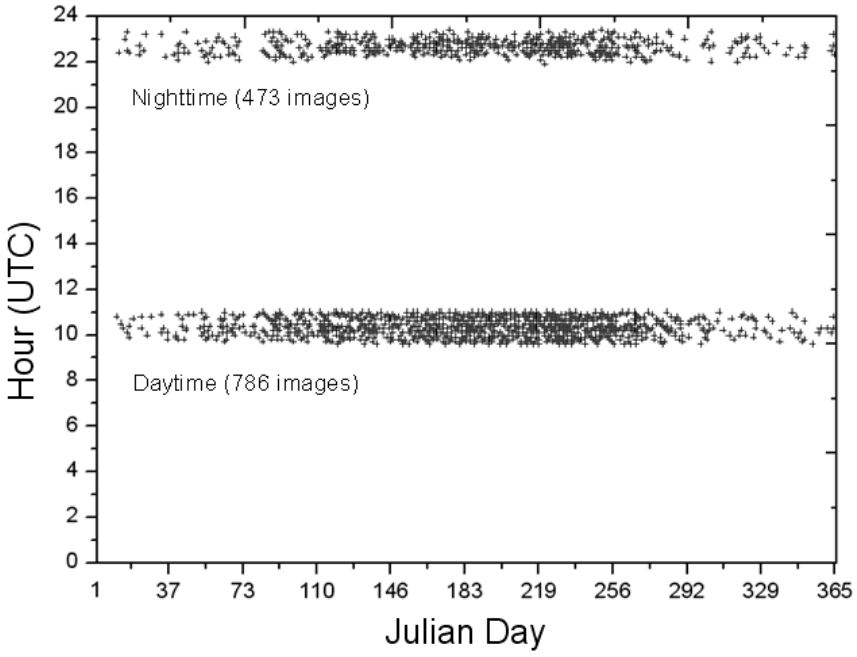

Figure 2: Acquisition date and time of all MODIS/Terra data for 2003-2008 used in this study.

WST, climatologies, anomaly maps and statistics

Maps of monthly mean daytime and nighttime water surface temperatures were produced from 2003 to 2008. The thermal amplitude was computed pixel-by-pixel by subtracting daytime and nighttime temperatures. To obtain the anomaly, the monthly mean temperatures from 2003 to 2004 were computed in a pixel-based procedure and then subtracted from each month for the entire time interval. The seasonal thermal amplitude was also analyzed. Descriptive statistics (lakewide mean, maximum and minimum) were computed for the WST maps to build a time series of daytime and nighttime monthly mean temperatures.

The surface energy budget was also calculated using the WST maps derived from MODIS/Terra.

Surface Energy Budget

A study of the energy exchange between the lake and atmosphere is essential for understanding the aquatic system behavior and its reaction to possible changes of environmental and climatic conditions (Bonnet, Poulin and Devaux, 2000). The exchange of heat across the water surface was computed using the methodology described by Henderson-Sellers (1986) as:

$$\phi_N = \phi_s(1-A) - (\phi_{ri} + \phi_{sf} + \phi_{lf}) \quad (1)$$

where ϕ_N is the surface heat flux balance, ϕ_s is the incident short-wave radiation, A is the albedo of water (=0.07), ϕ_{ri} is the Longwave flux, ϕ_{sf} is the sensible heat flux and ϕ_{lf} is the latent heat flux. The units used for the terms in Eq. (1) are W m^{-2}.

RESULTS AND DISCUSSION

Water Surface Temperature

Figure 3 shows the average monthly mean daytime and nighttime WST distributions at Itumbiara reservoir. Generally, the daytime temperatures decrease from boundary of the reservoir to the center. For nighttime, the processes is inverted. This inversion at night was observed by Sturman et al. (1999) and MacIntyre et al. (2002), who attributed this phenomenon to turbulent convection due to differential cooling. This cooling induces an effective lateral transport, replacing the water from the interior of the lake to the littoral zone (Imberger, 1985). The temperature for a given heat flux out of the water surface decreases more rapidly in the shallow water body due to the low thermal mass than in the deep regions (Wells and Sherman, 2001).

As shown in Figure 3, the spatial and horizontal variations of the daytime temperatures are at the minimum in May while the spatial horizontal variations of nighttime temperatures are the minimum during July and August. The water temperature daytime series show that January is the month with the smallest maximum temperature (26.5ºC), which starts to rise in February (30ºC). From March to July, the maximum temperature rises to around ~ 28ºC. From August to October, the temperature decreases to around ~ 7ºC. In November and December, the temperatures start to drop. The mean temperatures present the same observed patterns as the maximum temperatures.

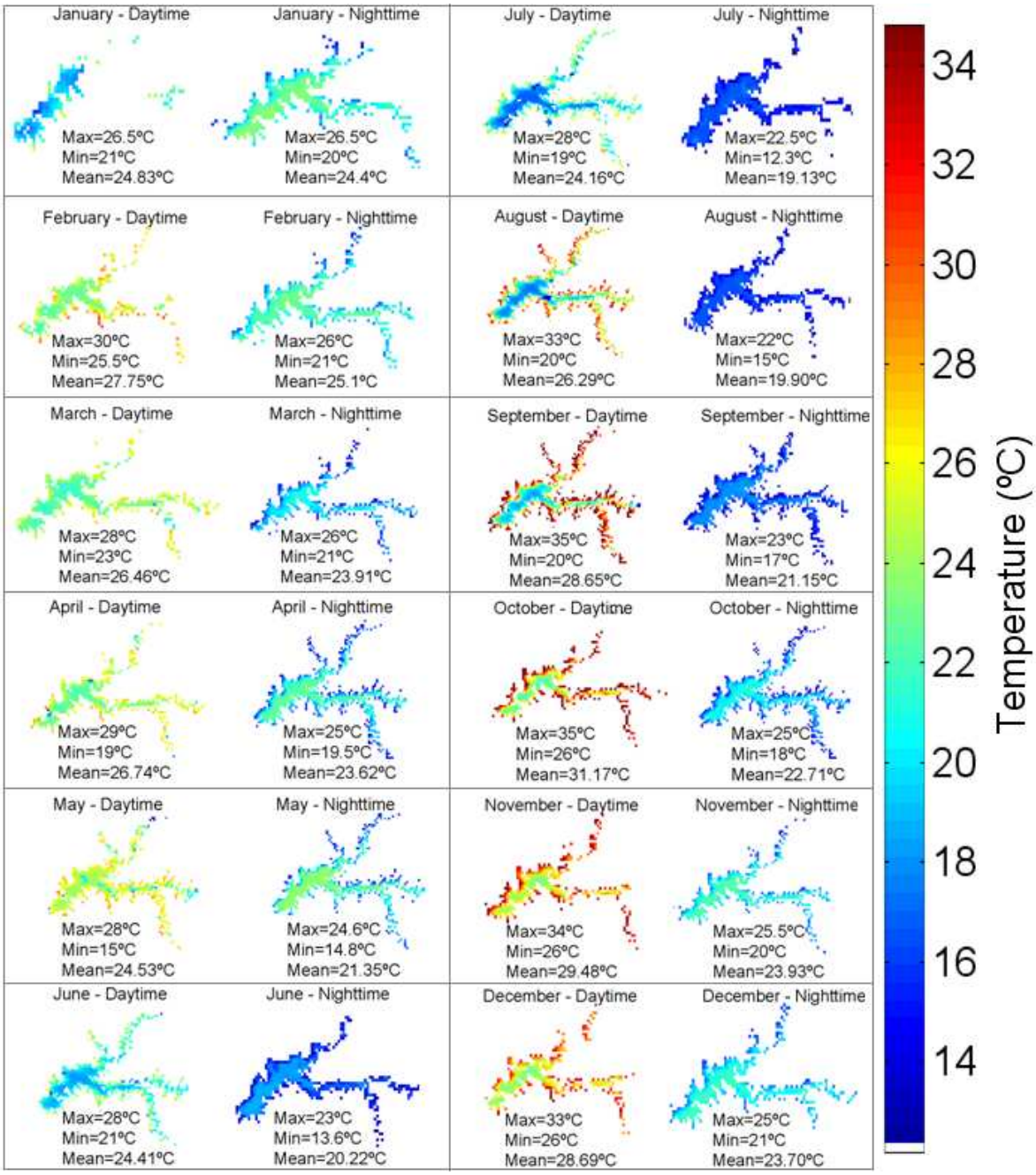

Figure 3: Monthly mean of daytime and nighttime surface water temperatures from 2003 to 2008.

Seasonal water surface temperatures

The seasonal maps were computed using the average monthly mean from 2003 to 2008 (daytime and nighttime) of the following months: summer (from December to March), fall (from March to June), winter (from June to September) and spring (from September to December). The seasonal maps of daytime were subtracted by nighttime seasonal maps to infer the seasonal thermal amplitude.

The analysis of the seasonal changes of water surface temperature shows that the differences in temperature between daytime and nighttime are negative for summer in most of the reservoir's area (Figure 4). This means that the nighttime temperatures are higher than the daytime temperatures during the summer. The greatest differences occur in the center of the reservoir (~-6ºC).

In fall, the temperature differences are near zero, with negative differences occurring in the central part of the reservoir. However, in winter these negative differences are replaced by patches of near-zero differences in the central portion of the reservoir. In the spring, these patches of near-zero amplitude are smaller, with the occurrence of positive differences (Figure 4).

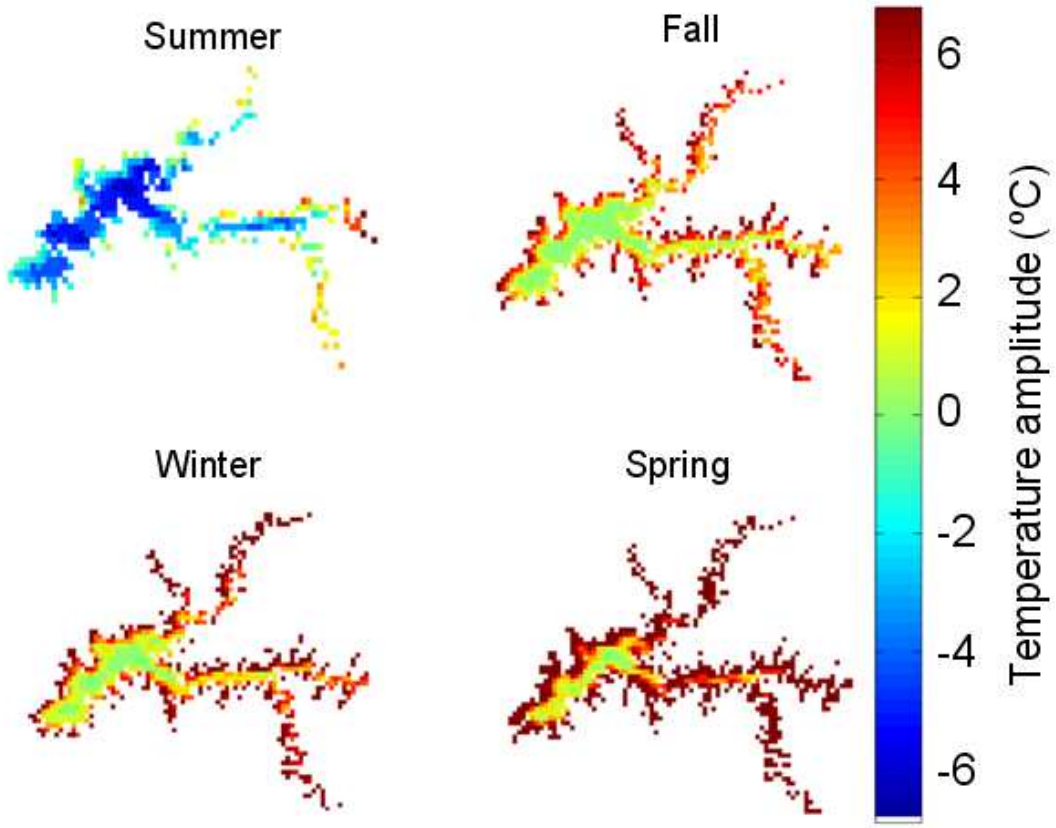

Figure 4: Monthly mean water surface temperature differences between daytime and nighttime over the seasons.

In conclusion, the temperature differences between the border and the central water body of the reservoir are positive from summer to spring. This is due to the low depth of these areas, which is less than 1 m. During spring, the highest positive temperature differences can occur (~6ºC). The nighttime temperatures can be higher than daytime temperatures during summer and fall. However, this is more pronounced in summer than in fall. The energy fluxes were computed to understand this variability observed in the results.

Surface energy budget for daytime and nighttime

The spatially effective surface heat balances are show in Figure 5. For January, February and April the northwest section of the reservoir gains more heat than the southeast section. This is because the preferable wind direction is from southeast to northwest as the wind drives the warm masses into the littoral zone by advection. For March, the southwest heats more than the northeast. During May, the greatest area of the reservoir loses heat, and only a small area in the main body of the reservoir gains heat. From June to July, heat loss dominates the whole reservoir, and the northwest losses are lower than the southeast losses. From August to December, the reservoir heats from the littoral zone to the center of the reservoir; but in October, it presents the greatest heat gradient between the littoral zone and the center of the reservoir.

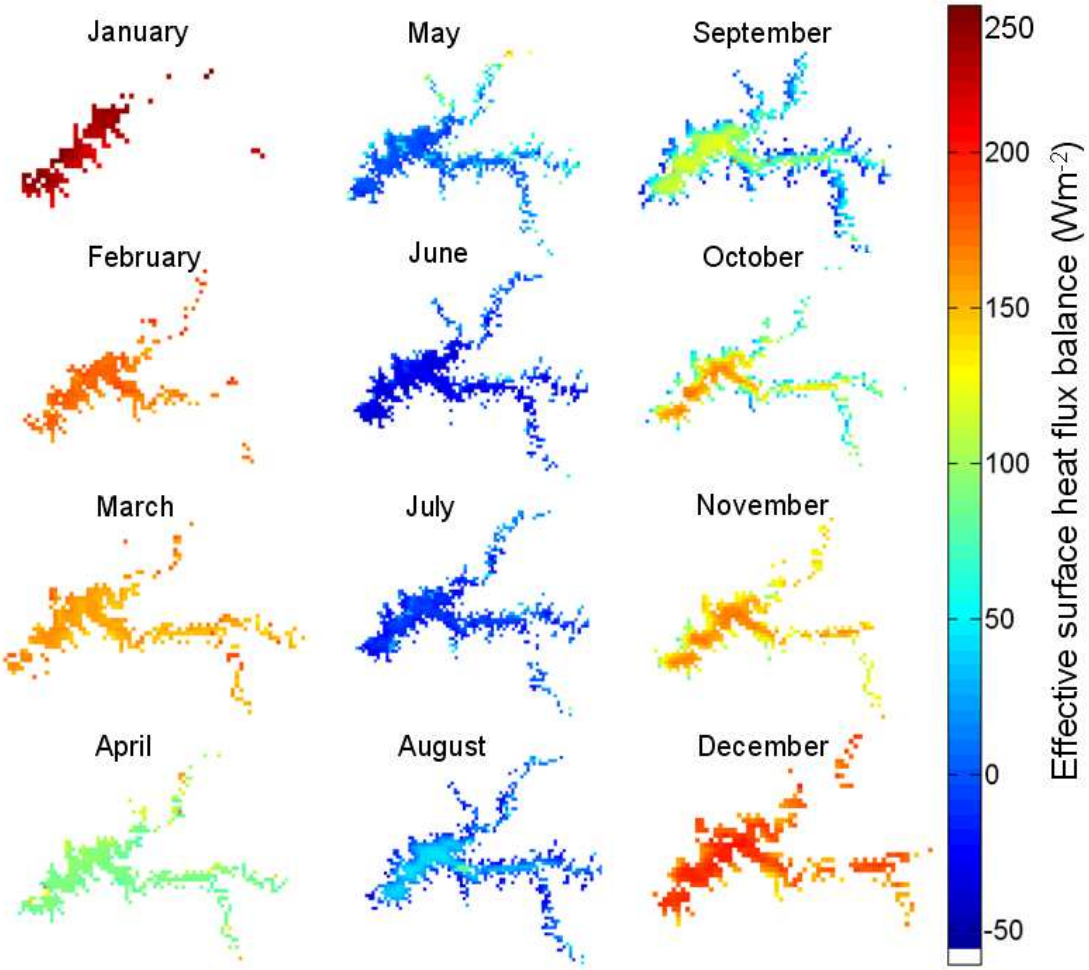

Figure 5: Spatially effective surface heat flux balance (Wm^{-2}) over the Itumbiara reservoir.

CONCLUSIONS

The objective of this study was to map the surface water temperatures and improve understanding of spatial and temporal variations in the Itumbiara hydroelectric reservoir. Our hypothesis of how meteorological and heat fluxes would affect the water surface temperature was developed and tested. The main conclusions are:

During the daytime, the water surface temperature heats from the center to the littoral zone. During nighttime, the processes invert due to the turbulent convection caused by differential cooling. The temperature, for a given heat flux out of the water surface, decreases more rapidly in the shallow water due to the low thermal mass. The seasonal analysis shows that, during summer, the water surface temperature is warmer than during nighttime. The interannual anomalies are higher in January and smaller in June for daytime and nighttime.

The reservoir gained heat from January to May and from August to December. It lost heat from May to August. The period of heat gain was also the period when the reservoir had a high potential to stratify, and during heat loss, it had the potential to mix. A difference exists between the heat balance near the dam and river confluences.

The statistical model shows that, for water surface temperatures measured at daytime, only the incoming shortwave radiation is needed for the model. For nighttime, it needs the longwave radiation, latent heat flux and sensible heat flux. The nighttime water surface temperature is more complex to model than the daytime surface temperature.

REFERENCES

Bonnet MP, Poulin M, Devaux J (2000) Numerical modeling of thermal stratification in a lake reservoir: Methodology and case study. Aquatic Science **62**:105-124.

Crosman ET, Horel JD (2009) MODIS-derived surface temperature of the Great Salt Lake. Remote Sensing of Environment. **113**:73-81.

Fischer HB, List EJ, Koh RCY, Imberger J, Brooks NH (1979) Mixing in inland and coastal waters. Academic Press: California.

Henderson-Sellers B (1986) Calculating the Surface Energy Balance for Lake and Reservoir Modeling: A Review. Reviews of Geophysics. **24**:625-649.

Kimmel BL, Lind OT, Paulson LJ (1990) Reservoir primary production. In: Thorton KW, Kimmel BL, Payne FE (ed.). Reservoir limnology. Ecological Perspectives. John Wiley and Sons. New York.

Lerman A, Imboden D, Gat J (1995) Physics and chemistry of lakes. Springer-Verlag, Berlin.

MacIntyre S, Romero JR, Kling GW (2002) Spatial-temporal variability in surface layer deepening and lateral advection in an embayment of Lake Victoria, East Africa. Limnology and Oceanography. **47**:656-671.

Oesch D, Jaquet J-M, Hauser A, Wunderle S (2005) Lake surface water temperature using advanced very high resolution radiometer and moderate resolution imaging spectroradiometer data: validation and feasibility study. Journal of Geophysical Research, **10(**C12014):1-17.

Oesch D, Jaquet J-M, Klaus R, Schenker P (2008) Multi-scale thermal pattern monitoring of a large lake (Lake Geneva) using a multi-sensor approach. International Journal of Remote Sensing. **29**:5785-5808.

Reinart A, Reinhold M (2008) Mapping surface temperature in large lakes with MODIS data. Remote Sensing of Environment. **112**:603-611.

Schladow SG, Palmarsson SO, Steissberg TE, Hook SJ, Prata FJ (2004) An extraordinary upwelling event in a deep thermally stratified lake. Geophysical Research Letters. **31**:L15504.

Sturman JJ, Oldham CE, Ivey GN (1999) Steady convective exchange flows down slopes. Aquatic Science. **61**:260-278.

Thiemann S, Schiller H (2003). Determination of the bulk temperature from NOAA/AVHRR satellite data in a midlatitude lake. International Journal of Applied Earth Observation and Geoinformation. **4**:339-349.

Wan, Z. (2008). New refinements and validation of the MODIS land-surface temperature/emissivity products. Remote Sensing of Environment. **112**:59-74.

Wells MG, Sherman B (2001) Stratification produced by surface cooling in lakes with significant shallow regions. Limnology and Oceanography. **46**:1747-1759.

Impact of a Hydroelectric Power Station on Water Mixing Processes within a Stratified Lake

C. Lemckert[1]*, Gibbes, B.R.[2], J. Zier[1] and, J. Udy[3]

[1] Griffith School of Engineering, Griffith University, Gold Coast, Queensland, Australia
[2] Centre for Water Studies, School of Civil Engineering, The University of Queensland, Brisbane, Queensland, Australia
[3] Queensland Bulk Water Supply Authority (trading as SEQWater), Brisbane, Queensland, Australia

Corresponding author, e-mail c.lemckert@griffith.edu.au

KEYWORDS
Power station; stratification; jet mixing; reservoir.

EXTENDED ABSTRACT

INTRODUCTION
It is well understood that atmospheric forcing, river inflows, convective currents and water withdrawal play an important role in reservoir dynamics. As such, these processes have and will continue to be well studied to ensure predictive schemes can be developed to enhance management strategies. However, it is becoming increasingly obvious that other processes also play a key role in reservoir mixing and water quality. These processes include groundwater inflows and evaporation that results in differential cooling and biological activity. More recently, it has been observed that hydroelectric power stations that use water supply reservoirs as their discharge and recharge point can also be considered an important reservoir mixing mechanism. In this situation a hydroelectric plant releases its water into a thermally stratified reservoir at a rate exceeding that of normal flood events – resulting in direct water mixing. The release events, whose duration is of O(hours), are therefore dynamically significant and likely to enhance internal wave activity (at least during the initiation of the flow) and related boundary mixing rates.

METHODOLOGY
A detailed field study aimed at quantifying the outflow jet from a hydroelectric power station was conducted on Wivenhoe Dam, Queensland, Australia. Wivenhoe Dam is the largest reservoir and the major water supply in South East Queensland (Gibbes et al, 2009; Gibbes and Grinham, 2010)). The power station releases water into Wivenhoe Dam, through a set of turbines, from an upstream storage (Splityard Creek Dam) during peak load periods when electricity prices are relatively high, thus lowering Splityard Creek and raising Wivenhoe water levels. During off peak periods when electricity is relatively cheap the station pumps water from Wivenhoe into Splityard Creek ready for its next release. As the power station operators do not have a calibrated model for the outflow behaviour of their plant an additional aim of this study was to quantify the flow rates relative to the power generating turbine and water property conditions. Flows exiting the power station were monitored primarily using two transecting ADCPs –one was mounted on a small inflatable raft drawn backwards and forwards across the power station outflow channel close to the power station outlet (initial inflow conditions) while the other was traversed a short distance away in order to quantify dilution rates and obtain a suitable data set for future model validation. Additional bed

mounted ADCPs (with one located near the power station outlet) were also deployed to monitor long term water column changes. The primary data set collected during the study was the result of a controlled release program provided by the power station operators. Inflows varied from 0 (no flow) to 600 m^3/s (maximum flow).

RESULTS AND DISCUSSION

Studies of the inflow revealed that the flows into the reservoir were highly turbulent in nature (Reynolds numbers typically exceeding 1x107) with flow rates encountered typically five times greater than that of a typical flood event.

Figure 1 presents a comparison of the power station outflows against the flow rates measured 50m from the effective outflow point. The data reveals that in this short distance the flow rate increased by 10% - hence significant water entrainment resulting in a dilution of 10% in this short distance.

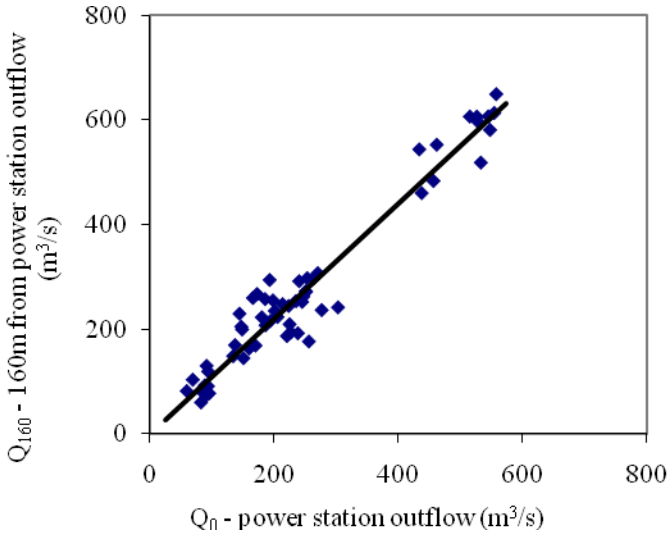

Figure 1. Plot of power station outflow at a distance 160m from the source (Q_{160}) vs power station outflow rate (Q_0). The line of best fit to the data is $Q_{160} = 1.1Q_0$ with R^2=0.94.

The results from the study showed that the power station would normally run at a $Q_0 \sim 250 m^3/s$, for periods up to 4 hours for no more than one inflow event per day. The flows are therefore significant in the mixing behaviour of Wivenhoe Dam and must therefore be included in all future modelling activities. Additionally, it is now evident that the reverse flow case initiates a selective withdrawal process that also requires further investigation as it too may be an important stratification controlling mechanism.

Therefore, power stations can have a significant effect on reservoir dynamics and their presence warrant careful modelling to be undertaken if the reservoir dynamics are to be accurately replicated.

REFERENCES

Gibbes, B. R., Barry M. E., Collecutt, G. R., Lemckert, C. J., Udy, J. and Lockington D. A. (2009) 1Preliminary modelling of hydrodynamics of purified recycled water inputs to Lake Wivenhoe, Proceedings of the 18th World IMACS Congress and MODSIM09 International Congress on Modelling and Simulation, Cairns, Australia, 13–17th July 2009

Gibbes, B. and Grinham, A. (2010) "Application and testing of a three-dimensional hydrodynamic model of Lake Wivenhoe using the ELCOM modelling platform" A research report prepared by the University of Queensland's Centre for Water Studies for Seqwater, March 2010, 45 pp.

Modeling circulation in Lake Huron

Dmitry Beletsky[1*], David Schwab[2], Eric Anderson[1] and Gregory Lang[2]

[1] University of Michigan, Ann Arbor, MI 48108, USA
[2] NOAA Great lakes Environmental Research Laboratory, Ann Arbor, MI 48108, USA

[*]Corresponding author, e-mail dima.beletsky@noaa.gov

KEYWORDS
Limnology; hydrodynamics; circulation; Lake Huron.

EXTENDED ABSTRACT

Saginaw Bay is a long (about 100km by 50km) and shallow bay in the south-east corner of Lake Huron (Figure 1). Like many coastal areas around the world, Saginaw Bay has been subjected to numerous stressors including toxic contaminants, nutrients, sediments, overfishing, and invasive species. The combined effect of these stressors has compromised the health of Saginaw Bay and resulted in the loss of many ecosystem features and services that people value. Several on-going projects dealing with the water quality of Saginaw Bay require detailed information on circulation in the Bay (and fine-scale circulation near the beaches on the inner bay) and water exchange with Lake Huron.

We employ the Princeton Ocean Model (Blumberg and Mellor 1987) for calculation of lake-scale hydrodynamic circulation. Over the past 10 years, the Princeton hydrodynamic model has been adapted for use in the Great Lakes and has been successfully applied both for long-term climatological simulations and for use in a real-time coastal forecasting system (Schwab and Bedford 1994; Beletsky and Schwab, 2001; Beletsky et al., 2003). The model is based on the three-dimensional, nonlinear Navier-Stokes equations. It employs a terrain-following vertical coordinate (sigma coordinate) to provide high vertical resolution even in shallow areas. For lake-scale simulations, meteorological data from the NWS surface observing stations and mid-lake weather buoys are used to synthesize overwater momentum flux and heat flux fields to drive the model to calculate circulation and thermal structure lake-wide and in Saginaw Bay in 1993, 1995, 1996 and 2008 on a 2 km grid.

Lake-wide model results show significant interannual variability in circulation patterns and water exchange between the inner bay and the outer bay. In general, waters of Lake Huron do not penetrate deep into Saginaw Bay due to peculiarities of local bathymetry. In particular, the presence of an anticyclonic gyre near the entrance of Saginaw Bay in summer significantly impacts water exchange between the lake and the outer bay. The size of this gyre varied between years, indicating potential importance of this phenomenon for interannual variability of chemical and biological processes in Saginaw Bay.

Nested grid model was developed for the inner bay on a 200 m grid to support research on forecasting beach closures due to contaminated river plumes. Results from the whole-lake simulations are used to specify the open water boundary conditions for the nested grid simulations. Model results are tested with current observations at several near-shore locations. Additional model validation is done with satellite imagery of Saginaw River plume. The model became operational in summer 2009 as a part of the Great Lakes Forecasting System.

Figure 1. Nested grid model of the inner bay of Saginaw Bay, Lake Huron.

REFERENCES

Beletsky,D., D.J. Schwab, P.J. Roebber, M.J. McCormick, G. S. Miller, and J.H. Saylor. (2003). Modeling wind-driven circulation during the March 1998 sediment resuspension event in Lake Michigan. *J.Geophys. Res*., 108(C2), 3038

Beletsky, D., and D.J. Schwab. (2001). Modeling circulation and thermal structure in Lake Michigan: Annual cycle and interannual variability. *J.Geophys. Res., 106, 19745-19771*.

Blumberg, A.F. and G.L. Mellor. (1987). A description of a three-dimensional coastal ocean circulation model. Three dimensional Coastal Ocean Models, Coastal and Estuarine Sciences, 5, N.S. Heaps [ed.] Amer. Geophys. Union, Washigton, D.C., pp 1-16.

Schwab, D.J. and K.W. Bedford. (1994). Initial implementation of the Great Lakes Forecasting System: a real-time system for predicting lake circulation and thermal structure. Water Poll. Res, J. Canada, 29(2/3), 203-220.

Process oriented modeling of Lake Ontario hydrodynamics

Leon Boegman[1]* and Yerubandi R. Rao[2]

[1] *Department of Civil Engineering, Queen's University, Kingston, ON, Canada*
[2] *National Water Research Institute, Environment Canada, Burlington, ON Canada*

**Corresponding author, e-mail leon.boegman@civil.queensu.ca*

KEYWORDS
Internal waves, Lake hydrodynamics, Lake Ontario, Reynolds-averaged modelling

EXTENDED ABSTRACT

INTRODUCTION
For small and medium sized lakes with a characteristic lengthscale (L) less than or equal to the Rossby radius (R), hydrostatic Reynolds averaged Navier-Stokes equation (RANSE) models have been shown to be capable of resolving the fundamental processes at the basin-scale, including surface seiches and internal Kelvin and Poincaré waves (e.g. Hodges, et al. 2000). However, for large lakes (e.g. the Great Lakes), where $L >> R$, these models are typically calibrated against temperature and current observations (e.g. León et al. 2005; Schwab & Bedford 1994; Huang et al. 2010). The ability of these models to simulate the fundamental processes in large lakes has not been investigated.

METHODS
A three-dimensional hydrostatic Reynolds-averaged Navier-Stokes equation model (ELCOM; Hodges, et al. 2000) has been applied to simulate the ice-free hydrodynamics of Lake Ontario during 2006. ELCOM solves the unsteady RANSE on a 2 km x 2 km horizontal z-level grid. Vertical grid spacing varies from 1 m near the surface to 16 m near the bed. The model is forced with 10-min meteorological data recorded by Environment Canada at stations 1263, 586 and 403 (Fig. 1).

RESULTS
The modelled water levels at stations 1266 and 1263 were compared to nearby water level observations from gauges. The seasonal trends were well modelled when the streamflow data was increased by 20%. Spectral energy plots of the water levels show statistically significant peaks in the model result and field data at 12-hrs and at the periods of the first (5.06 hr) and third (2.32 hr) longitudinal surface seiche modes.

Modelled temperature profiles were compared to observed temperatures at stations 403, 586 and 1266. The evolution of the temperature profile is well modelled (e.g. Fig. 2a,b), including the formation of a seasonal thermocline at a depth of ~ 15 m, surface layer mixing events (near days 180 and 200) and large and small scale oscillatory motions associated with baroclinic (internal) waves. Higher-frequency Poincaré wave oscillations are evident in the observations and model results along the thermocline (Fig. 2c,d). The dominant spectral peak in both the modelled and field data at station 1266 has a period of 16.38 hrs and is identified as an internal Poincaré mode, just below the inertial frequency, f =17.35 hrs. Topographic and internal Kelvin waves are simulated, but are under-resolved (not shown). We expect that these motions can be captured with an R/5 or ~1 km grid (Schwab & Beletsky 1998).

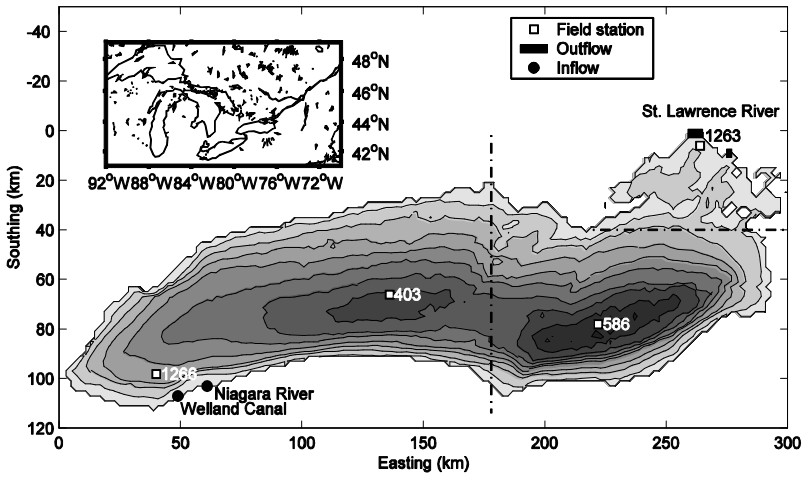

Figure 1. Bathymetric map of Lake Ontario showing the locations of the field stations, inflows and outflows. Distinct meteorological data was applied in each of the three regions delineated by the dash-dot lines as recorded at stations 1263, 586 and 403. The depth contour isobaths interval is 25 m.

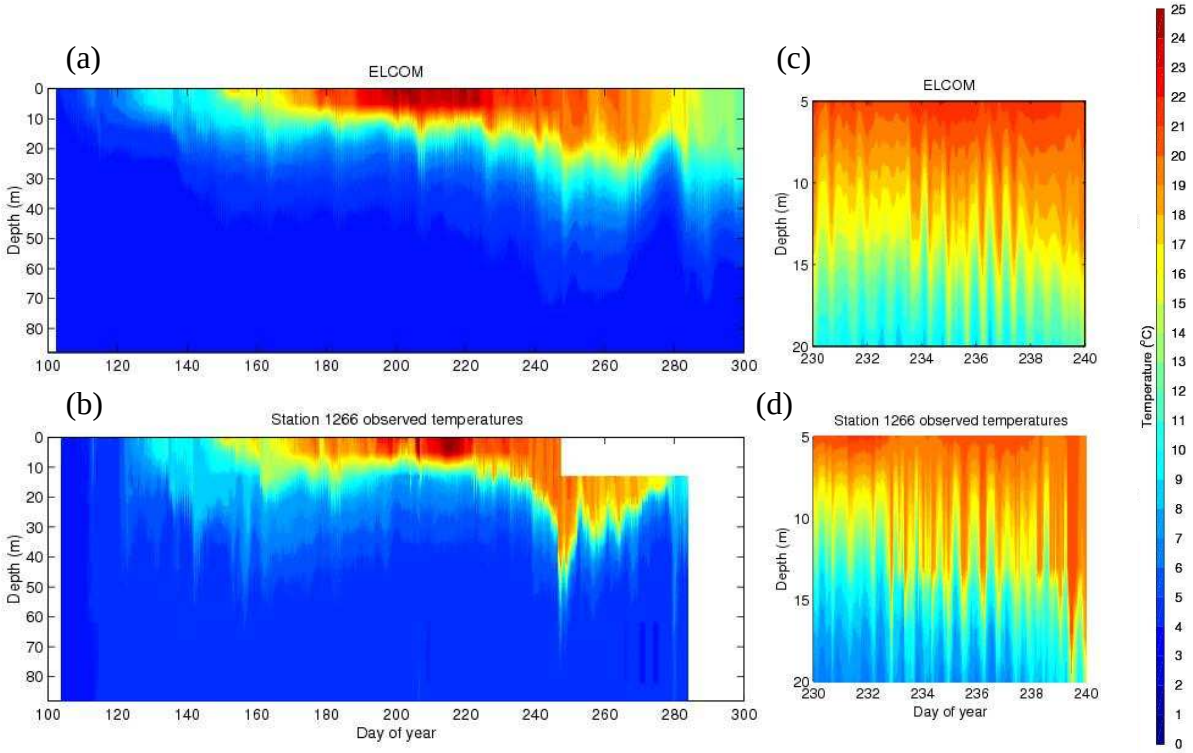

Figure 2. Modelled (a) and observed (b) temperature contours at station 1266. Detail showing modelled (c) and observed (d) Poincaré wave oscillation.

REFERENCES

Hodges BR, Imberger J, Saggio A, Winters KB. 2000. Modeling basin-scale internal waves in a stratified lake. *Limnol. Oceanogr*. 45: 1603-20.

Huang, A., Rao, YR, Lu, Y. 2010. Evaluation of a 3-D hydrodynamic model and atmospheric forecast forcing using observations in Lake Ontario. *J. Geophys. Res*. doi:10.1029/2009JC005601

León LF, Imberger J, Smith REH, Hecky RE, Lam DC, Schertzer WM. 2005. Modeling as a tool for nutrient management in Lake Erie: A hydrodynamics study. *J. Great Lakes Res.* 31(Suppl. 2) : 309-18.

Schwab DJ, Bedford KW. 1994. Initial implementation of the great lakes forecasting system: A real-time system for predicting lake circulation and thermal structure. *Water Poll. Res. J. Can*. 203-20

Schwab DJ, Beletsky D. 1998. Propagation of Kelvin waves along irregular coastlines in finite-difference models. *Adv. Water Res*. 22: 239-45.

Density of water from partial molal volumes

Bertram Boehrer[1], Peter Herzsprung[1], Martin Schultze[1] and Frank. J. Millero[2]

[1] *Helmholtz-Centre for Environmental Research - UFZ, Brueckstrasse 3a, 39114 Magdeburg, Germany*
[2] *Rosenstiel School of Marine and Atmospheric Science, Miami, Fl 33149, U.S.A.*

**Corresponding author, e-mail Bertram.Boehrer@ufz.de*

ABSTRACT
Chemical transformations must be reflected in the density function to simulate chemically stratified lakes. Partial molal volumes are used to calculate density from the chemical composition of lake water. A second order approximation for temperature dependence and ionic strength dependence is proposed for calculating density. The approach is assessed for seawater composition. In most cases, a very good representation of density based on the actual chemical composition of the lake water is achieved. This density function can easily be implemented into geochemical stratification models. This facilitates the numerical tackling of pressing questions, such as meromixis or double diffusive features or changes due to climate variation. This new approach is put into the context of other density approximations.

KEYWORDS
Density, molal volumes, physical limnology

EXTENDED ABSTRACT

Potential density is the central quantity to evaluate stability of a stratification. This stratification controls the vertical circulation of lake waters and the propagation of internal waves. Small differences control the processes and high accuracy approaches are needed for many applications. Density of water can be measured at a relative accuracy of about $2 \cdot 10^{-6}$ in the densitometer DSA 5000 manufactured by PAAR (Graz, Austria). This is about the accuracy that suffices for most limnological applications. There is no direct density measurement that supplies a similarly accurate measurement in the field.

Not for all purposes, samples can be taken to the laboratory. Alternative methods had to be developed to yield density values from easier to measure quantities. Usually temperature and electrical conductivity can be used to evaluate density on an indirect path. The currently used approaches can be categorized in four groups. Most of the numerical approaches can be read in Boehrer and Schultze (2008):

FRESH WATER EQUATION

Bührer and Ambühl (1975) proposed a third order polynomial for density of water of vanishing electrical conductivity. A conductivity contribution was added to density, depending linearly on electrical conductivity. This formula is in use for many alpine lakes, in some cases with small alterations. Based on such a formula, density profiles can be calculated based on easy to measure quantities such a temperature and electrical conductivity.

Similarly Chen and Millero (1986) proposed a formula, where salinity takes the place of electrical conductivity. Salinity is evaluated according to ocean approaches (Foffonoff and Millard, 1983) with a correction for low salinity limnic waters. This equation is proposed for any limnic water of salinity below 0.6.

OCEAN WATER

Lakes or estuaries connected to the sea, but also some lakes connected to salt deposits in the ground can resemble the chemical conditions of ocean water well enough, to use the ocean formula given by Fofonoff and Millard (1983). Salinity is based on a measurement of electrical conductivity and calculated over several intermediate steps. Based on this salinity, density is evaluated as a function of (potential) temperature and salinity. This formula is in common use, especially if any more detailed information on the chemical conditions in the limnic waters is missing. The reference of ocean waters is widely known also amongst limnologists. Strictly speaking, this formula is only valid for salinities between 2 and 42. For the complete formula see e.g. Boehrer and Schultze (2008).

LAKE SPECIFIC APPROACH

If a formula basing density on temperature and electrical conductivity is required for a certain lake, the most accurate approach is probably to collect two water samples from the lake. One of the samples should be at the high end of the electrical conductivity range encoutered in the lake and the second sample at the low end. (If electrical conductivity differences are small in the lake, the low conductivity sample may be produced by diluting the first sample with deionized water.)

The density of both samples is measured over the entire range of interesting temperatures. A numerical regression of 4^{th} order usually suffices to approach the measurements within the accuracy of the single density measurements. The density differences between both regressions are contributed to the different electrical conductivity of the samples. For a closer description of the approach, see Boehrer et al. (2009) dealing with the iron meromicitic Waldsee. Compared to above mentioned freshwater approaches, this lake specific approach can be applied to lakes of chemical gradients, as the reference of vanishing electrical conductivity is not used. This approach only uses the implicit assumption that the entire lake water lies along the mixing line between the two samples and density changes linearly with electrical conductivity.

DENSITY BASED ON MOLAL VOLUMES

This approach starts with the density temperature correlation of pure water. The contribution of all dissolved substances will be added in later steps. Such an approach is required, when in geochemical models the concentrations of dissolved substances are known and density needs to be based on the actual concentration of substances. Schmid (2004) has used such an approach when modelling the stability of the stratification, while dissolved gases, which contributed essentially to density, were removed from the deep waters of African lakes. Schmid (2004) included separate terms for methane and carbon dioxide.

In general, substances add their mass to a solution when being dissolved in water. However, also the volume of the solution changes. This volume change has been evaluated empirically. Coefficients of most interesting substances are available. Also the temperature dependence and dependence on concentration of dissolved substances are known (see Boehrer et al. 2010). Based on these coefficients also the volume of a sample of water with given solutes can be evaluated. Dividing mass of a solution by volume yields density. Hence the density change due to a chemical reaction can be simulated.

Boehrer et al. (2010) tested this approach quantitatively for ocean composition and concluded that the approach delivers very good results for any concentration over the temperature range most interesting for limnologists. The approach is straight forward and can be included in geochemical lake stratification models (Moreira et al. 2009).

REFERENCES

Boehrer, B.; Schultze, M. 2008. Stratification of lakes. Rev. Geophys. **46**, RG2005, DOI 10.1029/2006RG000210.

Boehrer, B.; Dietz, S.; von Rohden, C.; Kiwel, U.; Jöhnk, K.D.; Naujoks, S.; Ilmberger, J.; Lessmann, D. 2009a. Double diffusive deep water circulation in an iron-meromictic lake, Geochem. Geophys. Geosyst., **10**, Q06006, DOI 10.1029/2009GC002389.

Boehrer B., Herzsprung P., Schultze M., Millero F.J. (2010) Calculating density of water in geochemical lake stratification models (under revision)

Bührer, H., und H. Ambühl (1975), Die Einleitung von gereinigtem Abwasser in Seen, *Schweiz. Z. Hydrol. 37*(2), 347–368, doi:10.1007/BF02503411.

Chen, C.-T.A.; Millero F.J. 1986. Precise thermodynamic properties for natural waters covering only the limnological range. Limnol. Oceanogr. **31**, 657-662.

Fofonoff, N.P.; Millard, R.C. jr. 1983. Algorithms for commutation of fundamental properties of seawater, UNESCO technical papers in marine science 44.

Moreira S., Boehrer B., Schultze M., Samper J., (2009) A coupled hydrodynamic-geochemical model of meromictic lake Waldsee, Abstracts of the International Mine Water Conference, Oct. 2009, Pretoria, South Africa, ISBN 978-0-9802623-5-3, p. 892-897

Schmid M., Lorke A., Dinkel C., Tanyileke G., Wüest A. (2004) Double-diffusive convection in Lake Nyos, Cameroon. Deep-Sea Research Part I 51 (8), 1097-1111.

Combined use of the conservative tracers ^{18}O and SF_6 to detect groundwater inflow in the monimolimnion of a meromictic mining lake

Johann Ilmberger and Christoph von Rohden

Institute of Environmental Physics, University of Heidelberg, Im Neuenheimer Feld 229, D-69120 Heidelberg, Germany

*Corresponding author, e-mail Johann.Ilmberger@iup.uni-heidelberg.de

KEYWORDS
Groundwater-lake interaction, meromixis, tracer

EXTENDED ABSTRACT

INTRODUCTION
Meromictic lakes are characterised by an incomplete seasonal mixing of the hypolimnion, resulting in a closed-off monimolimnion. This (anoxic) layer is enriched in dissolved substances forming a chemocline, which separates the layers. The knowledge of any monimolimnic groundwater exchange is essential for the understanding of the geochemical reactions in the monimolimnion and might play an important role for its continuance.

METHODS
In order to detect groundwater exchange the measurement of one conservative tracer is normally not sufficient, as mostly the vertical transport coefficients in the monimolimnion are not known. However a combination of two conservative tracers can be used to eliminate the vertical transport.

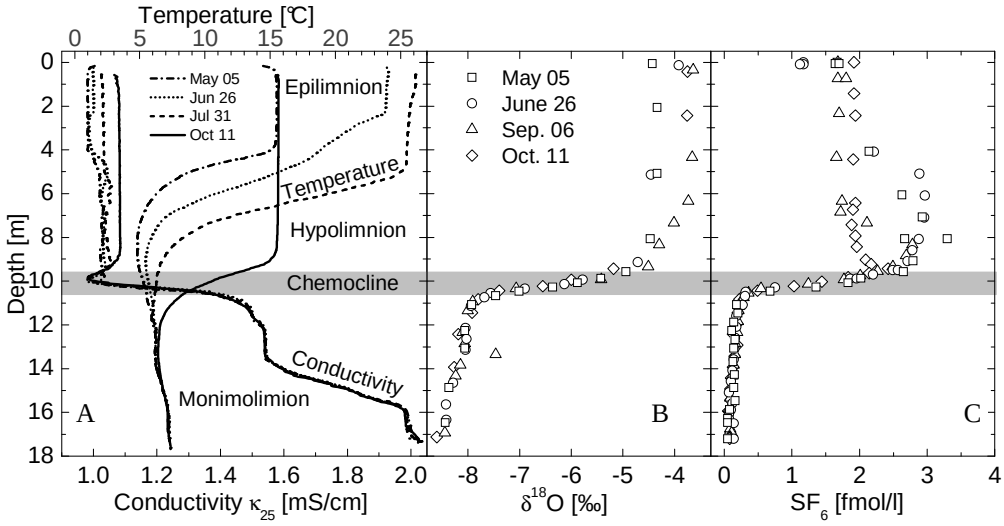

Figure 1: Lake Moritzteich, measured temperature and conductivity (A), $\delta^{18}O$ (B) and SF_6 (C) at different dates of 2006.

RESULTS AND DISCUSSION
We assume steady state, i.e. the tracer concentrations profiles do not change in time, which we use as first order approach for the measurements below the chemocline (Fig.1). This

assumption implies: steady vertical flux at the lake's bottom and at the chemocline and moreover (if present) a steady, probably depth depended, groundwater flushing.
Using Fick's first law and the mass balances for two tracers depth dependent, we end up with an equation that shows, if the correlation of two conservative tracers deviates from a straight line, then there has to be an exchange with groundwater (vonRohden et al., 2010).
In the case of Moritzteich we can clearly distinguish two regions, where, within the errors of the measurements, we have straight lines (i.e. no groundwater flushing) with different slopes (Fig.2). So we can infer a groundwater-lake exchange where c_{SF6} is *~0.3 fMol/l* and $\delta^{18}O \sim -7.8$ ‰. This corresponds to a depth of about *11 m* extending over *~2.2m* (Fig.1).

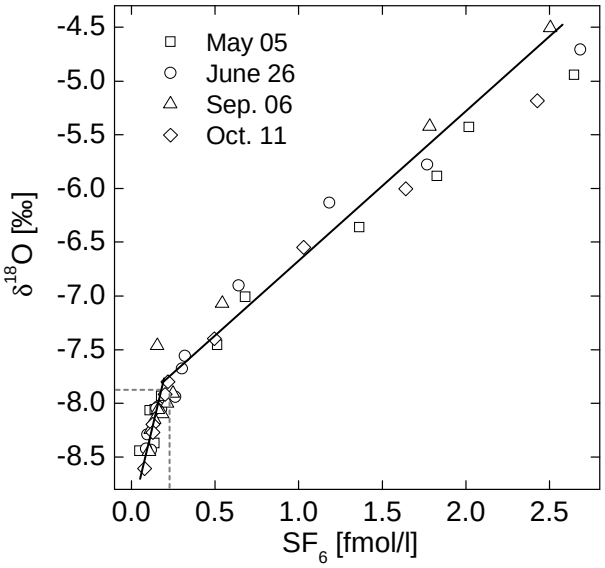

Figure 2: The change in slope of correlation of $\delta^{18}O$ and SF_6 marks the region of groundwater inflow

To quantify the exchange rate the tracer concentrations of the inflowing groundwater and the vertical flux at one single depth are required. In the case of Lake Moritzteich, we use as lower boundary the flux across the chemocline being close to molecular transport. The tracer concentrations of the inflowing groundwater are not known. In order to estimate the limits of the exchange rates, we calculated two scenarios: (1) SF_6-concentration of the inflow as *0* and (2) *0.2 fMol/l*. The first assumption implies old, SF_6-free groundwater entering the lake, whereas the second assumes a *~10%* addition of recent water.
The estimation of the groundwater exchange rate is *19* and *57 m^3/d* or *6* and *19 %* per year of the involved layer of *2.2 m*. The associated groundwater $\delta^{18}O$ values are rather high (*−8.5* and *−8.1 ‰*), but might be explained by the addition of water, which has undergone some evaporative modification to the groundwater (*−9.1 ‰*), entering the lake.
Applying the same procedure to the electrical conductivity, a sink can be identified in the upper chemocline and estimated to *24 µS/cm* per year, which presumably is due to precipitation of iron hydroxides.

CONCLUSIONS

From the change in slope of the correlation of two conservative tracers we can identify a groundwater inflow (if the inflow concentrations are not "binary mixed").
Adopting the general assumptions of steady state and close to molecular transport across the chemocline scenarios can be used to calculate the limits of the groundwater exchange. Correlating a non-conservative tracer to a conservative one (e.g. SF_6), we can identify and quantify a source or sink of the non-conservative quantity.

ACKNOWLEDGEMENT

This research was granted by the Deutsche Forschungsgemeinschaft (DFG)

REFERENCES

von Rohden, C., A. Seebach, K. Knöller, and J. Ilmberger. 2010: Assessing groundwater exchange in a meromictic lake using conservative tracers. Submitted.

Factors influencing the currents over a shallow bank in the Gulf of Finland

M.-J. Lilover*, J. Pavelson and T. Kõuts

Marine Systems Institute, Tallinn University of Technology, Akadeemia tee 21, 12618 Tallinn, Estonia

**Corresponding author, e-mail madis@phys.sea.ee*

KEYWORDS
Seiches; sub-surface currents; topographic forcing.

EXTENDED ABSTRACT

The Gulf of Finland is an elongated estuarine-like sub-basin of the Baltic Sea with a complicated dynamic activity. The main preconditions for the development of dynamic processes of different scale are the vigorous coastline and bottom topography of the gulf, the variable wind field over the gulf promoted by the mostly eastward moving atmospheric cyclones and a large freshwater inflow of the river Neva at the eastern end of the gulf. The circulation pattern of the gulf as well as the currents induced by different meso-scale processes have been intensively studied in the last decade by numerical models and also by acoustic current meter data analysis. In the present study we focus to the response of currents over the shallow Naissaar Bank to varying winds. In the Gulf of Finland the varying winds were found to give rise to considerable variations of wind-driven currents (Alenius *et al.*, 1998, Gästgifvars *et al.*, 2006) and to cause the upwelling/downwelling events with the related jets (Talpsepp *et al.*, 1994, Laanemets *et al.*, 2005). Moreover, the inertial oscillations and seiches with the accompanied currents are usually generated after the passage of wind fronts (Alenius *et al.*, 1998 and references therein). Still, there exists a deficit of experimental data about the bottom topography influence on currents. Considering our observation site on one of the banks at the entrance to the Tallinn bay (Fig. 1), the resultant near-surface currents will presumably be rather complicated. In the study, in order to explain observations, we consider the following constituents of the observed current: the wind-generated drift currents, the barotropic currents due to the wind-induced sea level gradients and the currents initiated by the passage of wind fronts (seiches, inertial oscillations). We determine the most energetic submesoscale harmonic oscillations of currents by means of spectral analysis. The residual current vector is formed by removal of these oscillations from the original series. Finally, the correlation between the wind and current residual vectors as well as the effect of the local bottom topography on the residual current are estimated.

Our study is based on the time series of current velocity measurement performed within 5 weeks on the Naissaar Bank in the northern part of the Tallinn Bay, Gulf of Finland in late autumn of 2008 using a bottom-mounted ADCP deployed at 8 m depth. The observation period was characterized by a variable strong mainly southerly wind with the speed exceeding 10 m s^{-1} during 60% of the whole period. The seiches with the periods of 31, 24, 19.5, 16 and 11 h and the maximum current magnitudes of 3–8 cm s^{-1} were provoked after passing the wind fronts. The contribution of inertial oscillations and diurnal tidal currents were less

important. Thus, altogether the variance of different oscillating currents formed 25% of the total variance leaving 75% to the low-frequency currents (with time scale >36 h).The low-frequency current correlation with the wind was 0.69 for the whole series and much higher (up to 0.90) within shorter steady wind periods. At the wind speeds less than about 10 m s^{-1} the current veered to the right from wind ~35º (Fig. 2) without any significant veering direction in vertical. During weaker decaying winds a counterclockwise veering was observed. The latter behavior deviating from the Ekman drift current was most likely caused by a barotropic geostrophic flow due to the sea-level gradient along the Gulf of Finland. In addition, the currents revealed two dominant directions, which were interpreted by the influence of the bottom topography. Firstly, during strong winds the flow was steered along the isobaths of the bank. Secondly, at times, in case of moderate winds and large sea level gradients along the gulf, the flow was directed along the 'channel' located to the north from our measurement site.

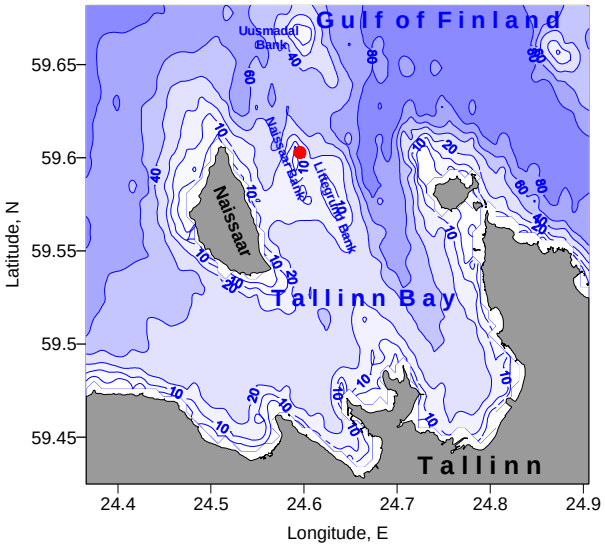

Figure 1. Map of the Tallinn Bay with bathymetry. The location of bottom-mounted ADCP is indicated by the dot.

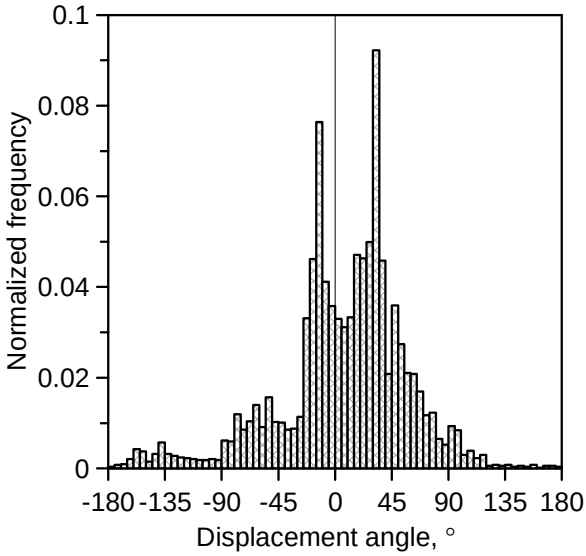

Figure 2. Normalized histogram of displacement angle between wind and current vectors.

REFERENCES

Alenius P., Myrberg K. and Nekrassov A. (1998). Physical oceanography of the Gulf of Finland: a review. *Boreal Env. Res.* **3**: 97-125.

Gästgifvars M., Lauri H., Sarkanen A., Myrberg K., Andrejev O. and Ambjörn C. (2006). Modelling surface drifting of buoys during a rapidly-moving weather front in the Gulf of Finland, Baltic Sea. *Estuarine Coast. Shelf Sci.* **70**: 567-576.

Laanemets J., Pavelson J., Lips U. and Kononen K. (2005). Downwelling related mesoscale motions at the entrance to the Gulf of Finland: observations and diagnosis. *Oceanol. Hydrobiol. Studies* **34**: 15-36.

Talpsepp L., Nõges T., Raid T. & Kõuts T. 1994. Hydrophysical and hydrobiological processes in the Gulf of Finland in summer 1987: characterization and relationship. *Cont. Shelf Res.* **14**: 749-763.

Wind-driven ocean upper layer model

A. Toompuu* and J. Heinloo

Marine Systems Institute, Tallinn University of Technology, Akadeemia tee 21, 12618 Tallinn, Estonia

**Corresponding author, e-mail alex@phys.sea.ee*

KEYWORDS
Ekman layer; modelling; turbulence.

EXTENDED ABSTRACT

The observed current dynamics in the wind-driven upper layer of the ocean deviates from the classical Ekman theory. So, the surface current veering from the wind stress direction differs in general from the value predicted by the Ekman theory and the currents' turn (clockwise in the northern hemisphere) with depth is often smaller than in the Ekman theory (Price et al., 1987). The deviations have been so far explained by complementing the Ekman theory with either the logarithmic boundary layer model, with the surface-wave-induced velocity bias, with the depth-varying eddy viscosity or with the ocean density stratification (Price and Sundermeyer, 1999). Our hypothesis is that the observed deviations of the surface current from the Ekman theory can be explained by the prevailing orientation of large-scale eddy rotation in the ocean upper layer supported by the velocity shear. The suggested model is based on the relevant turbulence theory (Heinloo, 2004) treating the turbulence as divided into the orientated (large-scale) and non-orientated (small-scale) constituents. The dominant effect is attributed to the orientated turbulence constituent interacting immediately with the average flow.

Let (x,y,z) be the wind-relative Cartesian coordinate system with the coordinate z directed downward, z=0 at the ocean surface, and the coordinate x directed down the wind. The flow is considered forced by the constant wind stress $\boldsymbol{\tau} = (-\tau,0,0)$, τ>0. The coordinate system is assumed right-hand in the Northern Hemisphere and left-hand in the Southern Hemisphere. Assuming the flow velocity $\tilde{u}=u_x+iu_y$, where i is the imaginary unit, depending on z only, the solution of equations of the applied theory for the specified flow in the non-stratified ocean has the form

$$\tilde{u} = \tilde{u}_1(0)\exp(-\frac{z}{h_{11}})\exp(-i\frac{z}{h_{12}}) + \tilde{u}_2(0)\exp(-\frac{z}{h_{21}})\exp(i\frac{z}{h_{22}}), \qquad (1)$$

in which

$$\tilde{u}_1(0) = \frac{\tau}{\mu_s}\frac{-\lambda_1 + B\lambda_2\exp(i\pi/4)}{\lambda_1^2 - \lambda_2^2} \quad \text{and} \quad \tilde{u}_2(0) = \frac{\tau}{\mu_s}\frac{\lambda_2 - B\lambda_1\exp(i\pi/4)}{\lambda_1^2 - \lambda_2^2}. \qquad (2)$$

In (1) and (2): $\lambda_1 = -h_{11}^{-1} - ih_{12}^{-1}$ and $\lambda_2 = -h_{21}^{-1} + ih_{22}^{-1}$, where the depth scales h_{11}, h_{12}, h_{21} and h_{22} are determined by the coefficients characterizing the medium physical properties (Heinloo 2004), while h_{21}>h_{11}>0, h_{21}>h_{22}>0, h_{12}>h_{11}>0 and $h_{12}h_{22} + h_{11}h_{21} = h_{12}h_{21} - h_{11}h_{22}$;

$B>0$ and $\mu_s>0$ are determined by the medium physical parameters and by the boundary condition of the average angular velocity of the eddy rotation at the ocean surface. The solution (1) includes the observed deviations of the velocity vertical distribution from the velocity predicted by the classical Ekman solution, following from (1) for $\tilde{u}_1(0)=0$, $h_{21}=h_{22}=\ell_E$, where ℓ_E is the Ekman depth scale, and $\tilde{u}_2(0)=|\tilde{u}(0)|\exp(i\pi/4)$.

In Fig.1 the solution (1) is compared with data on the flow velocity relative to the reference level at z=98 m measured in the Drake Passage, Southern Ocean adopted from (Lenn and Chereskin, 2009) and with the corresponding velocity distributions according to the Ekman solution. It can be seen in Fig.1 that the depth of the Ekman layer following from the suggested model and from the Ekman solution exceeds considerably the depth of the applied reference level of 98 m resulting in different estimates of the velocity *e*-folding depth. In particular, the stated in (Lenn and Chereskin, 2009) difference of 2-3 times between the velocity e-folding scale and the rotation scale (see also (Price *et al*., 1987; Schudlich and Price, 1998; Price and Sundermeyer, 1999)) would not show up for the reference depth compatible with the theoretical vertical distribution of velocity.

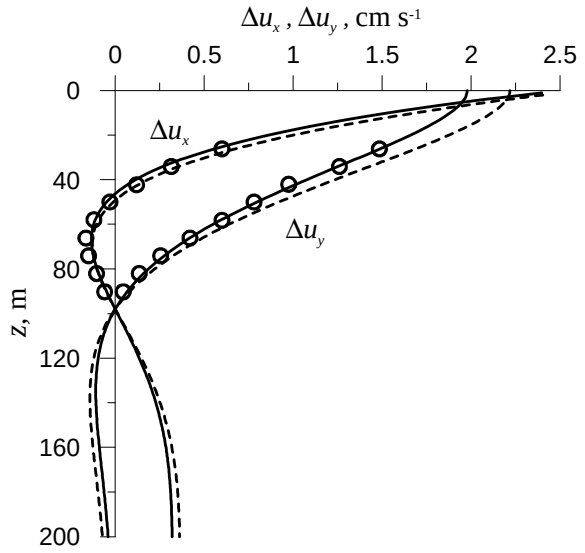

Figure 1. The depth-dependence of velocity components $\Delta u_x=\mathrm{Re}\Delta\tilde{u}$ and $\Delta u_y=\mathrm{Im}\Delta\tilde{u}$, where $\Delta\tilde{u}=\tilde{u}-\tilde{U}$ in which $\tilde{U}$ is the velocity at the reference level z=98 m, calculated according to the suggested model for B=1.7, h_{11}=14.0 m, h_{21}=44.2 m, h_{22}=43.6 m, $\tau\mu_s^{-1}$=0.115 s^{-1} (solid curves) and according to the Ekman model for the Ekman scale h_E=44 m, $|\tilde{u}(0)|$=3.2 cm s^{-1} (dashed curves) compared with data (circles) adopted from (Lenn and Chereskin 2009).

REFERENCES

Heinloo J. (2004). The formulation of turbulence mechanics. *Phys. Rev E*, **69**, paper 056317.

Lenn Y.-D. and Chereskin T.K. (2009). Observations of Ekman Currents in the Southern Ocean. *J. Phys. Oceanogr.*, **39** (3), 768-779.

Price J.F., Weller R.A. and Schudlich R.R. (1987). Wind-driven ocean currents and Ekman transport. *Science*, **238** (4833), 1534-1538.

Price J.F. and Sundermeyer M.A. (1999). Stratified Ekman layers. *J. Geophys. Res*., **104** (C9), 20467-20494.

Schudlich R.R. and Price J.F. (1998). Observations of seasonal variation in the Ekman layer. *J. Phys. Oceanogr*., **28** (6), 1187-1204.

Can we simulate the hydrodynamics of the European Shelf Sea by using a shallow water model?

Adolf Stips*, Elisa Garcia-Gorriz, Svetla Miladinova, Rodrigo Perez

European Commission – DG Joint Research Centre, Institute for Environment and Sustainability, Global Environment Monitoring Unit, Via E. Fermi 1 (TP 272), I-21020 Ispra (VA), Italy

*Corresponding author, e-mail adolf.stips@jrc.ec.europa.eu

ABSTRACT

The European larger Shelf Sea including the North Sea, Irish Sea, Gulf of Biscay and large parts of the Mediterranean Sea was simulated using the 3D hydrodynamical model GETM (General Estuarine Transport Model see http://getm.eu). The turbulence model included is the GOTM model (General Ocean Turbulence Model see http://www.gotm.net). Typical runs were covering the time period from 1985 to 2008, but the period of main interest was from 1998 to 2008. The model was run on spherical grids with different horizontal resolutions the results presented here are from a medium fine resolution setup of 5'x5' (1/12 degree). The area covered extends roughly from 20° West to 10° East and from 30° North to 61° North.

General vertical coordinates using 25 layers were applied. The meteorological forcing was derived from bulk formulae using six-hourly values on a grid from ECMWF interim re-analysis data. Initial and open boundary conditions were derived from the World Ocean Atlas (WOA2005) data. Climatological river runoff from the major rivers in the region of interest is considered in the simulations. The tidal forcing at the open boundaries towards the Atlantic Ocean was constructed from 13 partial tides from the TOPEX-POSEIDON data set. Observed Sea Surface Temperature (SST) data were taken from the NOAA/NASA Ocean Pathfinder satellite, see http://podaac.jpl.nasa.gov/sst.
Results are still preliminary, but it was possible to reproduce the basic circulation patters in the European Shelf Sea in sufficient detail. The prescribed *conditions* at the open boundaries are very critical for the quality of the simulations.

The ecodynamics of Lake Myvatn

A. Einarsson*

Myvatn Research Station, IS-660 Myvatn, Iceland and University of Iceland, Sturlugata 7, IS-101 Reykjavik, Iceland.

**Corresponding author, e-mail arnie@hi.is*

KEYWORDS
Population cycles; chironomids; sediment transport; limnology; shallow water, diatomite mining.

EXTENDED ABSTRACT

INTRODUCTION
Lake Myvatn and its surroundings is a unique landscape created by the interaction of water and the basaltic volcanism of the mid-Atlantic ridge straddling Iceland. The hills forming the backdrop of the lake were created by subglacial volcanism during the Pleistocene; the landscape on the shore is dominated by littoral cones (pseudocraters) formed as lava flowed into a precursor lake and interacted with its water logged sediment. The lake itself is partly fed by tepid groundwater, heated by subsurface bodies of magma. Most of the inflow, however, is cold groundwater that has dissolved nutrients from the extensive postglacial lava fields in the catchment. The critical nutrient is phosphorus which supports rich and diverse aquatic life, characterised by an abundance of chironomids and small crustaceans which in turn feed rich wildlife resources comprised of fish and waterfowl. The shallow, naturally eutrophic Lake Myvatn has caught the attention of naturalists since the early 19th century. In the last 40 years there has been a systematic attempt to map and understand its limnology (Jonasson, 1979; Einarsson *et al.*, 2004). What is emerging is a picture of a highly dynamic and vulnerable ecosystem responding to long term external forcing but also showing extreme short term quasi-cyclic fluctuations due to complex food web dynamics.

THE ECOSYSTEM
Ecological features of Lake Mývatn and the outflowing river Laxá exhibit large variation on a range of spatial and temporal scales. The two factors having the largest spatial effect are (1) the physical division of the lake into three main basins and (2) variation in chemical composition and temperature of the artesian springs feeding the lake. Variation in groundwater characteristics depends on percolation time and proximity to geothermal sources. Variation in precipitation is moderated by the porous volcanic soil and bedrock and the spring-water discharge is therefore very stable.

The primary producers, mostly diatoms and photosynthetic bacteria, go through a decomposing stage before being consumed by secondary producers which are mostly chironomid (midge) larvae and small crustaceans. Monitoring of the food web has revealed strong quasi-cyclic fluctuations that seem to be driven by processes internal to the food web rather than by external factors. It seems that the midge *Tanytarsus gracilentus* is a keystone species in this respect. Its larvae are dense enough to eat up available food and subsequently the population crashes. Other invertebrate populations follow suit because they rely on the

same resource. A mathematical model has been developed that describes the fluctuations which involve rapid switching between two modes of population behaviour, one stable the other oscillating (Ives *et al*., 2008). Studies of the model suggest that the ecosystem is sensitive to just small changes in the transport of organic particles (food) into the *Tanytarsus* habitat. Any reduction in these transported particles acts to deepen the fluctuations because they serve as a food reserve in lean years. The impact of small fish as predators may also be substantial but is probably most influential in the upper levels of the food web during lean years. Temporal variation in epibenthic chironomids and Cladocera translates into variable production of vertebrate predators (Arctic charr and ducks), body condition and mortality of fish and sometimes into return rates of migrating adult ducks (Gardarsson, 2006; Einarsson *et al.*, 2004).

Recycling of nutrients through internal loading is important. In winter, when the lake is ice-covered, the topmost 5 cm layer of sediment pore water has a hundredfold concentration of nutrients relative to the overlying lake water. The nutrients are released during the ice-free period by sediment resuspension, diffusion, bioturbation and recycling by the benthos. In spring, resuspension events sometimes lead to spikes in dissolved phosphorus and nitrogen, but there is little evidence of any major desorption of nutrients from suspended particles during such events later in the summer (Einarsson *et al.*, 2004).

Palaeolimnological studies indicate that primary production in the South Basin is increasingly benthic as the lake depth is reduced by sedimentation (around 2 mm yr^{-1}). Other trends include a decrease in *Tanytarsus* and *Daphnia* and an exponential increase in green algae and associated organisms.

Diatomite mining of the lake sediment in the period 1967-2004 created a new dimension in the spatial and temporal structure of the ecosystem. In the North Basin, where the mining took place, the distribution and density of waterfowl has changed as duck and swan habitat was reduced. Also, extensive sediment focusing into the mining pits is occurring there. Hydraulic modelling has been used to envisage the impact of potential diatomite mining in the South and East Basins. The main impact would be focusing of fresh detritus into the dredged pits. The estimated annual sediment focusing is one to two thirds of the annual net production of sedimented detritus in those basins, depending on mining scenarios and weather (Kjaran *et al.*, 2004). The predicted impact is one of reduced zoobenthic production and destabilization of the ecosystem (Einarsson *et al*., 2004; Ives *et al.*, 2008).

REFERENCES

Einarsson, A., Stefánsdóttir, G., Jóhannesson, H., Ólafsson, J.S., Gíslason, G.M., Wakana, I., Gudbergsson, G. & Gardarsson, A. (2004). The ecology of Lake Myvatn and the River Laxá: variation in space and time. Aquatic Ecology **38**, 317-348.

Gardarsson, A. (2006). Temporal processes and duck populations: examples from Mývatn. Hydrobiologia **567,** 89–100.

Ives, A.R., Einarsson, A., Jansen, V.A.A. & Gardarsson, A. (2008). High-amplitude fluctuations and alternative dynamical states of midges in Lake Myvatn. Nature **452**, 84-87.

Jonasson, P.M. (ed.) (1979). Ecology of eutrophic, subarctic Lake Mývatn and the River Laxá. Oikos **32**.

Kjaran, S.P., Hólm, S.L. & Myer, E.M. (2004). Lake circulation and sediment transport in Lake Myvatn. Aquatic Ecology **38**, 145-162.

Climate change and its effects on lakes in SW−Iceland

H.J. Malmquist*, F. Ingimarsson, H.R. Ingvason and S.M. Stefánsson

Natural History Museum of Kópavogur, Hamraborg 6a, IS-200 Kópavogur, Iceland

**Corresponding author, e-mail hilmar@natkop.is*

KEYWORDS
Climate change, Icelandic lakes, warming, conductivity, lake stratification.

EXTENDED ABSTRACT

INTRODUCTION
Significant changes have been observed in several climatic factors in Iceland for the past 200 years. Most notably, climate has been warming according to global warming in the northern hemisphere, with an increase in annual mean temperature of about 0.7°C per century, as measured during 1798−2007 in Stykkishólmur, W–Iceland (Björnsson *et al.* 2008). In the 20th century, there was a cold period between 1965−1986, but otherwise temperatures have been rising, especially in spring (April–May) and autumn (October–November). For the past 20–30 years, the last decade in particular, summer temperatures have also been very high.

The climate warming in Iceland has caused changes in hydrological and physico−chemical factors, including rapid glacial retreat, increased runoff and mechanical and chemical weathering fluxes in dissolved and suspended materials (Björnsson *et al.* 2008; Gíslason *et al.* 2009). So far, studies in Iceland on relations between climate change and hydrological factors have focused on glaciers and running waters. Less is known about climate change and its effects on lakes, but see Malmquist *et al.* (2009). This paper presents data on physico–chemical factors in six lakes in SW−Iceland in conjunction with climate warming.

SITE DESCRIPTION AND METHODS
Physico-chemical and biological factors, including temperature, conductivity and acidity, have been monitored every month since 2004 in several lakes in SW−Iceland. Sporadic measurements exist from some of the lakes back to the eighties in the last century. Here we present data on conductivity (adjusted to 25°C) in four lakes in the metropolitan area of Reykjavík: Lake Elliðavatn (2.02 km^2, mean depth 1.0 m, max. depth 2.3 m), Vífilsstaðavatn (0.27 km^2, mean depth 1.0 m, max. depth 1.5 m), Hafravatn (1.08 km^2, mean depth 8 m, max. depth 28 m) and Rauðavatn (0.32. km^2, mean depth 1.0 m, max. depth 1.4 m). Also presented are results on thermocline studies in Lake Þingvallavatn (83 km^2, mean depth 34 m, max. depth 114 m), Kleifarvatn (10 km^2, mean depth 29 m, max. depth 97 m) and Hafravatn. All lakes, except Hafravatn and Rauðavatn, are to a large extent springfed water bodies, situated in catchments dominated by permeable, volcanic basalt rocks from late Holocen age.

RESULTS AND DISCUSSION

Changes in Conductivity

Conductivity increased around 15% over the past seven years in all four lakes. In Elliðavatn (r = 0.40, n = 112, p<0.001) and Hafravatn (r = 0.61, n = 93, p<0.001), conductivity increased from around 80 µS cm^{-1} in 2004 to around 95 µS cm^{-1} in 2010. In Rauðavatn (r = 0.53, n = 85, p<0.001) and Vífilsstaðavatn (r = 0.64, n = 94, p<0.001), conductivity increased from around 130 µS cm^{-1} in 2004 to around 150 µS cm^{-1} in 2010. Earlier, sporadic measurements on conductivity in the lakes, dating back to 1993–1998, are in line with the observed trend.

The increase in conductivity coincides with climate warming in the metropolitan area, starting 25–30 years ago, resulting in increased lake water temperature, as best demonstrated in Elliðavatn, with an increase of 2.3–2.7°C on average in spring (April) and late-summer (August) (Malmquist *et al.* 2009). The increase in lake conductivity may be due to the climate warming, resulting in increased weathering rates of basaltic rocks in the catchments hence increased conductivity, as observed in catchments in NE−Iceland (Gíslason *et al.* 2009).

Lake Stratification

Based on available data from 1979, 1981–1982, 1984 and 2007–2009, direct stratification (≥ 1°C m^{-1} in the metalimnion) does apparently not develop in Þingvallavatn, the largest lake in Iceland. However, a weak thermocline may in some years develop in late summer (July-August) at 20–25 m depth, as e.g. in 2007 and 2009 when a gradient of 0.2–0.3°C m^{-1} was observed in the transitional zone (10–13°C at most in the epilimnion and ≤ 8.5°C in the hypolimnion) (Malmquist *et al.* 2010). In Kleifarvatn, measurements in 2005–2006 and 2008 revealed a weak thermocline at 20–25 m depth in late summer 2008, with a gradient of 0.2–0.3°C m^{-1} in the transitional zone (10–12°C at most in the epilimnion and ≤ 8.0°C in the hypolimnion). For Hafravatn, no thermocline was observed in 2003 or 2007.

In general, direct stratification, as commonly defined (Moss 1998), does apparently not develop in Icelandic lakes. Rather, the lakes appear to be more or less mixed from top to bottom throughout the year. We explain this by wind exposure due to open nature of Icelandic landscape. However, in very warm and calm periods, a weak thermocline may be present for a short time. Moreover, if predictions about climate warming in Iceland of 0.15–0.20°C per decade (Björnsson *et al.* 2008) come true, stronger and longer lasting thermocline may be expected in Icelandic lakes with accompanying effects on the biota.

REFERENCES

Björnsson H., Sveinbjörnsdóttir Á.E., Daníelsdóttir A.K., Snorrason Á., Sigurðsson B.D., Sveinbjörnsson E., Viggósson G., Sigurjónsson J., Baldursson S., Þorvaldsdóttir S. & Jónsson T. (2008). Hnattrænar loftslagsbreytingar og áhrif þeirra á Íslandi - Skýrsla vísindanefndar um loftslagsbreytingar. Umhverfisráðuneytið. (Global climate change and its effects in Iceland. The ministry of environment).

Gíslason S.R., Oelkers E.H., Eiriksdottir E.S., Kardjilov M.I., Gisladottir G. Sigfusson B., Snorrason A., Elefsen S., Hardardottir J., Torssander P. & Oskarsson N. (2009). Direct evidence of the feedback between climate and weathering. *Earth and Planetary Science Letters* 277: 213–222.

Malmquist H.J., Antonsson Þ., Ingvason H.R., Ingimarsson F. & Árnason F. (2009). Salmonid fish and warming of shallow Lake Elliðavatn in Southwest Iceland. *Verh. Internat. Verein. Limnol.* 30: 1127–1132.

Malmquist H.J., Ingimarsson F., Ingvason H.R. & Stefánsson S.M. (2010). Vöktun á lífríki og vatnsgæðum Þingvallavatns. Gagnaskýrsla fyrir árið 2009. (Monitoring pelagic biota and water quality in Lake Þingvallavatn. Year 2009.). Natural History Museum of Kópavogur. Report no. 1–10. 36 p. (English summary).

Moss B. (1998). Ecology of Fresh Waters. Third edition. Blackwell Publishing.

The significance of accurate hydrological modeling for long-term lake water quality predictions in volcanic zones

S.O. Palmarsson*, E.M. Myer, H. Sigurjonsson and S.L. Holm

Vatnaskil Consulting Engineers, Sudurlandsbraut 50, 108 Reykjavik, Iceland

**Corresponding author, e-mail sop@vatnaskil.is*

KEYWORDS
Climate change; Groundwater; Hydrological modeling; Lake water quality; Volcanic zones.

EXTENDED ABSTRACT

Lakes situated in porous lava fields of volcanic zones are essentially groundwater-fed, often with no significant surface inflows and a single river outlet. Groundwater typically enters the lake at its shores and bottom through springs, where groundwater naturally emerges from the subsurface. The permeability of the geological strata and the lakebed sediment, as well as the groundwater availability, determine the size (discharge) of the springs. Spring discharge can be very large where porous strata extend over large areas, particularly if geological conditions concentrate the groundwater to surface depressions such as lake areas.

Groundwater contributes to nearly 1000 m^3/s or about 20% of the total runoff in Iceland, with 200-300 m^3/s originating from glaciers (Sigurdsson, 2001). The largest portion of this groundwater surfaces in the highlands, at 200-800 m a.s.l., primarily in relation with geological strata and fissures at and near the active volcanic zone. Most of the largest rivers in Iceland have a large groundwater component, with over 30-50% of the common river discharge originating from groundwater springs. Some are almost entirely spring-fed rivers, such as Sogid and Laxa in Adaldalur, which are outlets of two of the largest lakes in Iceland, Lake Thingvallavatn and Lake Myvatn, respectively. The northern shore of Lake Thingvallavatn is the largest spring area in the country, with a flow of about 85 m^3/s, and the spring inflow in Lake Myvatn ranks as the fourth largest spring area in Iceland, with a flow of 32 m^3/s.

As is generally the case with lakes, the inflow and outflow is a basic forcing contributing to the lake circulation. Moreover, temperatures and chemical contents of inflowing water affect the lake water quality. Notably different from lakes with primarily surface inflows are the rather constant inflow rates, temperatures and chemical concentrations of the springs. Furthermore, a great spatial variability in these characteristics of the springs is common. In particular, if active volcanoes are in the region or if significant glacial contributions characterize the groundwater, the heterogeneity of groundwater temperatures and chemical concentrations may be apparent. This spatial variability results in spatial heterogeneity in the lake environment, including its ecosystem (e.g., Einarsson *et al.* 2004).

The utilization of groundwater and geothermal resources in a lake region may lead to modifications to groundwater flow paths, and changes in flow, temperature and chemical characteristics of the spring inflows to the lake. Such changes in the spring inflows may also

result from hydrologic alterations due to climate change (e.g., Johannesson, 2007). With potentially drastic effects to the lake ecosystem, it is very important to assess accurately the hydrological changes due to groundwater utilization or climate change. Future predictions on lake water quality are thus largely dependent on hydrological estimates.

This importance on hydrological simulations is demonstrated with simulations of the Lake Thingvallavatn and Lake Myvatn watersheds. Specifically, simulation results are presented on geothermal plant effluent fate and transport in the vicinity of the lakes and groundwater flow response to future climate scenarios. In this respect, runoff modeling was performed for several Icelandic watersheds according to predicted future climate scenarios that involve elevated air temperatures and precipitation during the years 2071-2100 compared to a reference period 1961-1990. The results demonstrate how less precipitation will fall as snow and more snow-melt will occur during the winter. Consequently, runoff in watersheds with little or no glacial melt water will increase substantially during the winter, whereas spring runoff tends to be smaller. On the other hand, in watersheds where runoff is dominated by glacial melt water, the increase is the greatest in the glacial melting period, i.e. in summer and early fall. It has been predicted that this significant increase in glacial melt will lead to thinning of the ice caps and retreat of glacier margins and even to near disappearance of the glaciers within the next 200 years (Johannesson *et al.*, 2007). The excessive retreat of the glaciers may lead to drastic changes in spring inflow rate, temperature and chemical characteristics at Lake Thingvallavatn's northern shore. Some effects in this regard may also be apparent in Lake Myvatn.

The spring inflows affect various important physical processes for lake mixing and thus water quality. It is expected that these processes may be altered in response to changes of the inflow characteristics. These responses are considered different for the shallow, eutrophic Lake Myvatn, compared to the deep, oligotrophic Lake Thingvallavatn. The persistent horizontal density gradients imposed by either cold or warm spring inflows, will lead to exchange flows in the littoral zones that may be complicated by diurnal heating and cooling by the meteorological forcing. The lake stratification dynamics in general will be affected, not only by the spatial variability of the horizontal density gradients, but by plunging cold spring inflows and warm spring inflows penetrating the interior of the lake along the surface. Questions arise with respect to internal wave dynamics and how cascade of energy from basin-scale to smaller scales will be affected. Furthermore, the steady inflow of groundwater at the lake bottom will modify near-boundary stratifications and forming of boundary layers may be affected. Lake Thingvallavatn and Lake Myvatn are suitable field laboratories to study these processes with respect to the particularities of the spring inflows. Such studies would furthermore provide much needed material to fill gaps in the description of their physical limnological characteristics and would support quite extensive ecological and chemical investigations already reported from these lakes.

REFERENCES

Einarsson A., Stefansdottir G., Johannesson H., Olafsson J.S., Gislason G.M., Wakana I, Gudbergsson G and Gardarsson A. (2004). The ecology of Lake Myvatn and the River Laxa: Variations in space and time. *Aquatic Ecology*, 38: 317-348.

Sigurdsson F. (2001). Grunnvatn sem orkuberi. Orkuþing 2001, p. 490-492 (in Icelandic).

Johannesson T., Adalgeirsdottir G., Bjornsson H., Crochet P., Eliasson E.B., Gudmundsson S., Jonsdottir J.F., Olafsson H., Palsson F., Rognvaldsson O., Sigurdsson O., Snorrason A., Sveinsson O.G.B. and Thorsteinsson T. (2007). Effect of climate change on hydrology and hydro-resources in Iceland. National Energy Authority, OS-2007/011.

Internal waves in weakly stratified Lake Lagarfljót

H. Ó. Andradóttir*

Faculty of Civil and Environmental Engineering, University of Iceland, Hjarðarhagi 6, 107 Reykjavík, Iceland

**Corresponding author, e-mail hrund@hi.is*

KEYWORDS
Internal waves, weak thermal stratification, sub-arctic lakes.

EXTENDED ABSTRACT

A fundamental understanding of lake physical responses to meterological forcing is necessary in order to assess the future impact of climate change on such aquatic systems. Lakes in northern climates differ from the better studied lakes at lower altitudes in that they experience a weak thermal stratification, which is solely present from mid June to mid September (e.g. Helgason and Axelsson, 2009 and Andradóttir, 2008). Relatively little focus has been on characterizing the internal wave activity in such weakly stratified systems. Rueda et al. (2003) studied basin scale internal waves in Lake Tahoe during weak winter density stratification, and found that the internal waves had periods greater than 5 days and vertical displacements as high as 30 m. MacIntyre et al. (2009) studied thermal and mixing dynamics in an Alaskan arctic lake. Their isotherm data show periodic fluctuations which are indicative of internal wave activity. Therefore, these prior studies suggest that one cannot make the simplifying assumption of neglecting the presence of internal waves in systems where the water temperature is “almost” uniform with depth.

The goal of this present study is to characterize the internal wave dynamics in one of Iceland´s largest (53 km^2) and deepest (max. 112 m) lakes, Lake Lagarfljót. The lake historically receives sediment rich glacial river water from Jökulsá í Fljótsdal, and more recently also from the Hálslón reservoir built on a nearby glacial river, Jökulsá í Dal, for the Kárahnjúkar hydroelectric project.

Thermistors consisting of Starmon mini from Star-Oddi Ltd. and TR-1060 loggers from RBR Ltd. were placed at regular depth intervals at three locations within the lake in the summers 2008 and 2009. In addition, near bottom water velocities were monitored with a Nortek Aquadopp Acoustic Doppler Velocitimeter (ADV). Vertical temperature, conductivity, pH and turbidity profiles were taken with a Sonde 6000 multiparameter profiler from YSI Inc. owned by the Insitute of Freshwater Fisheries in Iceland. Local weather and hydrological inputs were monitored by the Icelandic Meterological Office (2009, 2010).

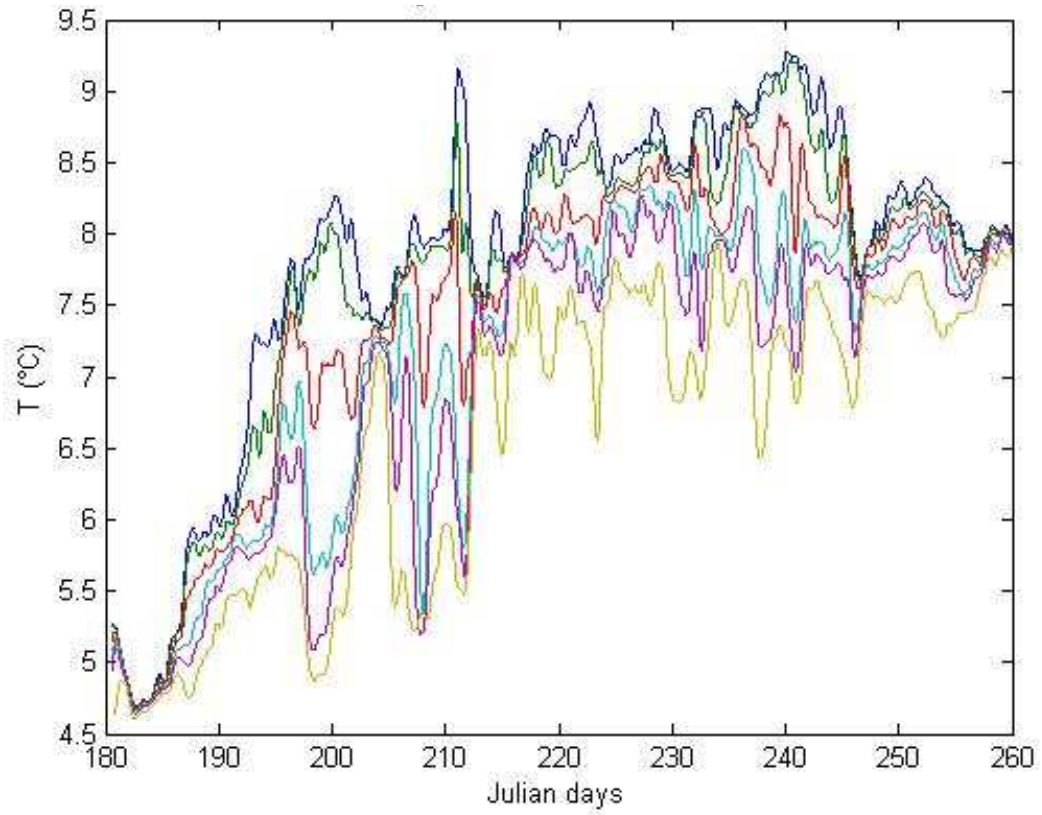

Figure 1. Filtered water temperatures at 9m (blue), 13m (green), 19 m (red), 25m (cyan), 29m (violet) to 37 m (green) depth in Lake Lagarfljót, July to October 2008

This talk will discuss the initial results of this monitoring program. As shown on Figure 1 Lake Lagarfljót is vertically stratified for 2 months, from July 5th to September 16th in 2008. The temperature difference between surface and bottom waters is on the order of 2°C. Under such weak stratificaion, internal waves with period on the order of 1-10 days are observed. Vertical displacements associated with these waves are in the range of 3-8 m. In addition vertical modes are detected, seen for example by spreading of the temperature time series around Julian day 200 in Figure 1.

ACKNOWLEDGEMENTS

This work was funded by the Landsvirkjun Energy Research Fund and the University of Iceland Research Fund.

REFERENCES

Andradóttir H.Ó. (2008). Thermal dynamics of sub-arctic lake Lagarfljót, In Ó.G. Blöndal Sveinsson (Ed), Nordic Hydrology and its global role, Vol. 1, NHP report no. 50, 82-93

Helgason V.K. and Axelsson E. (2008). Vatnshitamælingar Landsvirkjunar og Vatnamælinga á Austurlandi árin 1995-2007. Landsvirkjun LV2009-062

Iceland Meterological Office (2009, 2010). Weather and flow data bank, including extractions nr. 2009-10-28/01 and 2010-02-08/01.

MacIntyre S., Fram J. P., Kushner P.J., Bettez N.D., O'Brien W.J., Hobbie J.E., and George W. Kling (2009). Climate-related variations in mixing dynamics in an Alaskan arctic lake. Limnol. Oceanogr., 54(6), 2401-2417

Rueda F.J., Schladow S.G. and Pálmarsson S.Ó. (2003). Basin-scale internal wave dynamics during a winter cooling period in a large lake, J. of Geophysical Research, 108(C3), article nr. 3097

Modelling of physical processes in a large deep polar lake

Yerubandi R. Rao[1]*, Anning Huang[1], William M. Schertzer[1], Normand Bussières[2]

[1] *National Water Research Institute, Environment Canada, Water S&T Canada Centre for Inland Waters, Burlington, L7R 4A6, ON, Canada*
[2] *Climate Research Division, Atmosphere S & T, Environment Canada, 4905 Dufferin Street, Toronto M3H 5T4, ON, Canada*

**Corresponding author, e-mail Ram.Yerubandi@ec.gc.ca*

KEYWORDS
Hydrodynamic model, Great Bear Lake, Circulation, thermal structure

EXTENDED ABSTRACT

Polar lakes are highly sensitive to changes in the climate. Some of the largest increases in the air temperature anywhere in the world have been observed in the Mackenzie Basin. Rouse *et al*. (2007) suggested that Great Bear Lake is very responsive to climatic variability, being influenced by the relation between the length of the ice-free season and absorbed solar radiation. Currently, the lake has an ice-free period of ~ 4-5 months. The longest ice-free period occurred during an intense El Nino in 1998. Meyer *et al.* (1994) conducted a preliminary analysis of the impact of climate change on hypothetical lakes at different latitudes including Great Bear Lake. They suggested that the lake is currently in cold monomictic stage experiencing complete vertical mixing once in three years. Using a one-dimensional model , their preliminary climate changed simulations with Geophysical Fluid Dynamics Lab (GFDL) steady-state climate scenario suggested that under an atmospheric 2 x CO_2 increase, the consequent increase in air temperature would result in a reduction in the period of ice cover from 82% of the year to only 65%. As a result of air temperature increase, which was assumed to be as much as 9^oC, strong convective mixing in the lake could potentially occur in the spring and autumn months. This suggests that the lake could change its mictic state from cold monomictic to become dimictic (overturn twice yearly in the spring and the fall) with physical processes similar to temperate lakes such as the Laurentian Great Lakes. Such a change would have profound implications for the lake physical limnological characteristics (e.g. ice extent, ice-free period, water temperature) as well as on aquatic ecosystem components (e.g. fisheries) which the northern communities depend on. However, these predictions have major limitations because the meteorological forcing data were not applicable for this region and the model was not verified with measurements in the lake. Furthermore, large lakes like Great Bear Lake exhibit significant horizontal and vertical variability in thermal structure and circulation, which will have significant impacts on the local weather and climate. Therefore, the main objective of this paper is to study the current conditions of thermal structure during ice-free period and develop hydrodynamic models that can be used to assess the climate impacts. As part of Environment Canada's contribution to the International Polar Year (IPY), the impact of warming on the thermal characteristics of the Great Bear Lake is studied. During the summers of 2008 and 2009, time series observations of meteorological, hydrological and physical limnological parameters were obtained in the lake to characterize the thermal regime in the lake (Figure 1). Surface heat flux components

are computed from the meteorological measurements over the lake. These observations and the forecasted forcing from a regional version of the Canadian operational Global Environmental Multi-scale (GEM) model are used to simulate the ice-free hydrodynamics in the Great Bear Lake using a high-resolution, three-dimensional hydrodynamic model, namely, Princeton Ocean Model (POM).

The model predicted surface and sub-surface temperatures are close to observations. Surface currents generally followed the prevailing winds (Figure 2). The model simulates weak stratification and predicts mean cyclonic circulation reasonably well. By using POM we also studied the thermal response of the lake under warmer climate. Sensitivity experiments revealed that the temperatures in the upper water column increased by 2-5% with a 20% increase in the net heat flux with noticeable changes at the surface. Seasonal thermocline was established at much shallower depths (~10 m) for slightly longer period than the base conditions. By using Canadian Regional Climate Model (CRCM) scenarios for the base climate (1970-2000) and future warmer climate (2040-2070) we carried out hydrodynamic simulations in the lake. The largest increases in surface temperature were observed in the north-east corner (>2^{o}C) and near the southern shoreline (1-1.5^{o}C) in the Kieth Arm of the lake. In deeper regions of the lake surface temperatures are also increased by 0.5-1^{o}C in the future climate scenario.

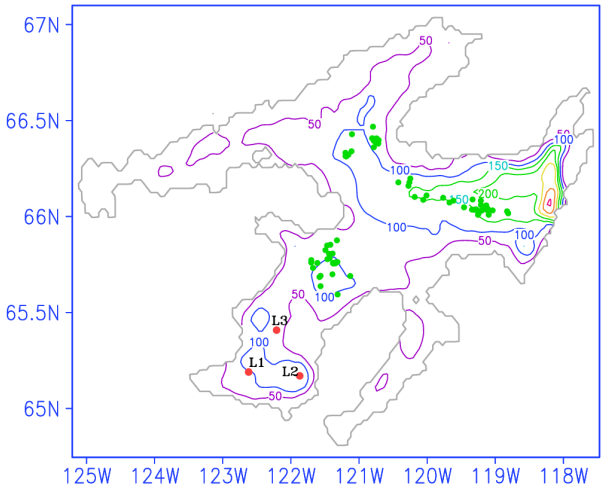

Figure 1. Bathymetry of Great Bear Lake in the model domain (in meters) and temperature moorings (blue) and APEX profiler locations (green).

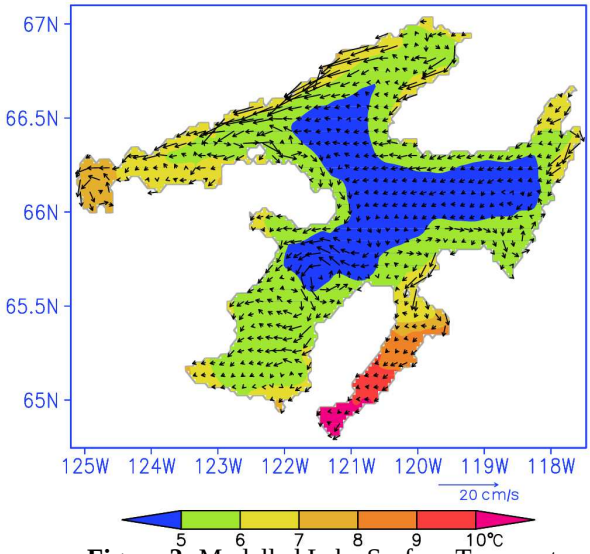

Figure 2: Modelled Lake Surface Temperature an currents averaged from Aug 1-Sept 30, 2008.

REFERENCES

Meyer, G., Masliev, I., and Somlyody, L. 1994. Impact of Climate Change on Global Sensitivity of lake Stratification, Working Paper WP-94-28, International Institute for Applied Systems Analysis, laxenburg, Austria, 56p.

Rouse, W.R., Blanken, P.D., Bussieres, N., Oswald, C.J., Schertzer, W.M., Spence, C., and Walker, A.E. 2008. An investigation of the thermal and energy balance regimes of Great Slave Lake and Great Bear Lake, J. Hydrometeor, 9:1318-1333.

Internal seiching in ice-covered lakes.

G. Kirillin[1]*, C. Engelhardt[1], S. Golosov[1], M. Leppäranta[2], N. Palshin[3], A. Terzhevik[3], G. Zdorovennova[3], R. Zdorovennov[3]

[1]*Department of Ecohydrology, Leibniz-Institute of Freshwater Ecology and Inland Fisheries, Berlin, Germany*
[2]*Department of Physics, Universityof Helsinki, Finland*
[3]*Northern Water Problems Institute, Russian Academy of Sciences, Petrozavodsk, Russia*

[*]*Corresponding Author, e-mail kirillin@igb-berlin.de*

ABSTRACT.

Basin-scale oscillations or seiches are intrinsic features of bounded water bodies: lakes, reservoirs and enclosed seas. There is little known about seiches in ice-covered lakes though several recent reports suggest an appreciable contribution of the lakewide oscillations in the circulation under ice. Based on temperature records from the winter 2007-2008 in two ice covered lakes, Pääjärvi in Finland and Vendyurskoe in Russia, we demonstrate a distinguished seiche signature in the isotherms displacements at periods from hourly to synoptic ones. The pattern of these lake-scale oscillations reveals several unique features suggesting their principal difference from the "normal" seiches in summer stratified lakes: In the deeper Lake Pääjärvi, the oscillations develop on the background of specific "lenticular" thermal stratification with vertical spacing of the isotherms increasing from the near-shore areas to the central parts of the lakes. As a result, the oscillations take place at higher vertical modes with upper isotherms oscillating in the counterphase to lower ones. All dominating *internal* seiche periods exceed the inertial period for the lakes' latitudes, suggesting strong effect of the Coriolis force on the oscillations and, as a result, concentration of the seiche-produced oscillations currents in the near-shore areas in form of Kelvin waves - the typical feature of large-scale geophysical flows. In the shallower Lake Vendyurskoe, the internal seiches appear only intermittently, whereas a strong signature of external seiches persist in the temperature records at the bottom slope — a feature specific for the strong near-bottom stratification in winter. These features make the spectrum of oscillations under ice much more manifold than that in the open waters, where usually only one vertical and one lateral mode dominate. The results have important implications for understanding the lateral mass transport from sediment and ice across the water column during the ice-covered season.

KEYWORDS

Seiches, ice-covered lakes, Kelvin waves, winter limnology

INTRODUCTION

Below we compare the patterns of the basin-scale waves in two ice-covered lakes revealed from the thermistor chains data in winters 2007-2008 and 2008-2009. The aims of the analysis were to identify spatial and temporal characteristics of the basin-scale motions under ice and to outline the similarities and differences of oscillations in the lakes with different morphometry.

STUDY SITES AND METHODS

The study is based on temperature data collected from Lake Pääjärvi in Southern Finland (Fig. 1a, maximum depth 87 m, surface area 13.4 km^2, volume 0.1 x 10^9 m^3) and from Lake Vendyurskoe in the Russian Karelia (Fig. 1b, mean depth 5.3 m, maximum depth 13.4 m, surface area of 10.4 km^2, water volume of ~5.5×10^7 m^3). Two thermistor chains (RBR TR-1050 and TDR-2050, accuracy 0.002^{o}C) were installed in each lake in similar configuration:

one chain in the central part of the lake and another one in the near-shore part. In Lake Pääjärvi an RDI Workhorse ADCP was installed in the near-shore part of the lake recording vertical current velocity profiles. The measurements period in Lake Pääjärvi covered 2 weeks in March-April 2008; in Lake Vendyurskoe the temperatures were recorded during the entire ice-covered period from December 2008 to May 2009.

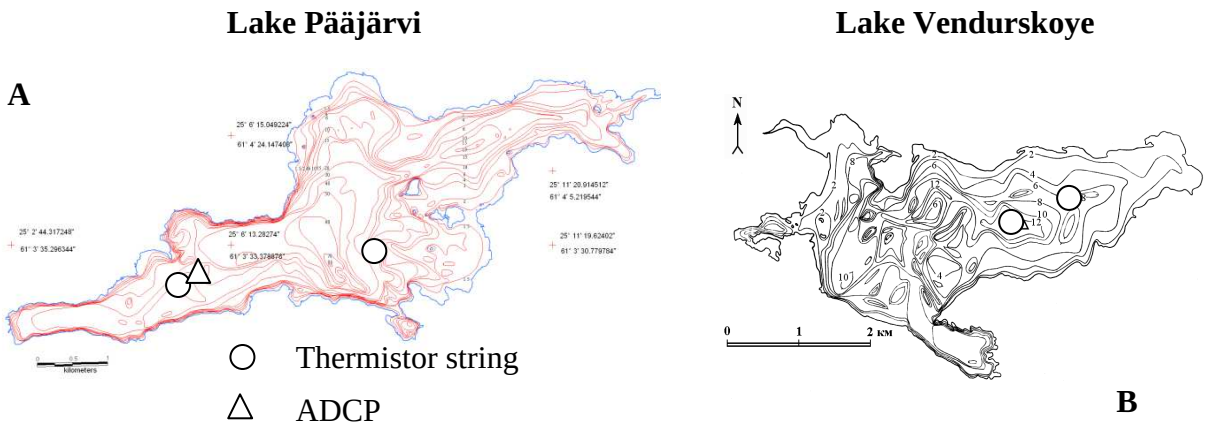

Figure 1 Bathymetrical maps of the two lakes with measurement site locations.

RESULTS:

Lake Vendurskoye, Winter 2008-2009

The background temperature evolution in Lake Vendyrskoe during the 5 months from the beginning of December to the end of April was characterized by an appreciable graduate heating of the water column through the heat flux from the sediment (Fig. 2).

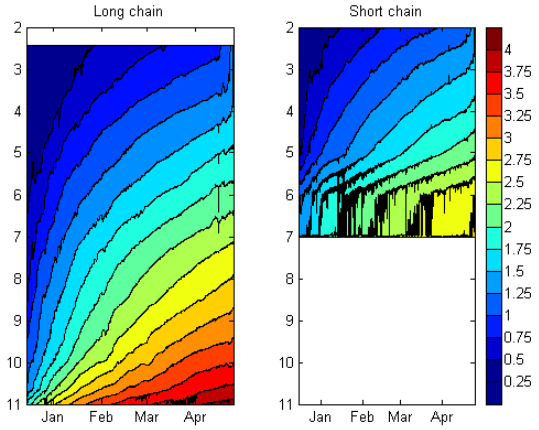

Figure 2 Isotherms evolution in Lake Vendyurskoye during the winter 2008-2009

At the shallow location ("Short" thermistor chain) pronounced short-term temperature variability was observed in the layer in the lower 2 meters of the water column between 5 and 7 meter depth. The highest amplitudes of the isotherm oscillations were observed at about 6 m depth, which coincides with the upper boundary of the near-bottom mixed layer (Fig. 3a-b). Among the detectable oscillation frequencies the shortest one of 26.1 minutes persists during the entire observations period (Fig. 3d) and is clearly distinguishable as a narrow peak in the temperature spectrum (Fig. 4a). These short-period oscillations are unambiguously ascribed to the *external* seiching: the same period of 26.1 min persists in the spectra of pressure records under the ice (Fig. 4b). In addition, exactly the same period was reported by Malm et al. (1997) to prevail in the current speeds and in the ice cover oscillations in Lake Vendyurskoe

in winter 1995-1996, and was shown to roughly coincide with the period of the longitudinal external seiche following from the Merian formula. The clear external seiche signal in isotherm displacements is rather surprising: typical external seiche amplitudes do not exceed 1 cm and have no remarkable effect on the vertical temperature distribution in open waters. Here, such an effect can be ascribed to the strong stratification in the lake bottom vicinity, conditioned by the stabilizing heat flux from the sediment: as a result, even small oscillations of the water body are followed by an appreciable temperature changes at the fixed locations of the temperature loggers.

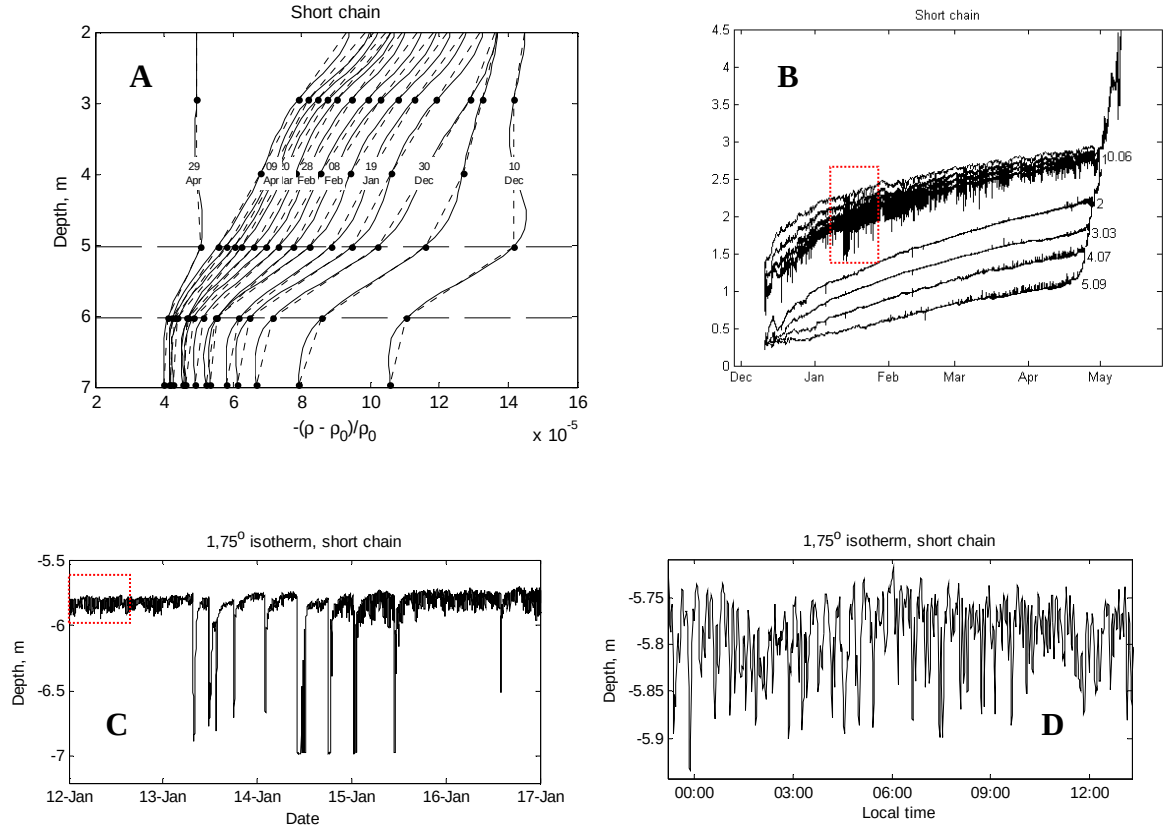

Figure 3 Stratification development and periodic oscillations in the near-shore area of Lake Vendyurskoye ("short chain"): (A) successive profiles of buoyancy. (B-D) temperature evolution at different water depths; (C) is a zoomed picture with internal seiching event; (D) is a zoom with shot-period oscillations driven by surface seiching.

Noteworthy, oscillations with longer periods, which could be ascribed to the *internal* basin-scale waves, were not associated with a single dominating frequency. Nevertheless, their periodic character is evident, as e.g., in the short burst of periodic isotherm oscillations with amplitudes up to 1 m and periods of 5-6 hrs observed on 13-16 January 2009 (Fig. 3c). The period of 5-6 hrs, which is also pronounced in the spectrum of the isotherm displacements (Fig.4a), exceeds remarkably the period of the inertial oscillations at the lake's latitude, $T_f = 1/f = 2.17$ hrs. Therefore, the observed oscillations could be ascribed to inertia-gravity waves of Kelvin-type balanced by the Earth rotation (Kirillin et al 2009). Consequently, the irregular shape of the lake explains the nonlinear shape of the waves, since the Kelvin waves propagate along the boundaries and are thereby strongly affected by the lake morphometry. The additional spectral peak in the vicinity of the inertial frequency f can be interpreted as a signature of the Poincare waves—an analogue of transverse seiches in non-rotating fluids—and provides by this an additional support to the rotational character of the internal basin-scale motions.

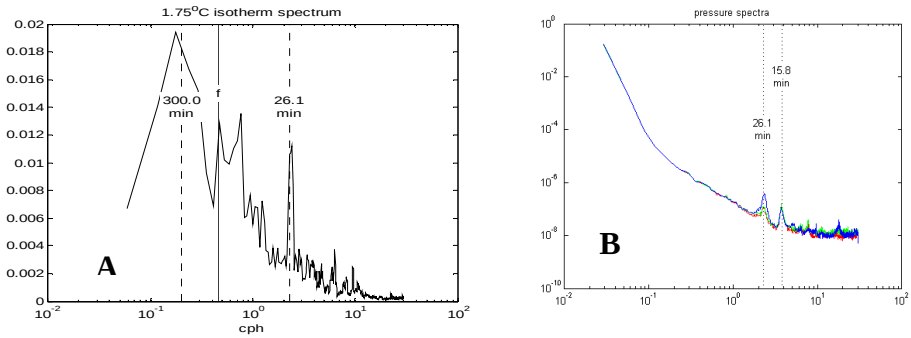

Figure 4 Spectra of (A) isotherm displacements and (B) pressure at the shallow site in Lake Vendyurskoye.

Central part of the lake

At the deep location in the middle of the lake (thermistor chain "Long") no significant short-term temperature oscillations were observed during the first phase of the ice-covered period from December to February. The situation had changed in the end of February: starting from this moment, clearly expressed periodic variations of the temperature existed in the lower 0.6 metres of the water column and were ceased in the beginning of April (Fig. 5c-d). The corresponding isotherm displacements have the amplitudes of about 0.5 m and the varying periods, among which the diurnal and semidiurnal periods are the most pronounced. The fact that the shape of the oscillations is very similar to that of the oscillations observed in the beginning of the ice-covered period at the shallow point, suggests the same origin of the oscillations, viz. the inertia-gravity basin-scale waves. Though the periods of 12 and 24 hrs coincide with the solar radiation cycle, it is not likely that the oscillations are directly driven by the radiatively-driven effects, which are rather small in the end of February under the snow-covered ice surface. More probably, the forcing is provided by 12-hour oscillations of the ice cover revealed in the low-frequency part of the pressure spectrum (Fig. 6b). The internal waves develop only 2.5 months after the lake surface freezing that can be associated with the seasonal changes in the vertical stratification in the lake: the waves appear when the near-bottom temperatures approach the maximum density value of 3.8°C. As a result, the vertical density stratification changes significantly, despite the vertical temperature gradients remain nearly the same (cf. vertical profiles of buoyancy $(\rho_O-\rho)/\rho_0$ and those of temperature in Fig. 5a,b): a layer of zero vertical density gradient develops near the lake bottom, where the internal waves propagate. Hence, presence of such a "mixed layer" with homogeneous vertical density distribution appears to be a necessary condition for development of the basin-scale waves with appreciable amplitudes. This condition explains also the existence of the waves only at the shallow measurement point in the beginning of the ice-covered period: the near-bottom layer of the constant density was created there by the shear mixing produced by the downslope density currents, whereas in the deep part of the lake the near-bottom density gradients remained high until the temperature approached the maximum density value (cf. vertical profiles of buoyancy in Figs. 3a and 5a).

Lake Pääjärvi, Winter-Spring 2008

Background stratification

The measurements period in Lake Pääjärvi covered the concluding stage of the ice-covered period starting from 29 March 2008. Therefore, we lack the information on the previous seasonal development of the background stratification in the lake. The vertical temperature and density distributions at the two measurement points reveal a mixed layer located between

1 and 7 meters depth (Fig. 7a-b), which developed, apparently, due to convective mixing driven by the solar radiation penetrating the ice (Mironov et al 2002).

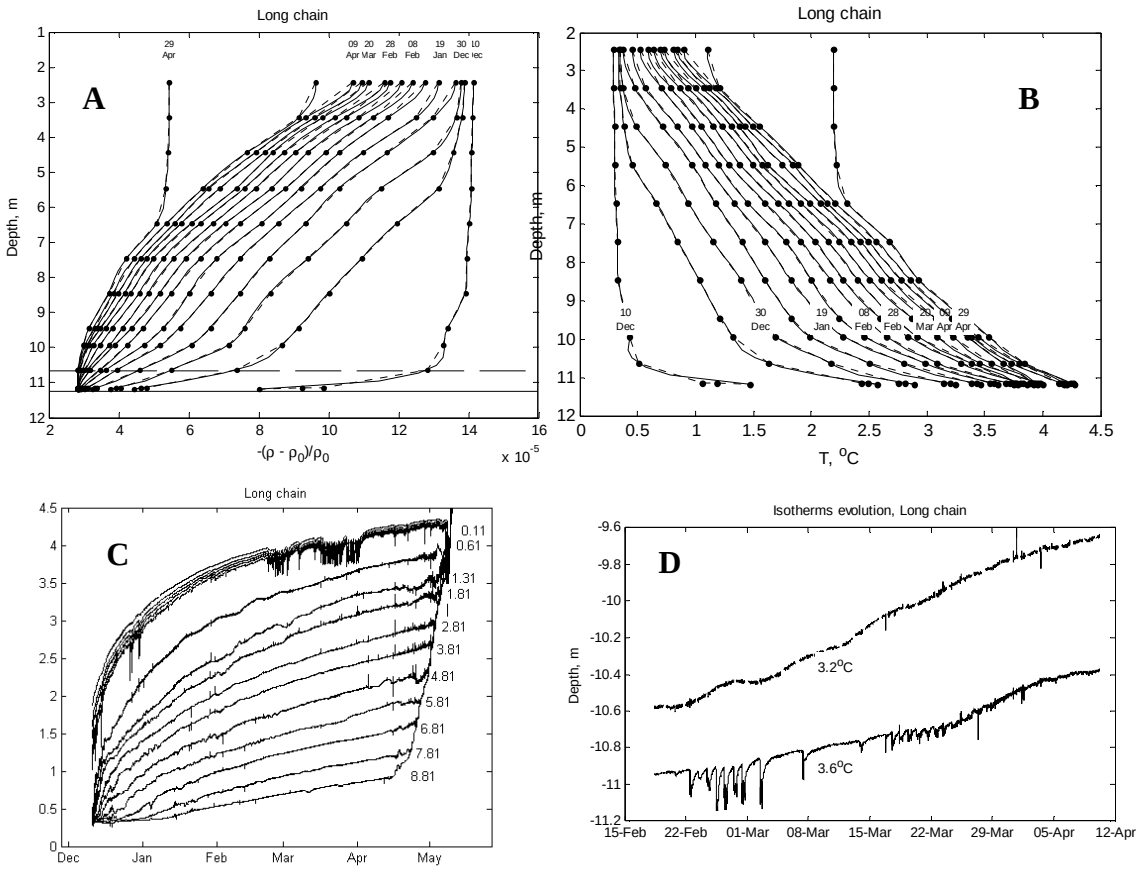

Figure 5 Stratification development and periodic oscillations in the deep area of Lake Vendyurskoye ("short chain"): successive profiles of (A) buoyancy and (B) temperature. (C) temperature evolution at different water depths; (D) isoterm evolution during the oscillations development in March-April.

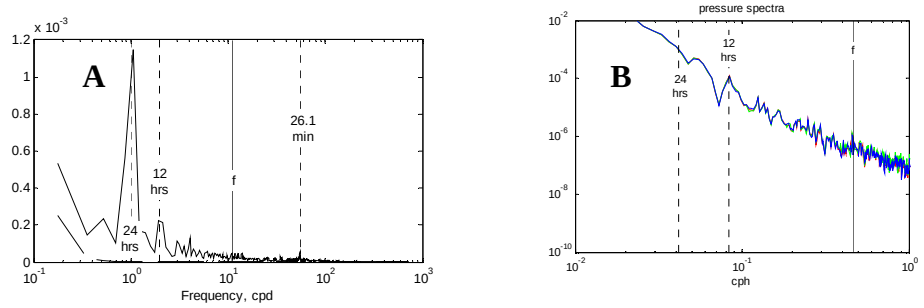

Figure 6 Spectra of (A) isotherm displacements and (B) pressure at the deep site in Lake Vendyurskoye.

The week preceding the observations start was characterized by a strong snowfall and formation of a 15 cm snow cover, which prevented further convection development. Direct radiation measurements under ice indicated quite low amount of the penetrated radiation (about 2W/m^2 daily mean) during the period from 29 March to 01 April. After that the snow cover melted and the radiative flux increased abruptly up to 40 W/m^2 in daily mean causing intense convection and rapid heating of the water column. Below we consider only the non-convective period between 29 March and 01 April, when the external radiatve forcing was damped and the temperature dynamics was dominated by the free basin-scale oscillations.

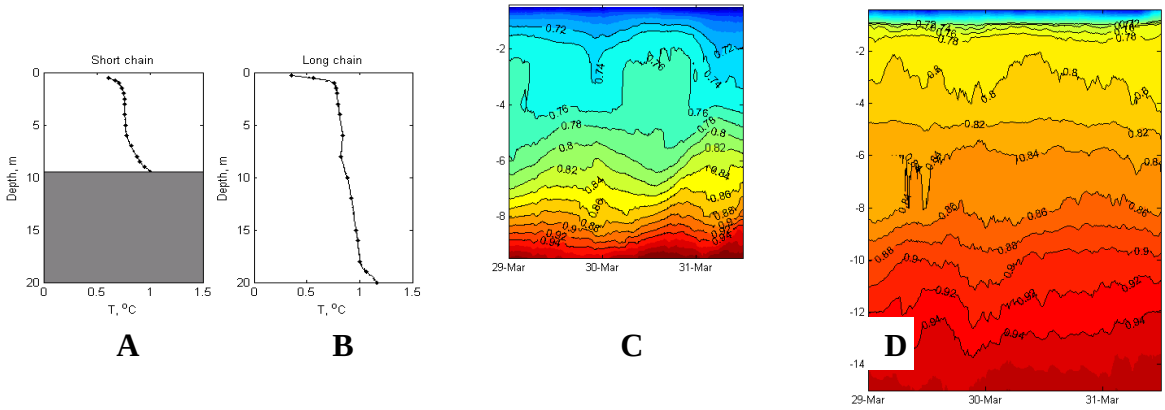

Figure 7 (A-B) Mean temperature profiles at the shallow ("short chain") and at the deep site ("long chain") in Lake Pääjärvi. (C-D) Isotherms evolution at both sites.

Basin-scale oscillations

The isotherm displacements during this period revealed strong vertical oscillations both at the shallow and deep measurement sites (Fig. 7c-d). Compared to the situation in Lake Vendyurskoye, the oscillations feature significantly higher amplitudes and longer periods. The most prominent period of oscillations amounted at about 33 hours and amplitudes of 1-2 m in the upper part of the water column. This period is an order of magnitude larger than the inertial period for this latitude. In addition, the estimation of the internal Rossby radius from the mean vertical density gradient as $R = Nh/f$, N being the buoyancy frequency, f being the inertial frequency, and h being the mean lake depth, amounts at ~500 m, i.e. an order of magnitude smaller than the typical lateral scale of the lake $L \approx$ 5-10 km. These values suggest significant effect of the Earth rotation on the basin-scale oscillations, which should in such conditions have the form of coastal-trapped Kelvin-type waves. The coastal-trapped character of the waves is supported by higher amplitudes and more distinct vertical structure of the isotherm oscillations at the near-shore site than in the deeper part of the lake (cf Fig. c and d).

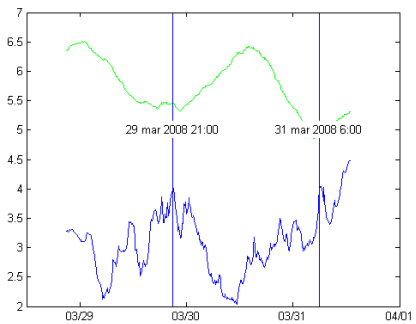

Figure 8 Evolution of the 0.8oC isotherm at the shallow (green line) and at the deep site, Lake Pääjärvi.

Comparison of the isotherm displacements at the shallow and deep sites reveals another remarkable feature of the waves, viz. the 180^o shift in the oscillations of the isotherms (see comparison of 0.8^{o}C isotherm displacements in Fig. 8). The distance between two sites coincides approximately with the half-length of the lake i.e. the *length of the basin-scale wave coincides with the lake size*. For standing basin-scale waves, the 1st "gravest" lateral mode is the sum of two waves with *wavelength twice the basin size* propagating in opposite directions. Such a wave has one crest and one trough located at the opposite sides of the lake. Hence, the observed wave appears to be of the 2nd lateral mode, i.e. has two symmetric crests/troughs at the opposite sides of the lake. Taking into account the fact that the wave speed of the ideal

Kelvin wave is the same as that of non-rotating linear seiche, the period of the *n*-th lateral mode wave can be estimated from the Merian formula:

$$T_n = \frac{2}{n}\frac{L}{C}, \qquad (1)$$

where $C = Nh$ is the wave speed, and n is the mode number. At n=2, substitution in (1) of the typical length and depth scales and the mean buoyancy frequency from the vertical temperature profiles yields period estimations close to the observed one of 33 hrs. E.g., adopting the estimations L = 7km, h = 20m, N^2 = 1e-5 s^{-2} results in $C = 6*10^{-2}$ m/s and T_2 = 32.5 hrs.

This observation suggests a remarkable qualitative difference of the basin-scale internal waves under ice from those in the open water lakes, where the 1st lateral mode always dominates. One explanation for the predominance of the 2nd lateral mode in the ice-covered lake could lie in the basin-scale distribution of the external forcing: under ice, the external forcing for basin-scale motions is provided by pressure differences between near-shore areas and the mid-part of the lake, e.g. by oscillations of the ice cover with maximum amplitude in the lake center, or by stronger heating of the shallow areas by solar radiation appearing at daily periods. This contrasts to the open-surface lakes, where seiches are created by the wind-driven horizontal gradient of the hydrostatic pressure across the entire lake with the water level rise at the downwind shore and the corresponding water level drop at the opposite upwind shore.

The observed waves reveal specific vertical structure, which is particularly noticeable at the shallow site. Three counter-phase oscillating boundaries, which can be approximately associated with the isotherms 0.74°C 0.78°C and 0.88°C (see Fig. 7) divide the water column in four layers – a structure typical for the 3rd vertical mode seiches. This 4-layered structure arises from the specific vertical temperature distribution formed to the end of the ice-covered period by both solar heating and the heat flux from the lake sediment. In the upper part of the water column two distinct layers are formed by the solar radiation penetrating the ice: the convectively mixed layer with the vertically homogeneous temperature distribution with depth of 4-5 meters, and a thin “conduction” layer just beneath the ice, where temperature rapidly increases from 0°C at the ice-water interface to that of the convectively mixed layer. In the lower part of the water column, just above the bottom, a layer of several meters depth with strong vertical temperature gradients is created by the heat inflow from the sediment. A quiescent part of the water column bounded by the sediment-heated layer below and the radiatively-heated convective layer above comprises the fourth layer. The vertical structure of this kind is inherent for relatively deep ice-covered lakes suggesting the 3rd vertical mode of internal seiches to be typical feature of ice-covered lakes.

An important consequence of the 3rd vertical mode seiches for the lateral transport is the multilayer structure of horizontal currents. The structure is recognizable in the vertical current velocity profiles recorded at the shallow site by an ADCP and averaged over the half-period of the seiche (Fig. 9): the west-east current velocity component (coinciding approximately with the main axis of the lake) has opposite directions in the neighboring layers and changes its direction at 180° within one seiche period (cf. red and black line in Fig. 9c). The structure is less pronounced in the lower layers, which are apparently affecter by the bottom friction and the near-bottom downslope currents driven by the temperature difference between shallow and deep areas of the lake. The south-north component of the velocity reveals a constant negative current with magnitudes up to 0.01 m/s, which is, apparently, a result of the lake-wide cyclonic circulation produced by the combined effect of the heat flux from the sediment and the Coriolis force.

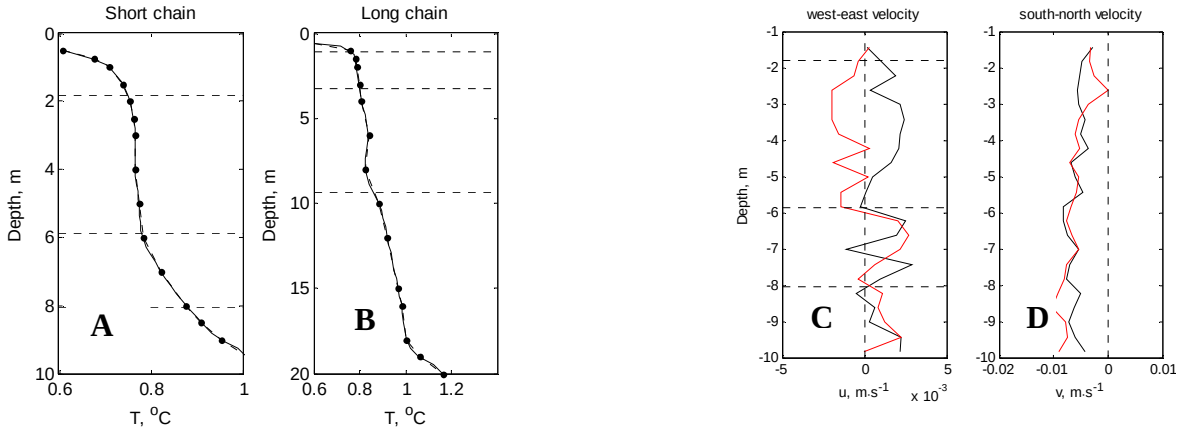

Figure 9. Four-layered structure of the 3rd vertical seiching mode (horizontal dashed lines) in the temperature profiles (A-B) and in the vertical velocity profiles (C-D). Red and black lines in Panels C-D represent velocity profiles averaged over two subsequent half-periods of the seiche.

CONCLUSIONS

The basin-scale motions in seasonally ice-covered lakes demonstrate a specific pattern, differing in many aspects from that in open surface conditions, and varying between shallow and deep lakes:

In shallow Lake Vendurskoye:

- There is a signature of surface seiching in the near-bottom temperatures conditioned, apparently, by the strong temperature gradients at the water-sediment boundary. The effect can potentially contribute to the mixing and transport between the sediment and the water column.
- Irregular appearance of the internal waves, confined within the thin (< 1 m) layer near the lake bottom. A necessary condition for internal waves of appreciable amplitude to develop is the homogeneous vertical density distribution within this layer. Therefore, in the starting phase of the ice-covered period in Lake Vendyurskoe, the internal oscillations were observed at the shallow site only, where the bottom boundary layer was vertically mixed by the downslope density currents. Although the vertical temperature gradient was permanently present near the lake bottom at the deep site in the central part of the lake, the near-bottom vertical density gradient had disappeared there in the second half of the ice-covered period, as soon as the temperature had approached the maximum density value. As a result, internal oscillations were present in the deep part of the lake from that moment to the start of the convective mixing by solar radiation.

In deep Lake Pääjärvi:

- Internal basin-scale oscillations with amplitudes up to several meters and period about 33 hours were present across the entire water column. A distinctive feature of the waves is their complex modal structure: the 2nd lateral mode and the 3rd vertical mode are clearly pronounced in the oscillations. The dominance of the 3rd vertical mode is apparently conditioned by the multilayer vertical density structure resulting from the two heating mechanisms - heat flux from the sediment and solar radiation. This fact allows suggesting high vertical seiching modes to be inherent for the majority of deep ice-covered lakes.
- Oscillations of the higher vertical modes are characterized by long periods exceeding significantly the inertial period at the lake's latitude. This suggests strong effect of the Earth rotation on the waves. The suggestion is supported by larger wave amplitudes in the shallower part of the lake. As a result, considerable wave currents develop in the near-shore area, potentially increasing mixing rates and affecting litoral-pelagial exchange.

AKNOWLEDGEMENTS

The study is the part of the research project “Heat and mass transport in seasonaly ice-covered lakes” funded by the German Research Foundation (DFG, ref KI-853/5).

REFERENCES

Kirillin, G. et al., 2009. Basin-scale internal waves in the bottom boundary layer of ice-covered Lake Muggelsee, Germany. Aq. Ecol., **43**(3), 641-651.

Malm, J. et al., 1998. Field study on currents in a shallow, ice-covered lake. Limnol/ Oceanogr., 43(7), 1669-1679.

Mironov, D. et al., 2002. Radiatively driven convection in ice-covered lakes: Observations, scaling, and a mixed layer model. J. Geophys. Res., 107(C4), doi:10.1029/2001JC000892.

Temperature driven flows in natural lakes

M.G. Wells*, M. Colman and P. Pernica

Department of Physical and Environmental Sciences, University of Toronto, Toronto, M1C1A4 Ontario, Canada

**Corresponding author, e-mail wells@utsc.utoronto.ca*

EXTENDED ABSTRACT

The strength and variability of thermal stratification can play an important role in structuring the distribution of biology in lakes. In this presentation I will discuss two important physical processes in lakes relating to the thermal stratification, namely (1) how wind driven currents can lead to internal waves in lakes and intermittent mixing water in the water column and (2) how differential cooling in the boundaries of lakes can lead to circulation due to the formation of cold gravity currents. Results from two field studies will be presented along with analouge laboratory studies.

In the first part of the talk I will present a detailed record of thermal stratification within the waters of Lake Opeongo to discuss the presence of intermittent mixing and internal waves. This lake is oligotrophic and dimictic. It is located in the Algonquin Provincial Park, Ontario, Canada (45^{o}42' N, 78^{o}22' W), with an area of 60 km^2 and mean depth of 20 m. It is typical of many hundreds of lakes located on the Canadian Shield. In order to capture the variability in internal wave dynamics in response to wind events, an array of fast response RBR temperature loggers and ADCP units were deployed from May 2009 until the autumn overturn in September 2009. The epilimnion of the lake experienced weak diurnal stratification, with typically change in 1^{o}C over the 5 m depth of the epilimnion. While this is an order of magnitude smaller than the strong stratification within the main thermocline, the presence of even a weak stratification can inhibit vertical mixing within the epilimnion and so influences the spatial distribution of plankton within the euphotic zone. Previous research in Lake Opeongo by Blukacz *et al.* (2009) has demonstrated that wind forcing strongly influences the patchiness of both phytoplankton and zooplankton in the eplimnion, on small scales of order 10 to 100 meters. Their specific findings were that for wind speeds less than 3 m/s and greater than 7 m/s, the horizontal distribution of plankton was uniform. However for intermediate wind speeds of 3 m/s - 7 m/s, they found that the distribution of zooplankton had the greatest horizontal patchiness.

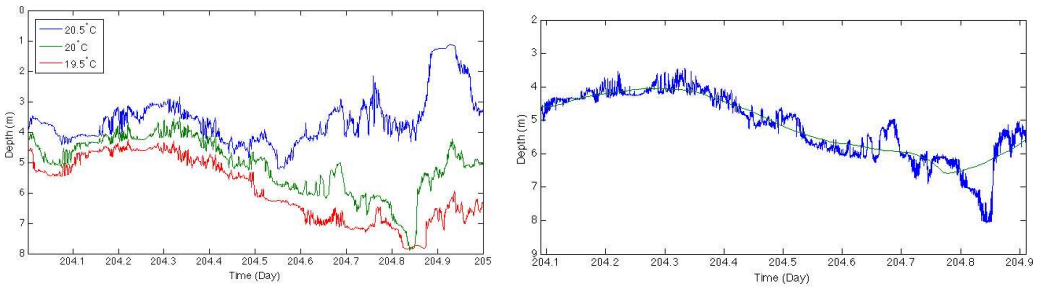

Figure1: a) Movements of isotherms during JD 204 (July 23, 2009) within the epilimnion of Lake Opeongo. b) The 20^{o}C isotherm is shown relative to the 4-hour mean depth indicating the presence of internal waves in the epilimnion.

The hypothesis that we are currently exploring is that when the eplimnion is weakly stratified, that wind forcing excites weak internal waves that locally displace vertical gradients of plankton. Figure 1a shows a typical time-series of isotherms within the epilimnion. For the day shown the water column is weakly stratified with 1°C < ΔT < 2°C over the course of the diurnal cycle, similar to 32% of the summer when ΔT >2°C. Figure 1b compares the position of the 20°C isotherm compared to the 4 hour mean. The fluctuations from the mean give an indication of the presence of internal waves. I will show how these internal waves in the weakly stratified epilimnion are related to wind speed, local gradient Richardson number and overturning events in the water column.

In the second part of the talk I will describe how the interaction of surface cooling with a sloping bathymetry can results in the generation of gravity currents. An example of this process was documented in a field study (Wells and Sherman, 2001) in 1994 –1996 in the Chaffey Reservoir, located in northeastern New South Wales, Australia (31° 21'S, 151° 89' E). We had found that for a given heat flux out of the water surface, the temperature of the water column decreases more rapidly in the shallow regions where the water column has less thermal mass than in the deep regions. The net result was the production of a cold gravity current, that transports cold, dense water from the shallow to the deep regions. In the Chaffey Reservoir such downslope flows lead to the formation of stratification, even during winter when penetrative convection is often assumed to cause complete overturning of the water column.

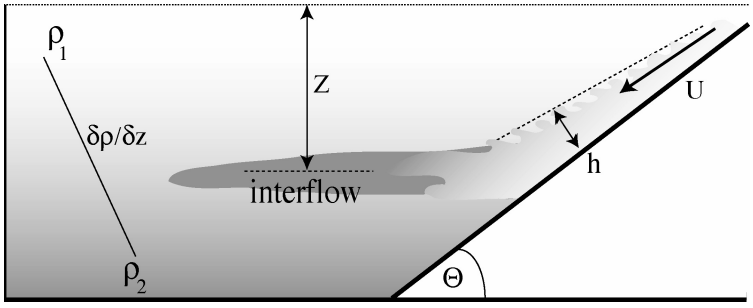

Figure 2: A sketch of a subsurface intrusion from a gravity current, with a velocity *U* and thickness *h*, flowing down a slope of angle Θ before intruding at a depth *Z* below the surface.

Similar gravity currents are seen in many other lakes, estuaries and in the coastal ocean. In a density-stratified lake or reservoir an "interflow" occurs after the gravity current separates from the boundary and intrudes into the layer where the flow is neutrally buoyant, as shown in Figure 2. The depth *Z* at which the intrusion occurs can determine where pathogens are placed, the locations of biological hot spots and whether nutrients from runoff will be emplaced in the euphotic or the benthic zones. I will present results from recent analogue studies that document how the depth of the intrusion scales with the buoyancy flux and stratification (Wells and Nadarajah, 2009) and how Coriolis forces influence the dynamics of these gravity currents (Cossu, Wells and Wåhlin 2010).

REFERENCES

Blukacz, E.A., Shuter, B.J., and Sprules, W.G. (2009) Towards understanding the relationship between wind conditions and plankton patchiness. Limn Oceanogr., **54**:1530-1540.

Cossu, R., Wells, M.G. and Wåhlin, A.K. (2010) Influence of the Coriolis force on the velocity structure of gravity currents in straight submarine channel systems. J. Geophys. Res. (under review)

Wells, M.G. and Nadarajah, P. (2009) The intrusion depth of density currents flowing into stratified water bodies. J. Phys. Oceanog. **39,** 1935–1947.

Wells, M.G. and Sherman, B. (2001) Stratification produced by surface cooling in lakes with significant shallow regions. J. Limn. and Ocean. **46,** 1747-1759

Internal wave-induced flow in shallow, stratified waters

M. Carr[1,2] and P.A. Davies[2]*

[1] *School of Mathematics and Statistics, University of St Andrews, St Andrews, KY16 9SS, UK*
[2] *Department of Civil Engineering, The University, Dundee, DD1 4HN, UK*

**Corresponding author, e-mail p.a.davies@dundee.ac.uk*

KEYWORDS
Internal waves; instability; wave breaking; stratified fluids.

EXTENDED ABSTRACT

INTRODUCTION
Internal solitary waves (ISWs) are ubiquitous features of lakes, semi-enclosed seas and coastal waters. They propagate as waves of depression/elevation, depending on whether the pycnocline is located nearer to the surface/bed than the bed/surface of the stratified water body in question. If the depth H of the water body is comparable with the amplitude of the wave, the passage of the ISW is associated with the generation of transient boundary currents at the bed (Carr & Davies, 2006) and these may become unstable. The manifestations of the instability, namely the production of arrays of vortices (Carr *et al*, 2008a) that propagate vertically through the water column, have implications for vertical mixing and sediment suspension. For sufficiently large amplitude ISWs, vertical mixing is also promoted by internal wave breaking by shear or convective instability at the pycnocline (Fructus *et al*, 2009; Carr *et al*, 2008b). The present study reviews recent experimental evidence of boundary layer instability and boundary layer separation caused by irregularities in bottom topography.

METHODS
Laboratory experiments were carried out using a long channel containing a stably-stratified, 3-layer system established with brine and freshwater mixtures and consisting of upper and lower layers of density ρ_1 and ρ_3 with undisturbed thickness h_1 and h_2 and separated by a pycnocline layer of thickness h_2 within which the density varied linearly between the upper and lower values. A gate inserted close to one end of the channel contained an excess volume of the upper fluid such that when the gate was removed an ISW propagated along the channel (Carr & Davies, 2006) with a prescribed phase velocity and amplitude. (Waves of depression or elevation could be chosen by suitable combinations of the layer thickness ratios). For the present cases, the bottom surface of the channel consisted of a flat plane and a section of transparent corrugated material over which the wave passed. Neutrally-buoyant tracer particles suspended within the fluid enabled the velocity fields within the fluid system to be visualised in a vertical plane illuminated from below by a thin sheet of light and recorded from the side by a digital camera. *DigiFlow* software was used to process the data.

RESULTS AND DISCUSSION
Fig 1 shows the disturbance field generated by the passage over the corrugated bottom surface of an internal solitary wave of depression, for two different elapsed times. The wave is travelling from left to right so that the interior flow is to the right (left) in the upper (lower)

layer and the boundary jet (close to $z/H = 0$) is directed to the right. In the early stages (Fig 1a) the interior flow is seen to generate a series of lee vortices behind the corrugations, while at longer elapsed times (Fig 1b) the boundary jet detaches the leading eddy and propels it vertically through the water column. For sufficiently large amplitude waves and corrugations, the detached vortex is able to disrupt the pycnocline and promote vertical mixing.

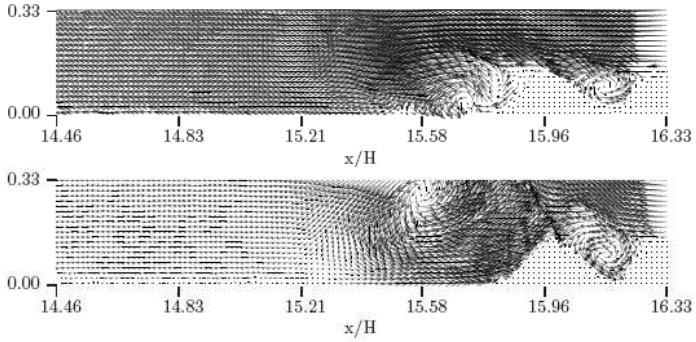

Figure1: Velocity field for an ISW of depression propagating (L to R) in a 3-layer fluid of depth H with celerity c over a corrugated bed, for elapsed times ct/H = (a) 16.8, (b) 18.1

In the case of ISWs of elevation, no vortex is formed at the leading edge and those formed downstream fill the troughs of the corrugations and propagate upwards with time. They deform the pycnocline after the wave has passed (when the pycnocline itself has returned to its undisturbed level). For sufficiently large amplitude corrugations – in particular, when the peaks reach or penetrate the pycnocline at rest - short internal waves are generated by the propagating ISW. When these waves are large enough, they grow and break as they propagate up and over the ISW. The resulting billows mix the pycnocline significantly on the downstream face of the ISW and behind the wave (see Fig 2).

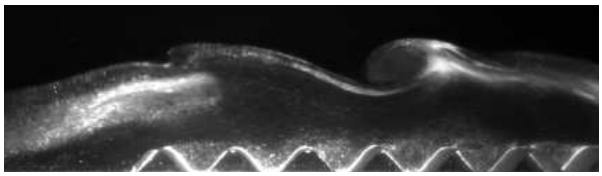

Figure 2: Photograph showing deformation of an ISW of elevation by bottom corrugations.

When the laboratory data are compared with numerical simulations using the model of Stastna and Lamb (2008), good qualitative agreement is obtained.

REFERENCES

Carr M. and Davies, P. A. (2006). The motion of an internal solitary wave of depression over a fixed bottom boundary in a shallow two-layer fluid. *Physics of Fluids*, **18**, 016601.

Carr M., Davies P. A. and Shivaram P. (2008a). Experimental evidence of internal solitary wave-induced global instability in shallow water benthic boundary layers. *Physics of Fluids* **20**, 066603.

Carr M., Fructus D., Grue J., Jansen A. and Davies P. A. (2008b). Convectively-induced shear instability in large amplitude internal solitary waves. *Physics of Fluids*, **20**, 126601.

Fructus D., Carr M., Grue J., Jensen A. and Davies P.A. (2009). Shear induced breaking of large internal solitary waves. *J. Fluid Mech*., **620**, 1-29.

Stastna M. and Lamb K.G. (2008). Sediment resuspension mechanisms associated with internal waves in coastal waters. *J. Geophys. Res*. **113**, C10016.

Spatial and temporal variability of turbulent hot spots in a large stratified lake

D. Bouffard[1]*, L. Boegman[1] and R.R. Yerubandi[2]

[1] *Department of Civil Engineering, Queen's University, K7L 3N6, Kingston, Ontario, Canada*
[2] *Environment Canada, Water Science and Technology, National Water Research Institute, 867 Lakeshore Road, L7R 4A6, Burlington, Ontario, Canada*

**Corresponding author, e-mail damien.bouffard@queensu.ca*

KEYWORDS
Microstructure profiles, Poincaré waves, SCAMP, Turbulence

EXTENDED ABSTRACT

INTRODUCTION
Recent temperature microstructure profiles from central Lake Erie have shown more unstable small scale density inversions than expected near the depth of the thermocline. These observations raise questions about the required spatial and temporal sampling to capture mixing events. The primary objective of the study is to analyze the spatial and temporal variability of turbulent mixing events in Lake Erie.

METHODS
Data is presented from two intensive measuring campaigns during the summers of 2008 and 2009 in Lake Erie. The data includes that from 13 moorings with high-frequency temperature loggers and acoustic Doppler current profilers (ADCP) and more than 600 SCAMP microstructure profiles.

RESULTS
SCAMP microstructure temperature profiles have been carried out along a longitudinal transect along the sloping lake bed from the western to central basins. This field work, thus, provides data to investigate the role of sloping boundaries in enhancing turbulence and mixing in the nearshore region (e.g. Lorke, 2007; MacIntyre et al., 2009). Dissipation of turbulent kinetic energy in the bottom boundary layer was not as elevated as measurements made in small lakes (e.g. Wüest et al., 2000). Moreover, analysis of dissipation rates in the thermocline, with respect to the nearshore or offshore location (Fig. 1), shows that the question of enhanced turbulence induced by the large scale internal wave field has to be addressed especially in the offshore region.

The main wind driven oscillation was identified as an anticyclonic Poincaré wave in this region of Lake Erie (e.g. Yerubandi et al., 2008). Our observations show that overturning events with a frequency near the Brunt Väisälä frequency are in phase with the crest of the Poincaré wave. These events had enhanced rates of dissipation of turbulent kinetic energy and

Poincaré wave induced shear. Due to the coarse spatial and temporal nature of microstructure measurements, this linkage between the large-scale internal waves and the small scale turbulence is of prime importance for turbulence modelling. Poincaré waves may be used to infer mixing rated for transport processes in the lake interior.

Some very energetic turbulence hot spots were identified and are tentatively explained by interactions between Poincaré waves and other important processes in Lake Erie such as upwelling and surface seiches. This work will provide a spatial and temporal map of turbulence which has never been done for large lakes.

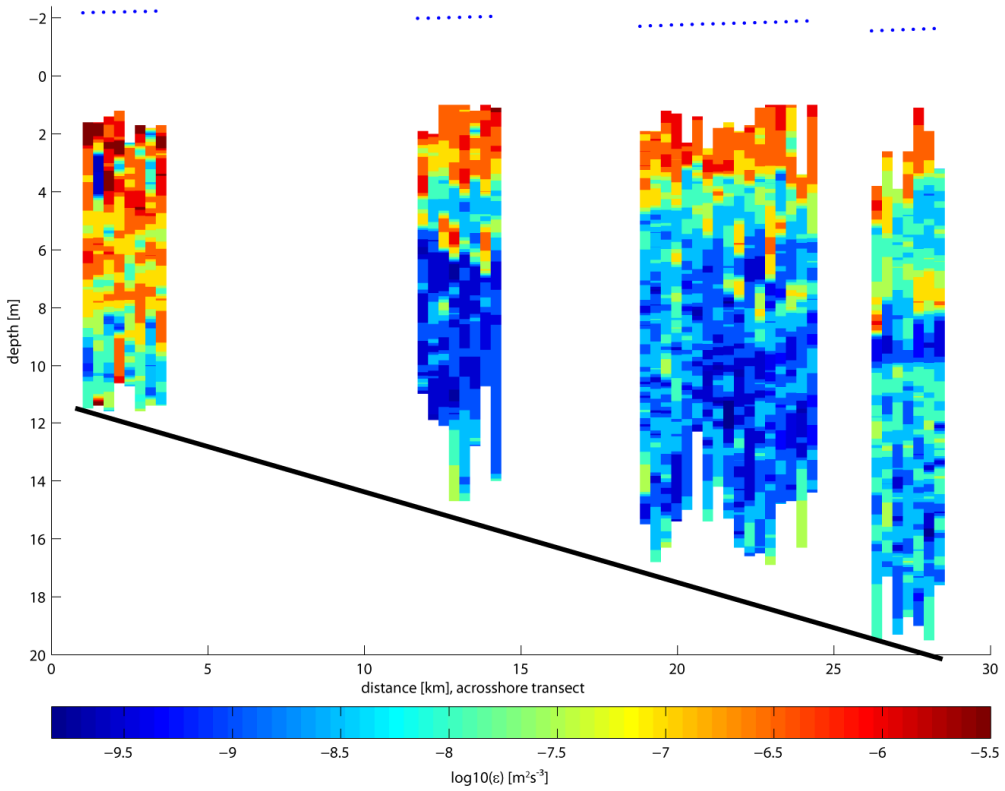

Figure 1: Dissipation map of acrosshore transect for 22 July 2008

REFERENCES

Lorke, A. (2007), Boundary mixing in the thermocline of a large lake, J. Geophys. Res., 112, C09019.

MacIntyre, S., Clark, J., Jellison, R. and Fram, J.P. (2009). Turbulent mixing induced by nonlinear internal waves in Mono Lake, California Limnol. Oceanogr., 54(6), 2255–2272.

Wüest, A., Piepke, G., and Van Senden, D.C., (2000). Turbulent kinetic energy balance as a tool for estimating vertical diffusivity in wind-forced stratified waters. Limnol. Oceanogr., 45, 1388–1400.

Yerubandi, R.R., Hawley, N., Charlton, M.N. and Schertzer W.M. (2008). Physical processes and hypoxia in the central basin of Lake Erie. Limnol. Oceanogr., 53(5), 2007–2020.

Vertical structure of the ex-fjord Powell Lake in British Columbia

Alfred Wüest[1,2]*, Roger Pieters[3], Rich Pawlowicz[3]

[1] *Eawag, Surface Waters - Research and Management, Kastanienbaum, CH-6047, Switzerland*
[2] *Institute of Biogeochemistry and Pollutant Dynamics, ETH, CH-8092 Zurich, Switzerland*
[3] *Ocean Dynamics Laboratory, Department of Earth and Ocean Sciences, University of British Columbia, Vancouver, B.C. CANADA V6T 1Z4*

**Corresponding author, e-mail alfred.wueest@eawag.ch*

EXTENDED ABSTRACT

Powell Lake, located ~100 km northwest of Vancouver on the Sunshine Coast of British Columbia (Canada), is a coastal ex-fjord containing at large depth ancient seawater trapped ~11,500 ± 1,000 yr BP during the early Holocene / late Pleistocene. As a result of the glacio-isostatic rebound of the Pacific Northwest, the lake surface was lifted by ~45 m asl (today ~55 m asl due to hydropower damming) and the former oceanic fjord is now separated by a rocky sill from the Strait of Georgia. Today, the lake covers an area of ~100 km^2 (~50/2 km long/wide), reaches up to ~360 m deep and consists of four sill-separated subbasins, which have very different characteristics.

The two most upstream North (McMillan) and West (Olsen) basins show the temperature-salinity-density characteristics of a usual low-saline, oligotrophic water body at temperate latitudes, including low temperature and high oxygen levels in the deep-water (indicating frequent deep convective mixing in winter). The two most downstream East and South basins show high deep-water salinity and temperature of up to ~17 psu and up to 9.4 ^{o}C, respectively and the water columns are permanently density-stratified (meromictic). The completely different fate of the long-term stratifications of the four basins is due to the hydrologic setting: Whereas in the upper two basins, sporadic particle-laden (turbid) energetic streamflows from the steep catchment intrude the deep-water and had therefore removed the salinity, the lower two basins have very small catchments and the weak direct runoff was not capable to erode the deep-water salinity. As a result, only diffusion has gradually removed salinity and therefore even today, the deepest layers contain still more than half of the original ocean salinity. The remaining ocean salts in the deep-water maintain high water column stability and therefore geothermal heat and biogenic gases (such as CO_2 and CH_4) have accumulated in the deepest 100 m of the water bodies over the ~11,000 yr since deep-water isolation.

In the talk, preliminary analysis of recent CTD and geochemical profiles will be presented and compared to profiles collected in the early 1980es and compared to the “double diffusive sisters” Lake Kivu and Lake Sakinaw (British Columbia).

REFERENCES

Osborn TR. (1973). Temperature microstructure in Powel Lake. J Phys Oceanogr 3 : 302 - 307

Perry, KA; Pedersen, TF. (1993). Sulfur speciation and pyrite formation in meromictic ex-fjords. Geochimica et Cosmochimica Acta, 57 (18): 4405-4418.

Reynolds, RC. (1978). Polyphenol inhibition of calcite precipitation in Lake Powell, Limnology and Oceanography 23 (4): 585-597.

Sanderson, B; Perry, K; Pedersen, T (1986). Vertical diffusion in meromictic Powell Lake, British-Columbia, J. of Geophysical Research Oceans, , 91 (C6): 7647-7655.

Toth DJ. and A Lerman (1975). Stratified lake and oceanic brine: Salt movement and time limits of existence. Limnology and Oceanography 20(5): 715-728.

Wilkin RT, Barnes HL (1997). Pyrite formation in an anoxic estuarine basin. Americal Journal of Science, 297 (6): 620-650.

Williams PM, WH Mathews and GL Pickard (1961). A lake in British Columbia containing old sea water. NATURE 191: 830-832.

Variability in the circulation in Kalbaksfjord, Faroe Islands

K. Simonsen[1]*, G. á Norði[2] and E. Gaard[2]

[1] *The University of the Faroe Islands, Nóatún 3, FO 100 Torshavn, Faroe Islands.*
[2] *The Faroe Marine Research Institute, Nóatún 1, FO 100 Torshavn, Faroe Islands.*

**Corresponding author, e-mail knuds@setur.fo*

KEYWORDS
Fjord circulation, wind driven circulation, fish farming.

EXTENDED ABSTRACT

INTRODUCTION
The fish farming industry in the Faroe Islands has grown to produce more than 50.000 tons of salmon in 2009, and plans are to increase the production. Due to the geographical position of the islands in the middle of the North Atlantic, the coast of the Faroes are relatively exposed for ocean waves. Consequently the farming is going on in the very limited areas of the sheltered fjords, and it is of vital interest of all involved parties that the farming is not affecting the environment in the fjords beyond sustainable limits. In order to estimate the production capacity of each of the fjords, an increased understanding of the circulation in the fjords are required.

One of these fjords are the 6.6 km long and 0.5-1.7 km wide Kalbaksfjord, which entrance is into the strait between the two main islands in the Faroes. The maximum depth of Kalbaksfjord is about 60 m and at the entrance is a sill with a maximum depth of 40 m. The tidal currents are generally quite strong in the sounds between the islands in the Faroes, with a dominating semi diurnal signal. However, the area at the entrance to the Kalbaksfjord is characterized by an semi-amphidromy in the semi-diurnal constituents, which leads to a very modest contribution from the tides in the circulation.

The primary production in this fjord is high, about 335 $gCm^{-2}y^{-1}$, but large variations occur during the production period (Gaard et al., 2010). This fjord also hosts a fish farming plant, which produce 2000-2500 tonnes during 18-24 months cycles.

In order to increase the understanding of the fjord circulation, including the variation in the natural production, and those also the fish farming production capacity of the fjord, two current profiler deployments were done in spring 2006.

METHODS
Current profiling
In the period from 22 March to 1 June, 2006, a RDI 300 kHz Workhorse Acoustic Current Doppler Profiler (ADCP) was mounted on the bottom at 38 m depth at station C1 and in the period from 22 March to 25 April, 2006, an AADI 600 kHz Recording Doppler Current Profiler (RDCP) was mounted at 48 m at station C2. Both instruments were located on the northern slope and were measuring in 2 m vertical bins (Figure 1).

Meteorological observations.
General meteorological observations from a station in Torshavn (T) about 4 km south of fjord and wind measurements from a road station at Sund (S) at the southern coast of the fjord were kindly made available by the Danish Metrological Institute and the Office for Public Works in the Faroes, respectivily.

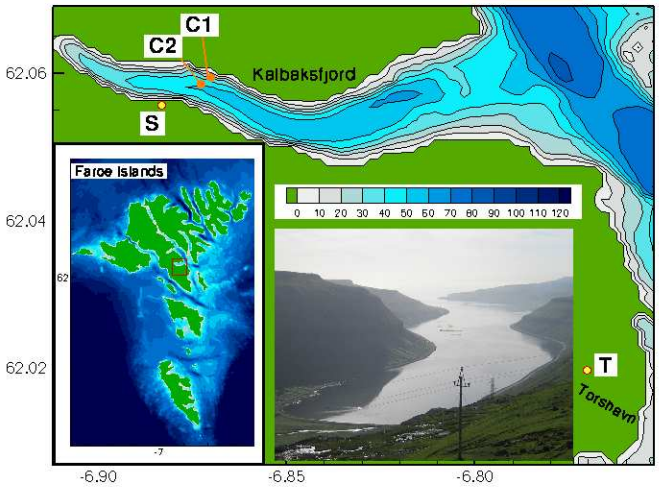

Figure 1. Bathymetric map of the Kalbaksfjord. Inserted is a map of the Faroe Islands and a photo of the fjord.

RESULTS AND DISCUSSION

The measured currents were generally of order 2-6 cm s^{-1} and only occasionally the currents exceeded 10 cm s^{-1}.

At both station the current profiles showed a persistent flow into the fjord at all depths. Due to continuity a similar, although not documented, outwards flow must exist along the southern coast, which implies a cyclonic circulation in the inner part of the fjord. In addition, the current also include a week diurnal tidal signal.

Due to the surrounding terrain the wind at station S is more unidirectional towards either East or West than measured at station T. However, it may be speculated that the observation at station T are more representative for outer part of fjord.

A relatively high correllation was found between the daily averaged easterly wind, i.e. into the fjord, at station S and east going current at particular at station C1, implying an anticyclonic circulation during these events, with a duration between one day and one week. On the contrary westerly wind reinforces the residual cyclonic circulation. The signal in the current lags the wind with approximately one day.

Below about 30 m depth at station C2 the flow was generally into fjord, but with frequent events of reduced or even outgoing flow. Not all these events are directly related to variations in the wind field.

It is not clear if the observed flow is part of a closed circulation loop in the inner Kalbaksfjord, or if it is directly related to the water exchange with the area outside the fjord. However, it is speculated that the cyclonic flow pattern do have a role in elevating nutrients from the bottom water into the production zone, and those partly explains the high primary production in this fjord. The observed correlation between the wind and fjord circulation may also provide an additional link between the changeable weather in the Faroes and the variable primary fjord production.

REFERENCES

Gaard, E., á Norði, G., and Simonsen, K., (2010), Environmental effects on phytoplankton production in a Faroese fjord, Subm. to Marine Biology Research.

Effect of submerged aquatic vegetation on turbulence induced by an oscillating grid: Application of a k-ε model

Dolors Pujol, Jordi Colomer, Teresa Serra and Xavier Casamitjana*

Department of Physics, University of Girona, 17071 Girona, Catalonia, Spain
**Corresponding author's e-mail: xavier.casamitjana@udg.edu*

ABSTRACT
Oscillating-grid turbulence (OGT) in a homogeneous fluid has been widely investigated. Here we present results of an experiment in which two different constructed canopies were placed at the bottom of a water tank. The first canopy was rigid, made of PVC cylinders, and the second was semi-rigid, made of nylon threads. We quantify the vertical distribution of turbulent kinetic energy (TKE), measured by an acoustic Doppler velocimeter. In our 30 experiments we used seven solid plant fractions (SPFs), three stem diameters (d) and three oscillation grid frequencies (f). Two source terms ($\sim(TKE)^{3/2}$) were added to a classical k-ε turbulence model to account for canopy dissipation. Results of the model show a good agreement with experimental data.

KEYWORDS
vegetation canopy, oscillating grid turbulence, k-ε turbulence model, turbulent kinetic energy, dissipation

INTRODUCTION
Much research has been carried out in laboratory flumes and in the field to determine the effect of emergent and submerged canopies (Mendez and Losada, 1999; Nepf, 1999; Nepf and Vivoni, 2000; Poggy et al., 2004). In all cases, the conversion of mean kinetic energy to turbulent kinetic energy follows from the interaction of the main flow with the canopy elements. This mechanical turbulence is caused by the wake turbulence generated locally by the stems, and the shear turbulence generated by the local velocity gradient (Neumeier, 2007). However, there are many field situations where there is not a predominant mean flow. For example, turbulence created by wind stirring or night convection in lakes and wetlands can interact with the plants and create an additional source of dissipation to produce turbulent kinetic energy. These situations can be simulated in the laboratory with oscillating-grid turbulence (OGT).

The turbulence generated by grids has been extensively studied, both theoretically and experimentally, in the laboratory. The design has been used to solve many scientific and engineering problems, such as the resuspension of sediment and transport, the mixing across density interfaces in stratified flows like thermoclines or haloclines (Hopfinger and Toly, 1976; Nokes, 1988), mass transfer across a shear-free water-air interface (Brumley and Jirka, 1987) and aggregation dynamics in natural and engineered systems (Serra et al, 2008). In the present work we extend the use of OGT to study the interaction of the TKE generated by the grid with two artificially constructed canopies: one rigid and one semi-rigid.

METHODS

The experiments were conducted with an OGT (Oscillating grid turbulence; Fig 1) that consisted of a Plexiglas box with interior dimensions of 28 x 28 x 49 cm. A Plexiglas grid was fitted over the top of the tank at a distance of z_0 = 0.02 m from the water surface. The square, 1 cm thick grid was composed of 5 x 5 bars, with a width between the bars of M = 0.05 m. It was placed horizontally, and oscillated vertically with a fixed stroke of s = 0.05 m, and variable frequencies of f =0.8, 1.6 and 2.8 Hz. A clearance of 5 mm between the sidewalls and the grid was maintained. The grid was suspended inside the tank at a height of 0.365 m from its bottom and was driven by a variable-speed motor located outside the tank.

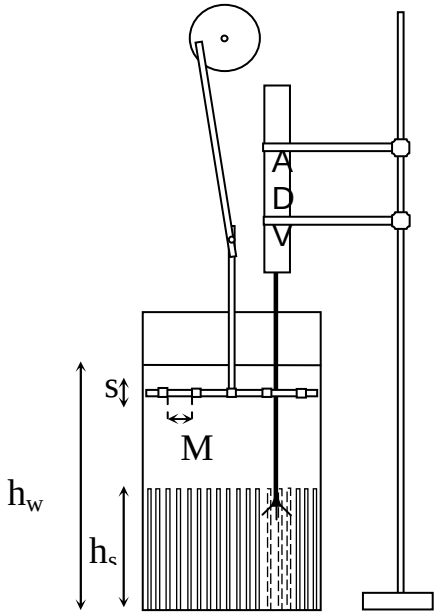

Figure 1: Schematic view of the laboratory experiment: (a) the structure of the device used in this study, where h_w is the height of the water column (0.41m); h_s is the height of the stem (0.17m) and s is the stroke of the grid situated at the top (0.05m).

Flow velocities were recorded with an acoustic Doppler velocimeter (ADV) (the Sontek/YSI 16-MHz MicroADV). The ADV has three acoustic receivers and one acoustic transmitter, and provides water velocity measurements in three directions: two horizontal flow components (u and v) and a vertical component (w). The acoustic frequency was 16 MHz, the sampling volume was 0.09 cm^3 and the distance to the sampling volume was 5 cm. The electronic noise of the measurements was smaller than the natural fluctuations caused by the turbulence. The ADV, which was operated manually, was mounted on a movable vertical frame so it could acquire single point measurements. For all experiments the ADV was placed at 7 cm og one side wall (1.4 mesh size) and at 12 cm from the other side wall (2.4 mesh size). In addition, the mesh endings were designed to not produce recirculation. For each experiment, a vertical turbulence profile was taken over a height of 0.05 - 0.25 m, with 13 height positions in total, from the bottom of the tank.

The rigid canopy consisted of rigid cylinders made of PVC. The density of the canopy was implemented by four different SPFs (the fractional plant area at the bottom occupied by stems) with values of 5%, 10%, 15% and 25%. The distribution of each SPF was made using a randomisation function. Three diameter values (d = 4mm, 6mm and 10 mm) were also used. The semi-rigid canopy was made of nylon threads, each 1.6 mm in diameter, stacked together at the base. Measured SPF's at the base of the canopy were 5%, 8% and 10%. It needs to be

pointed out that the SPF at the top of the canopy can be very different due to the induced waving of the stems.

MODEL

A standard k-epsilon model is used to model the vertical transport of TKE from the grid and through the vegetation. The governing equations are:

$$\frac{\partial k}{\partial t} = \frac{\partial}{\partial z}\left[\frac{\nu_t}{\sigma_k}\frac{\partial k}{\partial z}\right] - \varepsilon - S_k \qquad (1)$$

$$\frac{\partial \varepsilon}{\partial t} = \frac{\partial}{\partial z}\left[\frac{\nu_t}{\sigma_\varepsilon}\frac{\partial \varepsilon}{\partial z}\right] - C_2\frac{\varepsilon^2}{k} + S_\varepsilon \qquad (2)$$

$$\nu_t = C_\mu \frac{k^2}{\varepsilon} \qquad (3)$$

where k is the turbulent kinetic energy (TKE), ε is the dissipation rate, ν_t the eddy viscosity, z is the vertical coordinate, t is the time and σ_k (=1.0), σ_ε(=1.3), C_2 (=1.92) and C_μ (=0.09) are constants set up to widely accepted values. Apart from the canopy terms, S, these equations are standard. The term S_k is a TKE sink and accounts for the dissipation induced by canopy elements that short circuit the turbulence cascade. S_ε is analogous to S_κ but for the dissipation equation. Different models for S_κ and S_ε have been proposed for canopy air flows; however, these models have little physical basis beyond dimensional arguments (Sanz, 2002). We choose the simplest forms for both:

$$S_k = \alpha a k^{3/2} \qquad S_\varepsilon = \beta\frac{\varepsilon}{k}S_k \qquad (4)$$

where S_ε has been modelled as a logical extension of Kolmogorov's relation; a is the projected plant area per unit volume in the flow direction (Nepf, 1999); and α and β are dimensionless coefficients with no clear physical basis (Green, 1992). We chose β=1 and α was adjusted in order to fit the model with experimental data.

The coordinate z is taken positive downwards with its origin at the first measured value of TKE, which we take as k_o. Then the boundary conditions are:

$k=k_o$ $\varepsilon=\varepsilon_o$ at z=0

$\frac{\partial k}{\partial z} = 0$ $\frac{\partial \varepsilon}{\partial z} = 0$ at z = z_b (where z_b corresponds to the bottom of the tank).

The equations (1) - (4) are solved with the finite difference solver *pdepe*, implemented in MATLAB. As we do not know the value ε_o, we estimate as follows: for three different values of the grid frequency (0.8 Hz , 1.6 Hz and 2.8 Hz), values of ε_o were chosen in such a way that the experimental data fitted the theoretical curve. Fig. 2 shows the simulated steady state values, reached a few minutes after the initial time value (t = 0). The plot of k_o with the values obtained for ε_o showed a very good correlation (R^2 = 0.99) with a potential function $\varepsilon_o \sim k_o^{1.6}$.

This correlation is similar to the one found by Matsunaga et al. (1999), who found a value of 1.7 for the exponent of k_o. The potential function is then used to estimate the values of ε_o for all the simulations.

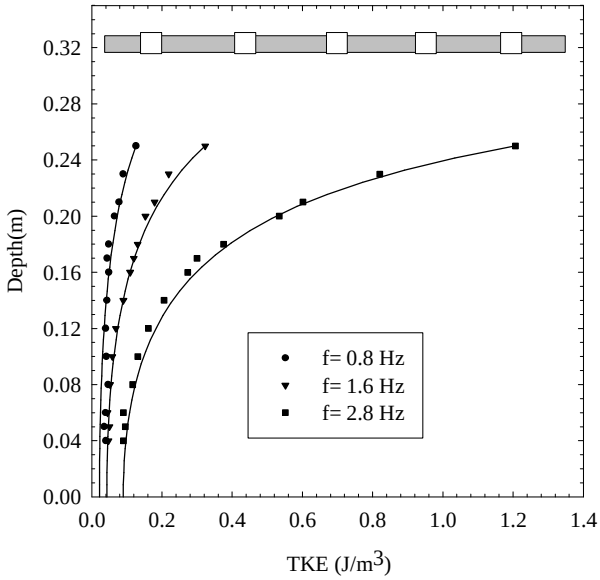

Figure 2: Experimental TKE profile with no canopy at frequencies of 0.8Hz (circles), 1.6 Hz (triangles) and 2.8 Hz (squares). Continuous lines are the predicted model values for the three cases. The mesh position is also shown.

RESULTS

ΔTKE values for different experiments are presented in Table 1. ΔTKE is the percentage difference between samples, at the same depth, corresponding to TKE with and without plants. One cm above the constructed canopy (hereafter hs+1), the ΔTKE was greatest and always positive, increasing with stem diameter, SPF and *f*. One cm below the top of the canopy (hereafter hs- 1), ΔTKE was positive for the rigid canopy and negative for the semi-rigid one. Down in the canopy, the ΔTKE suffered a progressive decrease, and well inside the canopy (hereafter hs/2, half the height of the stems), ΔTKE was nearly always negative.

In our 30 experiments, the largest TKE values were found above the constructed canopies. This result, and the fact that the TKE increased with the SPF, can be explained in terms of the TKE being redistributed at a lower volume compared to in the 'canopy-free' experiment, due to the presence of the constructed canopy. Most of the energy was concentrated above the canopy, and therefore the vegetation acted as a 'false rough floor' for the flow.

On the other hand, well inside the constructed canopies, at hs/2, the SPF was not the only variable, thereby reducing the TKE, the stem diameter also played an important role in dissipating turbulence. Specifically, the reduction in turbulence, or sheltering produced by the canopy, was enhanced as the stem diameter decreased and the SPF of the canopies increased.

Experimental results together with results of the model are presented in Fig. 3. For each graph there are two runs. In the first one the sources S (Equation 4), corresponding to canopy dissipation, were taken into account, while in the second they were not. As can be seen, the k-ε model solves the issue of canopy dissipation very well. The first three figures correspond to cases where the SPF = 25% and the diameters are of 4 mm, 6 mm and 10 mm. For the rigid canopy the decrease in the TKE at the base of the canopy is ~ 40% - 70%, except for where

the SPF = 5%, when dissipation is very small. For the semi-rigid canopy, decreases are considerably higher (see Table 2). The smallest diameter values gave the highest dissipation values. Table 2 differs from Table 1 because in Table 1 we compare experimental values with the values of Figure 2 with no canopy; in Table 2 we compare values of a model with canopy dissipation (very similar to experimental values) with values of a model with no canopy dissipation.

Fig. 4 is the same as Fig. 3 but with the semi-rigid constructed canopy. Here, dissipation at the base of the canopy is higher (Table 2). Two factors account for this behaviour. First, SPF values for semi-rigid canopies were calculated at their base. However, due to the morphology of the semi-rigid stems, where the thick stem at the base of the plant gradually divides at the top and its branches merge with the branches of its neighbours, the SPF on top of the canopy increases considerably. Second, we have seen that SPF increases dissipation; the waving generated in the stem motion introduces an additional form.

Values of α (Table 2) are between 0.5 and 4, and although there is not a clear physical interpretation of the meaning of this constant, α seems to decrease with the diameter and increase in line with the SPF. Its behaviour is related to the short circuiting of the energy cascade induced by the canopy. When turbulence eddies reach the top of the canopy, some of them will break up and cascade down to eddies of smaller diameter, eventually increasing the dissipation.

CONCLUSIONS

The canopy effects produced by OGT can be summarized as follows:

1. TKE on top of the canopy is higher than in a 'canopy-free' experiment. In fact, the top of the canopy "reflects" a certain amount of TKE, which is redistributed at a lower volume. Consequently, TKE increases.

2. OGT turbulence in a homogeneous fluid is an equilibrium between the diffusion of TKE and the dissipation rate of the energy. The presence of the canopy increases the dissipation by an amount of $\alpha a(TKE)^{3/2}$, where a is the projected plant density per unit volume in the flow direction. The coefficient α has no clear physical basis, but is related to the short circuiting of the turbulence cascade.

3. Dissipation increases with the semi-rigid plants. Two factors account for this behaviour: the increase in SPF in a vertical direction due to the movements of the plants, and the extra dissipation introduced by the waving of the plants.

Table 1: Summary of the 30 different situations studied with different SPFs, diameters and canopy models (R = rigid canopy model and SR = semi-rigid canopy model). For each situation the oscillation frequencies were 0.8, 1.6 and 2.8 Hz. The height of the plants was 17 cm. Table 2: α coefficient in Equation (4) and TKE reduction at the base of the canopy in the cases of Fig. 3 and 4. In all cases f = 2.8Hz.

			1.6 Hz			2.8 Hz		
	SPF (%)	d (mm)	h_s+1	h_s-1	h_s/2	h_s+1	h_s-1	h_s/2
RIGID CANOPY	5	4	19.6	27.9	-12.8	6.9	18.9	3.8
		6	20.0	35.2	-3.4	10.1	43.5	-1.9
		10	22.4	53.4	18.5	9.9	38.2	16.7
	10	4	16.5	20.0	-18.8	4.6	10.7	-31.9
		6	18.6	23.2	-1.06	12.8	28.6	-26.8
		10	24.6	41.6	-4.4	14.9	51.1	-7.6
	15	4	26.1	8.9	-26.0	6.9	0.4	-33.7
		6	40.6	21.5	-25.4	23.9	21.5	-39.5
		10	46.3	45.8	-6.4	29.5	43.3	-4.9
	25	4	42.0	-3.2	-28.8	12.2	-0.9	-50.7
		6	35.2	0.9	-30.0	29.1	25.6	-50.8
		10	55.9	37.0	-14.0	56.2	37.9	-4.2
SEMI RIGID CANOPY	5	4	25.5	-3.2	-18.2	12.2	-13.9	-34.5
	8		28.2	-5.0	-25.9	17.8	-15.0	-13.9
	10		35.7	-22.9	-34.6	36.5	-13.9	-52.9

Table 2: α coefficient in equation (4) and TKE reduction at the base of the canopy for the cases of Figures 3 and 4. All de cases correspond to f=2.8Hz

	SPF (%)	d (mm)	α	TKE
RIGID	25	4	0.7	62
		6	0.7	65
		10	0.4	42
	5	6	0.3	5
	15	6	1.1	65
SEMIRIGID	5	4	3.4	188
	10	4	3.4	527

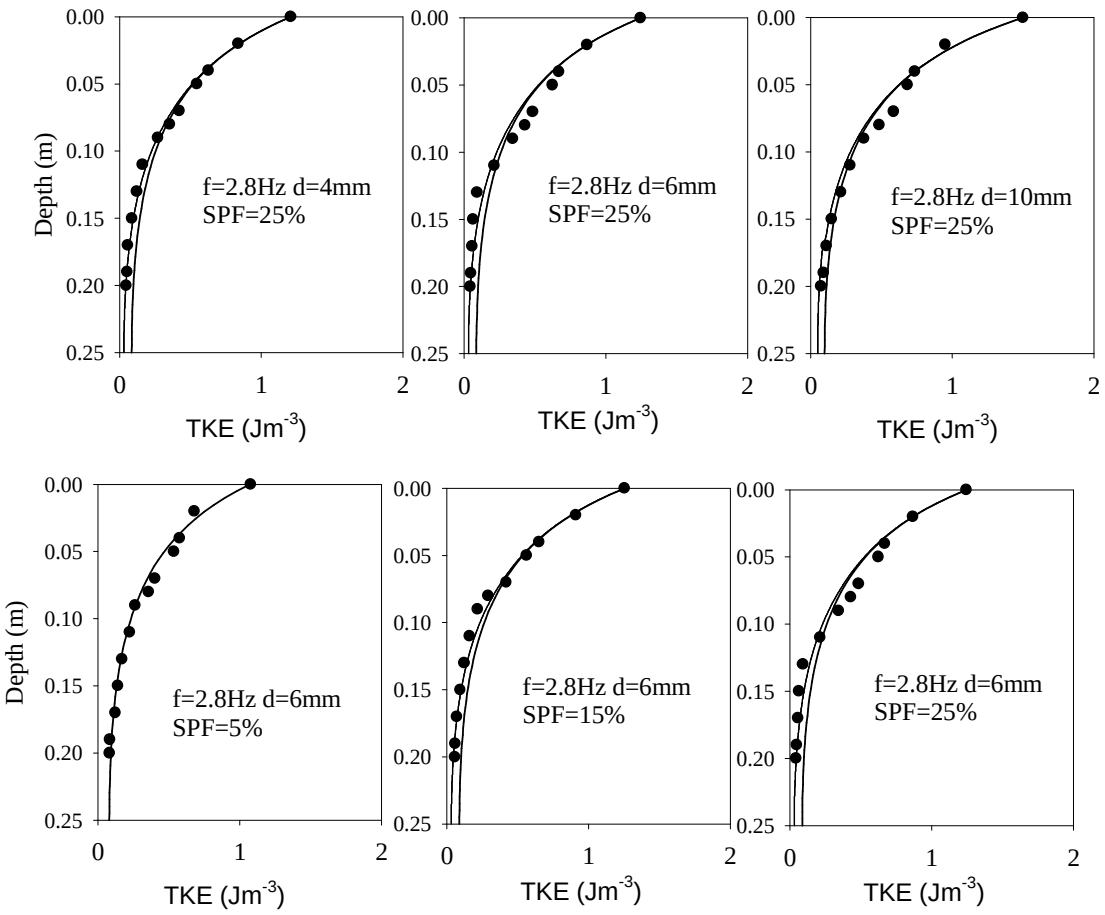

Figure 3: Experimental TKE profiles for the rigid canopy experiments (round circles) and predicted model profiles (continuous lines), for two cases: a k-ε model with source terms (see Equation 4), and a model with no sources. The best fit is provided by the model with sources.

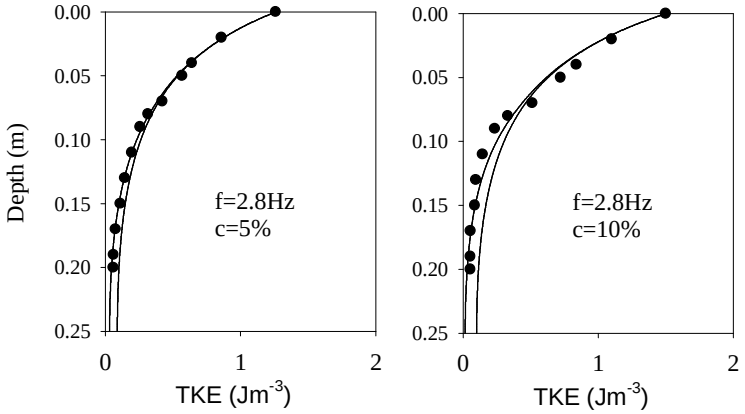

Figure 4: Experimental TKE profiles for the semi-rigid canopy experiments (round circles) and predicted model profiles (continuous lines), for two cases: a k-ε model with source terms (see Equation 4), and a model with no sources. The best fit is provided by the model with sources.

REFERENCES

Brumley, B.H., Jirka, G.H., 1987. Near-surface turbulence in a grid-stirred tank. J. Fluid Mech. 183, 235-263.

Green, S.R.,1992,. Modeling Turbulent Air Flows in a Stand of Widely-Spaced Trees, Phoenics J.5, 294-312

Hopfinger, E.J., Toly, J.A., 1976. Spatially decaying turbulence and its relation to mixing across density interfaces. J. Fluid Mech. 78, 155-175.

Matsunaga, N., Sugihara, Y., Komatsu, T., Masuda, A., 1999. Quantitative properties of oscillating-grid turbulence in a homogeneous fluid. Fluid Dyn. Res. 25, 147-165.

Mendez F.J. and Losada, I.J, 1999 Hydrodynamics induced by wind waves in a vegetation Field. Journal of Geophysical Research, 104, C8, 18383-18396.

Nokes, R.I., 1988. On the entrainment rate across a density interface. J. Fluid Mech. 188, 185-204.

Nepf, H.M., 1999. Drag, turbulence, and diffusion in flow through emergent vegetation. Water Resour. Res. 35, 479-489.

Nepf, H.M., Vivoni, E.R., 2000. Flow structure in depth-limited, vegetated flow. J. Geophys. Res. 105, 28547-28557.

Neumeier, U., 2007. Velocity and turbulence variations at the edge of saltmarshes. Cont. Shelf Res. 27, 1046-1059.

Poggi, D., Katul, G.G., Albertson, J.D., 2004. Momentum transfer and turbulent kinetic energy budgets within a dense model canopy. Boundary Layer Meteorology 111, 589-614.

Sanz, C. 2003 A note on k-ε modelling on vegetation canopy air flows Boundary layer , meteorology 108, 191-197

Serra, T., Colomer, J., Logan, B.E., 2008. Efficiency of different shear devices on flocculation. Water Res. 42, 1113-1121.

Modeling Mean Flow and Turbulence in Aquatic Vegetation

A.T. King[1]*

[1] *DeFrees Hydraulics Laboratory, School Civil and Environmental Engineering, Cornell University, 220 Hollister Hall, Ithaca, NY, USA*

**Corresponding author, e-mail atk6@cornell.edu*

KEYWORDS
Vegetation; flow; turbulence; RANS model.

EXTENDED ABSTRACT

Reynolds-averaged Navier-Stokes (RANS) models of flow through aquatic vegetation must capture a large number of length scales: water depth (H), plant frontal area per unit volume (a, an inverse length scale), stem diameter (d), and the distance(s) over which a and d may vary (e.g. in beds of rigid cylinders, which are often used to model aquatic vegetation in the laboratory, a and d vary only over the canopy height, h). We propose and test a k-ε type model that captures all of these length scales by separately treating two components of turbulent kinetic energy: TKE at the larger scale of vertical shear and TKE at the smaller scale of the plant stems.

There are two major existing k-ε models for flow through aquatic vegetation, found in López and García (2001) and in Katul *et al.* (2004), respectively. López and García add an extra production term to the TKE and dissipation equations of the standard k-ε model, $P_V \sim C_D a U^3$, where C_D is the drag coefficient and U is mean velocity. P_V is the rate at which energy of the mean flow is converted to TKE in the wakes of plants. Like López and García, Katul *et al.* include extra production, P_V, in the TKE and dissipation equations, but they also include an extra dissipation term, $W \sim C_D a U k$, where k is TKE. W approximates the rate of conversion of large-scale TKE (generated by vertical shear) into smaller-scale TKE in the wakes of plants. These two existing models explicitly incorporate the frontal area density, a, through the term(s) P_V (and W); they capture the canopy height, h, through variation of a over depth; and they capture the water depth, H, through boundary conditions. However, neither of these models incorporates the stem-scale, d. Both models perform well against existing data sets from submerged beds of rigid cylinders (e.g. Dunn et al., 1996), however, they both break down in the case of fully submerged vegetation where Tanino and Nepf (2008) have shown that TKE scales as $k \sim U^2 (C_D a d)^{2/3}$.

We propose a new k-ε model in which TKE is split into two components: k_S, at the scale of vertical shear, and k_V, at the smaller scale of the plant stems. In our model, $W \sim C_D a U k_S$ is a dissipation term for k_S and a production term for k_V. Dissipation of large-scale TKE may also occur through the cascade process, modeled by the standard dissipation equation with W added as an extra dissipation term. $P_V \sim C_D a U^3$ is a production term in the equation for k_V, and dissipation of k_V is modeled by $\varepsilon_V \sim k_V^{3/2}/d$, for consistency with Tanino and Nepf's (2008) findings. Preliminary testing indicates that the new model is promising. In Figure 1,

we compare the new model to those of López and García and of Katul *et al.* using experimental data from Dunn *et al.* (1996).

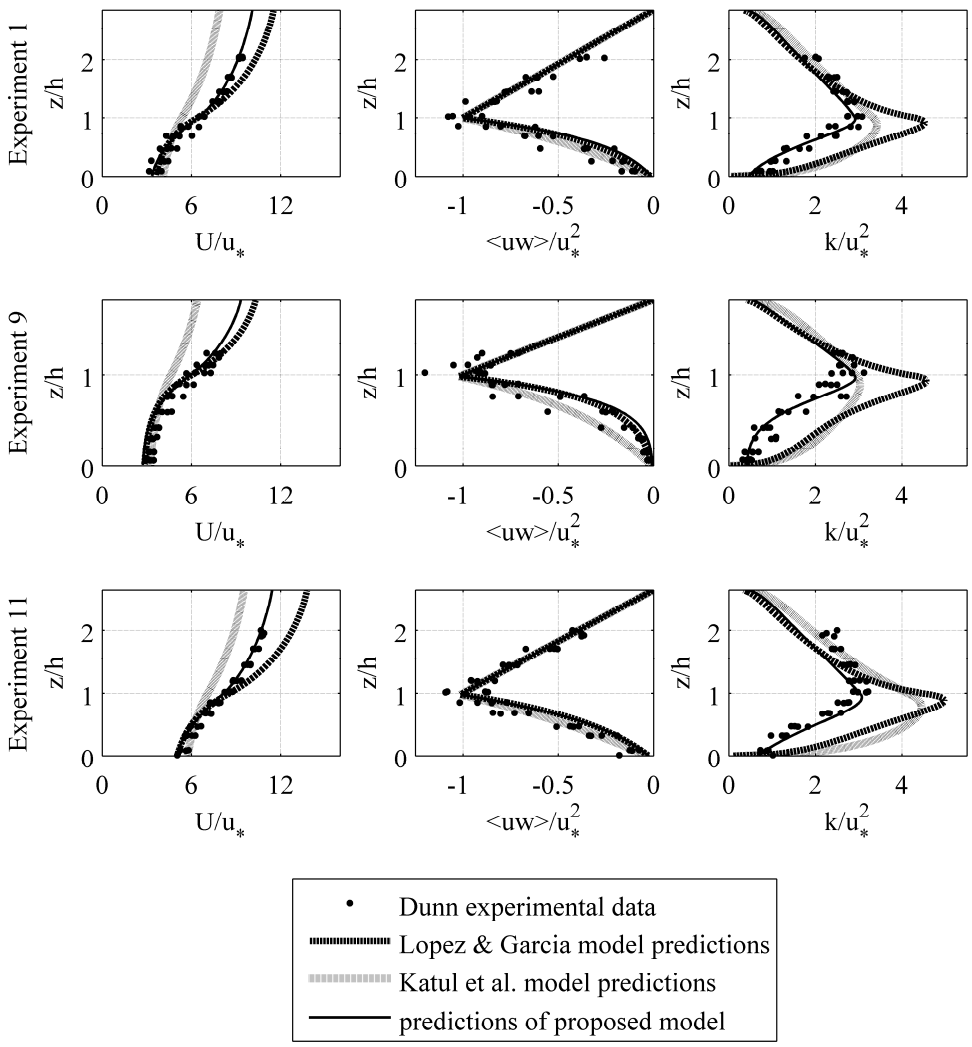

Figure 1. Vertical profiles of measured and modeled velocity statistics including mean velocity, *U*, Reynolds stress, <*uw*>, and total TKE, *k* for the Dunn *et al.* (1996) Experiments 1, 9, and 11. All statistics are normalized by u_*^2, the magnitude of the Reynolds stress measured at the top of the plant canopy.

REFERENCES

Dunn C., López F. and García M. (1996). Mean flow and turbulence in a laboratory channel with simulated vegetation. *Hydraulic Eng. Ser.*, **51**, Univ. of Ill., Urbana.

Katul G.G., Mahrt L., Poggi D. and Sanz C. (2004). One- and two-equation models for canopy turbulence. *Boundary-Layer Meteorology*, **113**, 81-109.

López F. and García M. (2001). Mean flow and turbulence structure of open-channel flow through non-emergent vegetation. *Journal of Hydraulic Engineering*, **127**, 392-402.

Tanino Y. and Nepf H. (2008). Lateral dispersion in random cylinder arrays at high Reynolds number. *Journal of Fluid Mechanics*, **600**, 339-371.

Velocity Variations in a Patterned Wetland from Lattice-Boltzmann Flow Modeling

E. A. Variano[1]*, M. C. Sukop[2], D. T. Ho[3], S. Anwar[4], and V. C. Engel[5]

[1] *Civil and Environmental Engineering, University of California, Berkeley, 623 Davis Hall, Berkeley, CA 94720-1710, USA.*
[2] *Earth Sciences, Florida International University, Miami, FL, USA.*
[3] *Department of Oceanography, University of Hawaii, Honolulu, HI, USA.*
[4] *South Florida Water Management District, West Palm Beach, FL, USA.*
[5] *South Florida Natural Resources Center, Homestead, FL, USA.*

**Corresponding author, e-mail variano@ce.berkeley.edu*

KEYWORDS
Computation Fluid Dynamics; Drag; lattice-Boltzmann; Everglades; Macrophytes; Vegetation

EXTENDED ABSTRACT

INTRODUCTION
The Everglades is a large and diverse landscape, covering ~1.5 million hectares in South Florida, USA. Of specific interest is the ridge-and-slough patterning found in the central Everglades. In this region, a complex and fragile set of feedback processes have sustained an alternating pattern of elongated sloughs (deep water areas with submerged vegetation) and ridges (areas of elevated peat surface colonized by emergent vegetation). Such patterning is thought to be a key habitat feature supporting wading birds and other Everglades wildlife. Understanding the exact mechanism by which this patterning is maintained is of immediate importance, because the landscape is being rapidly degraded in response to anthropogenic changes in the Everglades water budget [NRC 2003].

Those theories that describe ridge-slough maintenance based on hydrodynamic sediment transport [e.g. Larsen *et al.* 2007] require detailed descriptions of the flow through the Everglades, most notably the flow differences between ridges and sloughs. Recently, the authors of this paper participated in a series of tracer release experiments (EverTREx) that were much larger than previous tracer studies, covering areas up to 1 km^2. This data was reported in Ho *et al.* [2009] and Variano *et al.* [2009]. Herein we use these results to calibrate a numerical model that determines the velocity difference between ridges and sloughs.

METHODS
Simulations of the depth-averaged 2D shallow water equations are performed using a Lattice-Boltzmann (LB) model, described by Sukop and Thorne [2007]. This model is able to handle irregular boundaries in a very inexpensive manner, and also incorporate a spatially variable resistance term, which we use to account for the ridge and slough patterning. The structure of the patterned landscape is imported to the code starting with aerial photographs, which are then processed into greyscale images, with the pixel intensity corresponding to vegetation permeability. Having thus defined the geometry of the simulation domain, the LB model is used to assess the velocity differences between the ridge and slough vegetation regions.

Flow in the Everglades is typically slow enough (< 1 cm/s) that the surface water flow through vegetation can be modelled using Darcy's law for porous media flow. Leveraging the simplicity of this drag model, we accelerate computational speed by performing simulations at low Reynolds numbers and extrapolating results to values observed during field experiments.

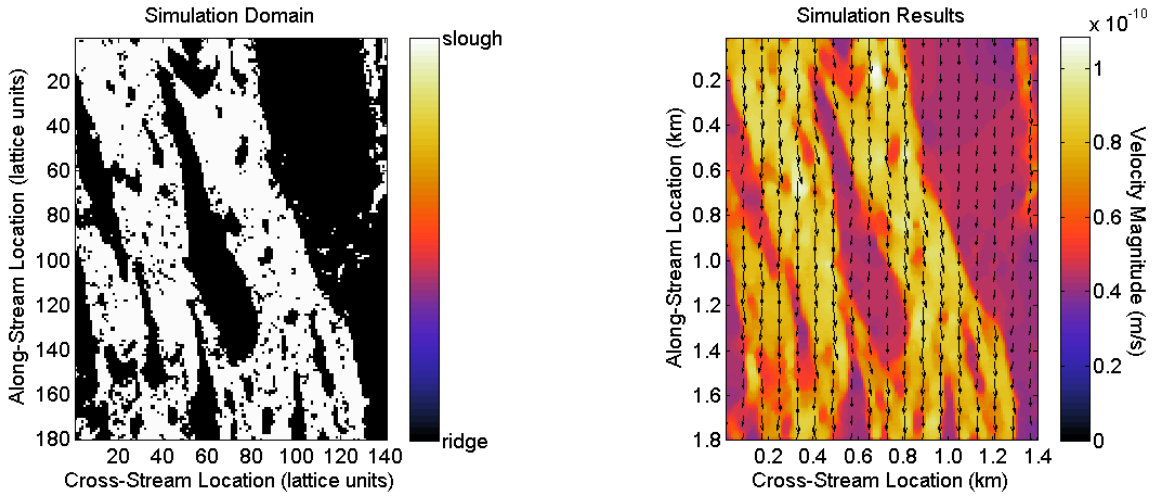

Figure 1. Simulation domain and results; note that vegetation domains are modelled in a binary manner and that simulation velocities are intentionally very small.

RESULTS AND DISCUSSION

The numerical model can rapidly simulate velocities in an area large enough to include several ridges and sloughs, e.g. Figure 1. From this, the effect of ridges and sloughs on flow patterns can be assessed, including the degree to which sloughs act to "channel" flow into high-velocity paths. This is important for assessing the relationship between the landscape patterning and the externally imposed velocity gradients. While the landscape acts to shape the flow, this effect can be overridden by hydraulic gradients imposed by water management operations. Such overriding is one hypothesized cause for the loss of landscape patterning in the ridge and slough landscape, due to disruptions in the historical sediment transport patterns [Larsen *et al.* 2007]. The relative permeability of the ridge and slough vegetation determines how susceptible the landscape is to disruptions of this sort. Using the LB model, we find that the ratio of ridge permeability to slough permeability is almost exactly equal to the ratio of velocities in these two vegetation regions. That is, the effects of irregular vegetation boundaries and nonlinear advection do not cause the flow to differ significantly from a simple balance between pressure gradient and Darcy-type drag. As a result, landscape susceptibility to management changes can be easily assessed by comparing permeabilities (measured with tracer releases or surveys of vegetation frontal area) and planned hydraulic gradients.

REFERENCES

Ho, D. T., V. C. Engel, E. A. Variano, P. J. Schmieder, and M. E. Condon (2009), Tracer studies of sheet flow in the Florida Everglades, Geophys. Res. Lett., 36, L09401.

Larsen, L.G., Harvey, J.W., and Crimaldi, J.P. (2007) A Delicate Balance: Ecohydrological Feedbacks Governing Landscape Morphology in a Lotic Peatland. Ecological Monographs 77, 591-614.

National Research Council (2003), Does Water Flow Influence Everglades Landscape Patterns?, Natl. Acad., Washington, D. C.

Sukop, M.C. and Thorne, D.T.J. (2007) Lattice Boltzmann Modeling: An Introduction for Geoscientists and Engineers. Springer. [Open source code distributed as LB2D_prime *http://www.fiu.edu/~sukopm/*]

Variano, E.A., Ho, D.T., Engel, V.C., Schmieder, P.J. & Reid, M.C. (2009) Flow and mixing dynamics in a patterned wetland: Kilometer-scale tracer releases in the Everglades. Water Resour. Res., 45, W08422.

A new model for mixing in turbulent open channel flows

J. Atkinson[1]*, S. Bennett[2], and H. Rubin[3]

[1] *Department of Civil, Structural and Environmental Engineering, University at Buffalo, Buffalo, New York, 14260 USA*
[2] *Department of Geography, University at Buffalo, Buffalo, New York, 14260 USA*
[3] *Department of Civil and Environmental Engineering, Technion-Israel Institute of Technology, Haifa, Israel*

**Corresponding author, e-mail atkinson@eng.buffalo.edu*

ABSTRACT
A variation of the traditional logarithmic velocity profile for turbulent open channel flow is developed that satisfies a zero gradient surface boundary condition and leads to an alternative description of eddy viscosity, relative to the classic Elder (1959) analysis. The differences between the proposed velocity profile and the standard logarithmic profile are not large, but the modified distribution of eddy viscosity is skewed upwards, with a maximum at a level one-third of the depth from the surface instead of at mid-depth, and has a peak value more than 50% greater than the value found in Elder's analysis. Using Reynolds' analogy, this result in turn leads to increased estimates of mixing coefficients, including longitudinal dispersion, and these results are shown to better represent mixing in both laboratory and natural channel experiments. Comparisons are made with experimental results found in the literature as well as flume experiments performed by the authors. These results are expected to have a broad impact on general studies of transport and mixing in open channel flows, providing improved estimates of diffusivities and longitudinal dispersion.

KEYWORDS
Open channel flow, turbulence, logarithmic profile, eddy viscosity, enhanced mixing.

INTRODUCTION
A common approach for representing turbulent open channel flow assumes negligible hydraulic gradient and leads to a logarithmic velocity profile, the so-called "law of the wall". However, this and other common profiles does not satisfy a zero-gradient surface boundary condition, so that a vanishing value of the eddy viscosity is then needed to achieve zero surface shear stress. This is the case with Elder's (1959) classic approach. The shear stress distribution assumed by Elder, however, results in a pressure distribution that is somewhat inconsistent with the common assumption of constant piezometric pressure distribution along the conduit while implementing Prandtl's mixing length theory.

Nezu and Rodi (1986) suggested the logarithmic profile was valid over about the lower 20% of the depth in open channels, although other studies have shown that this profile is valid over larger portions of the depth, up to 80% or greater (e.g., Nezu and Nakagawa, 1993; Still, 1986). Several researchers have adjusted the value of the von-Karman universal constant (κ) or the integration constant that arises in deriving the profile, in order to improve the logarithmic fit to the data throughout the entire depth. Other authors have used a wake

function, similar to boundary layer analysis, to account for the deviation of the logarithmic profile from observed data, where the value of the function in general depends on the Reynolds number of the flow (e.g., Coles, 1956; Coleman, 1981; Zippe and Graf, 1983; Nezu and Rodi, 1986). Nezu and Rodi (1986), for example, used a two-layer model for flow in open channels, in which a pure logarithmic profile was assumed for the lower region and a wake function was applied to adjust the upper region profile to provide a better fit to data. This model, however, still does not incorporate a zero-gradient boundary condition at the open channel surface. Guo et al. (2005) also used an empirical adjustment like a wake parameter (a "modified log-wake law") to provide improved fits of the logarithmic profile to velocity data measured in a series of wind tunnel experiments.

In the present study an alternative logarithmic velocity profile is proposed that is consistent with a theoretically derived distribution of shear stress and matches the required zero gradient condition at the surface. As shown below, the new profile also leads to a modified parabolic distribution of turbulent eddy viscosity, as derived by Elder (1959). In particular, the maximum calculated value for the eddy viscosity is 50% greater than the value obtained by Elder, and occurs at two-thirds of the height above the bed, rather than at mid-depth. Although the impact of the new profile is minor in terms of fitting measured velocity profiles, the impact on mixing coefficients in open channels can be significant.

BASIC FORMULATION

Velocity profile

For two-dimensional turbulent flow in a wide rectangular channel as shown in Figure 1, the steady state, Reynolds-averaged Navier-Stokes' equations of motion are

$$\rho \frac{\partial \left(\overline{u'w'}\right)}{\partial z} = -\frac{\partial p^*}{\partial x} + \frac{\partial \tau_{vis}}{\partial z}; \quad \text{and} \quad \rho \frac{\partial \left(\overline{w'^2}\right)}{\partial z} = -\frac{\partial p^*}{\partial z} \tag{1}$$

where ρ is the fluid density, *u'* and *w'* are velocity fluctuations in the longitudinal (*x*) and vertical (*z*) directions, respectively, τ_{vis} is viscous shear stress, given by

$$\tau_{vis} = \mu \frac{du}{dz} \tag{2}$$

where *u* is the local mean velocity in the *x* direction, μ is fluid viscosity, and p^* is piezometric pressure, defined as

$$p^* = p + \gamma Z \tag{3}$$

where *p* is pressure, $\gamma = \rho$ g is specific weight, *g* is gravitational acceleration, and *Z* is elevation. Both τ_{vis} and p^* also are assumed to be time-averaged. In addition, $du/dx = 0$ and the mean local velocity in the *z* direction is zero. Using eqn. (3), eqns. (1) may be rewritten as

$$\rho \frac{\partial \left(\overline{u'w'}\right)}{\partial z} = -\frac{\partial p}{\partial x} + \gamma \sin\alpha + \frac{\partial \tau_{vis}}{\partial z} \quad \text{and} \quad \rho \frac{\partial \left(\overline{w'^2}\right)}{\partial z} = -\frac{\partial p}{\partial z} - \gamma \cos\alpha \tag{4}$$

where α is the angle of declination of the channel bed with respect to horizontal (Figure 1).

Under two-dimensional steady state flow the pressure gradient in the *z* direction is not exactly, but nearly hydrostatic (Pai, 1981), so that the gradient of $\left(\overline{w'^2}\right)$ in eqn. (4) may be neglected. The total shear stress (τ) is commonly defined as the sum of viscous and turbulent terms, so

$$\frac{d\tau}{dz} = \frac{d}{dz}\left(\tau_{vis} - \rho\overline{u'w'}\right) = -\gamma J \tag{5}$$

where *J* is the hydraulic gradient,

$$J = -\frac{1}{\gamma}\frac{\partial p}{\partial x} + \sin\alpha \tag{6}$$

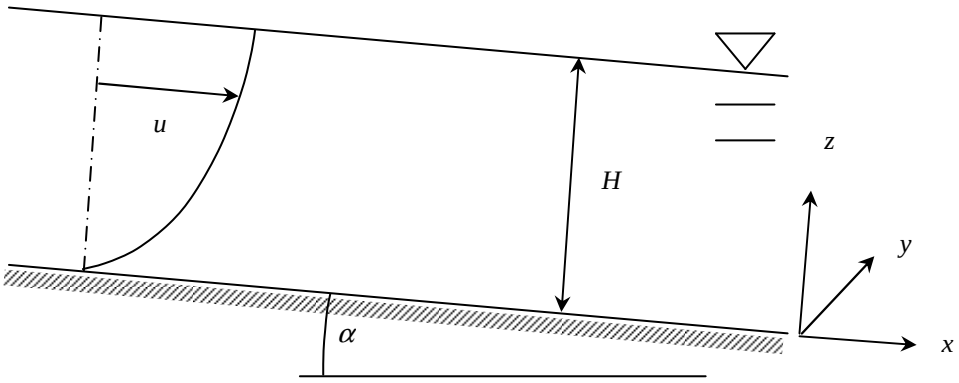

Figure 1. Definition sketch for wide rectangular open channel flow.

If the hydraulic gradient is neglected, $J \approx 0$, then eqn. (5) implies τ is uniformly distributed in the *z*-direction, which is an important assumption in deriving the logarithmic velocity profile as developed by Prandtl (1925, 1926). However, there is no uniform steady state open channel flow with $\alpha = 0$.

Based on mass and momentum conservation considerations, the turbulent fluctuations *u'* and *w'* have nearly identical absolute values and opposite signs. Further, according to Prandtl's mixing length theory, these velocity fluctuations can be represented by

$$|u'| \approx |w'| \approx L\frac{du}{dz} \tag{7}$$

where *L* is the mixing length, which represents a characteristic length scale of the turbulent eddies. In turbulent rough open channel flows the channel equivalent roughness (or the characteristic bed particle diameter) is considered as the characteristic length for momentum transfer and it is assumed that

$$L \cong \kappa z \tag{8}$$

where κ is Von-Karman's universal turbulence constant, having a value of about 0.4.

Introducing eqns. (7) and (8) into eqn. (5) and integrating gives

$$\tau_{vis} + \rho(\kappa z)^2 \left(\frac{dU}{dz}\right)^2 = -(\rho g J) z + c_1 \tag{9}$$

where c_1 is an integration constant. Near the channel bed (z = 0) the total shear is given by the viscous shear and is equal to the bed shear, $\tau_0 = \rho\, u_*^2$, where u_* is the shear velocity. Therefore, $c_1 = \tau_0$. Applying an overall force balance to a segment of the channel dx long, and assuming hydrostatic pressure distribution we obtain

$$\gamma HJ = \gamma H \sin\alpha = \tau_0 = \rho u_*^2 \quad \Rightarrow \gamma Jz = \rho u_*^2 \frac{z}{H} \tag{10}$$

where H is the water depth Also substituting for τ_{vis}, and rearranging,

$$\mu \frac{dU}{dz} + \rho(\kappa z)^2 \left(\frac{dU}{dz}\right)^2 = \rho u_*^2 \left(1 - \frac{z}{H}\right) \tag{11}$$

This last result is similar to many textbook derivations (e.g., Shames, 1992), except for the appearance of (z/H) on the right-hand-side, which arises from $J \neq 0$. Outside of the viscous sub-layer the viscous stress (first term on left-hand-side of eqn. (11)) may be neglected. If in fact the (z/H) term is neglected, then eqn. (11) can be solved to obtain the common logarithmic velocity profile,

$$U' = \kappa \frac{U}{u_*} = \ln \frac{z}{z_0} \tag{12}$$

where U' is the dimensionless velocity, z_0 is the virtual origin of the profile and κ = 0.4.

If the (z/H) term is not neglected, eqn. (11) leads to

$$U' = \kappa \frac{U}{u_*} = \left\{ 2(\eta - \eta_0) + \ln\left[\frac{(1-\eta)}{(1+\eta)} \frac{(1+\eta_0)}{(1-\eta_0)} \right] \right\} \tag{13}$$

where $\eta = (1 - z/H)^{1/2}$ and η_0 is its value when $z = z_0$. A general comparison of these two profiles is shown in Figure 2, where it can be seen that there are only minor differences, primarily near the surface, where eqn. (13) satisfies a zero gradient boundary condition.

Eddy viscosity

Using the definition of turbulent (or eddy) viscosity (ν_{turb}) in terms of a linearly distributed turbulent shear stress, as given by eqn. (5), yields,

$$\tau = \rho \nu_{turb} \frac{du}{dz} = \rho u_*^2 \left(1 - \frac{z}{H}\right) \tag{14}$$

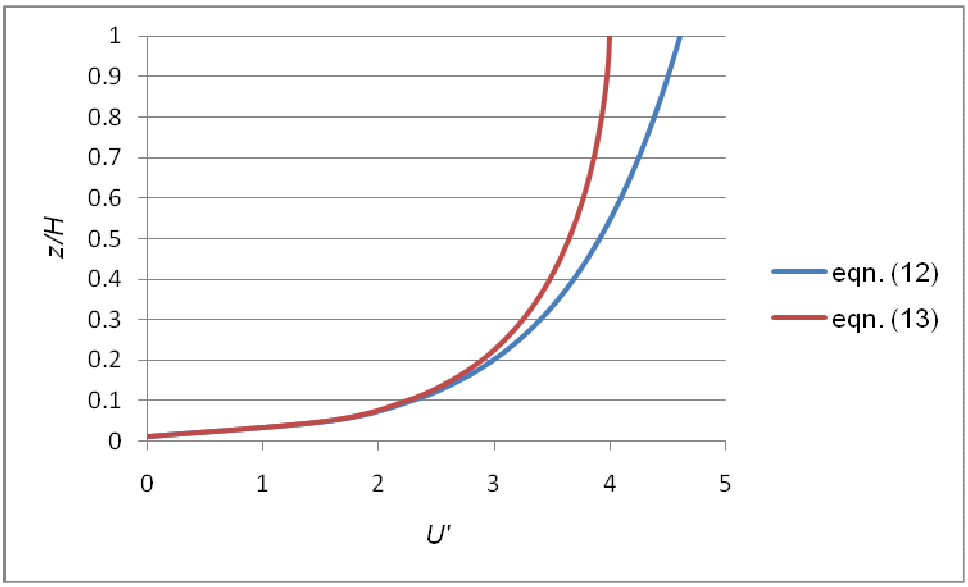

Figure 2. Comparison of two velocity profiles.

Using eqn. (12) to represent the velocity profile then leads to

$$\nu' = \frac{\nu_{turb}}{\kappa u_* H} = \frac{z}{H}\left(1 - \frac{z}{H}\right) \tag{15}$$

where ν' is a dimensionless viscosity. This equation is the classic result derived by Elder (1959). If, however, eqn. (13) is used, then

$$\nu' = \frac{\nu_{turb}}{\kappa u_* H} = \frac{z}{H}\left(1 - \frac{z}{H}\right)^{1/2} \tag{16}$$

Figure 3 is a comparison of the eddy viscosity values calculated by eqns. (15) and (16), where it can be seen that the modified velocity profile produces a significantly greater value for the eddy viscosity, nearly 50% greater than the traditional model, and that the peak value occurs at two-thirds height, rather than at mid-depth. This shift of the maximum eddy viscosity location towards the surface makes intuitive sense, since the effect of the solid bottom should have a stronger damping effect on turbulent motions contributing to the eddy viscosity than the free surface. Laboratory results from Bennett *et al*. (1998) also show that the peak value for eddy viscosity occurs in the upper half of the depth.

APPLICATIONS

An extensive comparison of eqns. (12) and (13), along with models incorporating a wake function, was conducted by Gomez (2006), using over 30 data sets from three different literature sources. He showed that the new profile provided similar and on average slightly better fits to the data as either of the other two alternatives. However, as suggested by the comparison in Figure 2, the differences were not great. The logarithmic profile is not expected to be theoretically valid over the entire flow depth, but it has been shown to be a good fit to data from many experiments, both in the laboratory and in natural channels. Thus the new profile proposed here, while addressing some of the inconsistencies of the law of the

wall, is not proposed as a significant change in the description of velocity profiles in turbulent open channel flow. Rather, the impact of this change on mixing is of greater interest, as suggested in Figure 3.

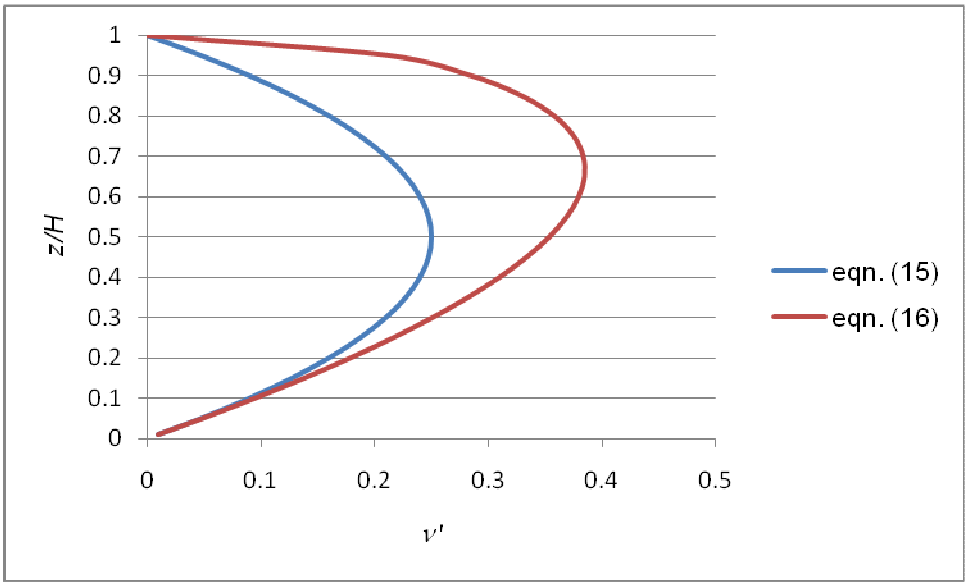

Figure 3. Comparison of two models for theoretical values of non-dimensional eddy viscosity.

Average vertical mixing coefficient

Fischer *et al*. (1979, p. 106) assumed the common logarithmic profile to be valid over the entire depth H, with the distribution of eddy viscosity given by eqn. (15). They also adopted this result as a representation of the local vertical diffusivity for heat or mass transport (by Reynolds' analogy) and calculated the average vertical turbulent diffusivity by integrating ν_{turb} over the channel depth. With $\kappa = 0.4$, this procedure resulted in

$$\nu_V = 0.067 u_* H \tag{17}$$

where ν_V is the average vertical diffusivity. Using the same dimensional scaling as in eqns. (15) and (16), this result also was written as

$$\nu'_V = \frac{\nu_V}{\kappa u_* H} = 0.167 \tag{18}$$

Fischer *et al*. (1979) showed that eqn. (18) was consistent with the measurements of Jobson and Sayre (1970), who performed experiments of the vertical mixing of dye in a flume. However, this seems to be a fortuitous result, since it may be argued that integration in the vertical direction should provide the effective average *horizontal* diffusivity, not the average vertical diffusivity.

Transverse and longitudinal mixing

Considering a flux calculation, the average transverse diffusivity is calculated by integrating the diffusivity over the flow depth. As before, Reynolds analogy is used to relate the eddy viscosity to the diffusivity values. Using Elder's model (eqn. 15), this process results in

$\nu'_T = 0.167$, where ν'_T is the average non-dimensional transverse diffusivity (i.e., same result as eqn. (18), which was obtained by vertical integration). Inn dimensional terms, this result corresponds to $\nu_T = 0.067 u_* H$. On the other hand, using eqn. (16) gives

$$\nu'_T = 0.27 \quad \text{or} \quad \nu_T = 0.11 u_* H \tag{19}$$

which is nearly double the result based on Elder's profile. Fischer *et al*. (1979) reviewed approximately 75 separate experiments in straight, rectangular channels and found that ($\nu_T/u_* H$) was nearly always between about 0.1 and 0.2, and they suggested an average value of $\nu_T \cong 0.15 u_* H$. The result of eqn. (19), based on the new profile, is much more closely aligned with this conclusion than is the result based on the traditional logarithmic profile.

Again following Fischer *et al*. (1979), longitudinal dispersivities can be estimated on the basis of velocity fluctuations from the mean, and the distribution of transverse diffusivities. A full evaluation of this quantity requires numerical integration. While that exercise is not repeated here, it is reasonable to expect that differences in calculated values should be obtained using the new velocity model, since there are obvious differences in the transverse diffusivity, as well as the velocity profile itself. The magnitude of the difference is difficult to evaluate without further specific data, and this would be a subject for further research.

DISCUSSION AND CONCLUSIONS

It should be emphasized that the only difference leading to the two results for velocity profiles, eqn. (12) for the standard logarithmic profile and eqn. (13) for the new profile, is the incorporation of a non-zero bottom slope, or more generally a non-zero hydraulic gradient. In addition, the proposed profile is consistent with a linear shear stress distribution and it has the added feature of zero velocity gradient at the surface, automatically satisfying a zero shear stress boundary condition there. Limited measurements such as those by Bennett *et al*. (1998) also show that maximum eddy viscosity occurs in the upper half of the flow, which is consistent with eqn. (16), derived from the new profile.

The difference in predictive capability of the new velocity profile, relative to other models including the well-known logarithmic profile, is relatively small, but of more direct interest for environmental applications, the impact on theoretical distributions of eddy viscosities and diffusivities is worth noting. In particular, estimates of eddy viscosity based on the new profile can be 50% larger than those determined when using a standard logarithmic profile. Moreover, averaged diffusivities found using the new approach are much more consistent with observed values as reported by Fischer *et al*. (1979). The approach suggested here will also have an important impact on estimates of longitudinal dispersivities, but further research is needed to develop more quantitative results.

REFERENCES

Bennett S.J., Bridge J.S. and Best J.L. (1998), Fluid and sediment dynamics of upper stage plane beds, J. Geophys. Res. 103 (C1): 1239-1274.

Coleman N.L. (1981). Velocity profiles with suspended sediment. J. Hydraul. Res., 19, 211 – 229.

Coles D. (1956), The law of the wake in the turbulent boundary layer, J. Fluid Mech. 1: 191-226.

Elder J.W. (1959), The dispersion of marked fluid in turbulent shear flow, J. Fluid Mech. 5: 544-560.

Fischer H. B., List E. J., Koh R. C.Y., Imberger J., and Brooks N. H. (1979), *Mixing in Inland and Coastal Waters*, Academic Press, San Diego.

Gomez Damian M. (2006), Alternative formulation of velocity profile in open channel flow, M.S. Thesis, Department of Civil, Structural and Environmental Engineering, University at Buffalo, Buffalo, NY.

Guo J, Julien P.Y. and Meroney R.N. (2005), Modified log-wake law for sero-pressure gradient turbulent boundary layers, Journal of Hydraulic Research 43 (4): 421-430.

Jobson H.E., and Sayre W.W. (1970). Vertical transfer in open channel flow, J. Hydr. Div. ASCE, 96, 703-724.

Nezu I. and Rodi W. (1986), Open channel flow measurements with a laser anemometer, Journal of Hydraulic Engineering 112 (5): 335-355.

Nezu I., and Nakagawa H. (1993). *Turbulence in Open Channel Flows*, Monograph Series, IAHR, Rotterdam, The Netherlands

Pai S.I., (1981). "*Modern Fluid Mechanics*," Van Nostrand Reinhold, NY

Prandtl L. (1925), Bericht uber untersuchungen zur aubgebildeten turbulenz, Z. Angew. Math. Mech., 5(2), 136-139.

Prandtl L. (1926), Über die ausgebildete turbulenz, Proc. 2nd International Cong. Appl. Mech., Zurich, 62-74; Translated as "Turbulent Flow", Nat. Adv. Comm. Aero. Wash., Tech. memo No. 435, 1927.

Shames I. H. (1992), *Mechanics of Fluids*, 3rd ed., McGraw-Hill, Inc., NY

Still B.L. (1986). Velocity profiles in the turbulent boundary layer: Pt. I. *Proc. Advances in Aerodynamics Fluid Mechanics and Hydraulics*, EM & HY Div. ASCE.

Zippe H.J. and Graf W.H. (1983). Turbulent boundary-layer flow over permeable and non-permeable rough surfaces. J. Hydr. Res. 21, 51-65.

Effects of lock operation and shipping on hydrodynamic conditions and geochemical fluxes in an impounded river

A. Mäck[1]*, C. Noss[1], H. Fischer[2] and A. Lorke[1]

[1] *Institute for Environmental Science, University of Koblenz-Landau, Fortstrasse 7, 76829 Landau, Germany*
[2] *Federal Institute of Hydrology (BfG), Am Mainzer Tor 1, 56068 Koblenz, Germany*

**Corresponding author, e-mail maeck@uni.landau.de*

KEYWORDS
Locking; hydrodynamic conditions; solitary wave; geochemical fluxes; methane.

EXTENDED ABSTRACT

INTRODUCTION
Hydrodynamic conditions in rivers provide the framework for the regulation of biogeochemical processes and play a key role in defining living conditions for the whole ecosystem. Anthropogenic alteration of flow regimes result in changed fluxes of organic matter and energy and changed physical properties of the water body which lead to different habitats and biocenosis. Dam construction, for example, reduces flow velocities and increases water residence times which enhances sedimentation rates, promotes the development of thermal stratification and can support primary production. Since in such systems the oxygenation of deeper layers is constricted, anaerobic degradation of organic matter can lead to methane production and its release to the atmosphere. In this study, we investigated the hydrodynamic conditions of an impounded river in Germany and its governing factors with special emphasis on its influence on methane emissions.

METHODS
The River Saar stretches along 246 km from its source in the French Vosges to its confluence with the Moselle near Konz, Germany and has a mean discharge of 80 m^3 s^{-1}. In the lower 93 km of the German part, six dams with storage heights between 3.5 and 14.5 m were built between 1977 and 2000 for shipping purposes. The impoundment leaded to reduced flow velocities and increased water depths, resulting in higher water residence times. This in turn promotes the development of thermal stratification (Becker et al. 2009) which effects water quality parameters, mainly dissolved oxygen.

In July 2009 we deployed thermistor chains (RBR TR-1060) combined with a pressure sensor (RBR TDR-2050) directly above ground and two optical oxygen sensors (Aanderaa 4330F, ENVCO D-Opto Logger) at two sampling sites (PS1, PS2). At a third site (PS3) an acoustic current Doppler profiler ADCP (RDI 600 kHz Workhorse Sentinel) was used to measure acoustic backscatter and flow velocities throughout the water column. All sampling sites are located in the impoundment between the dams of Serrig and Mettlach.

To estimate methane bubble flux rates in October 2009, we deployed an inverted funnel with a diameter of 1 m connected to a gas trap cylinder. This system sampled the bubbles

approximately 1.5 m below the surface. Deployment periods range from 5 to 23 hours. The trapped gas was gravimetrically quantified and analyzed using gas-chromatography.

RESULTS AND DISCUSSION

Locking of large ships had a significant impact on hydrodynamic conditions in the whole impoundment. Downstream locking at the upper dam in Mettlach is associated with the release of 24,327 m^3 water to the impoundment. This induced a soliton-like wave which propagates with a phase velocity of 7.83 ± 0.61 m s^{-1} (± 1 s.d.) to the dam in Serrig. The mean maximum amplitude of this solitary wave was 8.74 ± 1.05 cm (H_{max}). While the phase velocity correlates well with the theoretical parameters of a soliton for the given system (average depth = 5.5 m), the observed wave length is much longer (L = 5483 ± 488 m) than expected ($L_{theor.}$ = 1071 m).

Upstream lock operation in Serrig removes 36.000 m^3 of water from the reservoir. This causes a wave of depression of 5.89 ± 0.92 cm maximum height which propagates with a phase velocity of 5.39 ± 0.85 m s^{-1} to the dam in Mettlach. Both kinds of waves propagate along the whole 12.8 km long reservoir and are reflected back at the dams. Consecutive lock operation can reinforce the amplitude of these waves resulting in sinusoidal-like-shaped waves with wave heights up to over 20 cm and typical periods of 66.2 min. Spectral analysis revealed frequency peaks corresponding to the first, second and third mode of this wave, 32.9 min, 21.2 min and 15.2 min respectively.

Longitudinal mean flow velocities varied between -0.10 m s^{-1} and + 0.27 m s^{-1} and correlated well with passing waves. A downstream propagating wave crest was associated with a higher longitudinal flow velocity while an upstream moving crest reduced this velocity. In some cases, the wave was able to inverse the longitudinal flow velocity. Since the locks are mainly operated during the day, a typical diurnal rhythm was observed. In contrast to the height developed during daytime, the night shows a clear attenuation of the waves, if no further lock operation was run.

Fluxes of methane via bubbles varied throughout the sampling sites (0 -753.6 mg CH_4 $m^{-2}d^{-1}$), but showed a clear diurnal rhythm with an increase by a factor between 2 and 10 during the day (e.g. 305.4 to 753.6 mg CH_4 $m^{-2}d^{-1}$ at PS2). Enhanced ebullition rates during daytime are in accordance with the diurnal rhythm observed in the hydrodynamic forcing in July 2009 and indicate a significant impact of lock operation and ship traffic on the temporal dynamics of methane ebullition.

We also found a direct impact of shipping on biogeochemical processes. Passing ships caused enhanced acoustic backscatter signals which are likely to be related to ebullition events. The rise velocity observed in the acoustic backscatter data is in the same order of magnitude like the typical rise velocity of 5 mm methane bubbles and micro-bubbles (McGinnis et al. 2006).
It can be hypothesized that water level fluctuations associated with lock operation and ship-passage trigger ebullition events, despite a more detailed study with a higher temporal resolution of bubble flux is needed to confirm this hypothesis.

REFERENCES

Becker, A., V. Kirchesch, H. Z. Baumert, H. Fischer, and A. Schöl. (2009). Modelling the effects of thermal stratification on the oxygen budget of an impounded river. *River Res. and App.*

Mcginnis, D. F., J. Greinert, Y. Artemov, S. E. Beaubien, and A. Wuest. (2006). Fate of rising methane bubbles in stratified waters: How much methane reaches the atmosphere? *J. Geophys. Res.-Oceans* **111**.

Seiche-induced heat and mass exchange between the sediments and the near-bottom waters

J. Bernhardt*[1], K. Frindte[2], S. Jordan[3], M. Hupfer[3], H.-P. Grossart[2], C. Engelhardt[1] and G. Kirillin[1]

[1] *Department of Ecohydrology, Leibniz-Institute of Freshwater Ecology and Inland Fisheries, Berlin, Germany, Müggelseedamm 310, 12587 Berlin*
[2]*Limnology of Stratified Lakes, Leibniz-Institute of Freshwater Ecology and Inland Fisheries, Stechlin, Germany, Alte Fischerhütte 2, 16775 Stechlin*
[3]*Central Chemical Laboratory, Leibniz-Institute of Freshwater Ecology and Inland Fisheries, Berlin, Germany, Müggelseedamm 301, 12587 Berlin*

**Corresponding author, e-mail bernhardt@igb-berlin.de*

KEYWORDS
Convection; heat transport; laboratory experiments; mass transport; sediment-water-interface; seiches.

EXTENDED ABSTRACT

INTRODUCTION
Heat and mass transfer across the sediment-water-interface play an important role for energy and nutrient conversion and distribution in lakes. Vertical temperature measurements across the sediment-water interface (SWI) were performed in the littoral zone of stratified Lake Stechlin (Kirillin *et al.*, 2009). During stratified periods seiching occurs associated with changes in temperature, current velocity and direction in the bottom boundary layer. Seiche-driven upwelling of cold hypolimnion water into the littoral zone causes periodical inverse temperature gradients followed by the unstable stratification in the upper sediments (10-20 cm). The focus of this work is to establish simplified laboratory experiments on sediment cores to characterise the seiche-effect (periodic convective vertical fluxes) on heat and mass exchange between the sediments and the near-bottom waters more precisely than in the lake.

METHODS
Experiments
Laboratory experiments were performed with sediment and water from the littoral zone of Lake Stechlin to mimic and study the seiche-effect on heat and mass transport at the SWI. At once, experiments with two set-ups were conducted: set-up one with stable and set-up two with unstable temperature stratification. The 30 cm high sediment cores had an inner diameter of 10 cm. They were filled with homogenised mixed sediment (height 18.5 cm) topped with water (height 7.0 cm) 4 days before the experiment start. The set-ups were located in an incubator, where the initial temperature conditions of 18°C were set. The water above the sediment was artificially aerated and in this way well mixed. During the experiments vertical temperature profiles across the SWI (16 points) and conductivity (1 point) in the mixed water column were measured in 30 seconds temporal resolution. Both cores were closed with lids to prevent evaporation. Seiche induced instable temperature stratification was mimicked with colder water (8°C) above warmer sediment (18°C) in one core and stable stratification was forced in the other reference core with warmer water (28°C) above colder sediment (18°C). Therefore, at the beginning of the experiment the water temperature was switched from

initially 18°C to 8°C (28°C). The cooling (warming) was realised by thermostats that tempered the water column of each set-up. The inside of the water column was tempered by a cooling hose sitting at the inner core wall and the outside by tempered water around the core in the height of the water column. Then, 0.3 g dissolved NaCl- tracer (10 ml) was added to the water of each core. The experiment stopped after ca. 23 h and was repeated with new sediment cores.

Data processing

Heat transport

Time series from the vertical temperature profiles T (z = 22 cm, 1.3 cm spatial resolution) were used to calculate vertical heat fluxes Q (30 min averages) with time t and depth z for experiments with instable (convective = real vertical heat flux Q_r) and stable (diffusive = molecular heat flux Q_{mol}) temperature stratification. For the experiments with convective conditions Nusselt ($Nu = Q/Q_{mol}$) and Rayleigh (Ra) numbers were calculated and scaling analyses was performed (Nu(Ra)) to compare them to theoretical convection regimes (Kirillin *et al.*, 2009; Nield and Bejan, 2006). As well, fluxes and Nusselt numbers of experiments with diffusive conditions were compared with these of convective conditions.

Mass transport

For each experiment the decline in conductivity (NaCl -tracer) in the mixed water column was measured and conductivity time series were transformed into concentrations. The curves of the experiments with convective conditions were compared to these with diffusive conditions. Additionally, the concentration curves derived from measured conductivities were compared to calculated concentration curves valid for 1D-diffusion (Crank, 1975). Mass fluxes (1 h averages) in the water column J_w were calculated from the different time series of measured and calculated concentrations. Sherwood numbers Sh (analogue to Nusselt numbers) were used to compare mass fluxes of experiments with stable and unstable temperature stratification ($Sh = J/J_{mol}$).

RESULTS AND DISCUSSION

First laboratory experiments on sediment cores were conducted to characterise the seiche-effect on heat and mass exchange between the sediments and the near-bottom waters.

Heat transport

Experiments under instable temperature stratification showed in the first 6 hours after the water temperature was switched from 18°C to 8°C penetrative convection which reached up to 6 cm into the sediment. Convective heat transport was indicated by real heat fluxes (Q_r) that exceeded the molecular heat fluxes (Q_{mol}) by orders of magnitude for a few hours in the top sediment layer. Analysis in terms of the Nusselt numbers (Nu) revealed up to 50 times higher heat fluxes when penetrative convection took place in the sediment compared to conductive heat transport (Figure 1a). Nusselt and Rayleigh scaling revealed intermediate transport regime between Rayleigh-Bénard- regime for fluids and Darcy- regime for porous media (Figure 1b, see Kirillin *et al.*, 2009).

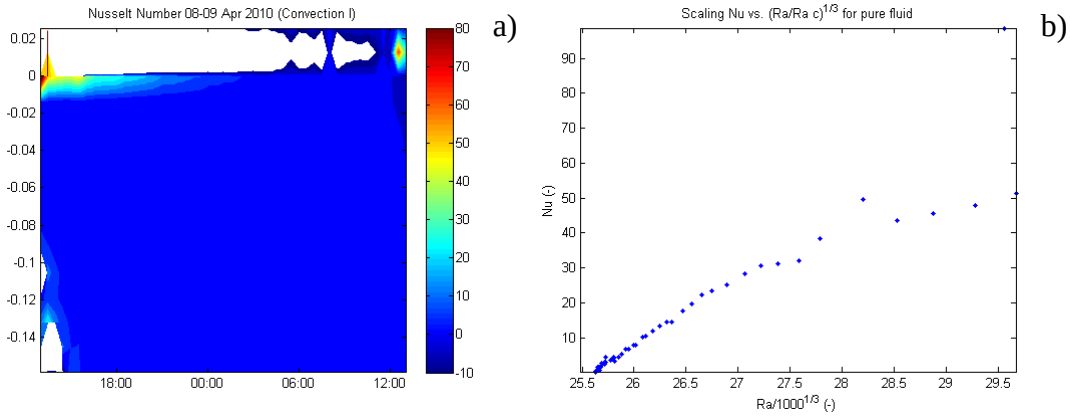

Figure 1. **a)** The Nusselt numbers during the laboratory experiment are high in the beginning of the experiment in the top layer of the sediment ($z < 0$). The water column is indicated by $z > 0$. **b)** The Nusselt-Rayleigh diagram shows Nusselt numbers at the SWI and Rayleigh numbers scaled for the Rayleigh-Bénard- regime resulting from laboratory experiments.

Mass transport

Periodic pore water convection in sediments is associated with convective mass fluxes, which increase the vertical mass transport of dissolved nutrients between the sediments and the lake water. Mass fluxes of the NaCl-tracer from the mixed water column into the lake sediment decreased with progressing time of the experiment as the concentration gradient between the water and the sediment declined. Under unstable temperature stratification the decline was linear (J) and under stable stratification exponential (J_{mol}). Sherwood numbers (Sh) showed up to 6 times – but generally 2 to 3 times – higher NaCl-fluxes from the mixed water into the sediment during convective transport regime compared to diffusive transport regime (Figure 2).

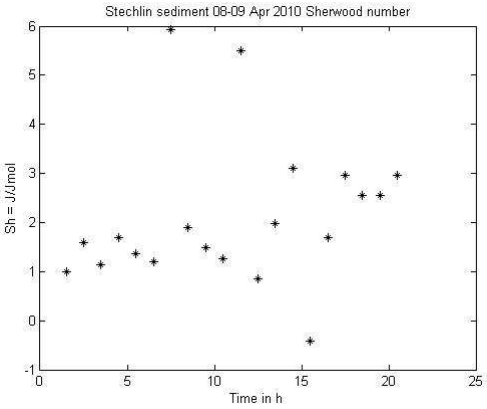

Figure 2. The Sherwood numbers increased during the experiment, thus the difference between convective mass fluxes and diffusive mass fluxes increased with time.

REFERENCES

Crank J. (1975). The mathematics of Diffusion. 2nd edn, Clarendon Press, Oxford; Oxford University Press. ISBN: 0198533446

Kirillin G., Engelhardt C., Golosov S. (2009). Transient convection in upper lake sediments produced by internal seiching. Geophys. Research Letters, **36**, L18601. doi:10.1029/2009GL040064

Nield, D.A., Bejan, A. (2006). Convection in porous media. 3rd edn, Springer, NY.

Cross wavelet, coherence and phase between water surface temperature and heat flux in a tropical hydroelectric reservoir

E.H. Alcântara*, J.L. Stech, J.A. Lorenzzetti, E.M.L.M. Novo

National Institute for Space Research, Remote Sensing Division, Brazil.

**Corresponding author, e-mail enner@dsr.inpe.br*

ABSTRACT

Water temperature plays an important role in ecological functioning and in controlling the biogeochemical processes of a water body. Conventional water quality monitoring is expensive and time consuming. It is particularly problematic if the water bodies to be examined are large. Conversely, remote sensing is a powerful tool to assess aquatic systems. The objective of this study was to analyze the time series of surface water temperature and heat flux to improve understanding of temporal variations in a hydroelectric reservoir. In this work, MODIS land-surface temperature (LST) level 2, 1-km nominal resolution data (MOD11L2, version 5) were used. All available clear-sky MODIS/Terra images from 2003 to 2008 were used, resulting in a total of 786 daytime and 473 nighttime images. Time series of surface water temperature was obtained by the monthly mean 3x3 window of three area of the reservoir: (1) first near the dam, (2) in the centre of the reservoir and (3) in the confluence of the rivers. Long-term environmental time series of continuously collected data are fundamental to identify and classify pulses and determining their role in aquatic systems. In-situ meteorological variables were used from 2003 to 2008 to calculate the surface energy budget time series. A correlation between daytime and nighttime surface water temperatures and the computed heat fluxes were made. The influence of the correlated heat flux in the water temperature was analyzed using the Cross-wavelet, coherence and phase analysis.

KEYWORDS
MODIS/Terra, hydroelectric reservoir, physical limnology.

INTRODUCTION

Research about water quality of reservoirs and lakes has been based mostly on point station datasets or along track lines obtained during cruises (Jerosch et al., 2006). High quality in situ measurements of water parameters are usually limited, and they are particularly critical for time series data and key variables. The detection of trends and sudden changes in the aquatic system is dependent on both the availability of long-term time series of environmental data and their proper analysis (Alcântara et al. 2010).
The objective of this paper is to analyze the time series of water surface temperature and heat balance of a tropical hydroelectric reservoir derived from satellite data.

STUDY AREA

The Itumbiara hydroelectric reservoir (18°25'S, 49°06'W) is located in a region stretched between Minas Gerais and Goiás States (Central Brazil) that was originally covered by tropical grassland savanna. The damming of the Parnaiba River flooded its main tributaries: the Araguari and Corumbá rivers. The basin's geomorphology resulted in a lake with a

dendritic pattern covering an area of approximately 814 km² and a volume of 17.03 billion m³ (Figure 1).

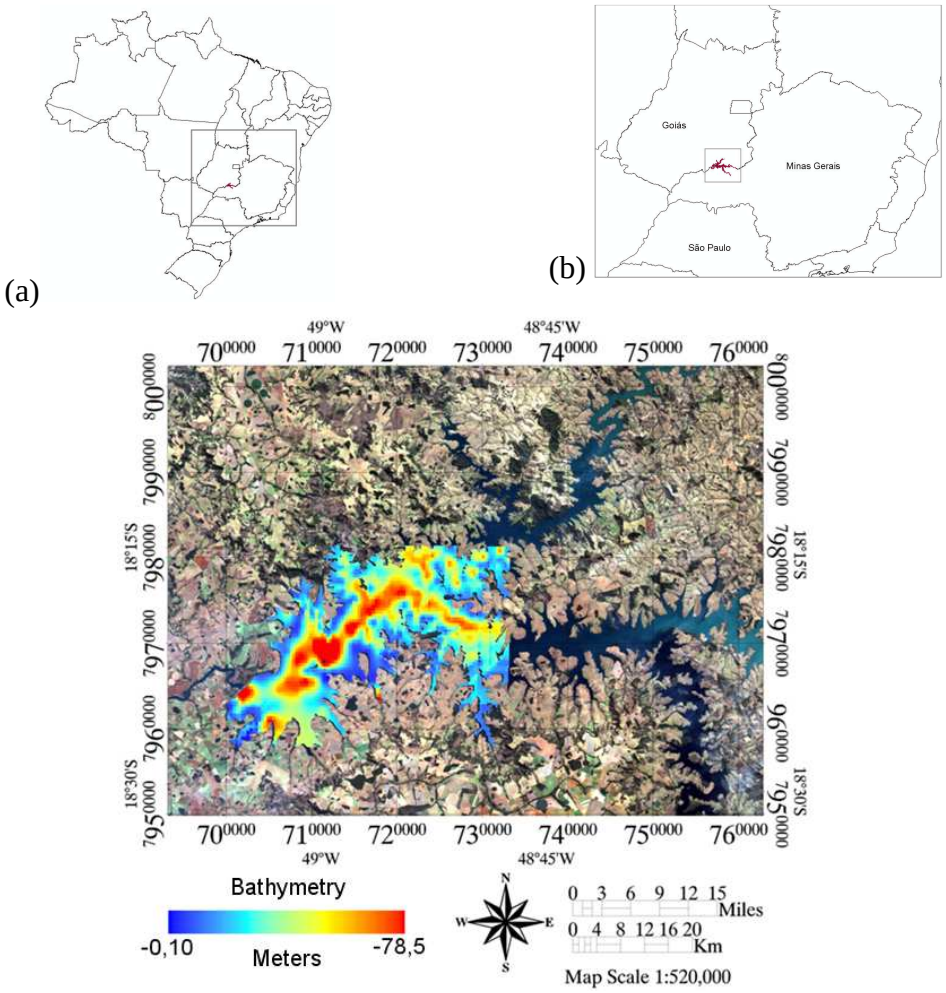

Figure 1: Localization of Itumbiara hydroelectric reservoir in Brazil's central area (a), at the state scale (b) and at the regional scale (c) with the bathymetric map.

METHODOLOGICAL APPROACH

Satellite data

MODIS water surface temperature (WST) level 2, 1-km nominal resolution data (MOD11L2, version 5) were obtained from the National Aeronautics and Space Administration Land Processes Distributed Active Archive Center (Wan, 2008). All available clear-sky MODIS Terra imagery between 2003 and 2008 were selected by visual inspection, resulting in a total of 786 daytime images and 473 nighttime images. A shoreline mask to isolate land from water was built using the TM/Landsat-5 image in order to isolate some anomalously cold or warm pixels remaining at some locations near the shoreline of the reservoir.

The WST-MODIS data were extensively validated for inland waters and were considered accurate (Oesch et al., 2005; Oesch et al., 2008; Reinart and Reinhold, 2008; Crosman and Horel, 2009).

Surface Energy Budget

A study of the energy exchange between the lake and atmosphere is essential for understanding the aquatic system behavior and its reaction to possible changes of environmental and climatic conditions (Bonnet, Poulin and Devaux, 2000). The exchange of heat across the water surface was computed using the methodology described by Henderson-Sellers (1986) as:

$$\phi_N = \phi_s(1-A) - (\phi_{ri} + \phi_{sf} + \phi_{lf}) \quad (1)$$

where ϕ_N is the surface heat flux balance, ϕ_s is the incident short-wave radiation, A is the albedo of water (=0.07), ϕ_{ri} is the Longwave flux, ϕ_{sf} is the sensible heat flux and ϕ_{lf} is the latent heat flux. The units used for the terms in Eq. (1) are W m^{-2}.

Time Series

The time series was constructed using the results obtained from the satellite imagery through the sampling in three regions of the reservoir (a window of $\overline{3x3}$). The figure 2 shows the regions where these sampling was taken.

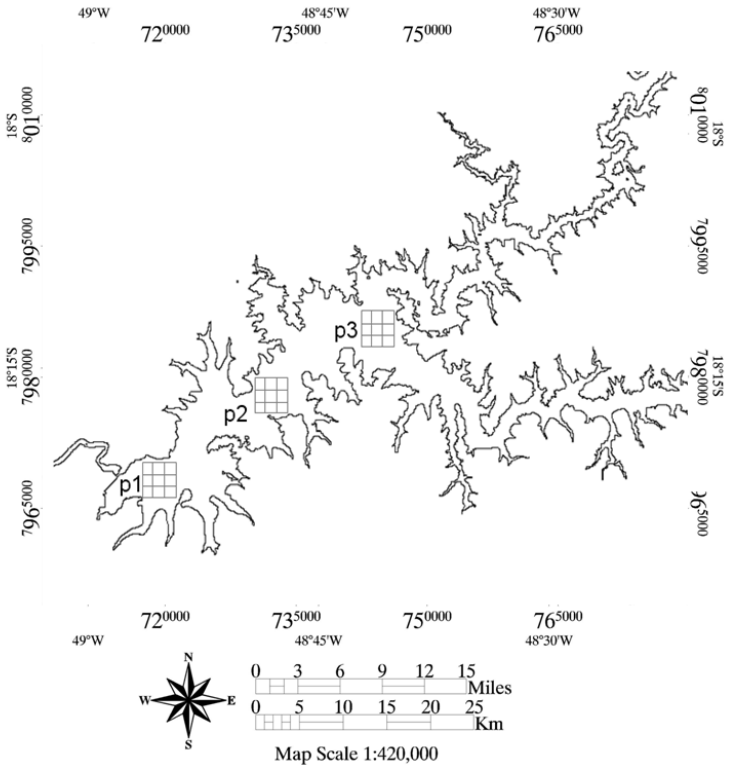

Figure 2: Sampling points location: p1 – region near de dam; p2 – central region of the reservoir and p3 – region under influence of the rivers.

Time Series Analysis

To show the relationship between WST and the significantly time series highlighted by Pearson's correlation the cross wavelet analysis was carried out and the coherence and phase analyzed (Grinsted, 2004).

The cross wavelet transform of two time series x_n and y_n is defined as $W^{xy} = W^x W^{y*}$, where $*$ denotes complex conjugation, so the cross wavelet power could be defined as $|W^{xy}|$ (Grinsted et al. 2004). The interpretation of complex argument arg(W^{xy}) can be interpreted

as the local relative phase between x_n and y_n in time frequency space. The cross wavelet power theoretical distribution of two time series with background power spectra P_k^x and P_k^y is given in Torrence and Compo (1998) as:

$$D\left(\frac{\left|W_n^x(s)W_n^{y*}(s)\right|}{\sigma_x\sigma_y} < p\right) = \frac{Z_v(p)}{v}\sqrt{P_k^x P_k^y} \tag{2}$$

where $Z_v(p)$ is the confidence level associated with the probability p for a pdf defined by the square root of the product of two χ^2 distributions. Cross wavelet power reveals areas with high common power.

Another useful measure is how coherent the cross wavelet is in time frequency space. The wavelet coherence could be defined following Torrence and Webster (1998) as:

$$R_n^2(s) = \frac{\left|S(s^{-1}W_n^{wy}(s))\right|^2}{S(s^{-1}\left|W_n^x(s)\right|^2).S(s^{-1}\left|W_n^y(s)\right|^2)} \tag{3}$$

where S is a smoothing operator; Notice that this definition closely resembles that of a traditional correlation coefficient, and is useful to think of the wavelet coherence as a localized correlation coefficient in time frequency space. The calculation procedures of cross wavelet and wavelet coherence were coded in Matlab 6.5 (The MathWorks, Inc., Natick, MA).

RESULTS

Statistical model for daytime and nighttime water surface temperatures

The Pearson correlation computed between the daytime and nighttime WST derived from the MODIS image against the heat flux terms is shown in Table 1. For daytime temperatures, the only significant correlated heat flux was the shortwave radiation; for nighttime temperatures, it was the longwave radiation, latent heat flux and sensible heat flux.

The multiple regression analysis shows that for daytime WST, the correlated heat flux terms explain 89% of the annual variation (RMS=0.89ºC, $\rho < 0.0013$). For nighttime, the heat flux terms explain 94% (RMS=0.53ºC, $\rho < 0.0002$). The representative equations of these relationships are presented in equations 2 and 3:

$$T_{daytime} = 18.78 + (0.02\phi_S) \tag{2}$$

$$T_{nighttime} = 38.17 - (0.31\phi_{ri}) + (0.55_{lf}) + (0.39\phi_{sf}) \tag{3}$$

where $T_{daytime}$ is the daytime water surface temperature (ºC), $T_{nighttime}$ is the nighttime water surface temperature (ºC), ϕ_s is the short wave radiation (Wm^{-2}), ϕ_{ri} is the long wave radiation (Wm^{-2}), ϕ_{lf} is the latent flux (Wm^{-2}) and ϕ_{Sf} is the sensible flux (Wm^{-2}).

Table 1: Pearson correlation coefficients for daytime and nighttime surface temperatures against shortwave radiation (ϕ_S), longwave radiation (ϕ_{ri}), sensible flux (ϕ_{sf}), and latent flux (ϕ_{lf}).

	Daytime water temperature	Nighttime water temperature
ϕ_S	0.64	-
ϕ_{ri}	-	-0.65
ϕ_{sf}	-	0.42
ϕ_{lf}	-	-0.64

Only values at a 95% significance level are shown.

Only the incoming shortwave radiation was needed to model the daytime WST. This is because when the shortwave radiation increases, the air temperature increases and transfers heat in the water column. However, the pattern of wind intensity and direction during the day is also important; with high wind intensity, the surface water loses heat through convection.
At night, the processes of convection and advection acting at the surface water and the balance of longwave radiation are important to drive the water temperature. Because of this, equation 3 is a subtraction of the joint effects of these three important fluxes.

Cross wavelet, coherence and phase

Daytime water surface temperature versus shortwave radiation (ϕ_S)

The cross wavelet between the daytime WST and the ϕ_S shows two band period of high common power: the first in the band period of 4.5-7 (regions 1 and 2) months, in special the semester from years 2004 and 2007; the second with the highest common power between 9-15 months (region 3) also with special attention in the years 2004 and 2007 (Figure 3-a).

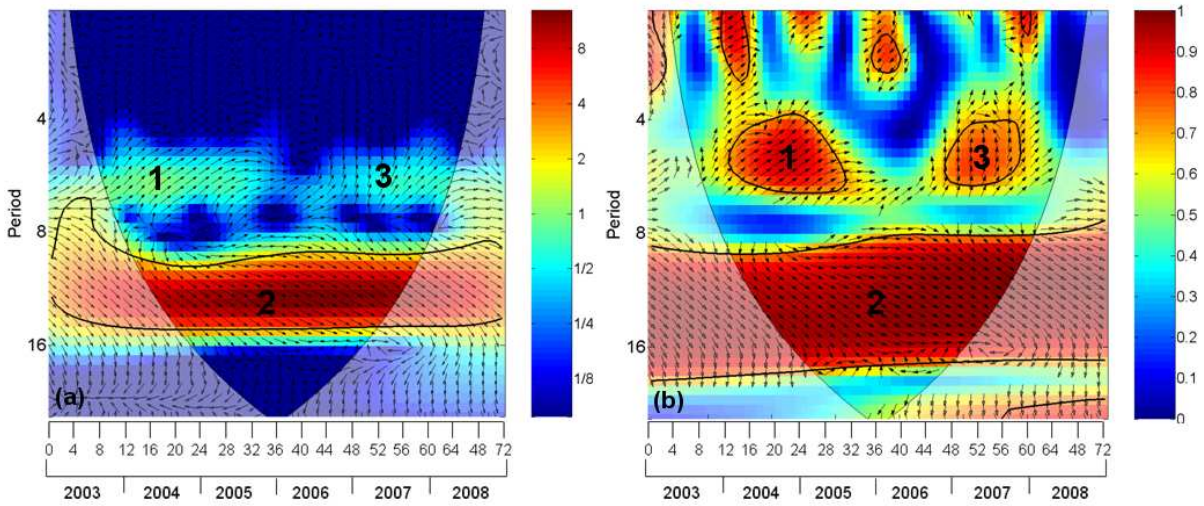

Figure 3: Cross wavelet between daytime WST and ϕ_S (a) and the coherence and phase (b).

The coherence in these common power periods (Figure 3-b) that: for the region 1 (period of 4-7 months) the ϕ_S is retarded 45º [~21 days] in relation to WST (from January 2004 to July 2005); for the region 2 (period of 8-16.5 months) the ϕ_S is advanced 45º [~1.5 months] in relation to WST and the region 3 (band period of 4.5-6.5) the ϕ_S is retarded 90º [~1.25 months] in relation to WST.

Nighttime water surface temperature versus longwave radiation (ϕ_{ri})

The cross wavelet analysis between the nighttime WST and ϕ_{ri} is show in the Figure 4. Five high common power was identified: (1) band period of 1-2 months localized between November 2004 and April 2005 (Figure 4-a), with ϕ_{ri} advanced 45º [~ 6 days] in relation to nighttime WST (Figure 4-b); (2) band period of 3-4 months localized between January and July 2007, with ϕ_{ri} advanced 90º [~27 days]; (3, 4) band period of 5-6 months end of 2005 until the beginning of 2006, with ϕ_{ri} advanced 135º [~2 months]; and (5) band period of 9-15 months localized between January 2004 until November 2007, with ϕ_{ri} advanced 135º [~6 months].

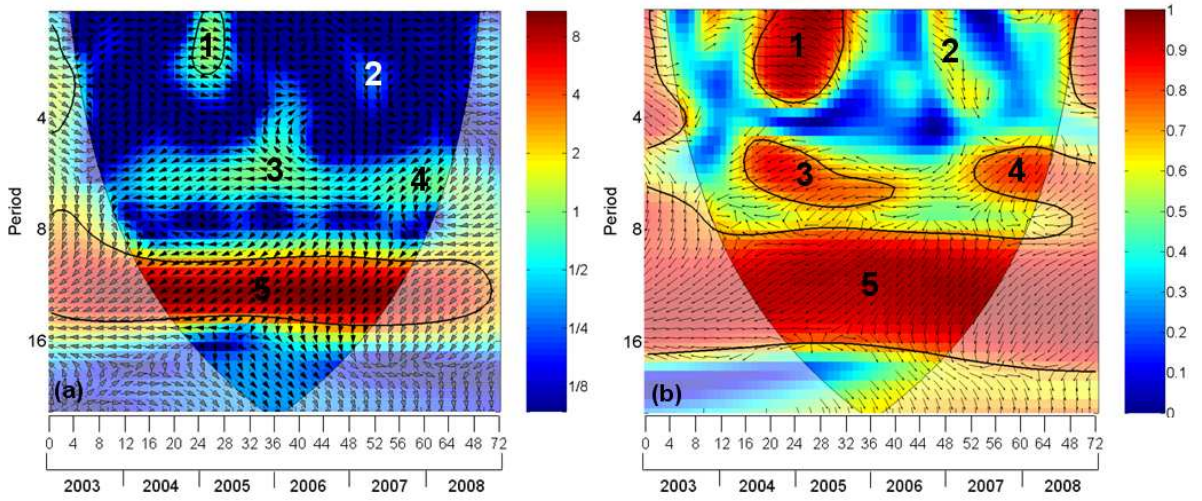

Figure 4: Cross wavelet between nighttime WST and ϕ_{ri} (a) and the coherence and phase (b).

Nighttime water surface temperature versus sensible flux (ϕ_{sf})

The cross wavelet analysis between the nighttime WST and ϕ_{sf} is show in the Figure 5. Four high common power was identified: (1) band period of 2-3 months localized from September to December 2004 (Figure 5-a), with ϕ_{sf} retarded 45º [~9 days] in relation to nighttime WST (Figure 5-b); (2) band period of 5-7 months localized from April 2004 to April 2005, with ϕ_{sf} advanced 135º [~2 months]; (3) band period of 5.5-7 months between May 2007 to March 2008, with ϕ_{sf} advanced 135º [~2 months]; and (4) band period of 9-15 months localized between February 2004 until November 2007, with ϕ_{ri} advanced 45º [~2 months].

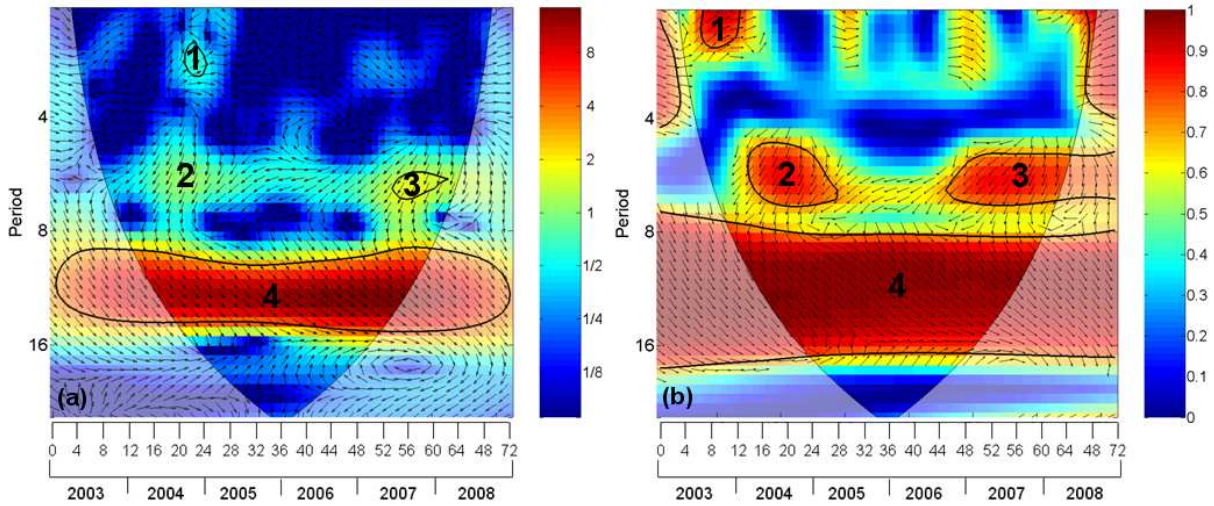

Figure 5: Cross wavelet between nighttime WST and ϕ_{sf} (a) and the coherence and phase (b).

Nighttime water surface temperature versus latent flux (ϕ_{lf})

The cross wavelet analysis between the nighttime WST and ϕ_{lf} is show in the Figure 6 and was identified four high common: (1) band period of 1-3 months localized from August 2004 to April 2005 (Figure 6-a), with ϕ_{lf} retarded 45º [~8 days] in relation to nighttime WST (Figure 6-b); (2, 3) band period of 6-8 months localized from April 2004 to January 2005, with ϕ_{lf} retarded 90º [~1.7 months]; (4) band period of 9-15 months between February 2004 to November 2007, with ϕ_{lf} and nighttime WST in anti-phase.

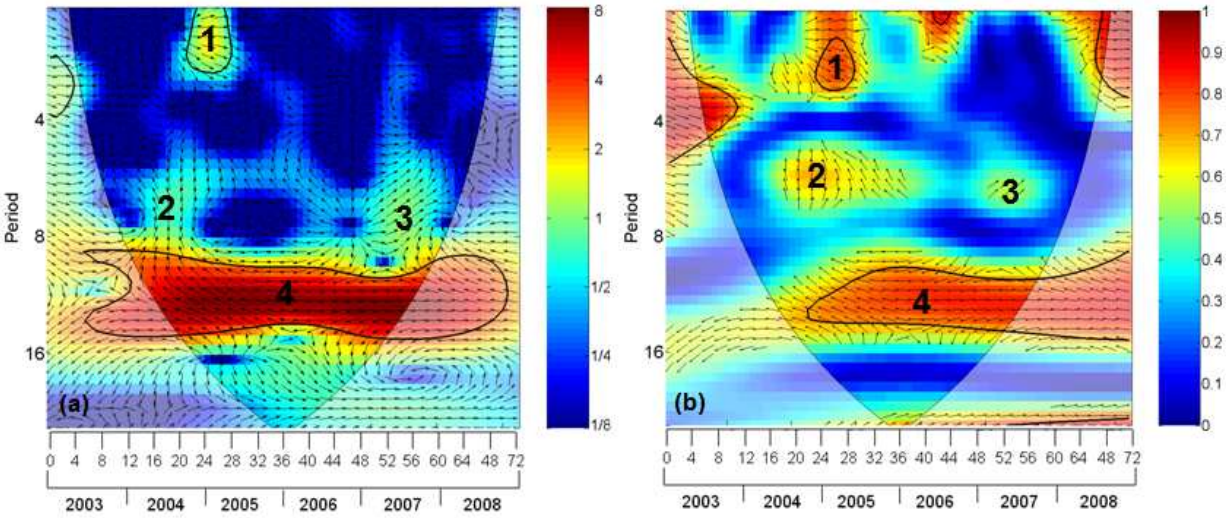

Figure 6: Cross wavelet between nighttime WST and ϕ_{lf} (a) and the coherence and phase (b).

CONCLUSIONS

The results obtained allow reaching the following conclusions:

(1) if we assume that the water surface temperature (WST) could be explained only the heat fluxes then for daytime WST only the shortwave radiation explain 89% of the temperature variability; to nighttime WST the longwave, sensible and latent flux explain 94%;
(2) The daytime WST and shortwave radiation presents a good agreement for periods of 6 (with shortwave retarded) and 12 months (with shortwave advanced);
(3) For nighttime WST and longwave the good agreement is present for 1, 3, 6 and 12 months, all with longwave advanced in relation to WST;
(4) The nighttime WST and sensible flux high common power for band periods of 2 (retarded), 6 (advanced) and 12 (advanced);
(5) Finally, the nighttime WST and latent flux with band periods of 2 (retarded), 6 (retarded) and 12 months (WST and latent flux in anti-phase).

ACKNOWLEDGMENTS

The authors would like to thank the FAPESP Project 2007/08103-2, INCT for Climate Change project (grant 573797/2008-0 CNPq). Enner Alcântara thanks CAPES grant 0258059.

REFERENCES

Alcântara, E., Novo, E., Stech, J., Lorenzzetti, J., Barbosa, C., Assireu, A., Souza, A. (2010). A contribution to understanding the turbidity behaviour in an Amazon floodplain, Hydrol. Earth Syst. Sci. **14**:351-364.

Bonnet MP, Poulin M, Devaux J (2000) Numerical modeling of thermal stratification in a lake reservoir: Methodology and case study. Aquatic Science **62**:105-124.

Crosman ET, Horel JD (2009) MODIS-derived surface temperature of the Great Salt Lake. Remote Sensing of Environment. **113**:73-81.

Grinsted, A., Moore, J. C., Jevrejeva, S. (2004). Application of the cross wavelet transform and wavelet coherence to geophysical time series, Nonlinaer Proc. Geoph. **11:**561–566.

Henderson-Sellers B (1986) Calculating the Surface Energy Balance for Lake and Reservoir Modeling: A Review. Reviews of Geophysics. **24**:625-649.

Jerosch, K., Schlüter, M., Pesch, R. (2006). Spatial analysis of marine categories information using indicator Kriging applied to georeferenced video mosaics of the deep-sea H˚akon Mosby Mud Volcano, Ecol. Inform. **1**:391-406.

Oesch D, Jaquet J-M, Hauser A, Wunderle S (2005) Lake surface water temperature using advanced very high resolution radiometer and moderate resolution imaging spectroradiometer data: validation and feasibility study. Journal of Geophysical Research, **10(**C12014):1-17.

Oesch D, Jaquet J-M, Klaus R, Schenker P (2008) Multi-scale thermal pattern monitoring of a large lake (Lake Geneva) using a multi-sensor approach. International Journal of Remote Sensing. **29**:5785-5808.

Reinart A, Reinhold M (2008) Mapping surface temperature in large lakes with MODIS data. Remote Sensing of Environment. **112**:603-611.

Torrence, C., Webster, P. (1999) Interdecadal changes in the ENSO-Monsoon system. Journal of Climate. 12:2679-2690.

Wan, Z. (2008). New refinements and validation of the MODIS land-surface temperature/emissivity products. Remote Sensing of Environment. **112**:59-74.

The impacts of the cold fronts on thermal stratification and water quality in a tropical reservoir (Brazil)

J.L. Stech, E.H. Alcântara*, J.A. Lorenzzetti, E.M.L.M. Novo, A.T. Assireu

National Institute for Space Research, Remote Sensing Division, Brazil.

**Corresponding author, e-mail enner@dsr.inpe.br*

ABSTRACT

Cold fronts arising from Antarctic and reaching the southeast Brazil region modify the wind field basic and have important impact over physical, chemistry and biological processes that act in the hydroelectric reservoirs. During the winter time these cold fronts can reach southeast Brazilian coast each six days and summer each fourteen days in average. Most part of them reaches interior of São Paulo, Minas Gerais and Goias States. Thus, the objective of this work is to analyze the influence of cold fronts passage in the thermal stratification and water quality of the Itumbiara (Goias, Brazil) hydroelectric reservoir. To reach this objective a collection o meteorological (wind direction and intensity, short-wave radiation, air temperature, relative humidity, atmospheric pressure), water quality (pH, dissolved oxygen, conductivity, turbidity) and water temperature in four depths (5, 12, 20 and 40 m) data were used. These data were collected using an Integrated System for Environmental Monitoring called SIMA, in high frequency, 10 minutes. SIMA, developed in partnership between the Vale do Paraiba University and the National Institute of Space Research INPE), is a set of hardware and software designed for data acquisition and quasi real time monitoring of hydrological systems. SIMA utilizes Brazilian satellites to transmit the data. The stratification was assessed by non-dimensional parameter analysis. The Lake Number an indicator of the degree of stability and mixing in the reservoir was used in this analysis. It was possible to observe the developing of upwelling and downwelling in different shores of the reservoir during the cold fronts passage. These phenomena can modify the chemistry and biological processes in the water body.

KEYWORDS

Thermal stratification, telemetric monitoring, Lake Number.

INTRODUCTION

Some authors (Stech and Lorenzzetti, 1992) had identified that the cold fronts arising from Antarctic reach the southeast Brazil region modifying the basic wind, atmospheric pressure and also the air temperature. During the winter time these cold fronts can reach southeast Brazilian coast each six days and summer each fourteen days in average. Most part of them reaches interior of São Paulo, Minas Gerais and Goias States.

These modifications were identified as a key for change the physical, chemistry and biological processes in the hydroelectric reservoirs (Tundisi et al. 2004). The response of each water body to meteorological conditions is revealed firstly by the thermal structure present in the water column (Ambrosetti and Barbanti, 2001).

Based on this the objective of this paper is to show the influence of the passage of cold fronts on the thermal stratification of a tropical hydroelectric reservoir in Brazil.

MATERIAL AND METHODS

Study area

The Itumbiara hydroelectric reservoir (18°25'S, 49°06'W) is located in a region stretched between Minas Gerais and Goiás States (Central Brazil) that was originally covered by tropical grassland savanna. The basin's geomorphology resulted in a lake with a dendritic pattern covering an area of approximately 814 km² and a volume of 17.03 billion m³ (Figure 1).

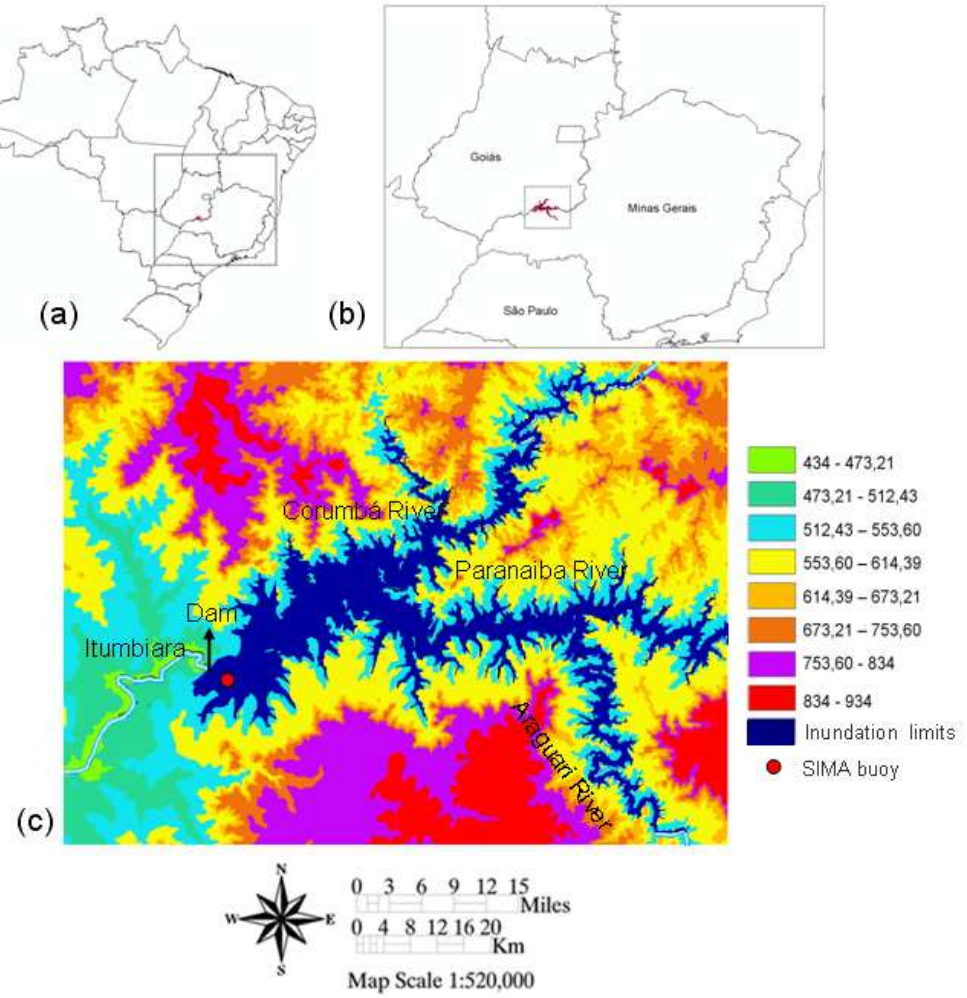

Figure 1: Itumbiara reservoir location in Brazil (a), between Minas Gerais and Goias States (b) and the topography near the reservoir and the location of the moored buoy (c).

Satellite data

The data of GOES-10 (Geostationary Operational Environmental Satellite) from May 31st to June 06th 2009 was used to capture the track of cold front pass over the Itumbiara reservoir.

Hydro-meteorological data

The meteorological (air temperature, humidity, air pressure and intensity wind) and limnological (water temperature in 5, 12, 20 and 40m depth) data from May 31st to June 06th 2009 was collected by a moored buoy called SIMA (Integrated System for Environmental Monitoring, see Stech et al., 2006) in each 1h.

Surface Energy Budget

A study of the energy exchange between the lake and atmosphere is essential for understanding the aquatic system behavior and its reaction to possible changes of environmental and climatic conditions (Bonnet, Poulin and Devaux, 2000). The exchange of heat across the water surface was computed using the methodology described by Henderson-Sellers (1986) as:

$$\phi_N = \phi_s(1-A) - (\phi_{ri} + \phi_{sf} + \phi_{lf}) \quad (1)$$

where ϕ_N is the surface heat flux balance, ϕ_s is the incident short-wave radiation, A is the albedo of water (=0.07), ϕ_{ri} is the Longwave flux, ϕ_{sf} is the sensible heat flux and ϕ_{lf} is the latent heat flux. The units used for the terms in Eq. (1) are W m^{-2}.

Lake Number - L_N

To indicate the degree of stability and mixing in the reservoir, due to the passage of cold front, the L_N was used (Imberger, 1998).

$$L_N = \frac{gS_t\left(1-\frac{Z_T}{Z_m}\right)}{\rho_0 u_* A_0^{3/2}\left(1-\frac{zg}{zm}\right)} \quad (7)$$

Where z_T and z_g are the height to the center of the metalimnion and the center of area, ρ_0 is the average density of the water column, u_* is the water friction velocity, A_0 is the surface area of the reservoir and S_t (gcm^{-1}) is an estimate of the stability of the reservoir calculated as (Hutchinson, 1957):

$$S_t = \frac{1}{\rho_0}\int_0^H g(h_v - z)\rho(z)A(z)dz \quad (8)$$

To calculate the stability of water column the reservoir bathymetry are needed.

Bathymetric Data

The bathymetry of the Itumbiara reservoir was made in two campaigns, the first from 11-15th May 2009 and second from 11-16 August 2009. The depth data was collected using an echo-sound LMS-525 from Lowrance, with a GPS (Global Positioning System) coupled. The depth data was treated in accordance to Merwade (2009).

RESULTS

Bathymetric Map

The results of the depth surveys show that the reservoir presents the highest depths in the line of flooded river with depths higher than 78m during the high water level; with a littoral zone with depth less than 2m. Other higher deep region is near the Dam where the depth reach 70m (Figure 3).

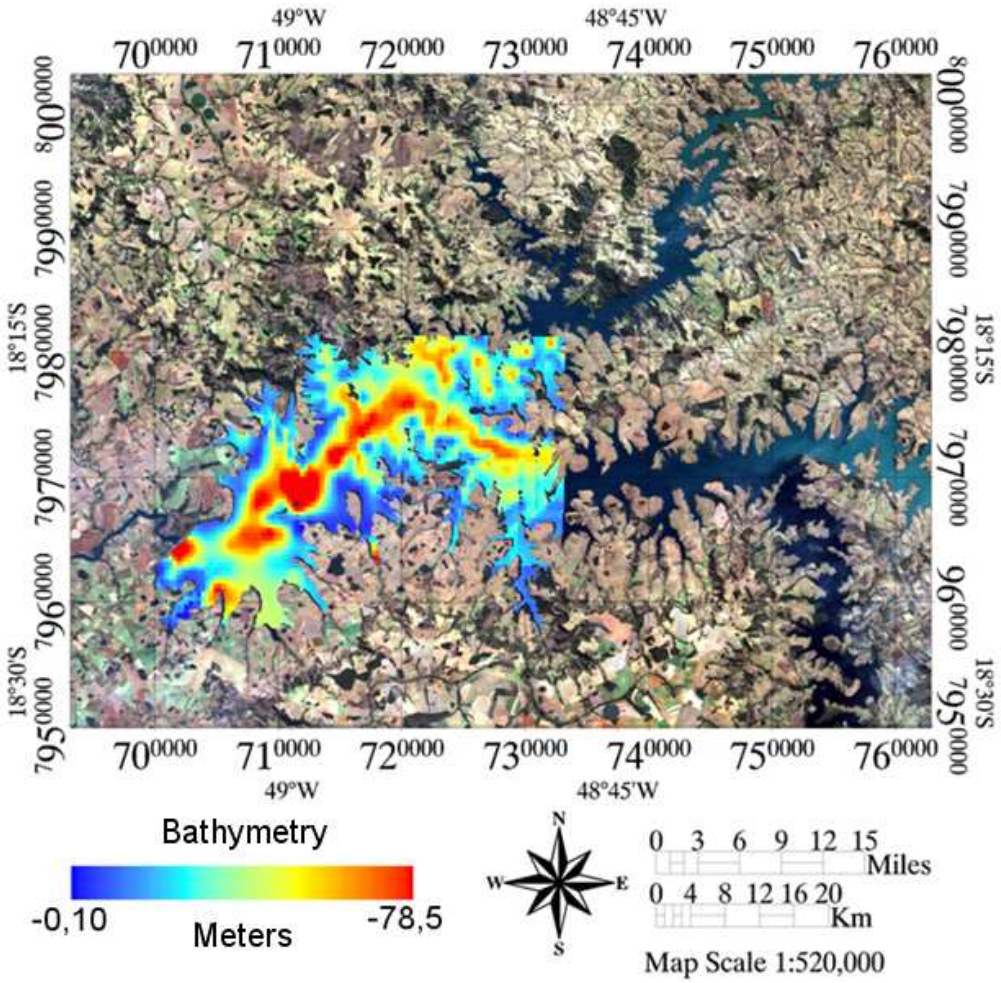

Figure 5: Bathymetric map of the Itumbiara reservoir.

Satellite data

Using the satellite GOES data is possible to see the extension and the hour of the cold front passage over the reservoir. The Figure 3 shows the evolution of the cold front passage over the reservoir and identifies the maximum activity of the front (Figure 3-b).

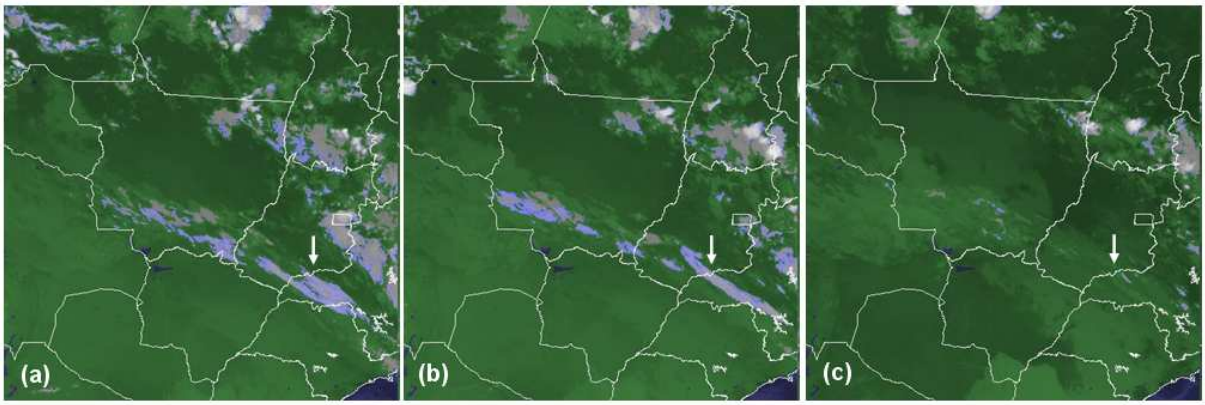

Figure 3: GOES-10 satellite data showed the evolution of the cold front passage over the reservoir: (a) 01st June 2009 at 08:00h, (b) 01st June 2009 at 09:45h (c) 01st June 2009 at 13:00h. The arrows indicate the location of the reservoir.

Meteorological and Limnological Data

The Figure 4 shows the meteorological and limnological parameters used in this study. It is clear that during the passage of cold front the atmospheric pressure and the air temperature decrease; in the other hand the wind shows a little increase and also the relative humidity. The water surface temperature decreases after the passage of the cold front as showed by Stech and Lorenzzetti (1992) for South Brazilian Bight..

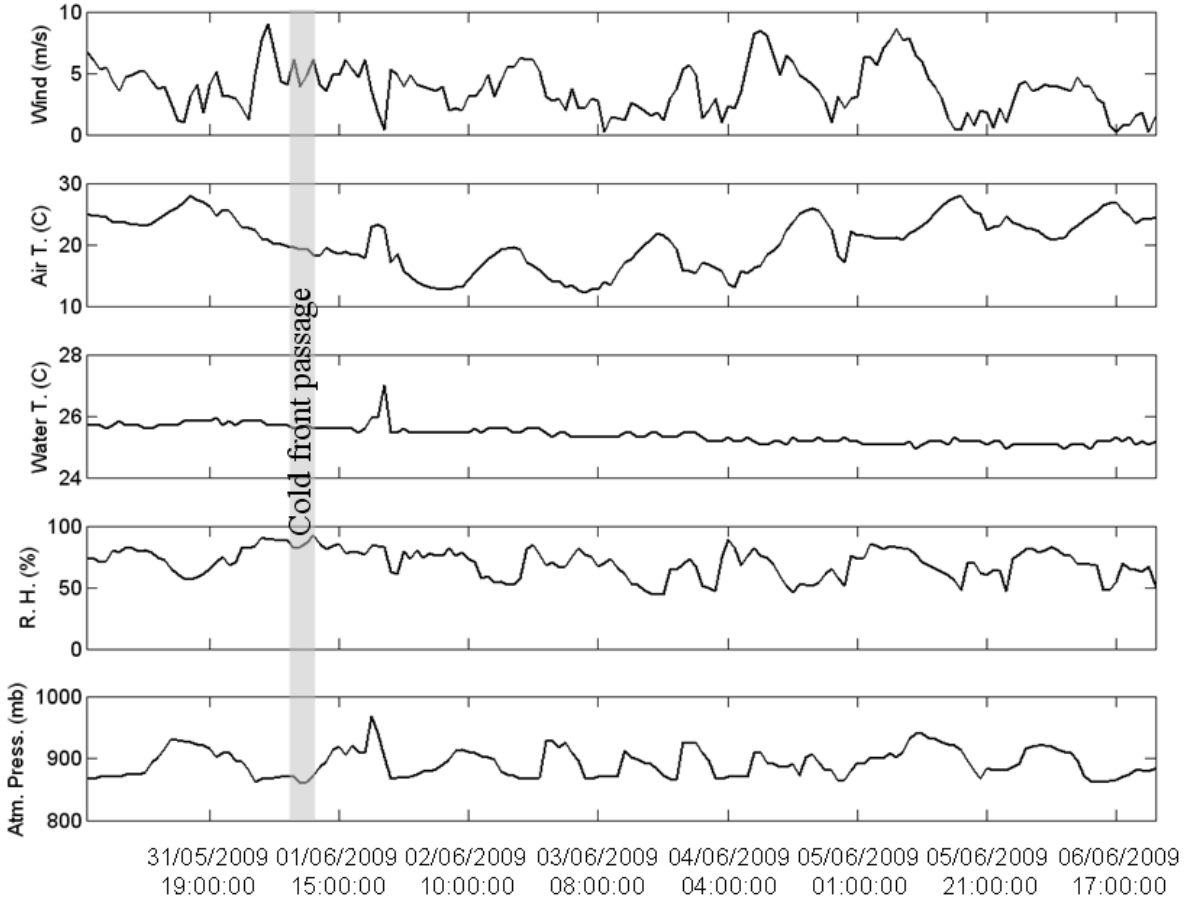

Figure 4: Meteorological (wind intensity, air temperature, relative humidity and atmospheric pressure) and limnological (water temperature) parameters collected by the SIMA buoy from May 31st to June 06th 2009.

This pattern observed before, during and after the passage of cold front is reflected in each component of the heat flux balance (Figure 5). During the passage of the cold front the intensity of the shortwave radiation decreases, with an increase of the longwave radiation. The sensible flux tends to be higher during and after the cold front passage if compared the period before the passage. The latent flux during the passage of the cold front tends to decrease, but after the passage the latent flux tents to increase again. The heat balance before the passage of cold front is positive when shortwave act in the systems; however during the passage the balance is negative and tends to normalize with the dissipation of the front.

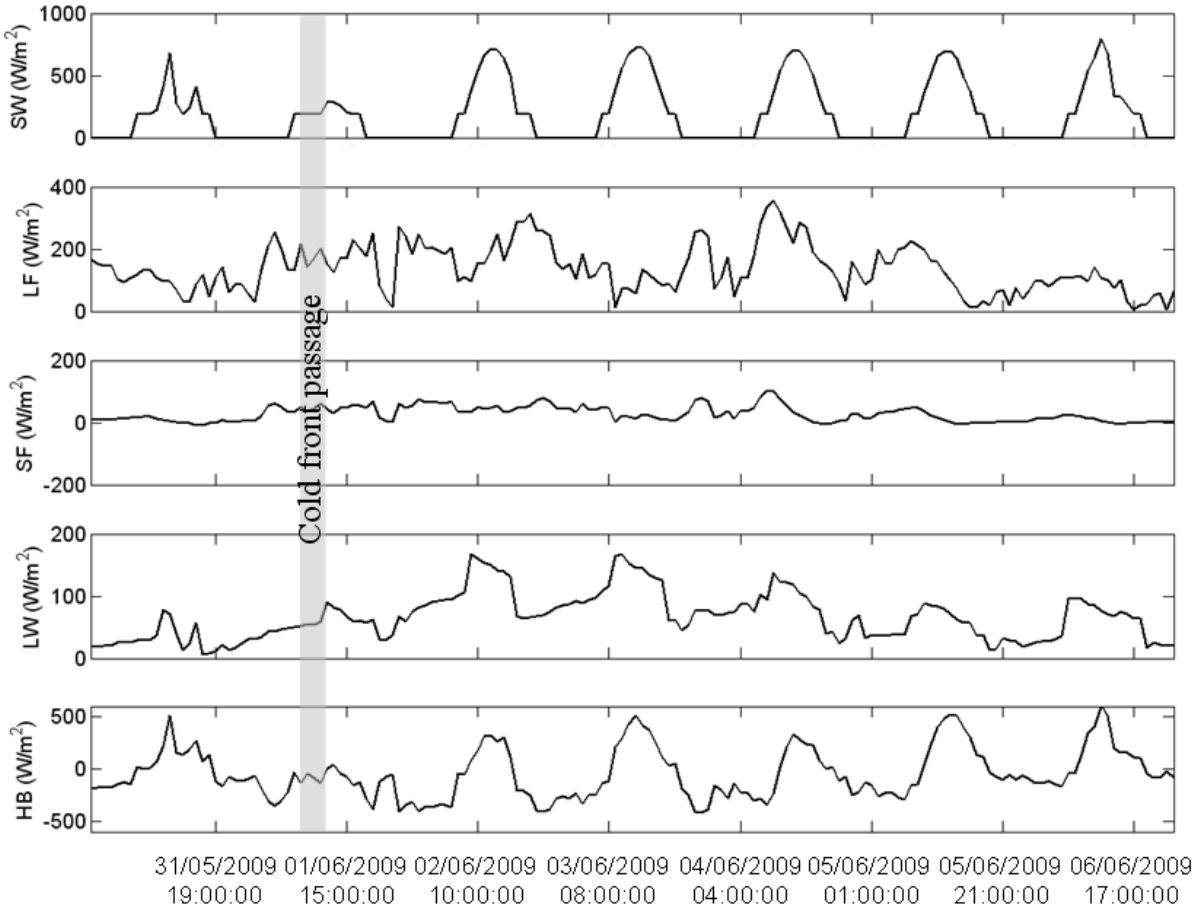

Figure 5: Heat flux components: SW – shortwave radiation, LF – latent flux, SF – sensible flux, LW – longwave radiation and HB – heat balance.

These pattern of meteorological and heat flux before, during the after the passage of the cold front will reflect in the water column temperature and stability (Figure 6). Before the passage of the front the water column presented a little temperature difference between the epilimnion and metalimnion; with the passage of the cold front the water temperature of the top-most layer decrease and the difference of temperature in the water column decreases also.

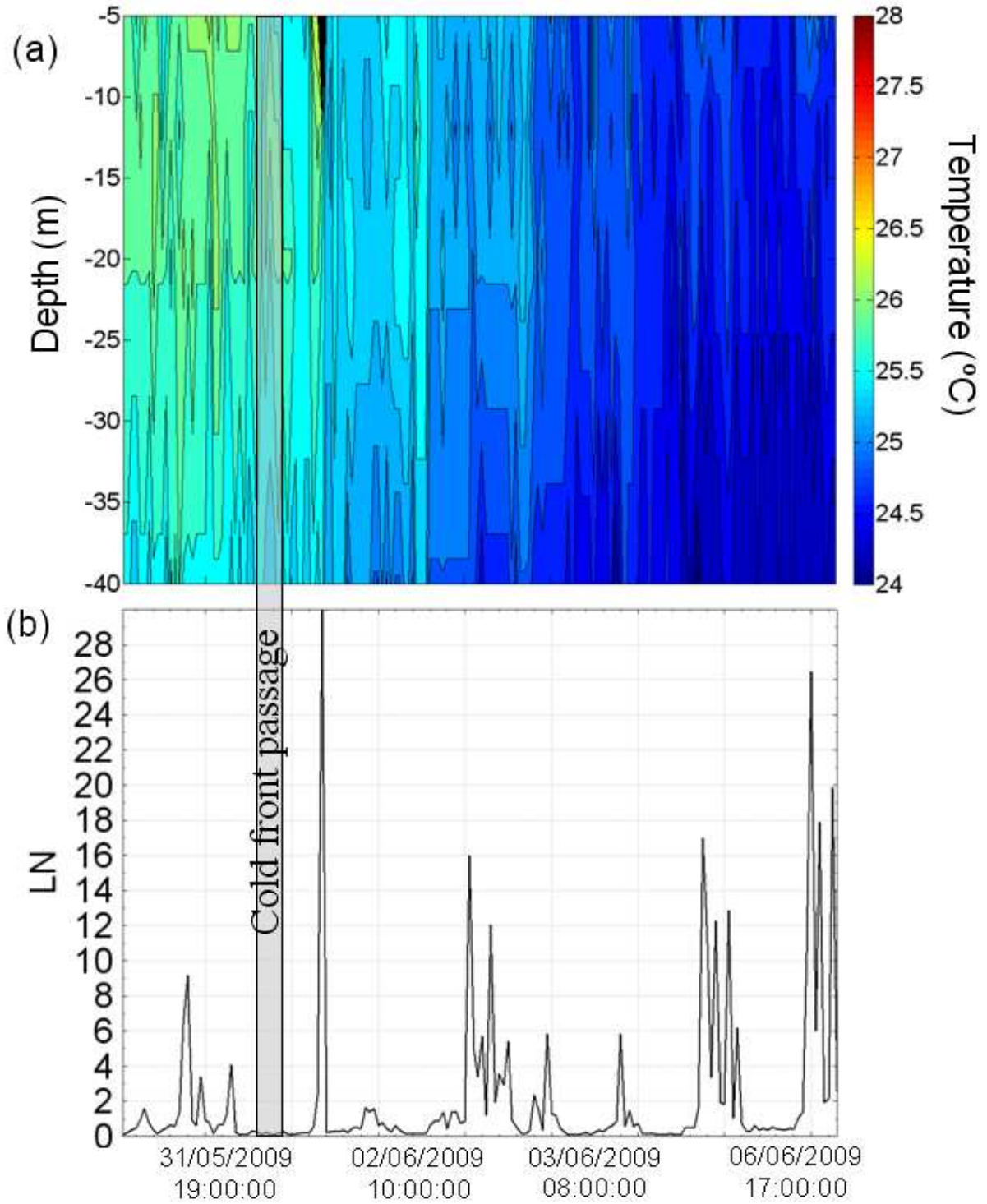

Figure 6: Thermal structure (a) and the Lake Number - L_N (b) for the Itumbiara Reservoir.

In accordance to Antenucci and Imberger (2003) when $L_N > 1$ there is no deep upwelling and when $L_N < 1$ the cold deep, often nutrient rich, water from the hypolimnion will reach the surface layer during the wind episode. All $L_N > 1$ occurred during the daytime when the incident shortwave radiation is present, but after the passage of the cold front the values of L_N increase during the heating phase. Often $L_N < 1$ occurred during the nighttimes, the unique exception is the day during the cold passage with L_N less than 1.

After the passage of the front the water from hypoliminion progressively cooler and the mixed layer goes up to the top layer. The fact of the L_N increases after the front passage during the daytime could be explained by the fact that during the cold front passage the water losses energy to the atmosphere and when the cold front dissipate the incident shortwave radiation heats the surface creating the condition enhancing the stability of the water column.
Tundisi et al. (2004) discuss that the most important finds of the cold front passage over a Brazilian hydroelectric reservoir is the release of iron and manganese; this is because this release could increase the costs of the drink water treatment.

CONCLUSION

The passage of cold front over a region decreases the atmospheric pressure and air temperature, enhancing the relative humidity. In tropical hydroelectric reservoir these modifications in the thermal structure can induce a great modification in the biological and chemical processes. Also when the upwelling event occur a cold water rise at the surface bring a nutrient rich masses that enhance the biological productivity in combination with light penetration into the water column.

ACKNOWLEDGMENTS

The authors would like to thank the FAPESP Project 2007/08103-2, INCT for Climate Change project (grant 573797/2008-0 CNPq). Enner Alcântara thanks CAPES grant 0258059.

REFERENCES

Ambrosetti, W.; Barbanti, L. (2001). Temperature, heat content, mixing and stability in Lake Orta: a pluriannual investigation. J. Limnol., **60**(1): 60-68.

Antenucci, J.; Imberger, J. (2003). The seasonal evolution of wind/internal wave resonance in Lake Kinneret. Limnology and Oceanography, **48**(5), 2055-2061.

Bonnet M.P.; Poulin, M.; Devaux, J. (2000). Numerical modeling of thermal stratification in a lake reservoir: Methodology and case study. Aquatic Science, **62**:105-124.

Henderson-Sellers, B. (1986). Calculating the Surface Energy Balance for Lake and Reservoir Modeling: A Review. Reviews of Geophysics, **24**:625-649.

Hutchinson, G.E. (1957). A treatise on limnology, geography, physics and chemistry. John Wiley, vol. 1, 1015p.

Imberger, J. (1998). Flux paths in a stratified lake: A review, p. 1– 18. In J. Imberger [ed.], Physical processes in lakes and oceans. Coastal and Estuarine Studies, Vol. 54. Am. Geophys. Union.

Merwade, V. (2009). Effect of spatial trends on interpolation of river bathymetry, Journal of Hydrology, **371**:169-181.

Stech, J.L.; Lorenzzetti, J.A. (1992). The response of the South Brazil Bight to the passage of wintertime cold fronts. Journal of Geophysical Research, **97**(C6):9507-9520.

Stech, J.L; Lima, I.B.T.; Novo, E.M.L.M.; Silva, C.M.; Assireu, A.T.; Lorenzzetti, J.A.; Carvalho, J.C.; Barbosa, C.C.F; Rosa, R.R. (2006). Telemetric Monitoring system for meteorological and limnological data acquisition. Verh. Internat. Verein. Limnol. **29**:1747-1750.

Tundisi, J. G., T. Matsumura-Tundisi, J. D. Arantes Junior, J. E. M. Tundisi, N. F. Manzini & R. Ducrot. (2004). The response of Carlos Botelho (Lobo, Broa) Reservoir to the passage of cold fronts as reflected by physical, chemical and biological variables. Brazilian Journal of Biology, **64**:177–186.

Modelling the diurnal migration of *Microcystis* in a stratified reservoir with a particle trajectory approach

Y.C. Chien and S.C. Wu*

Graduate Institute of Environmental Engineering, National Taiwan University, 71 Chou-shan Rd. Taipei, Taiwan 10673, Republic of China

**Corresponding author, e-mail scwu@ntu.edu.tw*

ABSTRACT

Sin-san Reservoir is a subtropical off-channel reservoir, and has developed a well stratified structure in terms of temperature and density from June to October annually. *Microcystis* blooms can be observed during this period of time every year. It is believed that *Microcystis* cells are capable of catching sun light in the euphotic zone and obtaining sufficient nutrients for growth in a well stratified water body, while other species of phytoplankton are not. The diurnal migration of *Microcystis* regulated by the change of buoyancy, which has been reported in the literature, may play a key role on this advantageous growth pattern. Cell density determines the velocity of floating or sinking in addition to the random movement due to turbulent mixing. It has been suggested that there are two mechanisms controlling the density of *Microcystis* cells, producing ballast material or compressing the gas vescles, which are both regulated by radiation intensity. A trajectory model which takes the diurnally changing solar radiation intensity and its influence on the movement of *Microcystis* cells into consideration has been developed. The results of simulation well describe the buoyancy regulated vertical migration within a 24-hour period. The established trajectory modeling approach would enable us to study the effects of desynchronized nutrient uptake and growth processed on the growth of *Microcystis* in stratified water bodies in the future.

KEYWORDS

Microcystis, buoyancy regulation, diurnal vertical migration, stratification, particle-tracking

INTRODUCTION

Sin-san Reservoir is one of the subtropical off-channel reservoirs in Taiwan, and has developed a well stratified structure in terms of temperature and density from June to October annually. *Microcystis* blooms can be observed during this period of time every year. It is believed that *Microcystis* cells are capable of catching sun light in the euphotic zone and obtaining sufficient nutrients for growth in a well stratified water body, while other species of phytoplankton are not. The diurnal migration of *Microcystis* regulated by the change of buoyancy, which has been reported in the literature, may play a key role on this advantageous growth pattern. Simulation of the movement of individual particles in a dynamic environment is an important tool for investigating ecological process in the ocean(Werner *et al*., 1993; Hare *et al*., 1999).

That cyanobacteria can regulate their buoyancy has been well documented (Walsby, 1970; Oliver and Walsby, 1984; Ibelings *et al*., 1991). This characteristic is considered to be important in contributing to the dominance of cyanobacteria in a wide range of aquatic ecosystems for its providing the advantage of altering position in the water column through physiological changes (Reynolds, 1987; Reynolds et al., 1987). The position of non-mobile

cyanobacteria cells or colonies in the water column depends on both the buoyancy of the cyanobacteria and the water motions. The short-term change of buoyancy is regulated by changing of the storage of carbohydrate in the cells (Kromkamp *et al*., 1986; Kromkamp and Walsby, 1990).

In the last two decades many attempts have been done to quantitatively describe the vertical distribution of *Microcystis* in water bodies (Visser *et al*., 1997; Wallace and Hamilton, 1999; Wallace and Hamilton, 2000; Wallace *et al*, 2000; Rabouille and Salençon, 2005). Some of these models of vertical migration could simulate the vertical trajectory of the position of colonies, but the colony size must be the same for all colonies at each run time. In natural water, the diameters of colonies are distributed. Each single colony has its own trajectory. Though some of these models could simulate the migration and growth of *Microcystis* population, the way to qualify population was using the total biovolume or carbohydrate content of population. This approach would average the 'behaviors' of different colonies, and could not trace the nutrient uptake rate of *Microcytis* nor the dynamic change of the individual cell density, which were all determined by the history of each cell.

The objective of this study is to develop a mathematical model which is able to simulate the vertical distribution of the population of *Microcystis* over time scales of hours and days in a subtropical reservoir with thermal stratification by the particle trajectory approach. Various physical factors such as diffusion, thermal stratification, temperature and sunlight intensity which affect the movement of *Microcystis* were considered in the present study.

Modelling the Movement of Microcystis

Diurnal change of the buoyancy of Microcystis occurs primarily through the change of the content of carbohydrate ballast (Thomas and Walsby, 1986). A simple empirical buoyancy regulation model for *Microcysis* has been used to predict the vertical position of colonies in turbulent environments is described in Wallace and Hamilton (1999) as described in (1).

$$\frac{dD}{dt} = k_r(D - D_{eq}) \tag{1}$$

where D is the rate of cell buoyancy change through the accumulation of stored cellular carbohydrate, D_{eq} is the equilibrium value of D and k_r is given by:

$$K_r = \begin{cases} \dfrac{1}{\tau_r}; & \text{for increasing light} \\ 0; & \text{for decreasing light} \end{cases} \tag{2}$$

where τ_r is the response time of adjustment of the rate of carbohydrate ballast accumulation. The form of Deq for *Microcystis aeruginosa* was found by Wallace and Hamilton (1999) to be best described by the equation suggested by Kromkamp and Walsby (1990):

$$D_{eq}(I) = \frac{d\rho(I)}{dt} = \frac{c_1 I(t)}{K_I + I(t)} - c_3 \tag{3}$$

where c_1 is the rate constant determining the increase in density with time, K_I is the irradiance at which the rate of density increase with time is half the maximal rate, and c_3 is the minimum rate of density decrease in the dark. In addition, the rate of cell buoyancy change in the dark due to a decrease of stored cellular carbohydrate is given by Visser *et al*. (1997) as

$$D = \frac{d\rho}{dt} = -c_2\rho - c_3 \quad (4)$$

where c_2 is the rate constant determining the decrease in density with time.

METHOD

Characteristics of the studied reservoir

Sin-san Reservoir is an off-channel reservoir located in the northwestern part of Taiwan with its water surface about 90 m above sea level, an average depth of 20 m and a total volume of 10 million cubic meters. The water is pumped into the reservoir from the nearby Keelung River through an inlet at the bottom, which is also the water outlet. The reservoir has developed a well stratified structure in terms of temperature and density from June to October every year with the highest surface temperature up to 32 ^{o}C and the hypolimnetic temperature about 17 ^{o}C.

There have been *Microcystis* blooms during late spring and early summer every year recently. When the surface water temperature increases gradually, the stability of the stratified structure of the water body gets higher. The nutrients in the epilimnion will soon be depleted due to limited vertical mass transfer and vigorous algal growth. It creates a better environment for the dominance of *Microcystis*, which favors high intensity of light and tolerates low nutrient concentration. However, *Microcystis* population declines as summer goes by. *Microcystis* blooms disappear in middle summer.

Model Structure and Scenario Setting

The developed one-dimensional model was intended to represent the vertical movements of a population of *Microcystis* colonies in the water column of a thermally stratified reservoir. Since the time range of the model simulation is only few days, the temperature profile of the water column was assumed to be constant during this short period of time. The processes that control the movement of the algal cells under this situation include the sinking or floating velocity of the individual cell and the turbulent mixing. A particle trajectory model was developed to describe the movement of a cohort of colonies of *Microcystis* with various colony size driven by the difference between cell density and the water density.

Particle-tracking method

The displacement of a single algal cell is contributed by advection due to sinking or floating, and mixing which can be modeled as a random walk (Csanady, 1973). A finite difference expression of the position of an algal cell including the displacement of one time step due to advection and random walk is defined by (1).

$$Z_n = Z_{n-1} + V\Delta t + R_n\sqrt{2K_z\Delta t} \quad (5)$$

where Z_{n-1} and Z_n are the initial and final depths, respectively, V is the vertical velocity (advection, and determined by grag force..), and final term is a random walk where K_z is the vertical diffusivity, R_n is a normal variate with zero mean and unit variance, and Δt is the time step. However, when turbulent diffusion varies spatially, as it does in nature and in the physical model, simple random walk models accumulate particles in regions of low diffusivity (Hunter, Craig, Phillips, 1993; Visser, 1997). Visser (1997) derived a more 'corrected' random walk model in which there is an additional non-random 'advective' component, $K'(Z_{n-1})$. The diffusivity is not estimated at the initial particle location, Z_{n-1}, but offset a distance $1/2\ K'(Z_{n-1})\ \Delta t$. Implementing this correction yields equation (2).

$$Z_n = Z_{n-1} + V\Delta t + K'(Z_{n-1})\Delta t + R_n\sqrt{2K_z[Z_{n-1} + 1/2K'(Z_{n-1})\Delta t]\Delta t} \quad (6)$$

When modeling the vertical distribution of the amount of *Microcystis* cells in the water column, the positions of a number of colonies, which are randomly distributed in water, will be tracked. The radii of the colonies are assumed to be in a normal distribution initially.

Sinking and floating velocity

The sinking velocity of a *Microcystis*, *V*, is calculated from the modified Stokes equation

$$V = 2gr(\rho - \rho_w)/(9\Phi n) \quad \text{(m/s)} \quad (7)$$

$$n = 10^{-3} \times [10^{(-1.65 + 262/(T + 139))}] \quad \text{(kg/(m s)} \quad (8)$$

where g is the gravitational acceleration (9.81 m/s^2), r is the radius of the sphere of volume equal to that of a *Microcystis* colony (m); $(\rho - \rho_w)$ is the difference between the density of a *Microcystis* colony (ρ) and of water(ρ_w), Φ is the coefficient of form resistance, and n is the viscosity of the water at the temperature T(℃)。

Density change

Equation (9) to (11) were used to predict the density change of Microcystis colonies. The finite difference expression of the cell density is given by (9)

$$\rho_{t+1} = \rho_t + D\Delta t \quad (9)$$

The sun light irradiation intensity which control the rate of the carbohydrate ballast accumulation is decaying with depth as described in (10)

$$I_z = I_0 e^{-\lambda z} \quad (10)$$

where I_z and I_0 are the sun light irradiation at depth of z and water surface, respectively.

The diurnal change of the surface irradiation, I_0, is approximated with a semi-sine curve function (Eq. 11)

$$I_0 = I_{\max} \times \frac{1}{2} \times \left(\sin(2\pi(t - 360)/1440) + abs(\sin(2\pi(t - 360)/1440))\right) \quad (11)$$

where I_0 is the surface light intensity at time t (minute), and $I_{\max}$ is the maximum daily surface light intensity. In addition, the time range of simulation is 72 hr, the time step is 1 minute, and the boundary depth is 20 meters.

Estimation of diffusivity

Many investigators have estimated diffusivity directly from temperature data (e.g., Jassby and Powell, 1975; Robarts and Ward, 1978; Michalski and Lemmin, 1995; Benoit and Hemond, 1996). The eddy diffusivity is varying continuously in time and space. Vertical turbulent mixing coefficient can be determined by the flux gradient method from integral changes of a tracer, such as temperature, over a certain time and a certain depth in the following way:

$$K_z = \left\{-1/\left[A(z)\frac{\Delta T}{\Delta z}\right]\right\}\int_z^{z_{\max}} A(z')\frac{\Delta T}{\Delta z}dz' \quad (12)$$

where *A(z)* is the reservoir surface area at depth *z*, *T* is temperature, *t* is time, and z_{max} is the bottom of the lake. The flux gradient method is valid during periods when lakes or reservoirs warm up but is not valid when convective cooling overwhelms wind induced mixing. Many investigators have applied this method to different lakes (e.g. Stauffer, 1992; Wüest *et al*.,2000; Lin, 2004). Thermal gradient and heat flux terms in the equation were smoothed by a moving average of two measurements across time, and the final K_z values are a moving average of the period (April 26- May 8, 2007) across depth.

Parameters Setting

The parameters setting of this simulation are shown in Table 1.

Table 1. The values of parameters used in the model simulation

Symbol	Description	Value	Units
c_1	Constant rate of density increase in the light	0.0127	kg/m^3/min
c_2	Constant rate of density decrease in the dark	0.001	kg/m^3/min
c_3	Minimum rate of density decrease in the dark	4.6E-5	kg/m^3/min
τ_r	Response time	20	min
K_I	Half saturated constant of irradiance	536.0	μ mol photons/m^2/s
I_{max}	Maximum surface irradiance	1000	μ mol photons/m^2/s
K_d	Light extinction constant under the water	0.5	1/m
r	Colony radius	400 ±300	μ m

RESULT AND DISCUSSION

Diffusivity calculated and temperature input

The vertical distribution of *Microcystis* colonies was simulated under the condition of a thermal stratified water, in which the temperature profile was measured on May 8 and kept constant (), and the diffusivity was calculated by the heat flux during this period of April 26 to May 8, 2007. The diffusivity near surface was quite large, and it declined down to the thermocline. The diffusivity at thermocline was quite low averagely, and the trend of the diffusivity at hypolimnion was similar to that at thermocline.

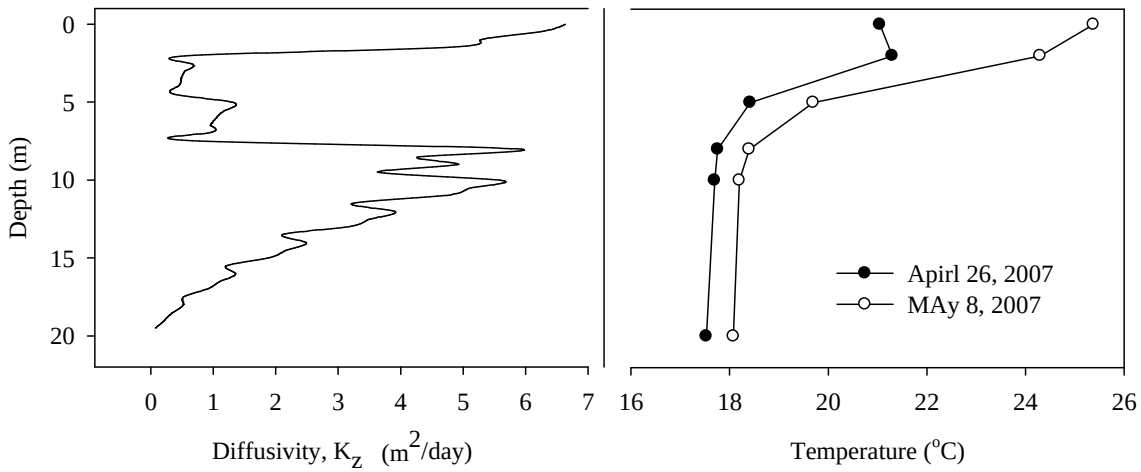

Figure 1. The estimated diffusivity and the measured temperature profiles used in the simulation.

Results of trajectory simulation

Eleven hundred colonies of *Microcystis* cells with their size in a normal distribution were evenly distributed over the whole water column at the beginning of the simulation. **Figure 2** shows the trajectories of 9 colonies in the water column, three of which were initially in epilimnion (0 m), three in thermocline (8 m), and three in hypolimnion (18 m). The initial depth of colonies seems not affecting the pattern of the vertical migration, which is sinking during the daytime and rising during the night. In summary, *Microcystis* colonies were (1) mostly sinking at daytime until afternoon; (2) some 'suspended' at thermocline (exception for No.410, 450, 954); (3) once sinking stop, rising sharply; (4) few colonies (No. 410, 450, 954) sunk to the bottom and never rising again.

Distribution of trajectory result

Figure 3 shows the distribution of colonies by integrating trajectory results. The distribution started diversely and gradually became converging to a clearly diurnal pattern after 20 hours of simulation. This simulation agrees with the real diurnal migration pattern of *Microcystis* observed in Sin-san Reservoir. Similar patterns repeated in the second and third day. The concentration peak sank gradually from midday until afternoon. However, once the sinking stop, the cohorts of colonies raised immediately. The reason of the simulation pattern might be due to that the parameters of density decreasing rate in the dark (c_2, and c_3) were too large. The larger density decrease rate caused the density of *Microcystis* colonies decrease in a quite short time. In addition, there were few colonies 'stuck' at the bottom due to the very low diffusivity at the bottom of hypolimnion.

CONCLUSIONS

In natural environment, phytoplankton is continuously mobilized by turbulence and density difference in the vertical gradients of light and temperature. The simulation involved tracking the vertical position of colonies with random normally distributed sizes. The model could be used to quantify the impacts of light, temperature and turbulence on the migration of colonies with different radius. Using the trajectory model of vertical migration, each colony is tracked, and the dynamic distribution of colonies can be obtained by integrating the mass of the *Microcystis* colonies along the depth. The advantage of this model is that it could also track the history of nutrient uptake of *Microcystis* by incorporating Droop's model (Droop, 1973) in the model in the future study.

ACKNOWLEDGMENTS

The authors are grateful to the Sin-san Reservoir Authority for its assistance on field investigation and to National Science Council for its partial financial support on this study through grant number NSC 96-2221-E-002-058-MY3.

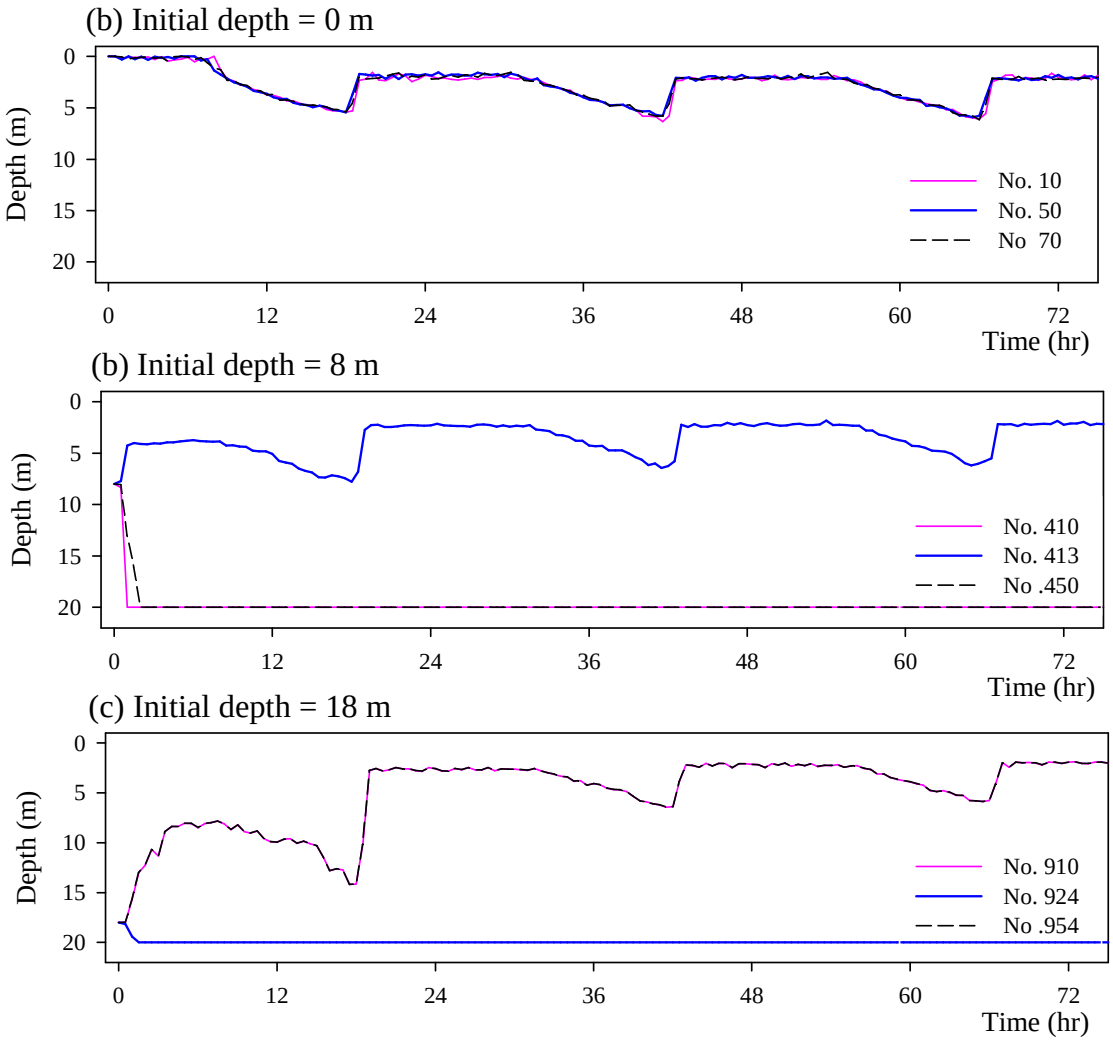

Figure 2. Simulated vertical trajectories of nine *Microcystis* colonies within 72 hours, three of which were initially in epilimnion (0 m) (shown in (a)), three in thermocline (8 m) (shown in (b)), and three in hypolimnion (18 m) (shown in (c)).

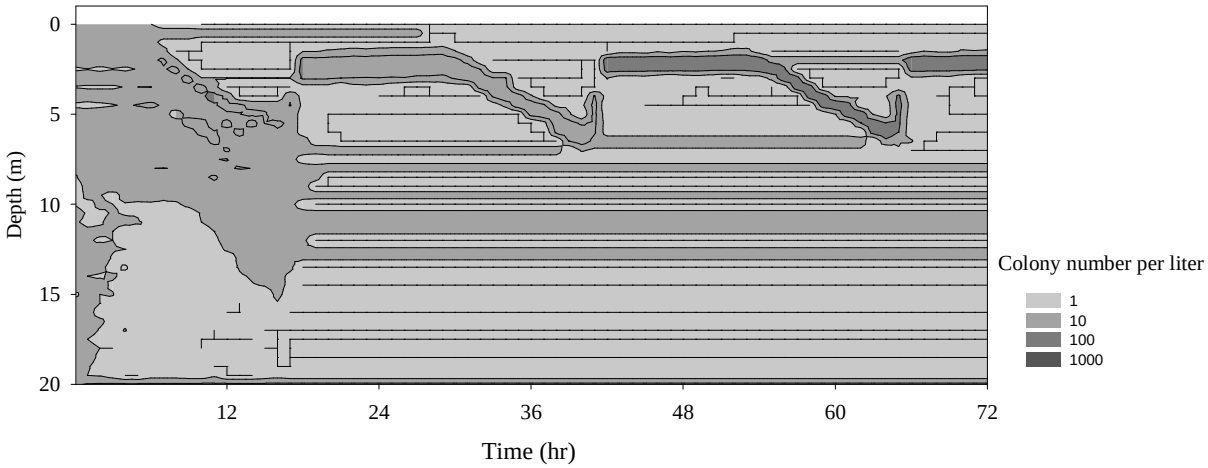

Figure 3. The simulation of the vertical distribution of colony density of total 1100 *Microcystis* colonies within 72 hours.

REFERENCES

Csanady G.T. (1973). Turbulent diffusion in the environment. Riedel: Dordrecht.

Droop, M. R. (1973) Some thoughts on nutrient limitation in algae. *J. Phycol.* 9: 264-272.

Hare J.A., Quinlan J.A., Werner F.E., Blanton B.O., Govoni J.J., Forward R.B.Jr, Settle L.R., and Hoss D.E.(1999). Larval transport during winter in the SABRE study area: results of a coupled vertical larval behavior-three-dimensional circulation model. *Fisheries Oceanography*. 8, 57-76.

Hunter J.R., Craig P.D., and Philips H.E. (1993). On the use of random walk models with spatially variable diffusivity. *Journal of Computational Physics*, 106, 366-376.

Ibelings B.W., Mur L.R., and Walsby A.E. (1991). Diurnal changes in buoyancy and vertical distributions in populations of *Microcystis* in two shallow lakes. *J. Plankton Res.* 13, 419-436.

Kromkamp J. and Walsby A.E. (1990). A computer model of buoyancy and vertical migration in cyanobacteria. *J. Plankton.* Res. 12, 161-183.

Kromkamp J., Konopka A., and Mur L.R. (1986). Buoyancy regulation in a strain of *Aphan* (cyanophyceae): The importance of carbohydrate accumulation and gas vesicle collapse. *J.Gen. Microbiol.* 132, 2113-2121.

Lin M.Y. 2004. Phytoplankton community structure analysis and stratified system dynamic modeling in Feitsui Reservoir. Thesis for Master of Science Graduate Institute of Environment Engineering of National Taiwan University.

Oliver R.L. and Walsby A.E. (1984). Direct evidence for the role of light-mediated gas vesicle collapse in the buoyancy regulation of *Anabaena flos-aquae* (cyanobacteria). *Limnol. Oceanogr.* 26, 285-294.

Rabouille S. and Salençon M.J. (2005). Functional analysis of Microcystis vertical migration: a dynamic model as a prospecting tool. II Influence of mixing, thermal stratification and colony diameter on biomass production. Aquat. Microb. Ecol. 39, 281-292.

Reynolds C.S. (1987). Cyanobacterial water blooms. *Adv. Bot. Res.* 13, 67-143.

Reynolds C.S., Oliver R.L., and Walsby A.E.(1987). Cyanobacterial dominace: The role of buoyance regulation in the billowing environment. *N.Z.J. Mar. Freshwater Res.* 21, 379-390.

Stauffer R.E. 1992. Efficient estimation of temperature distribution, heat storage, thermocline migration and vertical eddy conductivities in stratified lakes. *Freshwater Biol.* 27, 307-326.

Thomas R.H. and Walsby A.E.(1986). Buoyancy regulation in a strain of Microcysis. J.Gen. Microbiol. 131, 799-809.

Visser A.W. (1997). Using random walk models to simulate the vertical distribution of particles in a turbulent water column. Mar. Ecol. Prog. Ser. 158, 275-281.

Visser P.M., Passarge J., and Mur L.R. (1997). Modelling vertical migration of the cyanobacterium Microcysis. Hydrobiologia. 349, 99-109.

Wallace B.B., and Hamilton D.P. (1999). The effect of variations in irradiance on buoyancy regulation in *Microcystis aeruginosa*. *Limnol. Oceanogr.*44(2), 273-281.

Wallace B.B., and Hamilton D.P. (2000). Simulation of water-bloom formation in the cyanobacterium *Microcystis aeruginosa. J. Plankton Res.* 22(6), 1127-1138.

Wallace B.B., Bailey M.C., and Hamilton D.P. (2000). Simulation of vertical position of buoyancy regulating *Microcystis aeruginosa* in a shallow eutrophic lake. Aquat. Sci. 62, 320-333.

Walsby A.E. (1970). The nuisance algae: Curiosities in the biology of planktonic blue-green algae. *Water Treat. Exam.* 19, 359-373.

Werner F.E., Page F.H., Lynch D.R., Loder J.W., Lough R.G., Perry R.I., Greenberg D.A., and Sinclair M.M. (1993). Influences of mean advection and simple behavior on the distribution of cod haddock early life stages on Georges Bank. *Fisheries Oceanography*. 2, 43-64.

Wüest A., Piepke G., and Van Senden D.C. 2000. Turbulent kinetic energy balance as a tool for estimating vertical diffusivity in wind-forced stratified waters. *Limnol. Oceanogr.* 45(6), 1388-1400.

Scaling plankton persistence in complex flow networks

Javier G. P. Gamarra[1], Evan A. Variano[2*], and Mark B. Bain[3]

[1] *CIRRE-Institute of Biological, Environmental and Rural Sciences Aberystwyth University SY23 3DA, UK*
[2] *Civil and Environmental Engineering, University of California, Berkeley, 623 Davis Hall, Berkeley, CA 94720-1710, USA.*
[3] *Department of Natural Resources, Cornell University, Ithaca, NY 14853, USA*

**Corresponding author, e-mail variano@ce.berkeley.edu*

KEYWORDS
Flow Networks, Population Dynamics, Residence Time Distribution, Washout

EXTENDED ABSTRACT

INTRODUCTION
Populations of aquatic organisms are sensitive to both nutrient availability and transport by the ambient flow regime. The importance of advective transport is evident in the strong relationship between flowrate and productivity (Power *et al.* 1995, Jassby 2005), and excessive advective transport can cause populations to "wash out" (Speirs and Gurney 2001). We explore this extremum, at which advective transport is the primary determinant of population persistence. Furthermore, because riverine and estuarine flows are rarely unidirectional downstream, we explore the effect of advection patterns on population persistence. For this, we utilize an approach from network theory (*e.g.* Albert and Barabasi 2002), and describe advection patterns as weighted directed graphs. In this approach, the flow structure in a river or estuary is represented by an advection graph, which appears as a matrix in our coupled ecological-hydrodynamic model. From this model we derive an analytical formula relating the properties of the advection graph to the limits of population persistence.

METHODS
A set of n coupled differential equations represent the ecological processes at m locations. Each location can be considered a "cell" that is well-mixed, similar to continuously stirred flow-through reactor. Transport between the cells is governed by the mass-conserving advection graph, of size m x m. This describes the flow topology in a single matrix. This simplification of the flow is most valid at Peclet numbers of 1-10, based on the cell lengthscale. Nutrients are input at the upstream end of the flow domain, and any unused nutrients exit at the downstream end. The nutrients are consumed by a hypothetical autotroph species (e.g. phytoplankton), modelled using one of several different functional responses. Both the autotroph populations and nutrients are transported according to the advection graph.

All of the flow patterns we study share one important feature: a loop that connects an upstream location and a downstream location via a short path. We vary the strength and direction of flow in this loop (Q_a), thus obtaining a continuum of flow patterns. One region of this continuum ($Q_a < 0$) describes cases such as anastomizing rivers and vegetation-fringed channels, in which flow proceeds downstream via two different paths at two different speeds.

The other region of the continuum ($Q_a > 0$) describes a "recirculation" or "feedback" flow, in which some of the flow moves upstream and rejoins the main channel. Between these two regions ($Q_a = 0$) is the simple case of uniform downstream transport, such as a tanks-in-series transport model. In all cases, the inlet and outlet flows at the domain edges are Q_i.

RESULTS AND DISCUSSION

Analytical solutions relate the critical dilution rate to the Eigenvalues of the advection graph. The critical dilution rate δ_c is the flowrate Q_i (upstream of the loop) above which autotroph populations do not survive (often called "washout"). Results show that advection graphs that branch and then rejoin exhibit greatly enhanced population persistence (see Figure 1). This effect is highly nonlinear, such that small changes in Q_a can radically alter the range of flowrates for which populations can persist. In the case of $Q_a > 0$, even a small amount of feedback greatly increases the possibility of population persistence. In the case of $Q_a < 0$, the possibility of persistence increases rapidly as Q_a approaches Q_i. In both cases the increase in persistence is due to the loop's effect on the residence time distribution. By altering the flow so that some fluid particles remain in the system near indefinitely, the loop structure greatly reduces the probability of washout. Thus the geometry of a river or estuary can render washout irrelevant, thereby shifting the population dynamics to a regime dominated by nutrient availability. This model suggests that autotroph population's sensitivity to changes in flow patterns may be greater than those implied by considering flowrate alone.

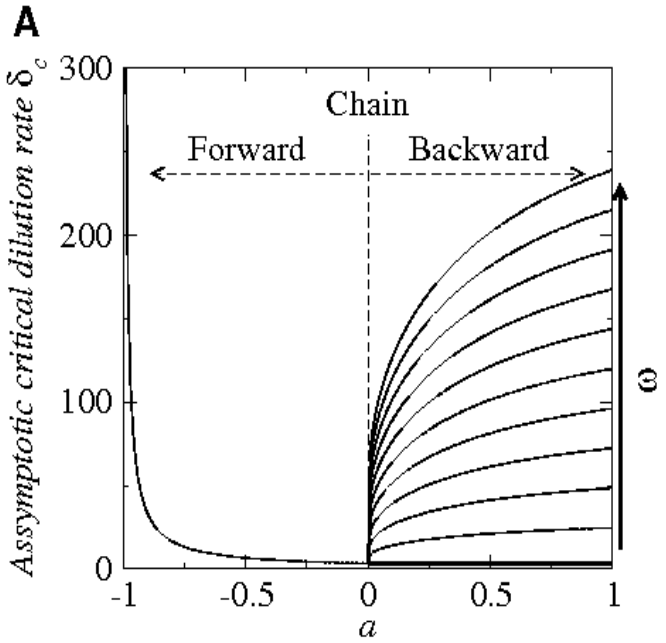

B

-(1+a)	1+a		
	-(1+a)	1+a	
		-(1+a)	1+a
a			-(1+a)

C

-1	1+a		-a
	-(1+a)	1+a	
		-(1+a)	1+a
			-1

Figure 1. (A) The effect of loop flow strength *a* (which is Q_a normalized by Q_i) on the persistence of autotroph species, as calculated from the flow network model. Larger values of δ_c correspond to improved population persistence. (B) Advection graph (or flow network) for a backward loop. (C) Advection graph for a forward loop. The advection graphs shown are for the case $m = 4$. The elements C_{ij} describe the nondimensional flowrates from cell i to j.

REFERENCES

Albert, R. & Barabasi, A.L. (2002). Statistical mechanics of complex networks. *Rev. Modern Phys.*, 74, 47-97.

Jassby, A.D. (2005). Phytoplankton regulation in an eutrophic tidal river (San Joaquin river, California). San Francisco Estuary and Watershed Science 3 (1).

Power, M.E.; Sun, A.; Parker, M.; Dietrich, W.E. & Wootton, J.T. (1995). Hydraulic food-chain models: an approach to the study of food-web dynamics in large rivers. Bioscience, 45, 159-167.

Speirs, D.C. & Gurney, W.S.C. (2001). Population persistence in rivers and estuaries. *Ecology*, 82, 1219-1237.

Using hyperspectral optical methods to examine the effect of turbulent mixing on ecosystem functioning in a coastal lagoon

O.N. Ross[1]*, J. Piera[1], E. Torrecilla[1], M. Lara[2], and E. Berdalet[2]

[1] Marine Technology Unit (UTM). Mediterranean Centre for Marine and Environmental Research (CMIMA, CSIC). Passeig Marítim de la Barceloneta, 37-49, E-08003, Barcelona, Spain.
[2] Marine Science Institute (ICM). Mediterranean Centre for Marine and Environmental Research (CMIMA, CSIC). Passeig Marítim de la Barceloneta, 37-49, E-08003, Barcelona, Spain

**Corresponding author, e-mail ross@icm.csic.es*

KEYWORDS
harmful algae; hyperspectral optics; shallow water; turbulence

EXTENDED ABSTRACT

INTRODUCTION
Phytoplankton play a pivotal role in driving and maintaining aquatic biodiversity and the marine food web as a whole and we need to establish causative links between phytoplankton growth, abundance, species success and succession and how they are affected by the driving environmental forces such as turbulent mixing. Traditional sampling methods, such as ship and satellite based observations only provide spot measurements within a highly dynamic and heterogeneous environment, lacking the necessary temporal and vertical resolution.

We are currently installing a hyperspectral optical sensor in a cabled coastal observatory in order to monitor the dynamics of the underwater ecosystem *in situ* and *in vivo*. Hyperspectral sensors provide ample spectral information to improve the identification of water column constituents, including a variety of phytoplankton species and functional groups (e.g., Sathyendranath et al 2007).

METHOD AND EXPECTED RESULTS
This is currently a work in progress and our overall objective is to develop methods based on hyperspectral optical data for the detection of phytoplankton functional groups (including Harmful algal bloom (HAB) species) and the characterisation of dynamic processes such as turbulent transport and photoacclimation at small scales. As a first step we develop a modelling tool (Fig. 1) with which we can test new analytical methods such as derivative analysis (Torrecilla *et al* 2009) for the identification and characterisation of phytoplankton groups and species using hyperspectral optical data. We coupled existing turbulence and individual based phytoplankton growth and photoacclimation models (Ross & Sharples 2007, Ross & Geider 2009) with HYDROLIGHT (www.sequoiasci.com) a radiative transfer software for the marine environment and OOPS (the Optical Ocean Plankton Simulator - www.kimsoops.net) in order to obtain time- and depth-resolved optical spectra (Fig. 2).

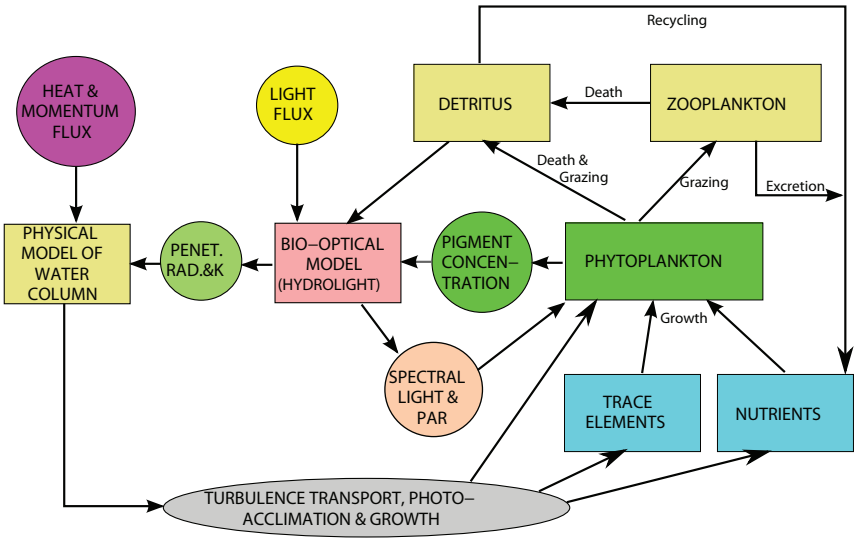

Figure 1. General framework of the coupled model (cf. Dickey *et al* 2002).

For the model validation we use hyperspectral observations and data analysis techniques as well as classical observations of turbulence through temperature microstructure. The model is applied to our field site at Alfacs Bay, a physically complex environment and an active aquaculture site 200km SW of Barcelona (NW Mediterranean) where recurring HAB events lead to chronic long-lasting closures of bivalve harvesting. Upon completion of this project, the model may serve as a 24h monitoring and early warning system for the occurrence of Harmful Algal Bloom events which regularly have severe economic impacts on the region.

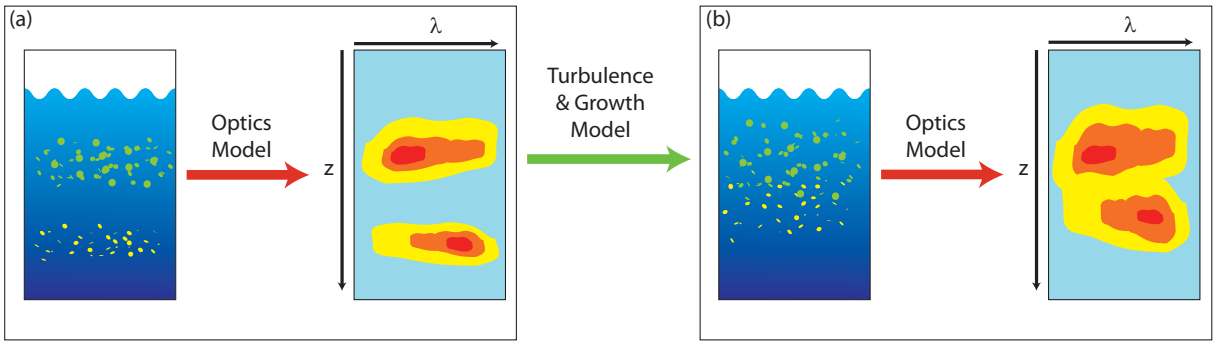

Figure 2. (a) An example distribution of two different phytoplankton groups (left panel) produces a particular optical depth spectrum (right panel). (b) After turbulence and growth have changed the physiology and location of the two groups, a different spectrum is obtained.

REFERENCES

Dikey T.D. (2002). Emerging ocean observations for interdisciplinary data assimilation systems. *J Mar Sys*, **40-41**, 5-48.

Ross, O.N. and J. Sharples (2007). Phytoplankton Motility and the Competition for Nutrients in the Thermocline. *Mar Ecol-Prog Ser*, **347**, 21-38.

Ross, O.N. and R.J. Geider (2009). New cell-based model of photosynthesis and photo-acclimation: accumulation and mobilisation of energy reserves in phytoplankton. *Mar Ecol-Prog Ser*, **383**, 53-71.

Sathyendranath, S. and T. Platt (2007). Spectral effects in bio-optical control on the ocean system. *Oceanologia*, **49**, 5-39.

Torrecilla, E., J. Piera and M. Vilaseca (2009). Derivative analysis of hyperspectral oceanographic data. In: Geoscience and Remote Sensing, I-Tech Publishers, Vienna. Chapter 3, pp. 597-618.

Benthic imagery survey of Asian clam in Lake Tahoe

A.L. Forrest[1]*, M. Wittmann[2], B. Allen[2], V. Schmidt[3], N.A. Raineault[4], W. Pike[1], A. Hamilton[1], L.P. Kost[1], B.E. Laval[1], A.C. Trembanis[4], and G. Schladow[2]

[1] *Environmental Fluid Mechanics Group, Department of Civil Engineering, University of British Columbia, Vancouver V6T 1Z4, BC, Canada*
[2] *University of California Davis Tahoe Environmental Research Centre*
[3] *Centre for Coastal Ocean Mapping, University of New Hampshire, Durham, NH 03824, USA*
[4] *Department of Geological Sciences, College of Earth, Ocean, and Environment, University of Delaware, Newark, DE 19716, USA*

**Corresponding author, e-mail forrest@civil.ubc.ca*

KEYWORDS
Asian clam; benthic imagery; autonomous underwater vehicle; Lake Tahoe; filamentous algae

EXTENDED ABSTRACT

The establishment and spread of the invasive bivalve, Asian clam (*Corbicula fluminea*), in Lake Tahoe has been of increasing concern to the Lake Tahoe community. This concern has motivated and focused research initiatives on the spread of *C. fluminea* and its affects on the native ecosystem. High-density populations (up to 6000/m^2) are displacing native benthic macroinvertebrate communities and are also thought to promote green filamentous algal (*Zygnema sp., Cladophora glomerata*) blooms. Benthic surveys conducted in 2008-2009 had identified population densities of *C. fluminea* in the southeast quadrant of the lake, but have not identified distribution in the remaining 75% of the 72 mile shoreline (Wittmann et al., 2008). The work presented here used benthic imagery collected with an Autonomous Underwater Vehicle (AUV) to investigate the distribution of *C. fluminea* in Lake Tahoe. Additionally, select environmental parameters were investigated to examine any potential association with clam distribution.

In the summer 2009, the Tahoe Environmental Research Centre partnered with the University of British Columbia to conduct a full lake survey using *UBC-Gavia*, a *Gavia* class AUV, as a platform to collect georeferenced benthic imagery and optical backscatter data. Derived data from the optical backscatter included turbidity (m^{-1} sr^{-1}), chlorophyll-*a* (μg L^{-1}), and colored dissolved organic matter (CDOM) (ppb). Survey goals were twofold; (1) conduct a single pass along-shore survey of the littoral region to determine lateral presence as a function of surficial bottom sediment clam shell matter, and (2) conduct a multi-pass across-shore survey to determine clam shell matter presence as a function of depth. Clam shells (2 – 27 mm in length) were detected as white reference points in the images and their presence used as a proxy for live clam populations. High-resolution images were collected at a constant altitude (height above the bottom) of 2.6 m above bottom at a frame rate of 4 Hz. All of the data collection missions were conducted at night to minimize the risk associated with operating an AUV in high boat traffic areas and also to maintain a normalized ambient light level in the collected imagery. An image-processing algorithm was written to estimate the relative density of clam shell abundance, corrected for altitude, in each frame. Initial versions of the algorithm counted the number of pixels in each frame above a certain color threshold but this was found insufficient due to variable strobe light intensity as a function of vehicle altitude and

orientation. Significantly improved predictions of clam shell matter were made using the median and mean deviations associated with each image. These were used for the rest of the presented work.

The collected data was then used to create a georeferenced species distribution map of the lake and revealed previously undiscovered regions where clam shell matter was abundant, particularly in areas along the western shoreline. The across-shore transects demonstrated variability between study sites and previously undiscovered potentially viable clam populations at depths greater than 80 m. A field campaign is currently underway to groundtruth the generated distribution map and also to confirm whether clam shell matter is a valid indicator of live clam populations. It was initially theorized that the optical backscatter show green filamentous algal dominant in clam-infested regions (Wittmann et al., 2008) however, no correlation was apparent when comparing results from two different areas. In contrast, relatively high concentrations of turbidity, CDOM and Chl-*a* were found in localized areas along the south shore. It is proposed that these result from a single nutrient point source although further work is required to examine the extent (both areal and vertical) that the plume extends into the lake. In addition, it was also observed that the Chl-*a* concentration was correlated with the CDOM measurement in the water column. It is possible to then conclude that one could be used as a proxy for the other if required. The results from this study provide new insights into the distribution of Asian clam within Lake Tahoe and how water column properties interact with these populations.

REFERENCES

Wittmann, M.E., Reuter, J.E., Schladow S.G., Hackley, S., Allen, B.C. Chandra, S., Caires, A. 2008. Asian clam (Corbicula fluminea) of Lake Tahoe: Preliminary scientific findings in support of a management plan. UCD- TERC Report. http://terc.ucdavis.edu/research/AsianClam2009.pdf

The net water budget of a lake without surface in- and outflow: a non-stationary approach

G. Kirillin[1], W. Philipp[2] , G. Nützmann[1] and C. Engelhardt[1]*

[1] Leibniz-Institute of Freshwater Ecology and Inland Fisheries, Department of Ecohydrology Müggelseedamm 310, D-12587 Berlin, Germany.
2 Technical University of Dresden, Institute of Hydrology and Meteorology, Helmholtzstr. 10, D-01069 Dresden, Germany.

**Corresponding author, e-mail engelhardt@igb-berlin.de*

ABSTRACT
The majority of the existing studies on the surface/groundwater balance in lakes assume stationarity of the groundwater flow at monthly or even annual scales. However, the groundwater exchange is closely connected to the water flows at the lake surface due to precipitation/evaporation, which are characterized by higher frequencies of temporal variability. Thus, the exchange between lake water and groundwater needs a non-stationary treatment. Whereas components of the water balance at the lake surface—the precipitation and the evaporation—can be estimated with reasonable accuracy from the standard meteorological observations, it is difficult to obtain the temporal variability of the groundwater flow in/out a lake from the field data on account of its high spatial heterogeneity. We present a method to estimate net groundwater input into the lake water budget as a rest term in the total water balance derived from high-resolution water level measurements by bottom-mounted pressure loggers. The method has demonstrated its reliability for estimation of the lake level variations on periods from sub-diurnal to perennial ones. The net groundwater flow revealed a pronounced seasonal component superimposed by perennial variations between wet and dry years, as well as by synoptic effects of lake water exfiltration into the groundwater aquifer following strong precipitation events. A strong relationship is derived between the groundwater flow and the water balance at the lake surface - the supposedly inherent feature of enclosed lakes with small watersheds.

KEYWORDS
Evaporation, groundwater flow, lake water budget, water level,

INTRODUCTION
In lakes without surface in- and outflow the groundwater flow is one of the most important components of water budget and external input of dissolved substances (Hood *et al.*, 2006; Nakayama and Watanabe, 2008). Both, experimental studies (Winter 1976; Lee *et al.*, 1980; Krabbenhoft and Anderson 1986; Cherkauer and Zager, 1989; Isiorho and Matisoff, 1990) as well as numerical modeling (Sacks *et al.*, 1992; Cheng and Anderson, 1993; Genereux and Bandopadhyay, 2001) were performed to study lake/groundwater interactions, often in combination with transport of solutes (Stephenson *et al.*, 1994; Sholkovitz *et al.*, 2003).

Most of the existing studies on the surface-groundwater balance in lakes assume a stady-state groundwater flow (Cheng and Andersson, 1994; Nützmann *et al.*, 2003). However, the groundwater exchange is driven by the time-dependent groundwater recharge and is closely connected to the water flows at the lake surface due to precipitation/evaporation, which are characterized by higher frequencies of temporal variability. The precipitation events are typically followed by the intensification or even changing of the direction of the net groundwater flow. This effect takes place on short daily or hourly time scales and remains out of scope of the methods with coarser time resolution. Hence, groundwater-surface water interactions are highly dynamic and a steady-state should not longer serve as a central, default assumption (Milly *et al.*, 2008). The exchange between lake water and groundwater varies with time and therefore needs a non-stationary treatment. Experimental techniques for the measurement of exchange between groundwater and lake water can only with difficulty be used for the total water budget (Nakayama and Watanabe, 2008). An alternative method for the evaluation of this budget could be the estimation of groundwater exchange as the residual in the balance between the water balance at the lake surface, in- and outflows, and lake volume (Pollman *et al.*, 1991). This method does not calculate the individual values of inflowing and outflowing components of groundwater, but provides valuable information on the net groundwater contribution to the water budget of the lake as an integral characteristic of the lake-groundwater interaction. Generally, changes in the groundwater recharge and the lake water level take place on temporal scales from synoptic (caused e.g. by local precipitation events) to seasonal (connected to variations in the groundwater recharge in the hydrologic year) to perennial ones (arising from variations in the annual sum precipitation-evaporation balance at the watershed). Thereby, the main temporal scales of this variability are determined by the regional climate, but the variability range is individual for every lake, depending on the watershed characteristics.

In this paper we estimate the groundwater climate of Lake Stechlin – a small enclosed lake without surface in- and outflows, located in north-eastern Germany. The estimation method consisted in determining of the net groundwater contribution into the lake water budget as a residual term in the total water balance derived from the known water level fluctuations in the lake. The water level fluctuations, in turn, were obtained from time-resolved pressure measurements at the lake bottom with sufficient accuracy and high temporal resolution. The dataset comprised two subsequent years 2006-2007, one characterized as “extremely dry” and another as “extremely wet” compared to the annual regional precipitation mean of 36 years. By this means, we were able to estimate the range of the groundwater flow variability on climatic scales that, complemented with the established seasonal and synoptic patterns, allowed us to reveal the typical features of groundwater interactions and to develop a simple relationship between them and the water balance on the lake surface.

METHODS

Study area

Lake Stechlin is situated in NE Germany (53°10'N, 13°02'E) about 100 km north of Berlin and has a surface area of 4.25 km^2 and an average volume of $96.88 \cdot 10^6$ m^3 (Koschel and Adams, 2003). The lake is a deepest one in the Brandenburg region with maximum and the mean depths of 68.5 m and 22.8 m respectively. The water level of Lake Stechlin is regulated by ground water inflow, by precipitation and evaporation, and by temporal runoffs through the surrounding sand layers (Richter, 1997; Nützmann *et al.*, 2003). The 80% of the 12.57 km^2 lake watershed is covered by forest. The subsurface watershed is also rather small

with the sharp rise of the groundwater table in the south–east and in the north–west directions. The summary discharge of in- and outflows is negligible (0.004 m^3s^{-1}).
To study the hydrologic budget of Lake Stechlin a stationary coupled water and chloride mass balance model has been developed before (Nützmann et al., 2003). A steady-state groundwater modeling study of Lake Stechlin watershed showed that with respect to different annual rainfall situations the subsurface flow regime is also changing (Holzbecher, 2001). According to this model, the groundwater flux G in Lake Stechlin is expected to reveal high temporal variability and to change its sign in the total water balance of the lake:

$$\frac{dV}{dt} = (p - e + g) * A, \quad (1)$$

where dV/dt [$m^3\ s^{-1}$] is the rate of change of the lake volume; A [m^2] is the lake surface area, p and e [$m\ s^{-1}$] are is the precipitation rate and the evaporation rate, correspondingly. Here, the precipitation rate p refers to the water volume falling directly on the lake surface, where the inflow from the land surface assumed to be negligible.

Estimation of the water balance components

Lake volume variations. We have used pressure measurements at the bottom of Lake Stechlin in order to estimate directly the fluctuations of the water level and, consequently, of the lake volume dV/dt (Eq. 1). Data on the water level fluctuations were collected in two subsequent years, from 27 January to 20 September 2006 and from 29 March to 4 September 2007 by a pressure sensor (TDR-2050 RBR Canada, absolute accuracy 0.03 db, resolution < 0.0006 db) installed at 30m depth in the southern part of Lake Stechlin at few centimeters above the sediment, and sampling continuously with 10s record interval. The annual precipitation rates amounted in these years at 489 mm/year in 2006 and at 906 mm/year in 2007, which are representative for wet and dry years, correspondingly (the annual precipitation in 1958–1994 varied between 427 mm and 815 mm with the mean value of 658 mm (Richter, 1997)). Thus, among with the resolution of the less-than-seasonal time scales, the dataset provided the opportunity for comparison of the G variability in dry and wet conditions.
The time variations in the water level h_W were determined from the hydrostatic balance,

$$\rho g \frac{dh_W}{dt} = \frac{d}{dt}(p_W - p_{Atm}), \quad (2)$$

where p_W is the measured pressure at the lake bottom, p_{Atm} is the atmosphere pressure, and ρ is the freshwater density. Taking into account the steep morphometry of Lake Stechlin and small amplitudes of the level fluctuations h_W, the associated variations in the lake surface area A assumed to be negligible, and the volume variations were estimated simply as

$$\frac{dV}{dt} = A\frac{dh_W}{dt}, \quad (3)$$

with A taken as 4.25 km^2. Under this assumption, Eq. (1) reduces to

$$\frac{dh_w}{dt} = p - e + g, \quad (4)$$

and the lake water level at any moment t is given by

$$h_w(t) = h_w(t_0) + P - E + G, \quad (5)$$

where t_0 is the time of the observations start, and $P(t) = \int_{t_0}^{t} p(\tau)\,d\tau$, $E(t) = \int_{t_0}^{t} e(\tau)\,d\tau$, and $G(t) = \int_{t_0}^{t} g(\tau)\,d\tau$ – are the accumulated precipitation, evaporation and groundwater input correspondingly.

Precipitation-Evaporation balance p - e. Data on the precipitation rate *p* and meteorological characteristics necessary for estimation of the evaporation rate *e* were adopted from the standard weather observations at the near-shore station provided by the German Weather Service (DWD) for the period 1957-2003 and by the German Environmental Agency (UBA) for 2004-2007. The small area of the lake suggests negligible difference between the measured precipitation over the land surface and that over the lake that is also supported by Richter's (1997) estimations.

Evaporation rate *e* is, along with the lake-groundwater exchange, one of the most uncertain components of the water balance (4) owing to complex interactions at the air-lake boundary. Apart from direct evaporation measurements, which are rarely available and are difficult to interpret at the lake-wide scale, a number of widely-used approaches exist for estimation of *e*, ranging from simple bulk-formulae to coupled models of the atmospheric and lake boundary layers. The choice of an appropriate method for a certain lake depends usually on available observational data and characteristic regime of the air-lake interaction. In particular, such factors as the fetch-dependent roughness of the lake surface, strong stability of the lower atmospheric boundary layer over the colder lake surface in summer and typically very low wind speeds in small wind-shadowed lakes are among the problems resulting in the lack of a universal parameterization of *e* suitable for any lake. Richter (1997) had obtained monthly evaporation totals at Lake Stechlin in 1958-2001 using measurements by evaporation pans installed directly over the lake surface. This dataset, when coupled with the meteorological observations at the lake shore and with the surface temperature measurements, gave us the opportunity of comparing different methods for *e* calculation in order to choose the one with sufficient accuracy for Lake Stechlin conditions.

The evaporation measurements were compared with outputs from several empirical evaporation formulae recognized in the literature (Haltiner and Martin, 1957; Kazmann, 1965; Richards and Irbe, 1969; Orlob and Selna, 1970; Richter, 1997), all of the form:

$$E = C \cdot f(u) \cdot (e_s - e_a), \qquad (6)$$

where $f(u)$ is a function of the wind speed u, measured at the height z_u above the lake level. e_s is the saturated water vapor pressure at water surface, e_a is the water vapor pressure at air temperature, C is an empirical coefficient.

The wind measurements at 10 m height from the near shore station were adjusted to z_u for each corresponding formula assuming the logarithmic wind profile within the surface boundary layer.

In addition to the 5 bulk evaporation formulae listed above, a more advanced scheme of the latent flux calculation was used, based on the model of the surface boundary layer of Zilitinkevich (1991) and implemented in the surface module of the lake temperature model FLake (Mironov *et al.*, 2010). In the scheme, the Monin-Obukhov similarity relations (see e.g. Yaglom, 1977) are used to compute turbulent fluxes of moisture. In case of strong stability in the surface air layer, when the gradient Richardson number exceeds its critical value and the Monin-Obukhov similarity relations yield zero fluxes, crude estimates of fluxes of momentum and of sensible and latent heat are obtained, assuming that the transport of momentum, heat and mass in the surface air layer is controlled by the molecular transfer mechanisms. A decision between turbulent and molecular fluxes and between fluxes in forced and free convection is made on the basis of flux magnitude.

The testing of the evaporation models was performed at the data from the period 1998-2001, for which daily water temperature measurements were available in addition to the standard meteorological observations.

RESULTS AND DISCUSSION

Evaporation estimates

In order to arrive at a reliable method for estimation of evaporation during the water level measurements in 2006-2007, we have compared the outcomes of several evaporation models against the monthly evaporation rates in 1998-2001 available from direct measurements with an evaporation pan installed on the lake surface (Richter, 1997). Generally, the data from the evaporation pan provide higher values than estimations given by all models tested (Fig. 1). This result can be referred, at least partially, to a known systematic overestimation of the true evaporation rate by the evaporation pan measurements (Winter, 1981; Eichinger, 2003). On the other hand all estimations given by non lake specific models yield similar values, which are several times lower than the measured evaporation rates, especially in summer (Fig. 1). The inconsistency is apparently conditioned by the specific features of the atmospheric boundary layer over the lake surface: a strong stability on account of the temperature difference between the summer air in summer and the cold surface of the deep lake, and low winds caused by the small lake area and the surrounding forest. Most of bulk-formulae are based on typical winds and stratification data over large open water bodies, particularly, over the ocean, and fail in these conditions. The Monin-Obukhov theory for the developed turbulent boundary layers underlying the FLake algorithm is also inapplicable for strongly stratified boundary layer (Cheng *et al.*, 2005). Still, the air-lake exchange of scalars, in particular, the water vapor, includes the transport by the intermittent turbulence in the strongly stratified air, and is essentially higher than that provided by the purely molecular exchange. In the absence of a theory adequately describing this exchange, the empirical formulae derived explicitly for such small and deep lakes are the most appropriate alternative for estimation of evaporation rates. The two formulae based on the small lake data are close to the pan measurements data, with the latter formula of Meyer (Kazmann, 1965) fitting slightly better to the data (RMS error 16.12 mm vs. 19.33 mm for the Richter (1997) formula). Therefore, the Meyer formula is adopted in the following for all estimations of the evaporation from the measured lake surface temperatures, and is coupled with the lake model FLake instead of its standard algorithm for calculation of the latent heat flux in the model scenarios.

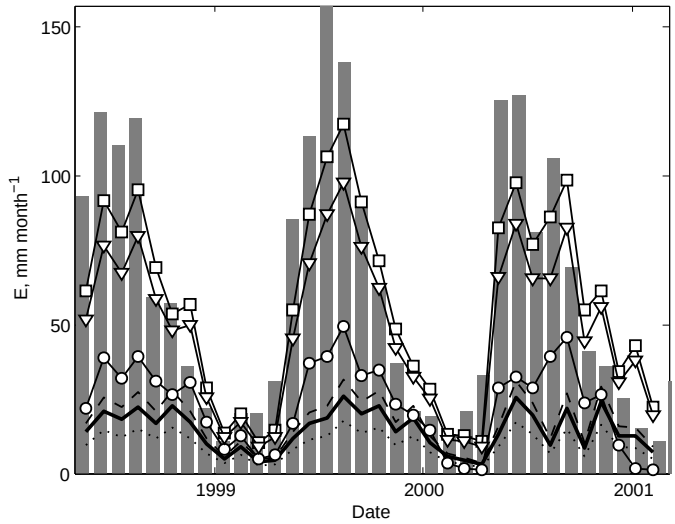

Figure 1. Monthly evaporation means from Lake Stechlin: evaporation pan measurements (gray bars) and those calculated after Richards and Irbe, 1969 (thick solid line), Orlob and Selna, 1970, dashed line), Haltiner and Martin, 1957 (dotted line); the Monin-Obukhov based Flake algorithm (Mironov *et al.*, 2010, line with circles), and the two lake-specific empirical formulae: Richter (1997, line with triangles) and Meyer (Kazmann, 1975, line with squares).

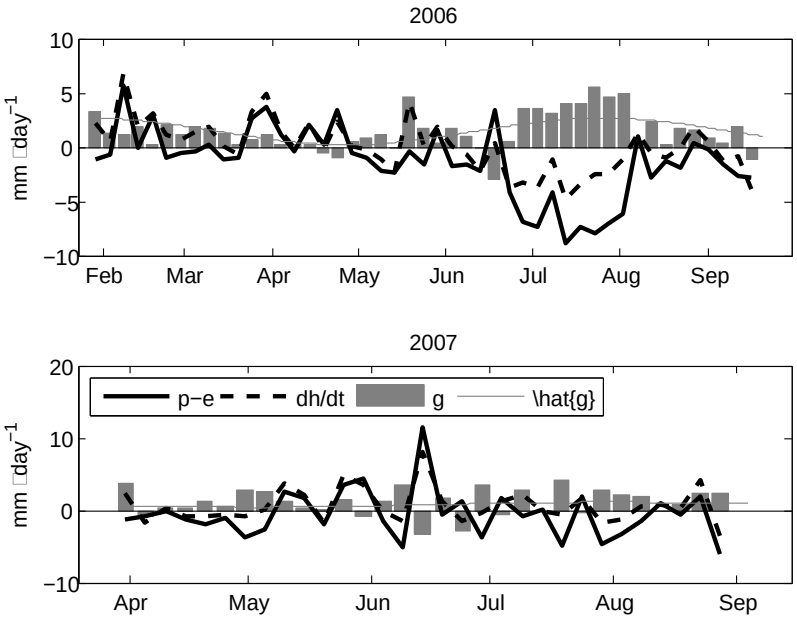

Figure 2. The water balance components in Lake Stechlin in (a) 2006 and (b) 2007. Thick solid line: precipitation-evaporation balance; dashed line: water level variability; gray bars: net groundwater inflow; thin gray line: approximation of groundwater inflow by Eq. (8).

Groundwater flow: short-term and seasonal fluctuations.
Qualitatively, the evolution of the lake level closely follows the cumulative precipitation-evaporation balance at the lake surface in 2006 as well as in 2007 (not shown). Among others, this fact demonstrates that the surface *P–E* balance determines, to a large degree, the short-term (days to months) variability of the water level in dry, as well as in wet conditions (Fig. 2). On the other hand, there is an additional positive component in the water balance in both years (the water level is higher that it would follow from the evaporation-precipitation balance only). In the absence of an appreciable permanent surface runoff, it is consistent to ascribe this discrepancy to the groundwater inflow. Approximating the accumulated groundwater inflow *G* by a linear fit, one arrives at a nearly constant groundwater contribution to the water level change at seasonal time scales of 1.45 mm/day in 2006 and 0.86 mm/day in 2007, which correspond to the net groundwater inflow of 6.17 10^3m^3/day and 3.67 10^3m^3/day, respectively. The residual variability in the groundwater inflow has remarkable differences between 2006 and 2007. In dry conditions of 2006 a pronounced seasonality persists in *G*, which is fairly well described by the sine function

$$\hat{G} = -A \sin\left(\frac{2\pi}{T}(t - T_0)\right) \text{ [mm]}, \tag{7}$$

or, correspondingly,

$$\hat{g} = -a \cos\left(\frac{2\pi}{T}(t - T_0)\right), \text{ [mm/day]}, \tag{8}$$

with the period *T* of 6 months, and the starting point T_0 set to 01 May (or 01 November) of the corresponding year. The seasonal amplitude amounts at A = 35 mm, or $a = 2\pi/T^*A$ = 1.2 mm/day. The same seasonal pattern is also present in 2007; is, however, much less expressed (the corresponding amplitudes are: A = 10 mm and a = 0.35 mm/day). In

addition, the seasonal periodicity in the wet year 2007 is masked by short-term oscillations of *G*, which are closely linked to the precipitation events in a particular manner: relatively strong precipitation events are immediately followed by negative *g* and corresponding drop of *G* (cf. the precipitation and groundwater lines in Fig. 2b). Thus, the precipitation produces short events of *exfiltration* of the lake water into the aquifer. That is, apparently, a result of the lake-groundwater pressure gradient produced after strong rains, which do not affect immediately the groundwater level, but increase the hydrostatic pressure in the lake by raising its water level.

Generally, the results demonstrate a direct relationship between the groundwater flow *g* and the water balance at the lake surface (*p*–*e*): the higher evaporation in dry conditions is, i.e the larger negative (*p*–*e*) are, the stronger is the groundwater inflow; in turn, when precipitation prevails over evaporation (*p*–*e* > 0) the groundwater flow changes its sign to negative. Based on the data from both 2006 and 2007, this relationship fairly agrees with the direct proportionality $g = -0.6(p–e)$ (Fig. 3), i.e. the net groundwater exchange constitutes roughly 60% of the water balance at the lake surface and changes its sign according to it. The absolute data scatter around the approximating straight line is larger during exfiltration, when precipitation prevails over evaporation. This can be explained by higher non-stationarity of the water budget and by a certain role of the surface runoff during the precipitation events, which is not accounted for in Eq. 1. Still, for both positive and negative (*p*–*e*), the correlation between the approximation and the data is 0.65, or about 42% of the relative variability is explained by the proposed relationship. The largest scatter around the straight line is found in the vicinity of the zero point (empty circles in Fig. 3): excluding them from the correlation estimation increases the predictive ability of the relationship up to 60%. Adopting this dependence of *g* on the surface water balance, the variations of the lake water level in Lake Stechlin can be expressed from (1) in a simple way as:

$$dh_W/dt = 0.4(p–e). \quad (9)$$

According to (9), the water level changes in the lake due to evaporative water losses and precipitation are damped to 60% by the lake-groundwater exchange, and the rest 40% should result in perennial water level variability (assumed the level is not artificially regulated).

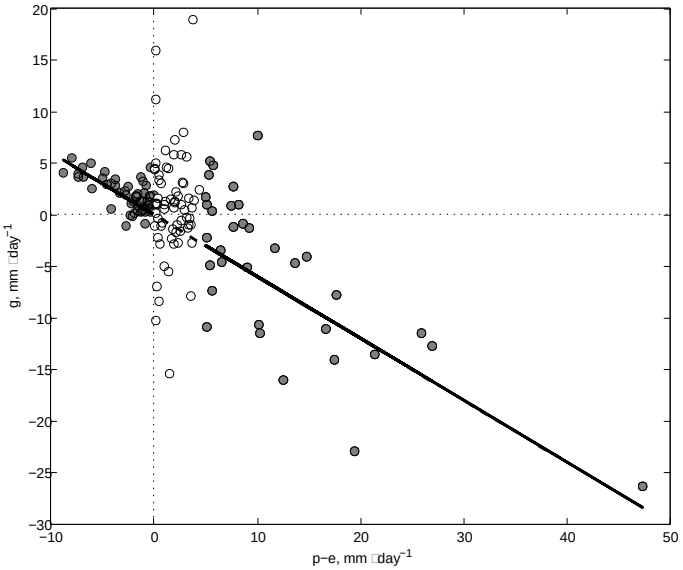

Figure 3. The net groundwater flow g in both 2006 and 2007 plotted against the surface water balance (p-e) (circles). Open circles correspond to the weak precipitation events with 0<(p-e)<5 mm/day. The solid line corresponds to the ratio g = -0.6(p-e).

CONCLUSIONS

One aim of the present study was testing of the routine pressure measurements by standard-accuracy sensors as a tool for estimation of the lake level variations in a wide range of temporal scales. The analysis of the net water budget components in Lake Stechlin has demonstrated a close relationship between the water balance at the lake surface and the net groundwater flow in the lake. This relationship reveals itself at different time scales and produces distinct variations in the lake-groundwater exchange with periods from synoptic (driven e.g. by the strong precipitation events), to seasonal (connected to the mean groundwater level), to perennial ones (conditioned by the interannual differences in the regional precipitation-evaporation balance). The fact that these variations are to a large degree determined by the concurrent variations in the atmospheric drivers suggests that the pattern of the net groundwater flow variability in Lake Stechlin can be extrapolated, at least qualitatively, at the majority of enclosed lakes with small watershed:

ACKNOWLEDGEMENTS

This study is part of the priority program AQUASHIFT that is funded by the German Science Foundation (DFG projects KI-853-3, BE-1383-7). We thank the German Environmental Agency (UBA) and the German Weather Service (DWD) for the observational data.

REFERENCES

Cheng, X. and Anderson, M.P. (1993). Numerical simulation of ground-water interaction with lakes allowing for fluctuating lake levels. Ground Water **31**, 929–933.

Cheng, Y., Parlange, M.B. and Brutsaert, W. (2005). Pathology of Monin-Obukhov similarity in the stable boundary layer, J. Geophys. Res., 110, D06101, doi:10.1029/2004JD004923.

Cherkauer D.S. and Zager J.P. (1989). Groundwater interaction with a kettlehole lake: relation of observations to digital simulations. Journal of Hydrology **109**: 167–184.

Eichinger, W.E., Nichols, J., Prueger, J.H., Hipps, L.E., Neale, C.M.U., Cooper, D.I. and Bawazir, A.S. (2003). Lake evaporation estimation in arid environments. IIHR Technical Report No. 430.

Genereux, D. and Bandopadhyay, I. (2001). Numerical investigation of lake bed seepage patterns: effects of porous medium and lake properties. Journal of Hydrology **241**, 286–303.

Ginzel, G. (1999). Hydrogeological investigations in the Stechlin-Nehmitz catchment area. IGB Report Nr. 9, 43-60 (in German).

Haltiner, G.J. and Martin, F.L. (1957). Dynamical and Physical Meteorology. Mc Graw Hill, New York, 1957, 470 pp

Holzbecher, E. (2001). The dynamics of subsurface water divides – watersheds of Lake Stechlin and neighboring lakes. Hydrological Processes, **15**, 2297-2304.

Hood, J.L., Roy, J.W. and Hayashi, M. (2006). Importance of groundwater in the water balance of an alpine headwater lake, Geophys. Res. Lett., **33**, L13405, doi:10.1029/2006GL026611.

Isiorho, S.A., and Matisoff, G. (1990). Groundwater recharge from Lake Chad. Limnology and Oceanography **35**(4) , 931–938.

Kazmann, R. G. (1975). Modern Hydrology, Second Edition, Harper & Row, New York.

Kirillin, G., Engelhardt, C. and Golosov, S. (2008). A mesoscale vortex in a small stratified lake, Environmental Fluid Mechanics **8**, 349– 366, doi:10.1007/ s10652-008-9101-8.

Koschel, R. and Adams, D. (Eds.), 2003. Lake Stechlin—An Approach to Understanding an Oligotrophic Lowland Lake, Arch. Hydrobiol., 58E. Schweizerbart, Stuttgart, Germany.

Krabbenhoft, D.P. and Anderson, M.P. (1986). Use of numerical ground-water flow model for hypothesis testing. Ground Water **24**(1), 49–55.

Lee, D.R., Cherry, J.A. and Pickens, J.F. (1980). Groundwater transport of a salt tracer through a sandy lakebed. Limnology and Oceanography **25**(1),45–61.

Milly, P.C.D., Betancourt, J., Falkenmark, M., Hirsch, R.M., Kundzewicz, Z.W., Lettenmeier, D.P. and Stouffer, R.J. (2008). Stationarity is dead: whither water management? Science **319**, 573–74.

Mironov, D., Heise, E., Kourzeneva, E., Ritter, B., Schneider, N. and Terzhevik, A. (2010). Implementation of the lake parameterisation scheme flake into numerical weather prediction model COSMO. Boreal Environ. Res. **15**, 218–230.

Nakayama, T. and Watanabe, M. (2008). Simulation of groundwater dynamics in North China Plain by coupled hydrology and agricultural models. Hydrological Processes **22**, 1150–1172. DOI: 10.1002/hyp

Nützmann, G., Holzbecher, E. and Pekdeger, A. (2003). Evaluation of water balance of Lake Stechlin with the help of chloride data. Arch. Hydrobiol. Spec. Issues Advanc. Limnol. **58**, 11-23.

Orlob, G.T. and Selna, L.G. (1970). Temperature variations in deep reservoirs. Proc. Am. Soc.Civ. Eng., **96**(HY2), 391-410.

Pollman, C.D., Lee, T.M., Andrews, W.J., Sacks, L.A., Gherini, S.A. and Munson, R.K. (1991). Preliminary Analysis of the Hydrologic and Geochemical Controls on Acid-Neutralizing Capacity in Two Acidic Seepage Lakes in Florida, Water Resources Res., **27**(9), 2321–2335.

Richards, T.L. and Irbe, J.G. (1969). Estimates of monthly evaporation losses from the Great Lakes 1950 to 1968 based on the mass transfer technique. paper presented 12th Conf. Great Lakes Res., Ann Arbor, Mich., Internat. Assoc. Great Lakes Res., May 5-7.

Richter, D. (1997). Bericht des Deutschen Wetterdienst 201: Das Langzeitverhalten von Niederschlag und Verdunstung und dessen Auswirkungen auf den Wasserhaushalt des Stechlinsees, Offenbach am Main.

Sacks, L.A., Herman, J.S., Konikow, L.F. and Vela, A.L. (1992). Seasonal dynamics of groundwater-lake interactions at Donana National Park, Spain. Journal of Hydrology 136: 123–154.

Sholkovitz, E., Herbold, C. and Charette, M. (2003). An automated dye-dilution based seepage meter for the time-series measurement of submarine groundwater discharge. Limnology and Oceanography, Methods **1**: 16–28.

Stephenson, M., Schwartz, J.W., Melnyk, T.W. and Motycka, M.F. (1994). Measurement of advective water velocity in lake sediment using natural helium gradients. Journal of Hydrology **154**, 63–84.

Winter, T.C. (1976). Numerical simulation analysis of the interaction of lakes and ground water. USGS Professional Paper 1001.

Yaglom, A.M. (1977) Comments on wind and temperature flux-profile relationships, Boundary-Layer Met., **11**, 89-102

Zilitinkevich S.S. (Ed.) (1991). Modelling of Air-Lake Interaction. Physical Background. Springer, 129 p.

Temperature in Hálslón reservoir

Victor Kr Helgason* and Andri Gunnarsson

Landsvirkjun, Research and Planning. Háaleitisbraut 68, 103 Reykjavík, Iceland

** Corresponding author, e-mail: victor@lvp.is*

KEYWORDS
Conference; Hálslón reservoir; temperature measurements; thermal layering.

ABSTRACT

Hálslón reservoir is contained by three dams, the largest being a 198 m high CFRD on the southern end of the Dimmugljúfur gorge. Hálslón stretches from Brúarjökull, an outlet glacier from Vatnajökull glacier, 25 km to the north and covers 61 km².

Three temperature dataloggers were suspended (1m, 10 m and 40 m depth) from a buoy in middle of June 2009 and retrieved around the middle of November the same year. The water temperature shows strong correlation with air temperature and wind data, with the correlation being higher in the upper layers at 1 m and 10 m depths than at 40 m depth. Temperature at 40 m depth is influenced by the temperature of the glacial melt water inflow originating from Vatnajökull glacier. From the recorded data, the positions of the thermal layers in the reservoir can be observed.

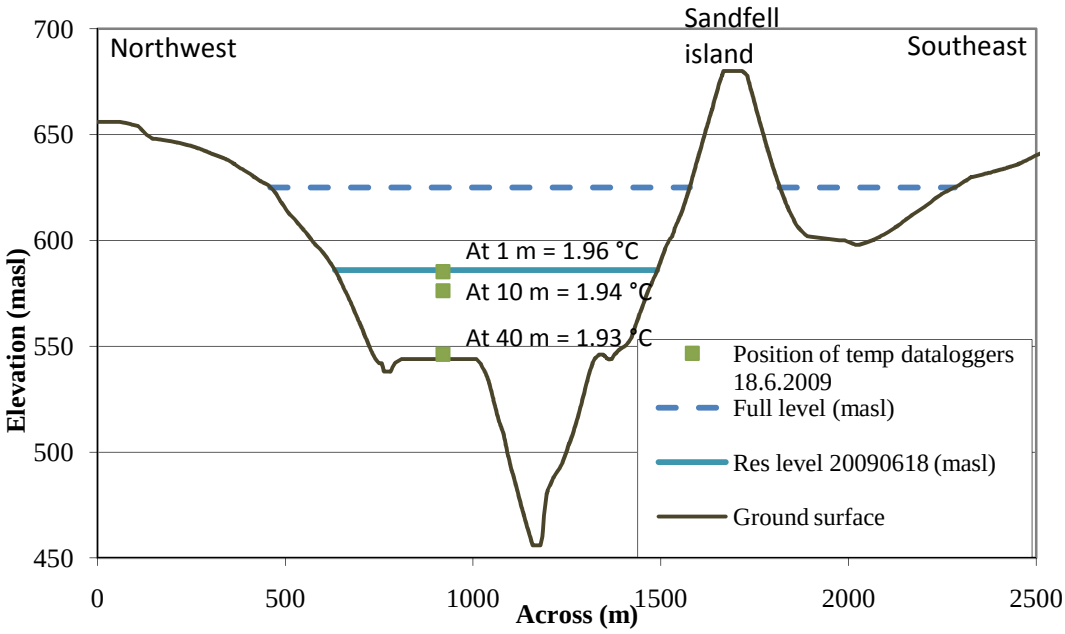

Figure1. Cross section of Hálslón reservoir in mid June

Modelling the thermal behaviour of subarctic water system during ice free conditions

M. Priet-Mahéo and H. Andradóttir

Faculty of Civil and Environmental Engineering, University of Iceland, Hjarðarhaga 6, 107 Reykjavík, Iceland

**Corresponding author, e-mail mcc1@hi.is*

KEYWORDS
Surface heat fluxes, temperature modelling, glacial river, spring river

EXTENDED ABSTRACT

INTRODUCTION
Water temperature is an important water quality parameter. In the age of climate change, the need for understanding how water systems heat up and cool down with varying meterological forcing is ever more pressing. In Iceland, water temperatures have been monitored regularly for as long as 15 years by Landsvirkjun and the Icelandic Meterological Office (e.g. Helgason and Axelsson, 2009). In addition, the Icelandic Meterological Office measures weather parameters such as air temperature and pressure, relative humidity, wind speed and direction. However, incoming short wave solar radiation is not commonly measured directly, making the assessment of impending surface heat fluxes difficult. The purpose of the present study is to assess surface heat fluxes and compute the evolution of water temperature from the tributary rivers of sub-arctic Lake Lagarfljót located in Eastern Iceland. These rivers can be divided into two categories: glacial rivers coming from the glacier Vatnajökull such as Jökulsá í Fljótsdal and spring rivers such as Keldá.

METHODS
In this preliminary study, net heat fluxes at the surface of the rivers are calculated from weather data from the Icelandic Meteorological Office using traditional methods described e.g. in Fisher et al. (1979) and Andradóttir (2000). Short wave radiations measurements being insufficient for our period of interest, are computed according to the methods described in Bras (1990) based on theoretical input and cloud cover data provided by the Icelandic Met Office.

In order to check the validity of the computed net heat fluxes, a simple 1D model is built based on the computation of net heat fluxes and applied to two tributary rivers of Lake Lagarfljót: a glacial river Jökulsá í Fljótsdal and a spring river Keldá í Suðurdal. The model assumes that because the rivers are shallow, the water is instantly fully mixed vertically. The governing equation is therefore:

$$\frac{dT}{dt} = \frac{H_{net}}{\rho C z}$$

with T the water temperature in °C, t the period in s, H_{net} the net surface heat flux in W/m², ρ the water density in kg/m^3, C the specific heat of water in J/(kg∗°C) and z the water depth in m. Modelled water temperatures are then compared to those measured by the Icelandic Meteorological Office.

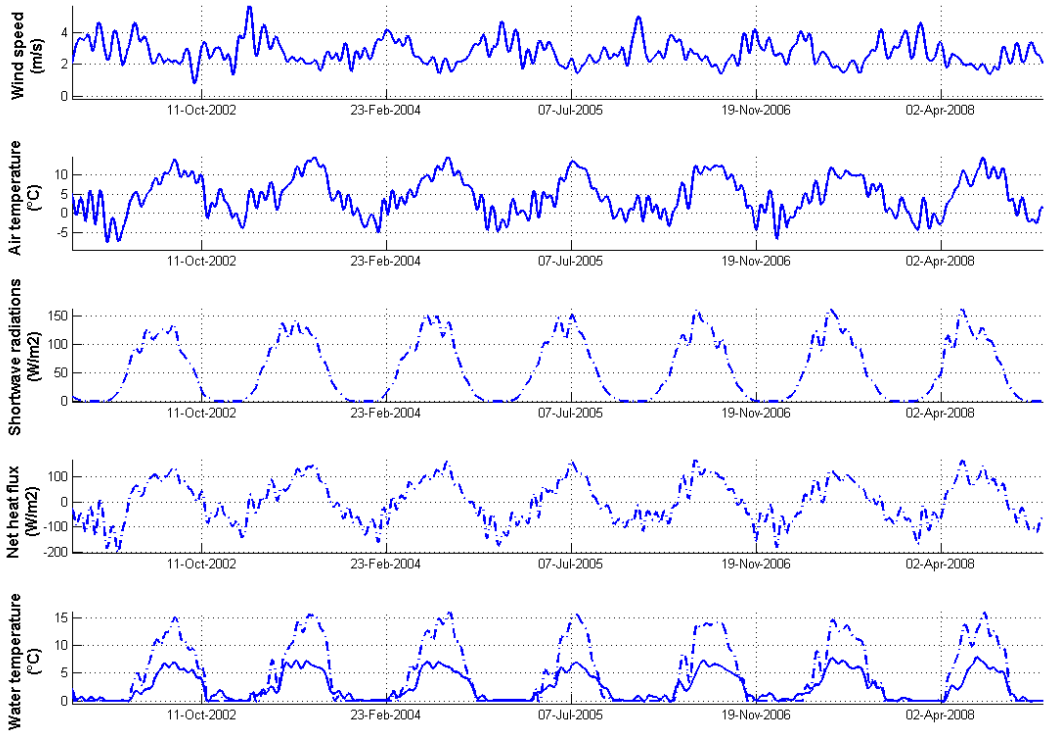

Figure 1 Comparison of the main components influencing the water temperature with the water temperature measurements and computation at Jökulsá í Fljótsdal. In solid line, measured data, in dash-dotted line, computed data from 2001-2008.

FIRST RESULTS AND DISCUSSION

Figure 1 shows the first results for the glacial river Jökulsá í Fljótsdal in 2001-2008. The calculated net heat fluxes appear to precede the river temperatures by less than a day which is consistent of the thermal inertia which is small as in such a shallow river (~1.5m deep). A simple water temperature model captures the general seasonal trends but with overestimates the temperature during the summer season. The RMS error for the glacial river is +/- 3.7°C while it is slightly less for the spring river (+/-3°C, not shown), suggesting that the cold glacial and groundwater source temperature needs to be taken into account in the computation and using a simple theoretical solar radiation adjusted for cloud cover might be insufficient in the present model. Future work will therefore focus on improving the river model. Once the river temperature model has been finetuned, the calculated net surface heat fluxes will be used as input to model the vertical temperature variation in sub-arctic Lake Lagarfljót.

ACKNOWLEGMENT

This work was funded by the Landsvirkjun Energy Research Fund and the University of Iceland Research Fund.

REFERENCES

Andradóttir H.Ó. (2000). Littoral wetlands and lake inflow dynamics, Ph.D. thesis, Massachusetts Institute of Technology, Cambridge

Bras, R. L. (1990). Hydrology: An Introduction to Hydrologic Science, Addison-Wesley-Longman, Reading, Mass, 643 pp.

Fischer, H.B., List, E.J., Koh, R.C.Y., Imberger, J., and Brooks, N.H. (1979). Mixing in inland and coastal waters. San Diego, Academic Press, 483 p.

Helgason, V., Axelsson, E. (2009). Vatnshitamælingar Landsvirkjunar og vatnmælingar á Austurlandi árin 1995-2007. Landsvirkjun.

Modeling underflows in Lake Thingvallavatn in varying surface shear conditions

A.L. Forrest[1]*, H. Andradottir[2], B.E. Laval[1]

[1] *Environmental Fluid Mechanics Group, Department of Civil Engineering, University of British Columbia, Vancouver V6T 1Z4, BC, Canada*
[2] *University of Iceland, Faculty of Civil and Environmental Engineering, 107 Reykjavik, Iceland*

**Corresponding author, e-mail forrest@civil.ubc.ca*

KEYWORDS
Underflows; entrainment; wind shear; autonomous underwater vehicles; vertical mixing

EXTENDED ABSTRACT

The fate of river inflows, and their associated entrainment rates, has been extensively studied in freshwater systems (Ellison and Turner, 1959; Dallimore et al., 2002). With some notable exceptions (Stefanovic and Stefan, 2002), the emphasis of field studies have been on summer stratified conditions even though a large percentage of the global lake inventory, particularly at high latitudes, undergoes winter stratification (e.g. weakly stratified and/or ice covered). Regardless of wind strength, ice cover isolates a weakly stratified water column from the direct influence of the wind. Irrespective if river inflows are forming a positively or negatively buoyant flow, isolation from wind shear will alter the mass flux path of the inflowing water into the main body of the lake. This work presents a unique field study of a negatively buoyant underflow and how the dynamic spring ice-cover break-up influences the initial mixing of the inflow with lake water.

During the winter months, Lake Thingvallavatn (88 km^2), Iceland is predominantly fed by a single groundwater source in a small, shallow (2–5 m total depth) embayment at the northern end of the lake which discharges at ~ 1–2 ºC greater than the lake that is near isothermal at ~ 1 ºC resulting in a negatively buoyant underflow which propagates into the lake. We characterize this system during the initial onset of spring ice break-up from Feb. 18 – 27, 2009. The dynamic nature of the moving ice allowed two different wind forcing scenarios, weak and strong forcing, to be identified and explored using a variety of conventional techniques (thermistor chains, vertical profilers, etc.) and the unconventional use of an Autonomous Underwater Vehicle (AUV) to measure horizontal profiles of water temperature beneath ice-cover, out to a distance of ~ 300 m away from the ice edge. This would have been impossible with almost any other technique as the ~ 10 cm thick rotten ice was not possible to safely sample from but was too thick to break through with a boat.

Although surface forcings were extremely variable during this time, samples were collected during two dominant wind regimes identified as; (1) weak wind forcing (either low wind speeds or ice cover), and (2) strong wind forcing (wind > 3 m s^{-1} and open water). During both of these regimes, the behavior of the underflow could be reduced to a two-dimensional flow problem; validated by comparing the measured underflow velocities with the ADV with the modeled predictions. Periods of transition between the two forcing conditions, characterized by dynamic, across-basin heterogeneity were also observed during the study period. Underflow behavior during these periods, generally associated with open water

conditions, was much more three-dimensional in nature and is thought to be related to a much greater degree with the wind direction than the two dominant regimes.

During the first regime, it was shown that the underflow is unmodified by convective processes associated with ice cover (e.g. radiatively driven convection) before plunging into the main body of the lake. The greatest contribution that these processes could account for in the observed temperature fluctuations was less than 3 percent of the observed temperature fluctuations. Entrainment rates estimated from constant-altitude AUV-collected CTD profiles, a novel estimation technique derived in this study, were in the range of $1.8 – 3.2 \times 10^{-3}$. As these predictions agree well with previous works (Cenedese et al., 2004), it is possible to conclude that it is possible to use standard formula to calculate entrainment under ice provided the bulk Richardson number for the underflow can be calculated. In contrast, during the second regime (strong wind forcing) enough mechanical mixing is provided to mix the underflow with the ambient water in the shallow bay.

It is possible to conclude that the ultimate fate of the underflow depends on the surface shear condition of the relatively shallow (2 - 5 m) receiving bay; low surface shear, due to either low wind speeds or ice cover, and high surface shear due to high wind speeds and no ice cover. During periods of low surface shear, the water column becomes stratified and bulk velocity can be approximated with simple two-layer, two-dimensional mass and energy budgets. During periods of high surface shear, input of wind energy exceeds buoyancy flux of the inflow resulting in mixing of the water column and dilution of the temperature signal of the underflow. The combination of the various data collection platforms used in this study was the only way to safely quantify three dimensional, time-evolving physical dynamics in this variable ice-cover subarctic lake.

REFERENCES

Cenedese, C., Whitehead, W.A., Ascarelli, T.A. and Ohiwa. M. (2003). A dense current flowing down a sloping bottom in a rotating fluid. *J. Phys. Oceano.*, **34**: 188 – 203.

Dallimore, C.J., Imberger, J. and Ishikawa, T. (2001). Entrainment and turbulence in saline underflow in Lake Ogawara. *J. Hydr. Engrg.* **127**(11): 937 – 948.

Ellison, T.H., and Turner, J.S. (1959). Turbulent entrainment in stratified flows. *J. Fluid Mech.* **6**: 423 – 448.

Stefanovic, D.L. and Stefan, H.G. (2002). Two-dimensional temperature and dissolved oxygen dynamics in the littoral region of an ice-covered lake. *Cold Regions Science Tech.* **34**: 159 – 178.

Turbulence modulation by suspended sediment in a zero-shear geophysical flow

S.J. Bennett[1], J.F. Atkinson[2]*, and M.J. Fay[1]

[1] *Department of Geography, University at Buffalo, Buffalo, New York 14261-0055 USA*
[2] *Department of Civil, Structural and Environmental Engineering, University at Buffalo, Buffalo, New York 14260 USA*

**Corresponding author, e-mail atkinson@buffalo.edu*

ABSTRACT
The effects of a suspended sediment load on fluid turbulence are investigated within a standard mixing box where a single oscillating grid is placed near the floor of the apparatus. Clear-water flow conditions for a given grid oscillation frequency are quantified using particle image velocimetry, and fluorescent tracer particles are used to discriminate the fluid phase. These measurements are repeated under identical boundary conditions for supply-limited and transport-limited suspensions using quartz-density fine sand. It is shown that the central region of the mixing box, dominated by highly turbulent, upward-directed flow velocities at the intersection of two depth-scale convection cells, undergoes significant turbulence suppression when sediment is present. Turbulence enhancement also is observed in the central region of the convection where the turbulent velocities are relatively small. It is suggested here that this experimental design is uniquely suited to examine unambiguously these fluid-particle interactions, and that turbulence suppression of this upward-directed flow field is an immediate consequence of having to maintain the suspended sediment load.

KEYWORDS
Turbulence modulation; particle image velocimetry; mixing box; zero-shear geophysical flow; suspended sediment.

INTRODUCTION
The effect of suspended sediment transport on turbulent, open channel flows has long been debated in the literature. Much of this debate has focussed on time-averaged profiles of velocity and Reynolds stress, the value of von Kármán's coefficient, and the magnitude, characteristics, and vertical distributions of turbulence intensities, mixing lengths, and eddy diffusion coefficients (see Best *et al*., 1997; Muste *et al*., 2005 and references therein), specifically how these parameters are altered in the presence of a suspended sediment load.

As noted by Best *et al*. (1997), three parameters often are used to delineate the effects of suspended sediment on fluid turbulence. These are (1) the ratio of sediment size to a characteristic turbulence length scale (e.g., Gore and Crowe, 1991), (2) the Stokes number, which is the ratio of particle response time to a representative fluid timescale (e.g., Elghobashi, 1994), and (3) the particle Reynolds number based on the slip velocity between the fluid and sediment phases (e.g., Hetsroni, 1989). Both Best *et al*. (1997) and Muste *et al*. (2005) applied these criteria to explain their experimental observations, employing either direct determination of these key parameters or suitable empirical relations for comparative

purposes. The results of applying these criteria, however, were met with varying success, and included (1) subtle rather than marked variations in velocity and turbulence signatures, (2) both enhancement and suppression of turbulence in the same flow, (3) inconsistency in the effects of sediment on turbulent flow, and (4) the recognition that the interactions of the sediment particles with coherent turbulent flow structures may not be adequately captured using time-mean values.

It is contended here that the experimental design to examine the effects of suspended sediment on fluid turbulence also can be improved. First, it is imperative that the fluid and sediment phases within a sediment-laden turbulent flow be clearly and unambiguously discriminated, therefore removing the potential that such turbulent signatures are, in fact, contaminated by the other phase. Second, it is imperative that the clear-water and sediment-laden flows are, in fact, hydrodynamically equivalent, thus removing any uncertainty about varying flow rates, boundary conditions, and energy gradients when sediment is introduced to the clear-water flow.

The current research program sought to quantify the effects of suspended sediment on fluid turbulence in a geophysical flow by specifically addressing these two experimental challenges. First, particle image velocimetry (PIV) is employed to quantify the turbulent flow field, where laser-induced fluorescent tracer particles coupled with lens-mounted polarized filters ensures that only the characteristics of the fluid phase are captured. Second, a standard grid-mixing box is employed (e.g., Thompson and Turner, 1975), such that the oscillation frequency and stroke of the grid can be externally controlled and total flow depth can be maintained, both with great precision. Thus, the objectives of the current paper are: (1) to quantify the time-mean and turbulent flow field within a mixing box using clear-water conditions, and (2) to quantify the variations in the time-mean and turbulence characteristics of the fluid phase in the presence of suspended sediment that is dilute (supply-limited) and concentrated (transport-limited).

METHODS

All experiments are performed in a polycarbonate mixing box 0.315 m wide and deep, and 0.393 m tall. An aluminum grid placed at the bottom box provides the source of turbulence, and this orthogonal grid consists of 10 10-mm square bars with 50-mm center-to-center spacing. The grid is mounted from above to a rotating eccentric arm and controlled by an external motor. The stroke of the grid as used here is 70 mm, and the speed of the motor is measured with an optical tachometer.

PIV is used to quantify all turbulence parameters within the box. This system comprises a dual-cavity 50 mJ Nd-YAG laser emitting 532 nm light and two 4 Mp cameras with 4 GB each of RAM. All data acquisition and synchronization are handled by an external timing hub, dedicated computer, and DANTEC software. Inside the box, at the apogee of the grid, a dual-level 3D calibration target (0.27 m wide and 0.19 m tall) is placed, and the cameras are mounted off-axis to the target (total angular difference of 16°). For this study, paired images are collected at 40 Hz, the interrogation areas are 32 pixels, and the central-difference adaptive correlation algorithm within the DANTEC software is used to derive the 3D vector fields. The laser light sheet enters the box at 80 mm from the sidewall, and is centered on the cross-bars of the grid, rather than the nodes. Hollow glass spheres 20 to 50 μm in diameter and dyed with Rhodamine B are used as fluid tracer particles, which fluoresce in the laser light sheet. Polarizing filters (>570 nm) are placed onto the camera lenses, thereby allowing

only these fluorescent tracer particles to be recorded to video. Each vector field comprises approximately 3479 vectors, and about 462 image pairs are used to derive time-averaged values of mean and turbulent velocities. All data reported here are actual measurements (no interpolations are used), and all time-averaged values have a minimum of 100 realizations.

Sand of varying concentrations is added to this box under these clear-water conditions. The quartz-density fine sand is 250 to 300 μm in diameter, and total dry mass added to the box ranges from 0.1 to 1 kg. Volumetric suspended sediment concentrations (m^3/m^3) are collected at-a-point using a siphon sampler. Both the volume of water and sediment removed after each sample extraction are replaced by an equivalent amount. These samples are decanted and the sediment oven-dried to determine total mass. Flow depth for all experiments is 0.292 m.

RESULTS AND DISCUSSION

Preliminary results of this experimental program are presented below. These include variations in the volumetric suspended sediment concentration within the box as a function of total concentration and vertical height, the time-mean and turbulent flow field using clear-water conditions, and the difference in these flow parameters using sediment-laden conditions.

Variations in suspended sediment concentration

Prior to full experimentation, it is important to determine the relationship between grid oscillation frequency *f* and volumetric suspended sediment concentration *C*, as normalized by the total volumetric sediment concentration in the box C_0. For varying heights *y* above the grid apogee ($y = 0$), as normalized by flow depth *d* above this datum, and for a given oscillation frequency $f = 2.33$ Hz, at-a-point values of C/C_0 show that these concentrations reach asymptotic values at slightly different input concentrations (Figure 1a). That is, suspended sediment concentration is supply limited until a threshold concentration of sand is added to the box. Based on this observation, and the chosen frequency *f*, two input sediment concentrations are selected for investigation: a supply-limited suspension ($C_0 = 0.00263$) and a transport-limited suspension ($C_0 = 0.00903$).

This distinction between supply-limited and transport-limited suspensions can be demonstrated by plotting C/C_0 as a function of relative height in the box y/d. Figure 1b shows that C/C_0 remains fairly constant with distance from the grid when $C_0 = 0.00263$, whereas when $C_0 = 0.00903$, C/C_0 remains fairly constant very near the grid ($y/d < 0.4$), but decreases significantly with distance away from the grid ($y/d > 0.4$). Thus for $f = 2.33$ Hz, suspended sediment is well-mixed and supply-limited when $C_0 = 0.00263$, but displays a strong vertical gradient and is transport-limited when $C_0 = 0.00903$. These will be the two sediment-laden conditions examined below.

Time-mean and turbulent flow using clear-water conditions

Time-mean 2D vectors (in the cross-stream *x* and vertical *y* directions; the transverse *z* velocity component is not shown here) and select streamlines for the clear-water conditions and $f = 2.33$ Hz are shown in Figure 2. Here, x/w is the relative distance across the box and *w* is the box width. Flow within the mixing box along this plane is characterized by two large convection cells, and the largest magnitude flow velocities are located in the center of the

field and vertically oriented where the two convection cells intersect. Varying the data collection rate from 40 Hz to 80 Hz had no effect on this time-averaged flow field.

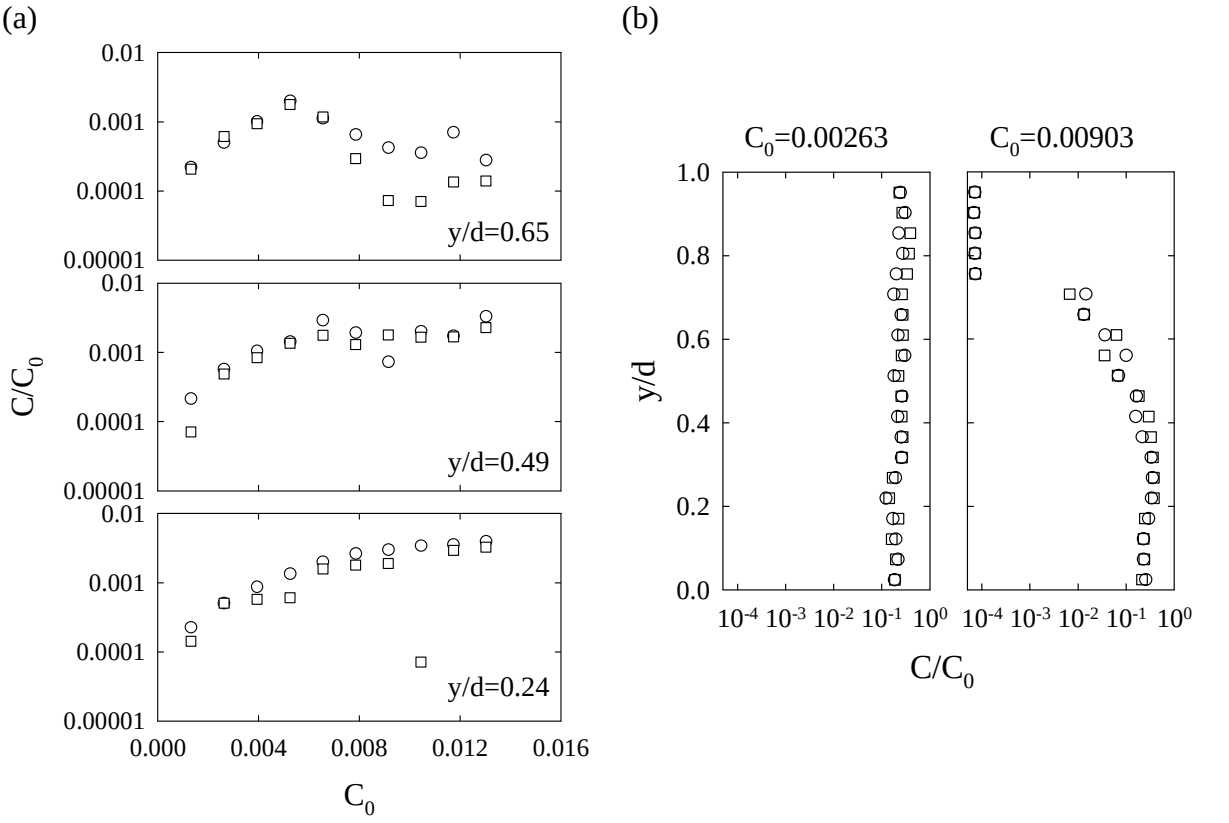

Figure 1. Using $f = 2.33$ Hz, variations in volumetric suspended sediment concentration (a) at-a-point at a given y/d within the mixing box for a range of C_0, and (b) as a function of y/d for two input concentrations C_0.

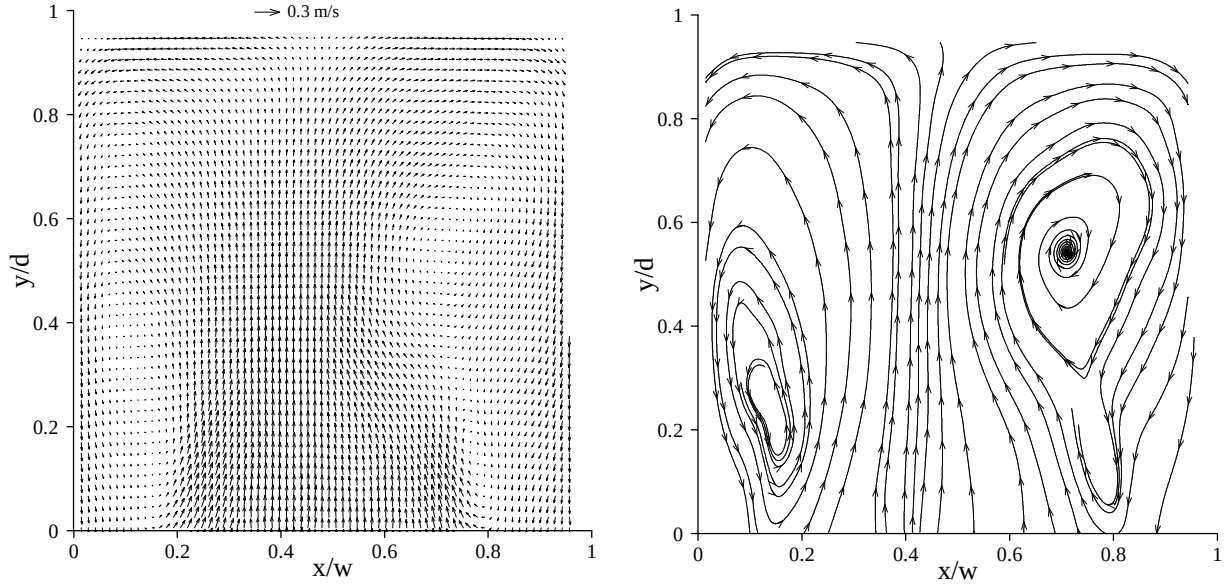

Figure 2. Time-averaged 2D flow vectors (on left) and select streamlines (on right) within the mixing box for clear-water conditions using $f = 2.33$ Hz.

Turbulence parameters for the clear-water flow conditions are shown in Figure 3. Here, the root-mean-square of the cross-stream u (x-axis; U_{rms}), vertical v (y-axis; V_{rms}) and transverse w components (z-axis; W_{rms}) and the turbulent kinetic energy (TKE) are defined as:

$$U_{rms} = \sqrt{\overline{u'^2}} \qquad V_{rms} = \sqrt{\overline{v'^2}} \qquad W_{rms} = \sqrt{\overline{w'^2}} \qquad TKE = 0.5\left(\overline{u'^2} + \overline{v'^2} + \overline{w'^2}\right)$$

where u, v, and w are the instantaneous velocities at-a-point, $u' = u - \overline{u}$, $v' = v - \overline{v}$, and $w' = w - \overline{w}$, and the overbar represents an at-a-point time-average. The distributions of turbulent velocities within the mixing box are in close association with distance from the grid and co-located with the highest magnitude velocity within the central portion of the convecting flow field.

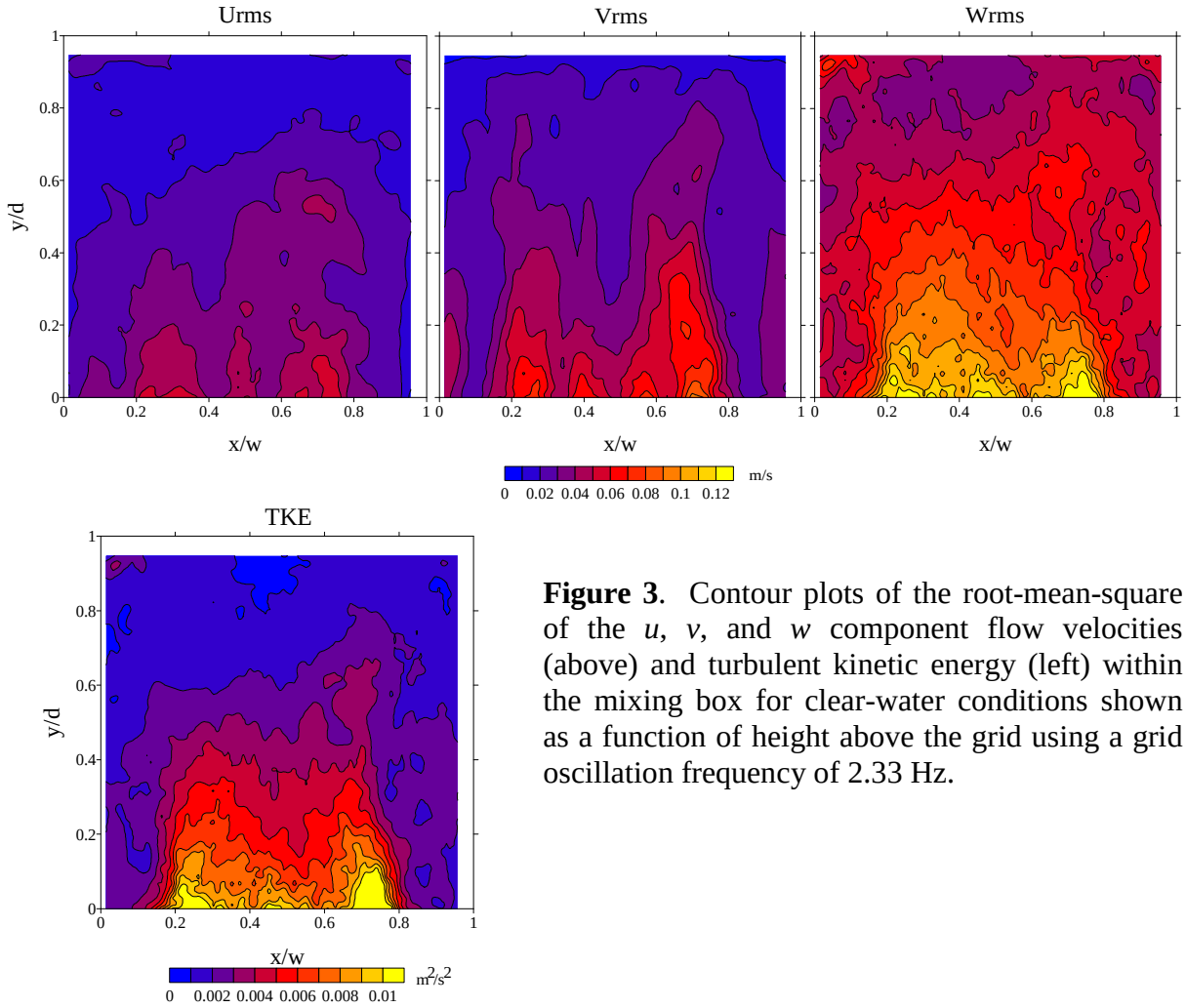

Figure 3. Contour plots of the root-mean-square of the u, v, and w component flow velocities (above) and turbulent kinetic energy (left) within the mixing box for clear-water conditions shown as a function of height above the grid using a grid oscillation frequency of 2.33 Hz.

Sediment-laden vs. clear-water turbulent flow conditions

Because the interest here in on the effects of suspended sediment on the turbulent flow field (the fluid phase only), the relative changes of the turbulence parameters as observed in the sediment-laden flow conditions can be determined. All time-mean and turbulent flow parameters for the two sediment-laden conditions (supply-limited and transport-limited) are determined, but only their differences in comparison to the clear-water conditions are shown below. In these cases, a normalized percentage difference (% difference) between the clear-water and sediment-laden conditions for the root-mean-square and turbulent kinetic energy values can be defined simply as:

$$\%\ \text{difference} = \frac{SL - CW}{CW} \times 100$$

where *SL* and *CW* refer to the sediment-laden and clear-water flow parameter in question, respectively.

The addition of sediment has a marked effect on the fluid turbulence signal within the mixing box. Figure 4 shows the percent differences between the sediment-laden and clear-water flow conditions for the root-mean-square velocity components. Modest reduction (suppression) of the turbulent velocities is observed for the supply-limited suspension for most of the flow field (up to –60%), whereas modest increases (enhancement) occurs near the central nodes of the convection cells (up to +60%). Yet when the sediment concentration increases and becomes transport-limited, the turbulence reductions become much more pronounced (up to –100%), and the turbulence enhancement within the convection cells also becomes greater in magnitude (up to +100%).

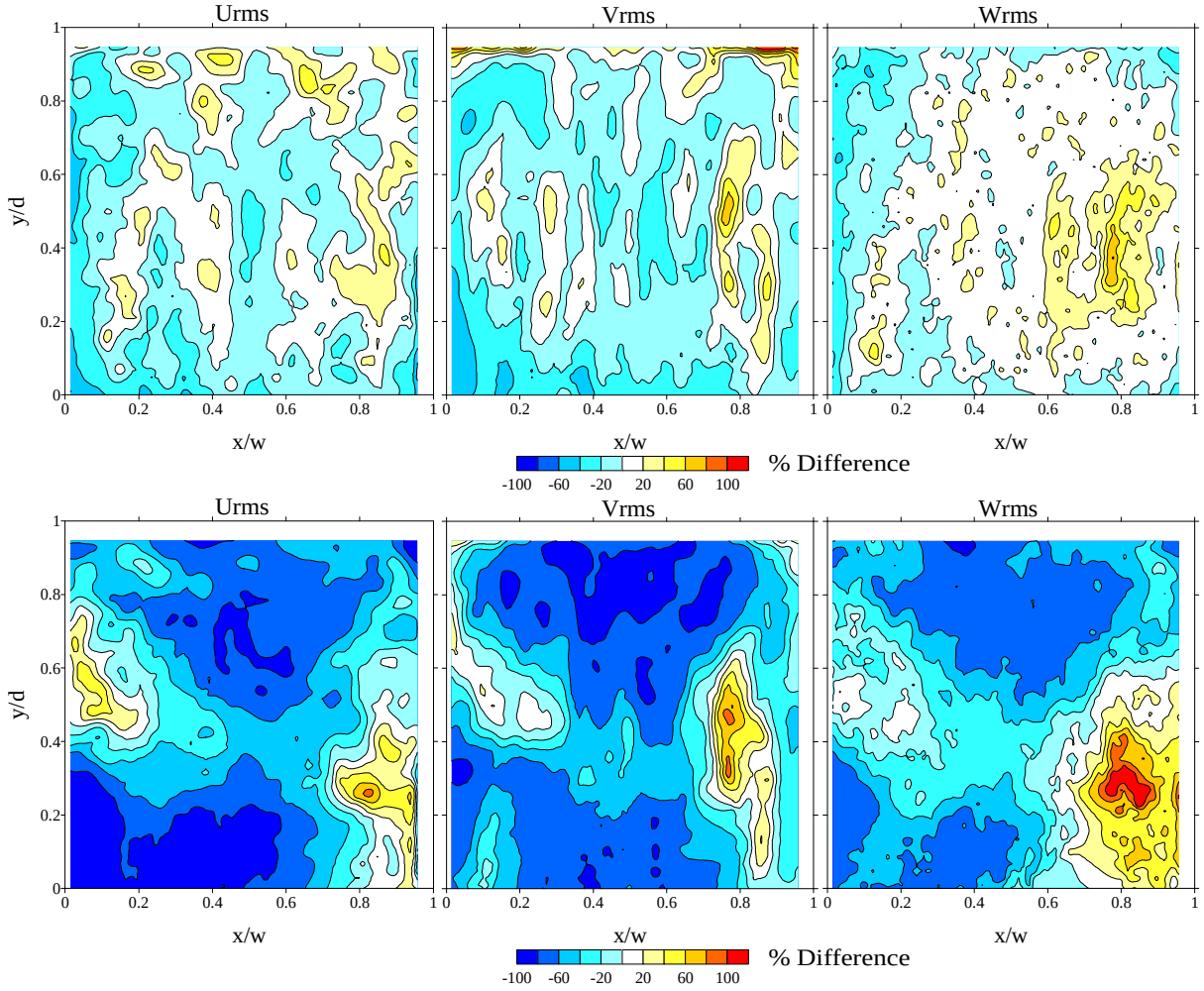

Figure 4. Contour plots of the percent difference in the root-mean-square of the *u*, *v*, and *w* component flow velocities (left to right) within the mixing box between the clear-water conditions and the supply-limited ($C_0 = 0.00263$, upper plots) and transport-limited ($C_0 = 0.00903$, lower plots) conditions, shown as a function of height above the grid using a grid oscillation frequency of 2.33 Hz.

Similar trends are observed in the comparison of the clear-water and sediment-laden turbulent kinetic energy signals. For the supply-limited condition, the change in turbulent kinetic energy for the sediment-laden flow is modest, with minor amounts of suppression and enhancement occurring in the central flow fields and markedly higher enhancement values within the convection cells. For the transport-limited condition, the change in turbulent kinetic energy for the sediment-laden flow is more pronounced, with greater amounts of suppression occurring in the central flow field (up to −120%) accompanied by markedly higher enhancement values within the convection cells (more than +200%).

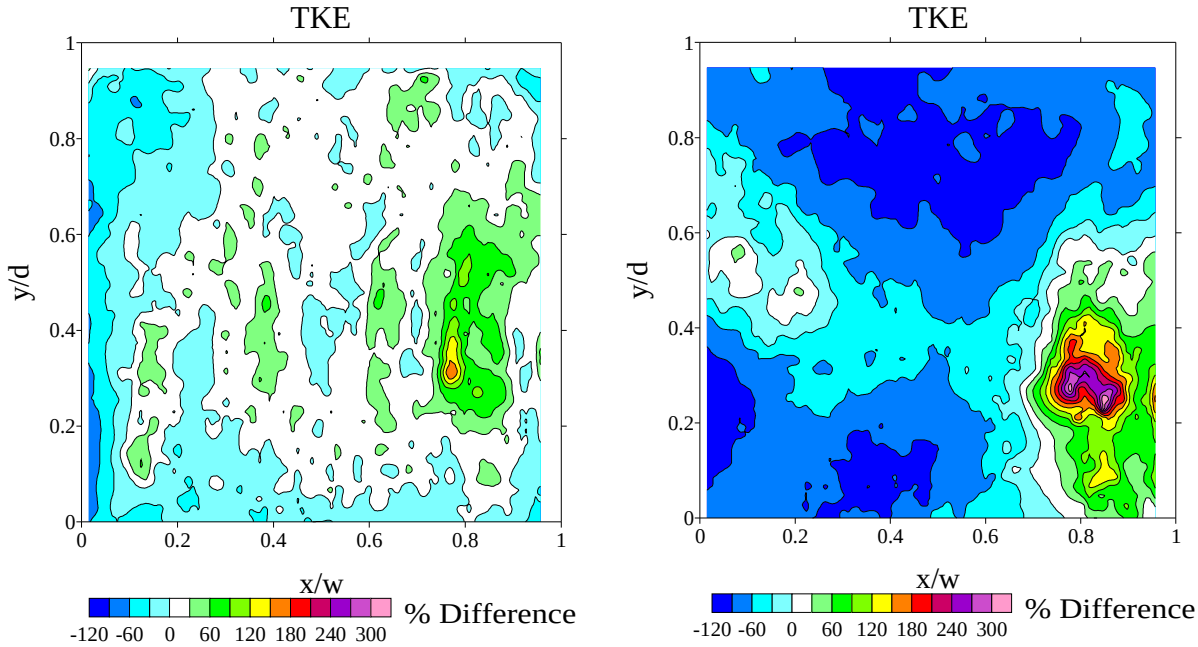

Figure 5. Contour plots of the percent difference in the turbulent kinetic energy within the mixing box between the clear-water conditions and the supply-limited ($C_0 = 0.00263$, on left) and transport-limited ($C_0 = 0.00903$, on right) conditions, shown as a function of height above the grid using a grid oscillation frequency of 2.33 Hz.

Discussion

While the causes for the turbulence modulation currently are under investigation, the magnitude and character of these signatures are clear and unambiguous within this experiment. Even with the addition of very modest concentrations of suspended sediment, significant departures of the turbulence from their clear-water values are observed. These effects are even more pronounced when the sediment-laden flow achieves transport-limited conditions, resulting in the suppression of fluid turbulence by as much as −100% within the primary flow field. It is no coincidence that the upward-directed fluid flow within this central region is most affected by this added sediment. It now is theorized that the maintenance of sediment suspension requires an upward directed net momentum flux equal and opposite to the immersed weight of the suspended load (Leeder *et al.*, 2005), and a similar mechanism is postulated here. That is, turbulence suppression occurs because turbulent energy of the fluid is being actively transferred to the sediment phase in order to suspend this load. Finally, it should be noted that while turbulence enhancement is observed on the downward arcs of convection cells, and most notably within the nodal regions, the magnitudes of these velocities are small in comparison to the central portion of the mixing box where turbulence suppression is most pronounced.

CONCLUSIONS

The effects of a suspended sediment load on fluid turbulence in open channel flows have long been discussed. It is contended here the use of particle image velocimetry and a standard mixing box can improve upon this previous work by employing two important experimental conditions: the creation of hydrodyamically equivalent flows, and the unambiguous discrimination of the fluid phase within sediment-laden flow. The objectives of the current paper are to quantify the time-mean and turbulent flow field within a mixing box using clear-water conditions, and to quantify the variations in these turbulent parameters in the presence of suspended sediment at two distinct concentrations (supply-limited and transport-limited).

Turbulent flow within a mixing box is quantified using PIV and fluorescent tracer particles for the fluid phase. Flow is characterized by two depth-scale convection cells whose central portion is dominated by highly-turbulent, upward-directed flow velocities. Upon the introduction of quartz-density fine sand to the box, this central region displays marked turbulence suppression, especially when the flow is transport-limited. Minor regions of turbulence enhancement also are observed, notably in the central regions of the convection cells where flow velocities are relatively small. These results provide qualitative support for the notion that the maintenance of a suspended load requires an upward-directed momentum flux, which is clearly modulated as load increases due to the transfer of turbulent energy from the fluid to the sediment phase. Finally, these results suggest that under ideal experimental conditions, the effects of a suspended load on fluid turbulence is clear, measurable, and unambiguous.

ACKNOWLEDGEMENT

This work has been financially supported by NSF-EAR 0640617 and NSF-EAR 0549607.

REFERENCES

Best, J.L., Bennett, S.J., Bridge, J.S., and Leeder, M.R. (1997). Turbulence modulation and particle velocities over flat sand beds at low transport rates. *J. Hydraul. Eng*., **123**, 1118-1129.

Elghobashi, S. (1994). On predicting particle-laden turbulent flows. *Appl. Sci. Res*., **52**, 309-329.

Gore, R.A., and Crowe, C.T. (1991). Modulation of turbulence by a dispersed phase. *J. Fluids Eng*., **113**, 304-307.

Hetsroni, G. (1989). Particles-turbulence interaction. *Int. J. Multiphase Flow*, **5**, 735-746.

Leeder, M.R., Gray, T.E., and Alexander, J. (2005). Sediment suspension dynamics and a new criterion for the maintenance of turbulent suspensions. *Sedimentology*, **52**, 683-691.

Muste, M., Yu, K., Fujita, I., and Ettema, R. (2005). Two-phase versus mixed-flow perspective on suspended sediment transport in turbulent channel flows. *Water Resour. Res*., **41**, W10402, doi:10.1029/2004WR003595.

Thompson, S.M., and Turner, J.S. (1975). Mixing across an interface due to turbulence generated by an oscillating grid. *J. Fluid Mech*., **67**, 349-368.

Hydrophysical processes in the gulf of Finland inferred from bottom-mounted ADCP measurements

L. Talsepp*, J. Elken, T. Kõuts, M.-J.Lilover, I.Suhova

Institute of Marine Systems, Tallinn, Estonia, Akadeemia Rd.21, 12618

**Corresponding author, e-mail talpsepp@phys.sea.ee*

EXTENDED ABSTRACT

A bottom-mounted ADCP was deployed near the southern coast of the Gulf of Finland at the position 59N 27.40, 24E 09.96 about 6 km offshore. The instrument was deployed for the period between 13 March and 30 June 2009. The mooring depth was 50 m. The 2 m cell size used enabled us to get currents from 20 levels. The instrument did not enable to measure currents in the bottom layer up to about 4 m distance from the depth (dead zone) and in the water layer about 3 m from the surface (influenced by side lobe of the instrument, surface waves and water level changes). In addition the wind data from Pakri peninsula and Tallinna Madal were available.

During a rather long measurements period we distinguished different hydrophysical processes that prevailed in different sub periods. Over the whole period of the experiment we observed oscillations with the near inertial frequency. In the period between 15 April and 15 May inertial waves were the main source of current variability. The amplitude of oscillations was up to 15 cm/s having the phase shift of 180 degrees between the surface and bottom layers. The westerly wind 5-10 m/s prevailed during that period.

In March and during the first decade of April we observed the dominating variability with the period of 4.5-5 days. The amplitude of these oscillations was up to 20 cm/s and currents appeared to be stronger in the near-bottom layer. In Fig.1 the northern component of the current in the near bottom layer is presented. We can see that currents variability is higher at 45 m depth, smaller at 41 m depth and smallest at 37 m depth.

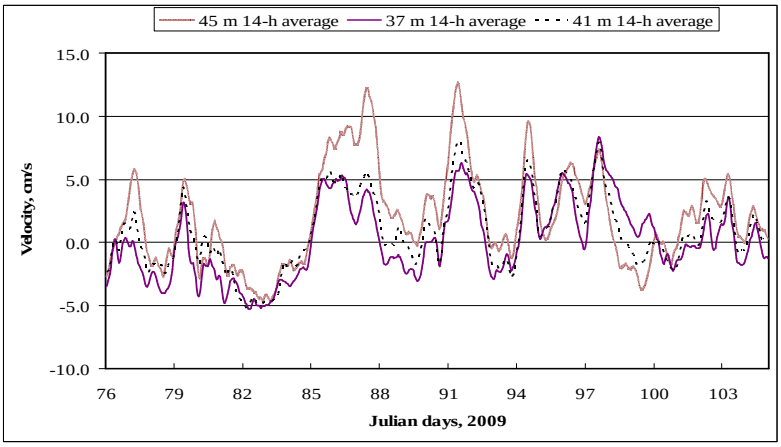

Figure1. The northward current velocity component at 37 m, 41 m and 45 m levels showing increase of the amplitudes of the dominating 4-5 day oscillations with depth, which corresponds to the theory of bottom-trapped topographic waves.

We also calculated the kinetic energy spectra of currents. The dominating peak in the kinetic energy spectra was at 5 days. The other peak was near the local inertial frequency. According to the kinetic energy spectra we can conclude that the kinetic energy increased with depth in the near bottom layer. We also noticed that there was more energy in the northern current component. That vertical variability of currents resembles the variability which the theoretical model of bottom-trapped topographic waves predicts and coincides with earlier observations of topographic waves in that region. However, this is a hypothesis about the existence of topographic waves as we rely only on the data of a single station. In the same period also variability of currents with inertial frequency was observed but the amplitudes were smaller (around 5 cm/s). The variable wind up to 15 m/s was mainly from the west in these days.

The variability of currents between 19 June and 25 June corresponded to the movement of a strong baroclinic eddy passing the experiment area. The expected eddy appeared in the layer from 15 to 35 m with maximum speed in the middle. Currents up to 20 cm/s were directed southward (south to south east) during the first five days and then slowly turned in the opposite direction. Earlier observations frequently revealed baroclinic eddies in that region. Again, because of single point measurements the eddy characteristics like the horizontal scale and spreading speed could not be established.

Current measurements near the southern coast of the Gulf of Finland are an excellent source for new knowledge of the general circulation in the eastern part of the Gulf of Finland and enable to test the corresponding model. To study the mean circulation in the southern part of the Gulf of Finland we calculated the mean current vector for the measurements period for every 2-meter layer. The mean current vector was directed eastward between the bottom and 12 m level and westward in the surface layer. Relying on these measurements we can conclude that in spring period in the southern part of the Gulf of Finland there exists a two-layer circulation pattern – in the bottom and intermediate layer the current is directed into the Gulf and in the upper layer out of the Gulf. The northward component of the mean current vector is positive at the bottom and negative in the surface layer. It means that during the measurements period nearer the southern coast the downwelling is the prevailing process – water is moving southward in the surface layer and offshore in the bottom layer. In Fig.4 the northward current components at the level of 45 m (bottom layer) and at the level of 5 m are presented. The strong downwelling occured between days 154 and 164 and between days 174 and 178. On these dates south-westerly wind prevailed.

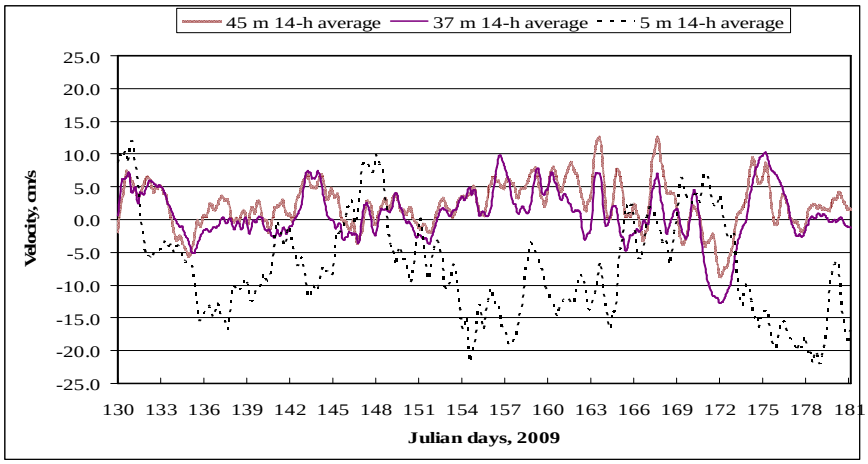

Fig. 2. The northward current velocity component at 5 m, 37 m and 45 m levels. The positive current velocity corresponds to the offshore current and negative velocity to the current directed to the shore

Dissolved oxygen dynamics in a shallow ice-covered lake

A. Terzhevik[1*], G. Kirillin[2], C. Engelhardt[2], S. Golosov[2], M. Leppäranta[3], N. Palshin[1], R. Zdorovennov[1], G. Zdorovennova[1]

[1] *Northern Water Problems Institute, Karelian Research Center, Russian Academy of Sciences, Petrozavodsk, Russia*
[2] *Department of Ecohydrology, Leibniz-Institute of Freshwater Ecology and Inland Fisheries, Berlin, Germany*
[3] *Department of Physics, University of Helsinki, Finland*

**Corresponding author, e-mail ark@nwpi.krc.karelia.ru*

ABSTRACT

Observational data recorded by a string of thermologgers TR-1060 and oxyloggers DO-1050 (RBR Ltd., Canada) deployed in Lake Vendyurskoe, Russian Karelia, during winters 2007-2008 and 2008-2009 demonstrated strong fluctuations experienced by dissolved oxygen (DO) content at different depths of a water column. The FFT analysis revealed that main periods corresponding to those fluctuations were in the range of 2.5-15 days. Putting forward a hypothesis on synoptical and/or seiche-like origin of those fluctuations, joint analysis of water temperature and DO data is performed.

Littoral zones as source of methane in lakes: Dynamics and distribution

H. Hofmann*, C. Seibt and F. Peeters

[1]*Environmental Physics Group, Limnological Institute, University of Konstanz, D-78465 Konstanz, Germany*

**Corresponding author, e-mail hilmar.hofmann@uni-konstanz.de*

KEYWORDS
Methane release, surface waves, spatial and temporal distribution, littoral

EXTENDED ABSTRACT

Lakes and reservoirs have been identified as an important source of atmospheric methane in global methane budgets. Methane is a major product of the carbon metabolism in lakes. Anaerobic carbon mineralization in terms of methanogenesis in anaerobic sediments can account for up to 50% of the overall carbon mineralised in freshwater lakes. A large proportion of the produced methane gets oxidised by methanotrophic bacteria at oxic water and sediment interfaces. The main emission pathways of methane from the water body to the atmosphere are summarised by Bastviken et al. (2004): ebullition from anaerobic sediments , diffusive flux across the air-water interface , plant mediated flux from littoral sediments , and the flux of methane stored in the anoxic water body during the stratification period that is rapidly released during overturning and mixing . The proportion of the individual pathway to the overall lake emission is highly dependent on lake characteristics, e.g., lake size, stratification pattern, nutrient load, and plant cover.

In the past, most of the investigations were focused on profundal sediments as source of methane, internal cycling, and methane oxidation in the water column. Methane produced in epilimnetic sediments is considered as important source for ebullition and the plant mediated flux that cause direct fluxes to the atmosphere. On the other hand, diffusive fluxes from shallow littoral zones were considered to be less important than fluxes from the anoxic profundal sediments.

The main differences between littoral and profundal sediments are the warmer water and sediment temperatures in the littoral during summer that favour higher methane production rates , but also the exposure to surface waves (Hofmann et al. 2008). In the absence of waves the exchange of dissolved methane above the sediment-water interface is dominated by molecular diffusion that limits the flux of methane to the water column and that is accompanied by high methane oxidation rates at the sediment-water interface . Waves cause intense oscillating currents (Hofmann et al. 2008) that accelerate the flux of methane above the sediment-water interface by advective sediment pore-water exchange (wave pumping) (Precht and Huettel 2003) and by resuspension (Hofmann 2007) that breaks up the upper sediment layer.

Simultaneous, high-resolution measurements of the surface wave field, wave-induced currents, the acoustic backscatter strength, and the concentration and distribution of dissolved methane were conducted in oligotrophic Lake Constance. In Lake Constance not only wind-generated, but also ship-generated surface waves contribute significantly to the surface wave field by generating a regular and periodic wave pattern (Hofmann et al. 2008). The measurements revealed that the passage of ship-generated wave groups cause single burst-like releases of methane into the water column that were directly connected to sediment resuspension (Hofmann et al. in revision). During these wave events, methane concentrations in the littoral zone were 50% higher than in the absence of waves. Hence, surface waves are an important trigger for the release of methane and increase the dissolved methane concentration in lake littoral zones, especially during the day when methane production in the sediments is high.

Experiments on the spatial distribution of dissolved methane revealed that near-shore as well as near-surface dissolved methane concentrations were higher compared to the open and deep water throughout the whole season (March-October) and especially during summer (Hofmann et al. in revision). This indicates an off-shore directed horizontal methane gradient and also a vertical gradient that is diminishing further off-shore. Furthermore, dissolved methane concentrations near-shore increased significantly during the course of the day (morning, midday, and evening), whereas methane concentrations further off-shore remained nearly constant. This resulted in an increased gradient between the high methane concentrations in the near-shore, shallow littoral zone and the low concentrations in the epilimnetic waters of the pelagic zone. The found diurnal and seasonal patterns are mainly caused by the course of water respectively sediment temperatures, which are linked to the methane production rates in the sediments, and lake dynamics, e.g., surface waves and currents.

These results support the hypothesis that the littoral zone may be an important source of dissolved methane for the whole lake, where the methane-rich water from the shallow littoral is transported laterally to the open water. Hence, surface-wave induced release of methane in shallow littoral zones and subsequent transport of dissolved methane to the pelagic zone increases the near-surface methane concentrations in large areas and thus enhances the overall flux of methane from lakes to the atmosphere.

REFERENCES

Bastviken, D., C. Cole, M. Pace, and L. Tranvik. 2004. Methane emissions from lakes: Dependence of lake characteristics, two regional assessments, and a global estimate. Global Biogeochem. Cycles **18:** GB4009, doi:10.1029/2004GB002238.

Hofmann, H. 2007. Characteristics and implications of surface gravity waves in the littoral zone of a large lake (Lake Constance). PhD Thesis. University of Konstanz.

Hofmann, H., L. Federwisch, and F. Peeters. in revision. Wave-induced release of methane: Littoral zones as source of methane in lakes. Limnol. Oceanogr.

Hofmann, H., A. Lorke, and F. Peeters. 2008. The relative importance of wind and ship waves in the littoral zone of a large lake. Limnol. Oceanogr. **53:** 368-380.

Precht, E., and M. Huettel. 2003. Advective pore-water exchange driven by surface gravity waves and its ecological implications. Limnol. Oceanogr. **48:** 1674-1684.

Extreme methane emissions from a temperate reservoir: The importance of ebullition

T. DelSontro[1]*, D.F. McGinnis[2], S. Sobek[3], I. Ostrovsky[4], W. Eugster[5], and B. Wehrli[1]

[1] *Eawag, Seestrasse 79, 6047 Kastanienbaum, & Insitute. for Biogeochemistry and Pollutant Dynamics, ETH, 8092 Zurich, Switzerland*
[2] *Leibniz Institute for Marine Science (IFM-GEOMAR), D-24148 Kiel, Germany*
[3] *Dept. of Ecology and Evolution, Limnology, University of Uppsala, 75 236 Uppsala, Sweden*
[4] *Israel Oceanographic & Limnological Research, Yigal Allon Kinneret Limnological Laboratory, Migdal 14950, Israel*
[5] *Institute of Plant, Animal and Agroecosystem Sciences, ETH, 8092 Zurich, Switzerland*

**Corresponding author, e-mail: tonya.delsontro@eawag.ch*

KEYWORDS
Ebullition; hydropower reservoirs; methane bubbles; emission to the atmosphere.

EXTENDED ABSTRACT

Methane (CH_4) is one of the most important greenhouse gases (IPCC, 2005). Lakes and reservoirs have been identified as important, but overlooked, sources to the global CH_4 budget. CH_4 emission pathways include dissolved gas exchange at the water surface, bubble transport (ebullition), and degassing at the turbines of a hydropower dam or further downstream (Soumis, *et al.*, 2005). Ebullition is an extremely effective pathway as bubbles mostly bypass oxidation at the sediment surface or in the water column and directly emit CH_4. The stochastic nature of ebullition, however, makes it incredibly difficult to estimate; thus the aim of this study was to compare the traditional funnel method for measuring ebullition with a mass balance system analysis, atmospheric CH_4 measurements, and hydroacoustic surveying.

A yearlong CH_4 survey was conducted at 2.5 km^2 Lake Wohlen, a 90-yr-old run-of-river hydropower reservoir along the Aare River downstream of Bern, Switzerland. Dissolved CH_4 ($[CH_4]_d$) profiles were measured monthly at the river inflow and at the dam. Sediment surface and water surface CH_4 diffusion and CH_4 oxidation in the water column were measured and/or calculated. Gas trap funnels measured ebullition near the seabed; drifting chambers captured total surface CH_4 emissions. A bubble dissolution model was used to assess fractions of CH_4 dissolving into the water and emitted to the atmosphere from bubbles. Complete method details in DelSontro, *et al.* (2010). Drifting chamber campaigns were accompanied by hydroacoustic surveys using an echosounder (Simrad EK60, 120 kHz). Eddy covariance measurements of atmospheric CH_4 fluxes (EC/CH_4) over the lake were made in conjunction with a cavity ringdown laser spectrometer (Los Gatos Research DLT-100). For details, see Eugster and Plüss (in press).

It was discovered that $[CH_4]_d$ increased by an order of magnitude along the reservoir and the $[CH_4]_d$ accumulation was exponentially correlated with water temperature (T) (Figure 1a). The bubble dissolution model predicted that 70% of bubble-conveyed CH_4 would reach the atmosphere, resulting in ~470 mg CH_4 m^{-2} d^{-1} emitted to the atmosphere at T=17°C. Sediment and surface diffusions did not vary much with season and played a much lesser role in CH_4

emissions than ebullition. Methane oxidation was negligible in this oxic reservoir with an average 2-day residence time.

A system analysis was developed to better constrain the stochastic pattern of ebullition. Assuming no ebullition in winter (T<10°C), sediment diffusion was estimated based on $[CH_4]_d$ accumulation in water at a given flow rate. The $[CH_4]_d$ accumulation and T regression was used to estimate $[CH_4]_d$ from dissolving bubbles at various T regimes which, at T=17°C, agreed well with funnel measurements (140 and 220 mg CH_4 m^{-2} d^{-1}, respectively). Using the bubble dissolution model results, sediment ebullition and atmospheric emissions were calculated and agreed well with empirical results. Considering all CH_4 dissolved into the water from rising bubbles will either degas at the turbines or further downstream, Lake Wohlen thus emits ~156 mg CH_4 m^{-2} d^{-1} on average throughout the year (140 tons/yr; Figure 1b), the highest recorded for a temperate reservoir to date (Soumis, *et al.*, 2005) and of which ~80% is from ebullition.

Drifting chambers captured emissions (mean, 855 mg CH_4 m^{-2} d^{-1}) much higher than those estimated with the system analysis at 17°C, but chambers were deployed in a highly active ebullition area. The chamber emissions agreed, however, with the peak CH_4 emissions measured by EC/CH_4 in the same region and are comparable to emissions estimated via hydroacoustics. These findings further highlight the importance in a potentially warming climate of (1) temperature-correlated CH_4 ebullition emissions from temperate water bodies, and (2) these promising techniques for quantifying them.

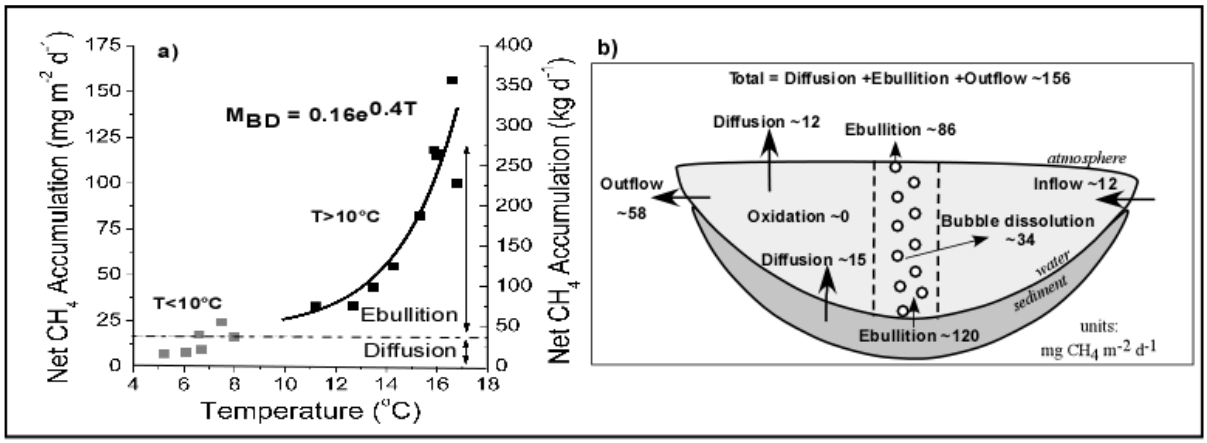

Figure 1. **a)** M_{BD}, bubble dissolution, can be calculated when T>10°C. **b)** CH_4 fluxes estimated mostly from the system analysis. Modified after DelSontro, *et al*. (2010).

REFERENCES

DelSontro, T., McGinnis, D.F., Sobek, S., Ostrovsky, I. and Wehrli, B. (2010). Extreme methane emissions from a Swiss hydropower reservoir: Contribution from bubbling sediments. *Environ. Sci. & Tech.* **44**(7), 2419-2425..

Eugster, W. and Plüss, P. (in press). A fault-tolerant eddy covariance system for measuring CH_4 fluxes. *Agric. Forest Meteorol.* doi: 10.1016/j.agrformet.2009.12.008.

Forster, P., Ramaswamy, V., Artaxo, P., Bernsten, T., Betts, R., Fahey, D.W., Haywood, J., Lean, J., Lowe, D.C., Myhre, G. *et al.* (2007). Changes in atmospheric constituents and in radiative forcing. In: S. Solomon, et al. (eds.), *Climate change 2007: The physical science basis. Contribution of Working Group I to the 4th Assessment Report of the IPCC.* Cambridge University, Chapter 2.

Soumis, N., Lucotte, M., Canuel, R., Weissenberger, S., Houel, S., Larose, C., Duchemin, E. (2005). Hydroelectric reservoirs as anthropogenic sources of greenhouse gases. In: J.H. Lehr and J. Keeley (eds.), Water Encyclopedia: Surface and Agricultural Water. Wiley-Interscience, pp. 203-210.

Physical characterization of oxygen fluxes across the water column in the central North Sea

L. Rovelli*, M. Dengler, J. Schafstall, M. Schmidt, S. Sommer, P. Linke and D. F. McGinnis

IFM-GEOMAR, Leibniz Institute of Marine Sciences at the University of Kiel, Kiel, Germany

**Corresponding author, e-mail lrovelli@ifm-geomar.de*

KEYWORDS
Dissolved oxygen fluxes; galvanic oxygen sensor; turbulence; vertical transport; North Sea

EXTENDED ABSTRACT

We investigated turbulence and vertical transport at the "Tommeliten" site in the Norwegian sector of the central North Sea during the R/V Celtic Explorer (CE0913) cruise from 8 - 11 August 2009. The sediments at this site are rather flat, sandy and non-permeable, with the presence methane seeps, as well bacterial mats and seep-related fauna. The hydrography of the ~70 m deep water column was characterized by a mixed surface layer extending to about 20 m depth and a well-mixed ~30 m thick bottom layer that was separated by a stratified interior layer (Figure 1). Amplitudes of tidal velocities were as large as 0.3 m s^{-1} in the bottom boundary layer.

Dissipation rates of turbulent kinetic energy (ε) determined from microstructure shear profiles was weak (~10^{-9} W kg^{-1} - the detection limit of the profiler) in the thermocline but increased to 10^{-7}-10^{-6} W kg^{-1} approaching the sea floor and the surface (Figure 1). Vertical turbulent eddy diffusivities (K_Z, Figure 2) ranged from 10^{-6} m^2s^{-1} in the stratified interior to 10^{-3} m^2s^{-1} and 10^{-4} m^2s^{-1} in surface and bottom boundary layers respectively; the pseudo-velocity, defined as $t = L^2 / 2K_z$ with L=1m (Figure 2) was on the order of hours to several weeks/months in the stratified interior.

High-resolution dissolved oxygen (DO) profiles were measured with a fast galvanic AMT oxygen sensor (response time 0.2 s) mounted on the microstructure probe. The sensor is capable of resolving oxygen fine structures (1 cm scale), i.e. the structures in the stratified interior, that are completely overlooked by standard slow DO sensors (Figure 1). Vertical turbulent DO fluxes were calculated using the gradient method with locally-measured dissipation rates of turbulent kinetic energy. The average downward turbulent DO flux from the thermocline to the bottom water was estimated to be 4.4 ± 1.4 mmol m^{-2} d^{-1}. The AMT sensor now allows us to resolve the before unrealized steep gradient in DO, and to properly characterize the downward fluxes. With benthic DO fluxes from chambers on the order of ~7 mmol m^{-2} d^{-1}, the water column depletion should therefore be about 3-4 mmol m^{-2} d^{-1}. This agrees with the observed DO concentrations of about 200 µmol L^{-1} (67% sat) and points to the thermocline being a significant source of DO. Previously, fluxes would have been grossly underestimated due to the inadequate response time of the traditional membrane sensors.

The results of the study show that the acquisition of high-resolution constituent profiles together with local microstructure measurements are necessary to characterized the dynamics of a system with regard to constituent fluxes and to set proper boundary conditions for modeling applications.

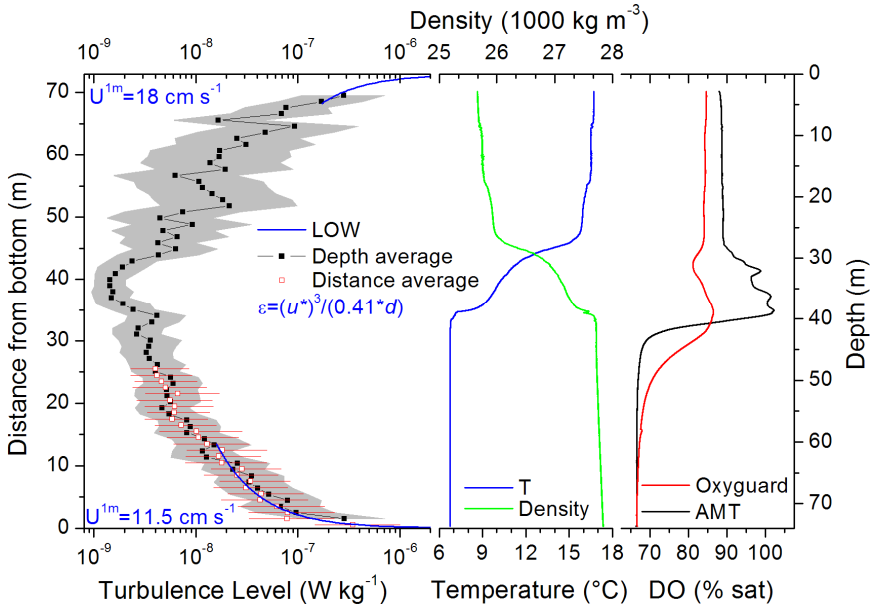

Figure 1. Averaged profile of dissipation rates of turbulent kinetic energy (ε). Left: averaged ε -profile (black line) and intermittency (grey area), the distance from bottom averaged profile (red dots and bars); LOW scaling (d=depth,distance) and U^{1m} velocities. Center: Representative temperature and density profiles to locate the mixed and stratified layers. Right: DO profiles from the same cast from a standard Oxyguard® sensor (red line) and from the galvanic sensor (AMT GmbH, Rostock, GER)

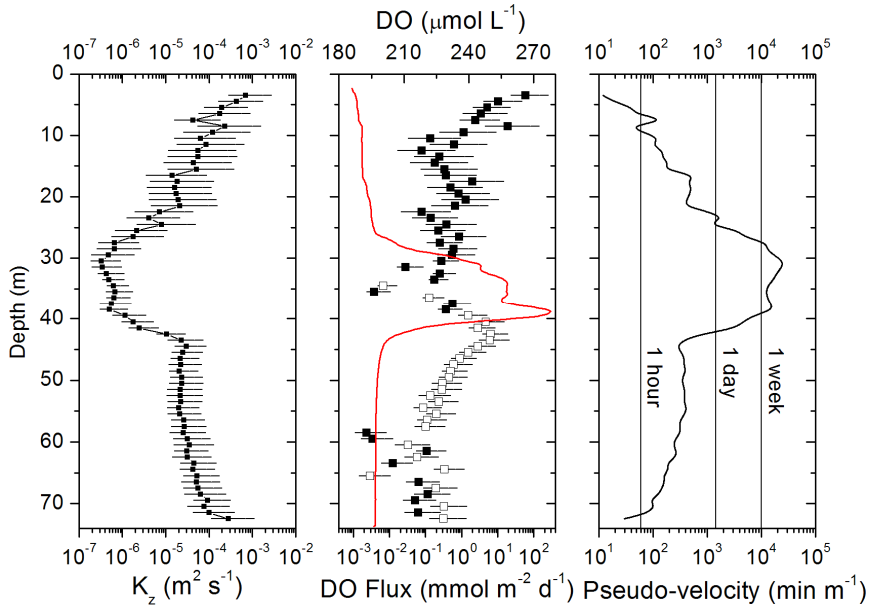

Figure 2. Turbulent DO flux. Left: Vertical turbulent eddy diffusivities K_z and intermittency bars. Center: turbulent downward (white squares) and upward (black squares) DO fluxes, observed DO profile (red line); Right: Pseudo-velocity, the amount of time required for a particle to diffuse through a length L=1 m assuming the present of a concentration gradient

Using the source as the solution: oxygenation effects on Mn cycling and water quality

L.D. Bryant[1]*, P.A. Gantzer[2], J.C. Little[1]

[1] *Environmental and Water Resources Engineering Program, Civil and Environmental Engineering Department, Virginia Tech, Blacksburg, Virginia 24061, USA.*
[2] *Gantzer Water Resources Engineering LLC, Kirkland, Washington 98034, USA.*

**Corresponding author, e-mail lebryan1@vt.edu*

ABSTRACT

The state of world water supplies is rapidly deteriorating with over one billion people lacking access to safe drinking water. In response to this water crisis, alternative approaches for improving water quality are being explored. For example, hypolimnetic oxygenation systems (HOx) are increasingly used to improve water quality in stratified reservoirs by elevating dissolved oxygen (O_2) concentrations in the water column and suppressing sediment-water fluxes of reduced species. Soluble metal flux from the sediment to the water column is one of the most common natural sources of increased metal concentrations in reservoirs, especially during hypolimnetic anoxia. Manganese (Mn) is particularly problematic from a drinking water perspective as source water with elevated Mn levels can be difficult to treat due to complex Mn redox kinetics.

This research is based on an unusually holistic approach to water treatment that enhances ecosystem conditions (e.g., trophic state, fish health) while specifically focusing on decreasing aquatic Mn levels, thus minimizing treatment required once the source water reaches the treatment plant. Using Carvins Cove Reservoir, a primary drinking-water-supply-reservoir for Roanoke, Virginia (USA), as a full-scale 'laboratory' in which redox conditions can be controlled via HOx in an otherwise entirely natural aquatic ecosystem, we obtained in-situ data with dialysis membrane porewater samplers ("peepers") and a microprofiler to evaluate the influence of HOx on sediment-water fluxes and subsequent water quality. Water column profile and bulk sediment data were also collected. Results show that sediment-water fluxes of O_2 and Mn are strongly affected by HOx, with significant decreases in total and soluble Mn in source water observed during oxygenation. By quantifying Mn biogeochemical cycling as a function of oxygenation and demonstrating that HOx may be successfully used to improve drinking water quality, this work contributes to the shifting global perspective on water resource management.

INTRODUCTION

Hypolimnetic oxygenation systems (HOx) are used by drinking water and hydropower utilities, as well as other lake and reservoir managers, to replenish dissolved oxygen (O_2) while preserving stratification (Wüest et al., 1992; Singleton and Little, 2006; Gantzer et al., 2009a). Increasing hypolimnetic O_2 while maintaining stratification in drinking water reservoirs is desirable because this allows the oxygenated hypolimnion water (which is relatively free of algal matter and other debris as compared to the epilimnion) to be used as source water (Gafsi et al., 2009). One of the primary goals of oxygenation from a drinking-water perspective is to improve source water quality by suppressing the release of reduced

chemical species (e.g., manganese; Mn) from the sediment to the hypolimnion (Beutel, 2003; Moore, 2003). It has been established that oxygenation can significantly decrease soluble Mn levels in the hypolimnion (Chiswell and Zaw, 1991; Gantzer et al., 2009b) as the reduced metals are oxidized by increased hypolimnetic O_2 and precipitate to the sediment. However, it has also been shown that technical lake management procedures such as oxygenation can fail to effectively decrease reduced species flux from the sediment in some systems (Gächter and Wehrli, 1998; A. Matzinger, unpubl.). O_2 dynamics and corresponding biogeochemical transformation processes are highly variable at the sediment-water interface (SWI) due to the extremely steep gradients in chemical, physical, and microbial properties that occur in this region (Santschi et al., 1990). Thus, as increased levels of oxide precipitates reach the sediment, potentially significant changes in the sediment O_2 uptake rate (J_{O2}) and metal fluxes at the SWI may occur (Jørgensen and Revsbech, 1985; Zhang et al., 1999). As a result, the influence of HOx on sediment-water fluxes of reduced species may not be as well understood as the influence on the water column.

Conceptually, HOx-induced increases in turbulence and near-sediment O_2 and metal concentrations will have a direct effect on sediment-water diffusive flux. Mass transport of soluble species at the SWI is governed by diffusion through the diffusive boundary layer (DBL), a mm-scale laminar layer immediately above the sediment (Jørgensen and Revsbech, 1985). Diffusive flux at the SWI is therefore controlled by the concentration gradient ($\partial C/\partial z$) within the DBL, which is in turn regulated by turbulence in the overlying water of the bottom boundary layer (BBL) and subsequent DBL thickness (δ_{DBL}). Natural variation in turbulence has been shown to have a significant effect on δ_{DBL} and sediment-water fluxes (Lorke et al., 2003; Brand et al., 2009; Bryant et al., 2010).

While previous work has established that oxygenation increases J_{O2} via elevated near-sediment O_2 and turbulence levels (Moore et al., 1996; Beutel, 2003), the influence of HOx on other sediment-water fluxes (e.g., J_{Mn} for Mn) has not been comprehensively evaluated. The complex nature of biogeochemical cycling at the SWI must be taken into account when assessing the effect of HOx on O_2 and Mn dynamics. Furthermore, much of the work that has been done on using oxygenation to improve water quality has largely focused on the water column (Chiswell and Zaw, 1991; Matthews et al., 2006; Gantzer et al., 2009b) and most of the studies that have been performed on sediment-water fluxes have been largely theoretical or laboratory-based (Moore et al., 1996; Beutel, 2003). We therefore performed a study that focused specifically on how HOx operations affect J_{Mn} and resulting water quality. Our study was based on O_2 and Mn data collected primarily in situ characterizing both the sediment and water column in a drinking-water-supply reservoir equipped with an HOx. By evaluating the vertical distribution of O_2 and Mn at the SWI, the incorporation of Mn into the bulk sediment, and subsequent source water quality as a function of HOx operation, we aim to promote greater understanding of (1) biogeochemical cycling at the SWI and (2) how to successfully manage HOx operation for the suppression of reduced chemical species.

MATERIALS AND METHODS

Study site and instrumentation – Our study focused on Carvin's Cove Reservoir (CCR), a drinking-water-supply reservoir managed by the Western Virginia Water Authority (WVWA) in Virginia, USA (Fig. 1). CCR is eutrophic and has a maximum depth of 23 m, width of ~600 m, and length of ~8000 m. A linear bubble-plume HOx (Mobley et al., 1997; Singleton et al., 2007) was installed by WVWA in CCR in 2005 and since that time ongoing field campaigns have been performed to monitor performance (Gantzer et al., 2009a,b). The CCR HOx is comprised of two parallel lines of porous tubing (each individual line consists of two

tubes that are each ~1 cm in diameter and 625 m in length) located in the deepest section of the reservoir near the WVWA treatment plant outtake (Fig. 1).

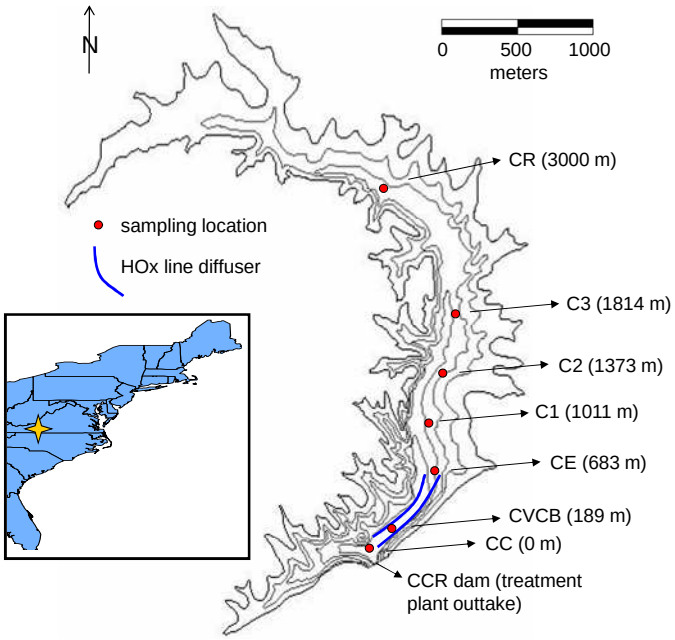

Figure 1. Map of Carvin's Cove Reservoir (CCR) showing locations of the seven sampling sites (CC, CVCB, CE, C1, C2, C3, and CR) and the hypolimnetic oxygenation system (HOx).

To evaluate sediment-water fluxes in CCR, a network of in situ and laboratory measurements was obtained from 2005-2008. Focused field sampling typically lasted from March (at the start of stratification) through November (post fall turnover). Samples were obtained primarily from sites near the HOx (CC and CVCB), mid-reservoir (CE-C3), and in the back region (CR) to characterize the influence of the HOx at a reservoir-wide scale (Fig. 1). O_2 microprofiles of the SWI were obtained using both an in situ microprofiler and microsensor profiling of sediment cores in the laboratory. In-situ porewater analyzers ("peepers"; Hesslein, 1976; Urban et al., 1997) were used to obtain soluble Mn profile data at the SWI. Water samples from different elevations in the water column and also from water overlying the sediment of core samples was used to track changes in total and soluble Mn. Bulk sediment data characterizing total Mn in the upper sediment were also obtained. Additional data were collected for background information and companion studies. Water column profiles were obtained using a CTD (Conductivity-Temperature-O_2 as a function of Depth) probe to track water column O_2 levels and density stratification as a function of temperature.

Flux analyses – Peeper profile data were used to estimate J_{O2} and J_{Mn}, respectively. While chemical and biological processes may influence sediment-water metal fluxes, solute flux models of the SWI are typically based on diffusive transport (Achman et al., 1996; Lavery, 2001). Diffusive flux (J_i) for species (i) O_2 and Mn was evaluated using Fick's first law of diffusion (Rasmussen and Jørgensen, 1992):

$$J_i = -\varphi D_{si} \frac{\partial C}{\partial z} \qquad [\text{mmol m}^{-2}\ \text{d}^{-1}] \qquad (1)$$

where φ is sediment porosity (m^3 voids m^{-3} total volume), D_{si} is the species-dependent diffusion coefficient in sediment (m^2 s^{-1}), and $\partial C/\partial z$ is the linear concentration gradient immediately below the SWI (μmol m^{-4}).

RESULTS AND DISCUSSION

We will first present data from a single field campaign in summer 2008 to emphasize the direct influence HOx has on both sediment O_2 availability and corresponding near-sediment Mn levels. We will then present a longer-term data set characterizing HOx-induced variations in J_{Mn}, the influence of biogeochemical cycling, and subsequent source water quality.

Immediate response of O_2 and Mn to HOx operations – During summer 2008, CCR HOx flow was maintained almost continuously at 51 m^3 hr^{-1} (or ~1580 kg O_2 d^{-1}). However, in the summer the HOx was turned off for an experimental campaigns (~1 week in duration) to track the response of the vertical O_2 distribution at the SWI and corresponding J_{O2}. In August 2008, the MP4 was deployed mid-reservoir at C3 (Fig. 1), ~1000 m upstream of the end of the HOx, and data were collected continuously from August 19 to 30. Data were downloaded and batteries for the MP4 microprofiler were exchanged daily. The HOx was turned off for ~48 hrs from August 19 to 21.

In response to halting HOx operations, the O_2 at the SWI (C_{SWI}) and near-sediment Mn levels changed drastically (Fig. 2). After the HOx was turned off from 19-21 August, SWI O_2 levels dropped to 0 μmol L^{-1} for over a week until the vertical O_2 distribution was finally re-established. A significant increase in total and soluble Mn is observed during this anoxic period, which clearly reveals the controlling influence that HOx operations have on sediment O_2 availability and metal cycling near the SWI. Based on ratios of total and soluble Mn, it is evident that Mn remained almost completely in the soluble form. This may likely be attributed to the fact that Mn reduces relatively easily under low (< ~40 μmol L^{-1}) O_2 conditions, especially at the pH of natural waters (Balzer, 1982; Davison, 1985; Crittenden et al., 2005). The observed delay (~8 days) in the restoration of the vertical distribution of O_2 and Mn at the SWI may be attributed to both sediment resuspension and time required for a uniform flow pattern in the reservoir to be re-established by the HOx plume.

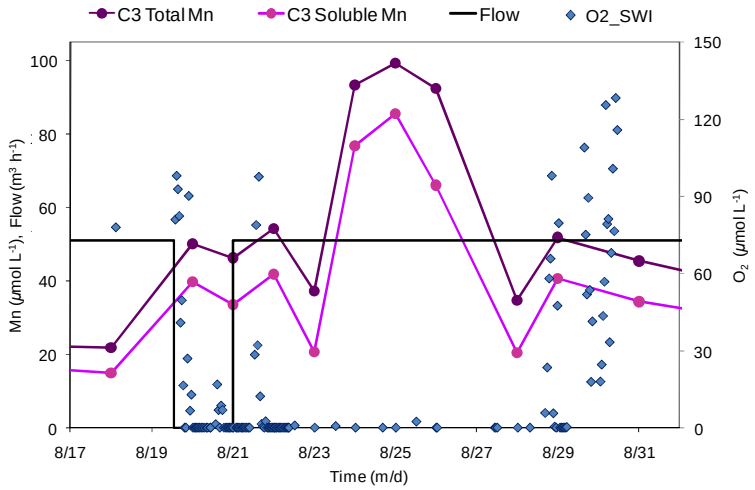

Figure 2. Correlation between near-sediment Mn levels (as characterized by sediment core water sample data), HOx flow, and O_2 levels at the SWI (as characterized by MP4 microprofile data) during the August 2008 campaign at C3.

HOx-induced variation in J_{Mn} and hypolimnetic Mn – A multi-year data set was used to evaluate the influence of variable HOx operations on J_{O2}, J_{Mn}, and corresponding source-water Mn levels (Fig. 3). Trends observed in J_{Mn} behavior are directly reflected in the response of J_{O2}, indicating that sediment-water fluxes of both chemical species were similarly affected by

HOx operations; due to this similarity, only J_{Mn} data are presented in Fig. 3. Our results indicate that J_{O2} is at least partially attributed to oxidation of reduced species (e.g., Mn) based on the parallel response in J_{O2} and J_{Mn}. Overall, J_{O2} and J_{Mn} were found to be strongly influenced by HOx operations (Fig. 3). Following an extended period of oxygenation, J_{Mn} peaked at 0.67 mmol m^{-2} d^{-1} corresponding with maximum J_{O2} = 26.8 mmol m^{-2} d^{-1} in the near-field region during August 2008. After the HOx was turned off for one month in July 2006, fluxes dropped to minimum values of J_{Mn} = 0.2 mmol m^{-2} d^{-1} and J_{O2} = 0.0 mmol m^{-2} d^{-1} while hypolimnetic Mn (at 1 and 4 m) increased substantially. Estimates of J_{Mn} and J_{O2} shown in Fig. 3 are comparable to values obtained from similar freshwater lake systems (Johnson et al., 1991; Belzile et al., 1996; Lorke et al., 2003). An initial increase in J_{Mn} very likely occurred immediately after HOx operations were halted and Mn was released as the sediment went anoxic (as shown in Fig. 2). The temporal scale of peeper measurements (two-week deployment period allowing for equilibrium to be established in situ), however, did not facilitate capturing such rapid changes in flux.

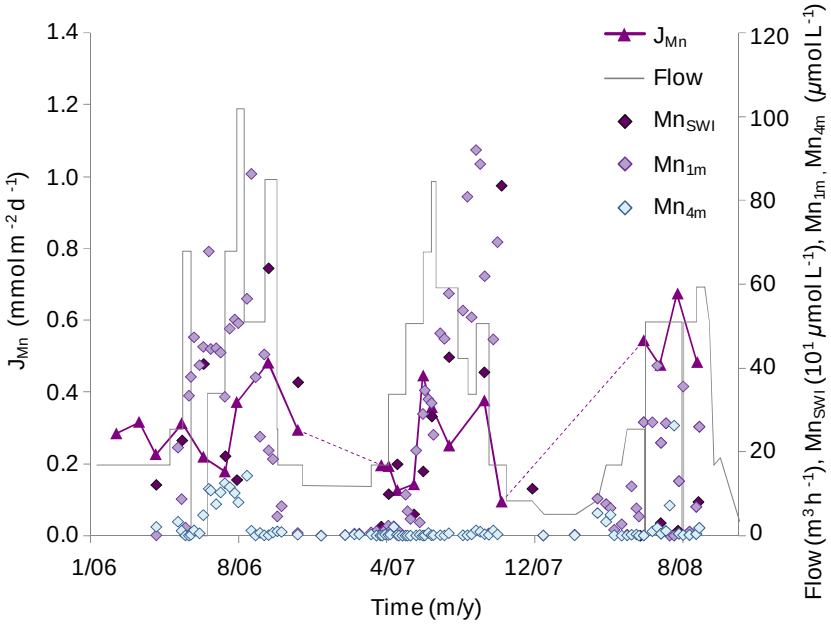

Figure 3. Correlation between J_{Mn}, HOx flow, and Mn concentrations directly at the SWI, 1 m above the sediment (benthic region), and 4 m above the sediment (mid-hypolimnion). Data shown were obtained near the HOx at CVCB. Dashed lines indicate periods between seasons of focused field sampling.

Biogeochemical cycling effects – Sediment-water metal flux results (Fig. 3) may appear to be in direct conflict with the overall goal of using HOx to reduce Mn levels in the water column. Conceptually, the response of J_{Mn} is logical per Fick's Law (Eq. 1). As evidenced by peeper profiles (data not shown) and corresponding J_{Mn} estimates (Fig. 3), HOx operation increased $\partial C/\partial z$ for diffusive transport of Mn out of the sediment into the water column. Conversely, J_{Mn} decreased when the HOx was turned off which may be attributed to decreased $\partial C/\partial z$ as near-sediment soluble metals increased significantly (Fig. 2-3) and the DBL was no longer maintained (Bryant et al., 2010).

While J_{Mn} is shown to be enhanced by HOx operations, released Mn was ultimately suppressed from the hypolimnion, which may be attributed to near-sediment biogeochemical cycling. As shown by Mn data in Fig. 2-3, although J_{Mn} and Mn levels near the sediment (both at the SWI and 1 m above) typically increased in response to HOx operation, Mn levels

in the bulk hypolimnion (4 m above the sediment) remained negligible excluding the period when the HOx was turned off in 2006. Similar results for J_{Mn} were observed both near the HOx (Fig. 3) and mid-reservoir (C3; data not shown). Hence, our results indicate that while HOx operations may increase soluble metal flux out of the sediment, elevated levels of O_2 maintained by HOx operation oxidize the soluble metals as they diffuse from the sediment. Following oxidation, metal oxide particles precipitate back to the sediment, thereby sustaining an HOx-supported Mn redox cycle in the near-sediment region.

Simple mass balance calculations were performed to further evaluate the influence of near-sediment biogeochemical cycling on hypolimnion water quality. Maximum bulk hypolimnetic Fe and Mn concentrations were estimated based on CC 2006 Mn flux data shown in Fig. 3, total Fe and Mn sediment trap data for the lower hypolimnion over the HOx (P. Gantzer, unpubl.), initial hypolimnetic Mn levels (Fig. 3), and average volumes of both the bottom meter and the full depth of the hypolimnion. It was assumed that no Mn was removed via oxidation/precipitation throughout the season; thus, all Mn diffusing out of the sediment and/or precipitating from the bulk water were retained in the volume assessed (benthic (1m) region or full hypolimnion). While actual Mn levels at 1 m above the sediment initially approached estimated maximum Mn levels at 1 m, the maximum Mn surpassed actual Mn levels considerably by mid-season. Average hypolimnetic Mn data (based on water samples obtained mid-hypolimnion at 7 m above the sediment) remained low and fell far below estimated maximum Mn at 7 m, with the deviation indicating a net gain of Mn to the sediment. These simple calculations characterizing the influence of biogeochemical cycling indicate that while moderate Mn suppression occurred in the near-sediment region, biogeochemical cycling and/or dilution effects prevented enhanced Mn levels released by J_{Mn} from reaching the bulk hypolimnion. Thus, while the previously discussed results show increased J_{Mn} from the sediment due to HOx operation (Fig. 3), overall suppression of metal fluxes to the bulk water is maintained via biogeochemical cycling and elevated O_2 in the benthic region, as indicated by negligible hypolimnetic levels of Mn during periods of oxygenation (Fig. 3) and supporting mass balance calculations.

CONCLUSION

This study supports the viability of using HOx to improve drinking water quality by decreasing source water Mn levels. Although J_{Mn} was enhanced by HOx operation, results indicate biogeochemical cycling facilitated by elevated O_2 in the benthic region prevented released metals from reaching the bulk water. While only Mn was evaluated in this study, additional species (e.g., iron, nitrite, methane) may also contribute to sediment O_2 uptake (Maerki et al., 2009; Matzinger et al., unpubl.). These results emphasize that O_2 allocated for the oxidation of enhanced fluxes of reduced species and subsequent incorporation of these species into the sediment must be taken into account for successful HOx operation. Ultimately, source water levels of Mn were shown to be substantially reduced by ongoing HOx operation (Fig. 3), thus decreasing treatment required at the plant. This work should promote greater understanding of controls on sediment-water fluxes and resultant water quality. Furthermore, our results should aid in optimization of CCR HOx operations and source-water quality and should also be of benefit to managers of similar lake and reservoir systems.

Acknowledgements – The authors thank Elizabeth Rumsey, Kevin Elam, and the staff at Western Virginia Water Authority who offered invaluable support in the field and with laboratory samples. We acknowledge financial support from the National Science

Foundation (NSF IGERT Program) and the Western Virginia Water Authority. The research described in this paper was partially funded by the United States Environmental Protection Agency (EPA) under the Science to Achieve Results (STAR) Graduate Fellowship Program. EPA has not officially endorsed this publication and the views expressed herein may not reflect the views of the EPA.

REFERENCES

Achman, D. R., B. J. Brownawell, and L. Zhang. (1996). Exchange of polychlorinated biphenyls between sediment and water in the Hudson River Estuary. Estuaries **19**: 950-965.

Balzer, W. (1982). On the distribution of iron and manganese at the sediment / water interface: thermodynamic versus kinetic control. Geochem. Cosmochim. Acta **46**: 1153-1161.

Belzile, N., J. Pizarro, M. Filella, and J. Buffle. (1996). Sediment diffusive fluxes of Fe, Mn, and P in a eutrophic lake: contribution from lateral vs bottom sediments. Aquat. Sci. **58**: 327-354.

Beutel, M. (2003). Hypolimnetic anoxia and sediment oxygen demand in California drinking water reservoirs. Lake and Reservoir Mgmt. **19**: 208-221.

Brand, A., C. Dinkel, and B. Wehrli. (2009). Influence of the diffusive boundary layer on the solute dynamics in the sediments of a seiche-driven lake: a model study. J. Geophys. Res. **114**: G01010, doi:10.1029/2008JG000755.

Bryant, L. D., C. Lorrai, D. F. McGinnis, A. Brand, A. Wüest, and J. C. Little. (2010). Variable sediment oxygen uptake in response to dynamic forcing. Limnol. Oceanogr. **55**: 950-964.

Chiswell, B., and M. Zaw. (1991). Lake destratification and speciation of iron and manganese. Environ. Monit. Assess. **19**: 433-447.

Crittenden, J. C., Trussell, R. R., D. W. Hand, K. J. Howe, and G. Tchobanoglous. (2005). Water Treatment: Principles and Design. John Wiley & Sons, Inc.

Davison, W. (1985). Conceptual models for transport at a redox boundary. *In*: Stumm, W. [Ed.], Chemical Processes in Lakes. John Wiley & Sons.

Gächter, R., and B. Wehrli. (1998). Ten years of artificial mixing and oxygenation: no effect on the internal phosphorus loading of two eutrophic lakes. Environ. Sci. Technol. **32**: 3659-3665.

Gafsi, M., A. Kettab, S. Benmamar, and S. Benziada. (2009). Comparative studies of the different mechanical oxygenation systems used in the restoration of lakes and reservoirs. J. Food Agric. Environ. **7**: 815-822.

Gantzer, P. A., L. D. Bryant, and J. C. Little. (2009a). Effect of hypolimnetic oxygenation on oxygen depletion rates in two water-supply reservoirs. Water Res. **43**:1700-1710.

Gantzer, P. A., L. D. Bryant, and J. C. Little. (2009b). Controlling soluble iron and manganese in a water-supply reservoir using hypolimnetic oxygenation. Water Res. **43**: 1285-1294.

Hesslein, R. (1976). An in-situ sampler for close interval porewater studies. Limnol. Oceanogr. **21**: 912-914.

Johnson, C. A., M. Ulrich, L. Sigg, and D. M. Imboden. (1991). A mathematical model of the manganese cycle in a seasonally anoxic lake. Limnol. Oceanogr. **36**: 1415-1426.

Jørgensen, B. B., and N. P. Revsbech. (1985). Diffusive boundary layers and the oxygen uptake of sediments and detritus. Limnol. Oceanogr. **30**: 111-122.

Lavery, P., C. Oldham, and M. Ghisalberti. (2001). The use of Fick's First Law for predicting porewater nutrient fluxes under diffusive conditions. Hydrol. Process. **15**: 2435-2451.

Lorke, A., B. Müller, M. Maerki, and A. Wüest. (2003). Breathing sediments: The control of diffusive transport across the sediment-water interface by periodic boundary-layer turbulence. Limnol. Oceanogr. **46**: 2077-2085.

Maerki, M., B. Müller, C. Dinkel, and B. Wehrli. (2009). Mineralization pathways in lake sediments with different oxygen and organic carbon supply. Limnol. Oceanogr. **54**: 428-438.

Matthews, D. A., and S. W. Effler. (2006). Assessment of long-term trends in the oxygen resources of a recovering urban lake, Onondaga Lake, New York. Lake and Reservoir Mgmt. **22**:19-32.

Matzinger, A., B. Müller, P. Niederhauser, M. Schmid, and A. Wüest. (2010). Hypolimnetic oxygen consumption by sediment-based reduced substances in former eutrophic lakes. Unpubl.

Mobley, M. H., G. E. Hauser, D. F. McGinnis, and R. J. Ruane. (1997). Diffuser system modeling and design for dissolved oxygen enhancement of reservoirs and releases. Proceedings of the 27th IAHR Congress, San Francisco, CA.

Moore, B. C. (2003). Downflow bubble contact aeration technology (Speece Cone) for sediment oxygenation. Proceedings of the Second International Conference on Remediation of Contaminated Sediments [eds. M. Pellei and A. Porta].

Moore, B. C., P. H. Chen, W. H. Funk, and D. Yonge. (1996). A model for predicting lake sediment oxygen demand following hypolimnetic aeration. Wat. Resour. Bull. **32**:1-9.

Rasmussen, H., and B. B. Jørgensen. (1992). Microelectrode studies of seasonal oxygen uptake in a coastal sediment: role of molecular diffusion. Mar. Ecol. Prog.-Ser. **81**: 289-303.

Santschi, P., P. Höhener, G. Benoit, and M. Buchholtz-ten Brink. (1990). Chemical processes at the sediment-water interface. Mar. Chem. **30**: 269-315.

Singleton, V. L., and J. C. Little. (2006). Designing hypolimnetic aeration and oxygentation systems: a review. Environ. Sci. Technol. **40**: 7512-7520.

Singleton, V. L., P. A. Gantzer, and J. C. Little. (2007). Linear bubble plume model for hypolimnetic oxygenation: full-scale validation and sensitivity analysis. Water Resour. Res. **43**(2): W02405.

Urban, N. R., C. Dinkel, and B. Wehrli. (1997). Solute transport across the sediment surface of a eutrophic lake: I. Porewater profiles from dialysis samplers. Aquat. Sci. **59**: 1-25.

Wüest, A., N. H. Brooks, and D. M. Imboden. (1992). Bubble plume modeling for lake restoration. Wat. Resour. Res. **28**: 3235-3250.

Zhang, H, W. Davison, and C. Ottley. (1999). Remobilisation of major ions in freshly deposited lacustrine sediment at overturn. Aquat. Sci. **61**: 354-361.

Sampling strategies for multi-scale characterisation of biological and hydrodynamic interactions: the role of *lothir* observatories

J. Piera[1]*, O.N. Ross[1], E. Torrecilla[1], S. Pons[1], I. F. Aymerich[1,2], J. J. Dañobeitia[1], R. Quesada[2], M. L. Artigas[3], E. Berdalet[3]

[1] *Marine Technology Unit (UTM). Mediterranean Marine and Environmental Research Centre (CMIMA, CSIC). Passeig Marítim de la Barceloneta, 37-49, E-08003, Barcelona, Spain.*
[2] *Technical University of Catalonia. Castelldefels School of Technology. Av. del Canal Olímpic, s/n, 08860 Castelldefels, Spain.*
[3] *Marine Science Institute (ICM). Mediterranean Marine and Environmental Research Centre (CMIMA, CSIC). Passeig Marítim de la Barceloneta, 37-49, E-08003, Barcelona, Spain.*

**Corresponding author, e-mail jpiera@cmima.csic.es*

KEYWORDS
Scientific methods; scientific instrumentation; underwater observatories.

EXTENDED ABSTRACT

INTRODUCTION
Hydrodynamics play a primary role in aquatic ecosystems, affecting processes across a wide range of temporal and spatial scales. The research on biological-physical interactions requires the multi-scale characterization of the environmental changes derived from the transport mechanisms and the response of organisms to these changes.
Typically, field observations provide the main source of data for such types of characterizations. One of the pivotal questions to resolve in the planning process of any observation is the number of samples and the sampling rate required for an effective analysis of the field data. Several authors have pointed out the need of adapting the sampling strategy to the observed process (Dickey, 2009).
In many cases, the final decision is highly dependent upon logistic or economical restrictions of the field observations (maximum number of samples that can be analysed, memory capacities to store data, limits on power or data transmission…). In the present contribution, the data size and sampling rate selection are proposed in a formal way, considering two main aspects

(1) **The Nyquist criteria** to set up the sampling rate. The sampling rate setup based on the Nyquist criteria requires a previous knowledge of basic dynamical properties of the parameter under study. In particular, the maximum frequency component of the signal f_{max} in the frequency domain. In order to avoid aliasing effects, it is necessary to set a minimum threshold of the sampling frequency as 2 f_{max}. Although the Nyquist criterion is a well known concept, it has not been considered in many applications as we demonstrate below.
(2) **The time-frequency resolution trade-off** in non-stationary signals. In many cases, due the non-stationary properties of the environmental signals, it is necessary to apply time-frequency tools to infer their dynamical properties.

METHODS

An example of a high resolution time series of a nutrient (nitrate) is the one was obtained using In Situ Ultraviolet Spectrophotometer (ISUS) from the Land/Ocean Biogeochemical Observatory in Elkhorn Slough (LOBO) details of the observatory can be found at Jannasch *et al.* (2008). As ISUS is based on spectrophotometry measurements, the instrument is able to collect data at high sampling rate (1 sample every hour). This sampling rate is much higher than those established at conventional methodologies based on laboratory analysis (where usually the sampling rate is set to 1 sample every week or month). The first plot of the figure provides a qualitative estimation of the information lost using conventional methodologies. It is possible to compute the spectrogram of the high resolution time series to estimate some of the dynamical properties for estimating the minimum sampling requirement (see figure caption)

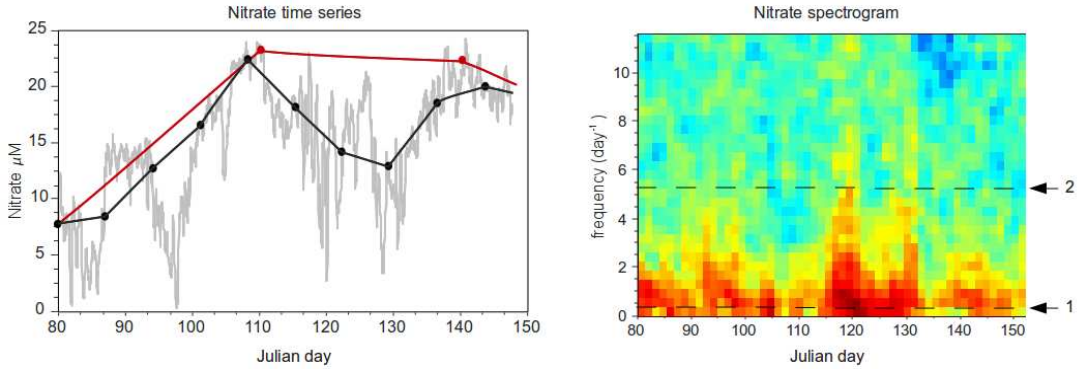

Figure 1. Left: High-resolution of nitrate time series (in grey) compared with more conventional sampling rates for biological or chemical data: weekly (black) or monthly (red). Right: Spectrogram estimated from the high-resolution time series. Arrow 1 indicates the localization of the frequency corresponding to weekly sampling and arrow 2 the threshold for the minimum sampling frequency according Nyquist criteria (~11 samples per day)

DISCUSSION

It seems clear that conventional observational methodologies should be improved in order to provide the data for the analysis of physical-biological interactions at different scales. There is a need to overcome the present technological restrictions to reach to the concept of LOTHIR (long-term & high-resolution) observatories. Biological information should be obtained at similar sampling rates to those required in physical characterization. There are several proposals to improve biological observing systems for obtaining biological information at the same scales of physical data. A good example of new biological instrumentation is the Environmental Sample Processor. (Scholin *et al.* 2006). Although instruments based on genomics or image analysis are providing a valuable new type of environmental information, they usually lack on the capability to cover all the scales. Alternatively, methods based on high-resolution optical information (Torrecilla *et al.* 2009) seems a good alternative for multiscale characterization, but at much lower taxonomic discrimination.

REFERENCES

Dickey T. (2009). Progress in Multi-disciplinary Sensing of the 4-Dimensional Ocean. Proceedings of SPIE.

Jannasch, H.W., Coletti, L.J. , Johnson, K. S., Fitzwater, S. E., Needoba, J. A., & Plant, J.N. (2008) The Land/Ocean Biogeochemical Observatory: A robust networked mooring system for continuously monitoring complex biogeochemical cycles in estuaries *Limnol. Oceanogr.: Methods* **6**, 263-276

Scholin, C. S. Jensen, B. Roman, E. Massion, R. Marin, C. Preston, D. Greenfield, W. Jones, K. Wheeler. (2006). The Environmental Sample Processor (ESP) – An Autonomous Robotic Device for Detecting Microorganisms Remotely using Molecular Probe Technology. Proceedings, OCEANS 2006 MTS/IEEE Conference. Boston, MA. Marine Technology Society, Columbia, MD.

Torrecilla E., Piera J., and Vilaseca M. (2009). Derivative Analysis of oceanographic hyperspectral data, Geoscience and Remote Sensing, In-tech publisher, Vienna, Chapter 29, pp. 597-618.

Mixing and secondary circulation in stratified oscillating boundary layers near sloping topography

L. Umlauf* and H. Burchard

Leibniz-Institute for Baltic Sea Research, Warnemünde, Germany

**Corresponding author, e-mail lars.umlauf@io-warnemuende.de*

ABSTRACT

The interaction of shear, stratification, and turbulence in boundary layers on sloping topography is investigated with the help of an idealized theoretical model, assuming uniform bottom slope, homogeneity in the upslope direction, and negligible rotational effects. It is shown theoretically that the irreversible vertical buoyancy flux generated in the boundary layer is directly proportional to the molecular destruction rate of small-scale buoyancy variance, which can be inferred e.g. from temperature microstructure observations. Dimensional analysis of the equations for harmonic boundary-layer forcing (in lakes typically originating from internal seiching motions) reveals that the problem is governed by 3 non-dimensional parameters (slope angle, roughness number, and ratio of forcing and buoyancy frequencies). Solution of the equations with a second-moment closure model for the turbulent fluxes demonstrates the periodic, shear-induced generation of gravitationally unstable boundary layers during upslope flow and restratification during the downwelling, both consistent with available observations in lakes. Investigation of the non-dimensional parameter space with the help of this model reveals a systematic increase of the bulk mixing efficiency in the boundary layer for (a) steep slopes and (b) low-frequency forcing, where boundary layer re-stratification during downwelling was identified as the mechanism leading to the strongest mixing rates. Basin-scale effective diffusivities resulting from boundary mixing correspond to the values obtained by other means for small to medium-sized lakes that are known to be dominated by boundary mixing processes.

Seasonal variation of mechanisms governing sediment dynamics in South San Francisco Bay

Andreas Brand*[1], Jessica Lacy[2], Kevin Hsu[1], Dan Hoover[2], Steve Gladding[1], and Mark Stacey[1]

[1] *Dept. of Civil and Environmental Engineering, UC Berkeley, Berkeley, California, 94720, USA*
[2] *U.S. Geological Survey, Pacific Science Center, 400 Natural Bridges Drive, Santa Cruz, California 95060, USA*

**Corresponding author, e-mail andreas_brand@berkeley.edu*

KEYWORDS
San Francisco Bay, sediment resuspension, shallow water, waves.

EXTENDED ABSTRACT

The ecology and water quality of South San Francisco Bay is closely coupled to its sediment dynamics. Due to mining activities and the industrial development during the last 150 years, sediments are highly contaminated with pollutants like mercury and chlorinated organic compounds. Sediment resuspension determines the bioavailability of these contaminants for the organisms in the bay. In addition, resuspension also plays a crucial role for the overall sediment transport and the export of these contaminants into the pacific. Resuspended sediment influences the nutrient cycle and productivity of the bay directly by controlling the light availability and enhancing nutrient release. Therefore, understanding the governing mechanisms of sediment resuspension is of crucial importance for the assessment of the ecological dynamics in the South San Francisco Bay. The extent of sediment resuspension depends on currents, wind, and waves as well as on the bed roughness, sediment density, and erodibility. In particular, turbulence and wave formation are expected to vary over the diurnal tidal cycle.

In order to investigate the interrelation between these factors, we deployed an array of stations in spring and fall 2009 to measure horizontal and vertical gradients of turbidity together with fluid flow, turbulence, and pressure along and across the shoal-channel transition. Three stations were located 500 m from the channel (channel depth ~13 meters) at 2.59 m MLLW depth and one station 2000 m from the channel at 2.19 m MLLW depth. We calibrated the backscatter of the Acoustic Doppler Velocimeters (ADV) against sediment concentration using water samples taken during the deployment. The simultaneous determination of sediment concentration and velocity at high frequency allowed us to determine sediment fluxes using the eddy correlation technique. The sediment grain size distribution was determined from grab samples. In addition, we monitored the in-situ particle size distribution of suspended sediment using a LISST 100 Type B. Wave properties were estimated from velocity spectra following Wiberg and Sherwood (2008). Bed roughness was calculated from the measured Reynolds stresses and the mean velocities over one ADV burst using the law of

the wall. These data were used for the estimation of combined current-wave shear stress using the model developed by Styles and Glenn (2000).

Sediment resuspension generally followed the tidal cycle with maximum vertical fluxes around 0.03 g m^{-2} s^{-1} during spring tide and 0.01 g m^{-2} s^{-1} during neap tide at times of maximum current induced shear. Corresponding sediment concentrations were approximately 35 and 15 g m^{-3} during spring and 70 and 40 g m^{-3} in fall. The modal particle size of resuspended sediment (100 mm) was ten times as high as the modal bed grain size of 10 mm determined in the laboratory, indicating the resuspension of flocs from the cohesive bed sediment. Regular diurnal wind patterns with maximum wind speeds around 10 m s^{-1} were observed during both campaigns. The efficiency of wind wave formation depended mainly on the phasing between tides and winds. Higher waves were mainly at high water levels. Wind waves with a root mean square height greater than 0.2 m enhanced sediment resuspension significantly producing sediment fluxes over 0.08 g m^{-2} s^{-1} and sediment concentrations over 140 g m^{-3} at the station further from the channel. The influence of these wind events was significantly smaller at the stations closer to the channel. These wind-enhanced resuspension events occurred primarily during flood tides after low water, which appears to be a result of an increase in wave induced bottom shear stress with decreasing water depth. Two strong wind events with a duration of approximately two days occurred at the end of the fall campaign with wind speeds of up to 20 m s^{-1}. These storm events resulted in extremely high sediment concentrations of 400-600 g m^{-3} at all stations and vertical sediment fluxes of over 0.3 mg m^{-2} s^{-1}.

Under conditions without significant wave shear, peak sediment concentrations at both stations in fall were approximately twice as high as during spring, suggesting a seasonal variation in the depth of the sediment erodible by shear induced solely by tidal currents. During both campaigns we observed an increased susceptibility to wind enhanced erosion at the station closer to the shore. During fall, the hydraulic roughness z_0 at this station was significantly higher (the modal value was 5.5×10^{-4} m) than at the stations closer to the channel (modal values of 7.5×10^{-5} m). The increased roughness height closer to the shore results in significantly enhanced bottom shear under presence of waves compared to the stations closer to the channel during fall. This explains partly the increased response of this station to wind-wave induced resuspension. Still, we observed only a minor difference in hydraulic roughness at both stations during spring (modal values of 3.6×10^{-5} m closer to the channel and 2.8×10^{-5} m closer to the shore). We assume that a difference in sediment response at high shear velocities caused the elevated sediment fluxes and concentrations under wind waves at the station closer to the shore during the spring campaign.

The use of ADVs allowed us to measure sediment concentrations, fluxes, turbulence and wave properties simultaneously. The driving forces of the variability in sediment dynamics during these studies were the spring-neap cycle and the phasing between wind and tidal elevation. Still, the extreme sediment concentrations and fluxes observed during two storms suggest the importance of intermittent events on the sediment dynamics in South San Francisco Bay.

REFERENCES

Styles R. and Glenn S.M. (2000). Modeling stratified wave and current bottom boundary layers on the continental shelf. Journal of Geophysical Research -Oceans 105 (C10), 24119-24139.

Wiberg, P.L. and Sherwood C.R. (2008). Calculating wave-generated bottom orbital velocities from surface-wave parameters. Computers & Geosciences 34 (10): 1243-1262. doi:10.1016/j.cageo.2008.02.010.

The dynamics of benthic boundary layer in Lake Biwa

M. Kumagai[1]*, D. Nover[2,3], S.G. Schladow[2,3] and C.R. Goldman[4]

[1] *Lake Biwa Environmental Research Institute, Yanagasaki, Otsu, Shiga 520-0022, Japan*
[2] *Environmental Dynamics Laboratory, Department of Civil and Environmental Engineering, University of California, Davis, CA 95616, USA*
[3] *Tahoe Environmental Research Center, University of California, Davis, CA 95616, USA*
[4] *Tahoe Research Group, University of California, Davis, CA 95616, USA*

**Corresponding author, e-mail kumagai-m@lberi.jp*

KEYWORDS
ADCP, AUV "Tantan", benthic boundary layer, Lake Biwa, Reynolds stress

EXTENDED ABSTRACT

INTRODUCTION
Classic theory of the benthic boundary layer (BBL) in lakes and oceans has been developed to explain the physical problems near flat bottom boundaries under a strong outer flow (Bowden, 1978). However, in lakes and reservoirs with sloping boundaries the BBL is periodically oscillating due to internal waves and is therefore sometimes unstable. Cold water moves up and down along the slope in synchronization with the period of the internal waves and the BBL becomes unstable when colder water is moved above warmer water leading to convective mixing (Lorke et al. 2005). This study was conducted at Lake Biwa, the largest lake in Japan with an area of 670 km^2 and maximum depth of 104 m. The BBL at Biwa is formed during the stratification season from May to October and it oscillates with long periods of 2-4 days. The DO of the BBL has become increasingly depleted since the 1970s and recoded its lowest DO concentration below 1 mg/L in 2007. The AUV "Tantan" found many dead fish on the bottom in December of 2007. In this study, we investigate the dynamics of the BBL to understand the physical factors that likely affect the low DO "dead zone" in Lake Biwa.

METHODS
A 1200 kHz RDI Workhorse Acoustic Doppler Current Profiler (ADCP) was deployed at 18 m above the lake bottom on the area of 92 m depth in the North Basin of Lake Biwa from July 10 to 28 in 2009 to measure the current velocity profile at every 0.5 m over 15 m (30 bins). The ADCP was operated in pulse-incoherent mode and data were saved in beam coordinates. The burst sampling interval was 10 minutes for 30 seconds at each interval to calculate the Reynolds stress. Fine scale profiling of water temperature, dissolved oxygen and turbidity were conducted at the same place where the ADCP was deployed using an F-Probe (high accuracy CTD) with 1 mm intervals on July 10 and 28 before and after the instrument mooring.

RESULTS AND DISCUSSION
Using current velocity fluctuations, the friction velocity and Reynolds stress on the bed were calculated using the variance technique proposed by Lohrmann et al. (1990) and the vertical profiles of the friction velocity and Reynolds stress are depicted in Fig. 1 with water temperature, dissolved oxygen and turbidity measured by the F-Probe on July 10. The friction velocity was almost constant between 74 m and 82 m depth, but it fluctuated below 83 m.

Reynolds stress had a similar distribution as the friction velocity. The height of the BBL likely changes periodically with the oscillation of water due to internal waves, and the thickness was 6-7 m. Very high Reynolds stress was seen in the BBL, and this suggests the bottom sediment could be re-suspended (Otsubo and Muraoka, 1988). In this layer, water was well mixed, dissolved oxygen (DO) concentration was low, and turbidity was high.

The fine data measured by the F-probe also revealed the existence of multiple sub-layers within the BBL. Those sub-layers show the possibility of other dynamical balances between density, turbulence, viscosity and biogeochemical processes. Instability of water temperature was also found in the BBL, but the profiles of dissolved oxygen and turbidity showed more complex structures than water temperature. In the sub-layer of 1 – 2 m height above the lake bottom, dissolved oxygen decreased and the turbidity increased sharply. The oxygen consumption in the BBL is closely related to the intensity of stratification in water (with clear implications for climate change) and the sediment oxygen demand (eutrophication). We thought this was induced by re-suspension of bottom sediment due to large Reynolds stress, but the recent results from AUV "Tantan" suggested another mechanism for enhanced high turbidity in the BBL.

In December of 2007, "Tantan" took many pictures of dead fish on the lake bed below 90 m depth apparently due to low concentrations of DO following a warm winter and hot summer, which may be the result of climate change. "Dead zones" at lake bottoms are now expanding world-wide and the study of the BBL is becoming increasingly important. Because the DO demand in the BBL is quite high, we worry about the future deterioration of environments near the lake bottom. If the onset of eutrophication coupled with enhanced thermal stratification at Lake Tahoe, California/Nevada, were to continue this could eventually produce boundary layer problems there as well.

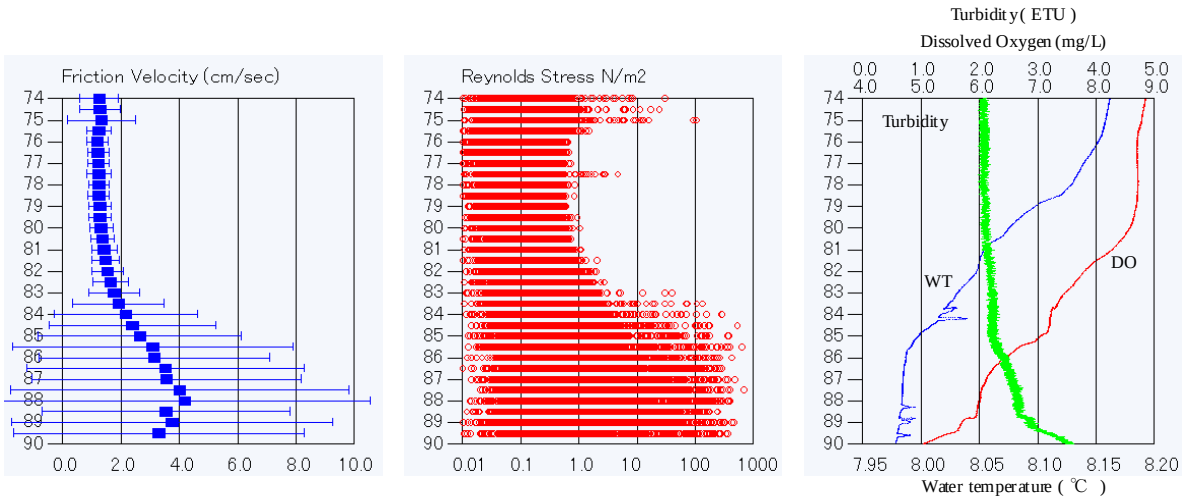

Fig. 1 Friction velocity above the lake bottom (left), Reynolds stress (middle) and F-Probe profiles (right).

REFERENCES

Bowden, K.F. (1978). Physical problems of the benthic boundary layer. Geophysical Surveys. 3: 255-296.

Lohrmann, A., B. Hackett, and Roed, L.D. (1990). High resolution measurements of turbulence, velocity, and stress using a pulse-to-pulse coherent sonar, J. Atmos. Oceanic Technol.,7, 1437.

Lorke A., F. Peeters and Wuest A. (2005). Shear-induce convective mixing in bottom boundary layers on slopes. Limnol. Oceanogr. 50(5): 1612-1619.

Otsubo K. and K. Muraoka (1988). Critical shear stress of cohesive bottom sediments. J. Hydr. Engrg. 114: 1241-1256.

Instrument comparison: Laser diffraction, microscopy and flow cytometry for assessing fine particle concentration and size distribution

Daniel M. Nover[1,2*], Stephen Andrews[1,2], Travis Schuler[2], Monika Winder[1], Debbie Hunter[3], John E. Reuter[1,3] and S. Geoffrey Schladow[1,2]

1. *Tahoe Environmental Research Center, University of California, Davis, 1 Shields Ave., CA 95617, USA*
2. *Dept. of Civil and Env. Engineering University of California, Davis, 1 Shields Ave., CA 95617, USA*
3. *Department of Env. Science and Policy University of California, Davis, 1 Shields Ave., CA 95617, USA*

[*]*Corresponding Author, email: dmnover@gmail.com*

KEYWORDS
Flow cytometry, Lake Tahoe, laser diffraction, particle measurement

EXTENDED ABSTRACT

INTRODUCTION
The fate and transport of particulate matter and associated nutrients and pollutants are among the most important factors affecting freshwater quality. Although research efforts over the past ~50 years have generated a great deal of knowledge about the dynamics of large particles, limits to analytic techniques have prevented the investigation of very fine particles (<10 um) until recently (Pedocchi and Garcia 2006). Because very fine particles are so small, they tend to stay in suspension longer than larger particles, exerting an influence on water quality that is out of proportion to their contribution to suspended solids concentrations (Jassby et. al. 1999). Additionally, fine particles are important due to the integral role they play in light scattering and water clarity.

Increasing interest in particle dynamics combined with technological advances in fields as diverse as cancer research and limnology has generated numerous methods for quantifying particle size, shape and distribution both in-situ and in the lab (Fugate et. al.). Unfortunately, different methods for quantifying fine particle concentrations and particle size distributions rarely produce identical results (Serra et. al. 2001). Additionally, methods vary dramatically in terms of the information one can gain from the data produced (Monfort and Baleaux 1992). For example, although gravimetric methods are useful for investigating suspended solids concentrations, these methods obscure the particles that make up the sample and consequently, little information is obtained about the nature of the particles or the particle size distribution before filtration. Laser diffraction generates data regarding particle concentration and size distribution, but gives no information about particle composition.

METHODS
In this study, five instruments are compared for their ability to measure particle shape, size, size distribution, concentration, and composition (Table 1). The instruments include two laser diffraction instruments; a bench-top particle counting spectrometer (LiQuilaz-S05-HF - manufactured by Particle Measuring Systems, Inc.) and a Laser In-situ Scattering Transmissometer (LISST-100x – manufactured by Sequoia Sci.), a MoFlo cell sorter and flow cytometer (Cytomation), and two microscopes; an Axio Observer A1 light microscope (Zeiss) and a scanning electron microscope with x-ray fluorescence (Philips). All instruments are

used to analyze replicate samples representing a broad range of particle populations, including glass microspheres, phytoplankton monocultures, and natural particle samples of mixed composition.

Table 1. Matrix showing the particle attributes that can be assessed by the listed instruments. Note that no single instrument can evaluate all relevant particle attributes.

Particle Attribute / Instruement	Shape	Size	Particle Size Distribution	Composition	Concentration
LiQuilaz	No	Yes	Yes	No	Yes
LISST	No	Yes	Yes	No	Yes
Cell Sorter	Yes	Yes	No	Yes	Yes
Light Microscope	Yes	Yes	Yes	No	Yes
SEM	Yes	Yes	No	Yes	No

RESULTS AND DISCUSSION

Using light microscope data to represent the "truth" makes it clear that the instruments that represent particle size distribution (PSD) vary considerably in their results. While particle concentrations are generally similar, the LiQuilaz systematically undersizes particles in the case of both nearly spherical algal cells and glass microspheres (Figure 1). The LISST basically "correctly" sizes and counts the particles in both of the above monoculture examples. Data from flow cytometery (not shown), suggests that all three of these instruments underrepresented the true particle concentrations.

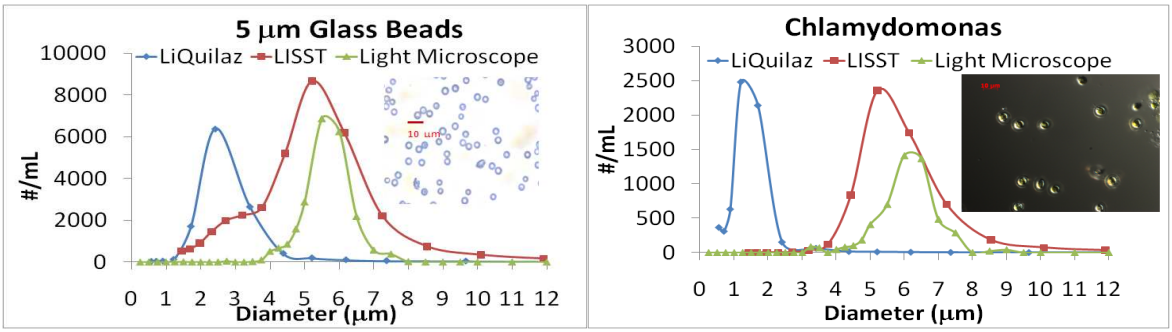

Figure 1. Particle size distribution measured by two laser diffraction instruments and a light microscope.

The results of this study are presented with the goal of identifying implications and strategies for long-term monitoring of fine particles. This is essential, as fine particle concentrations form the basis of the lake clarity restoration efforts at Lake Tahoe, CA-NV, USA.

REFERENCES

Fugate, D. C. and C. T. Friedrichs. (2002). "Determining concentration and fall velocity of estuarine particle populations using ADV, OBS and LISST." Continental Shelf Research **22**(11-13): 1867-1886.

Jassby, A. D., C. R. Goldman, et al. (1999). "Origins and scale dependence of temporal variability in the transparency of Lake Tahoe, California-Nevada." Limnology and Oceanography **44**(2): 282-294.

Monfort, P., and Baleaux, B. (1992). "Comparison of flow cytometry and epifluorescence microscopy for counting bacteria in aquatic ecosystems." *Cytometry*, 13, 188–192.

Pedocchi, F. and M. H. Garcia. (2006). "Evaluation of the LISST-ST instrument for suspended particle size distribution and settling velocity measurements." Continental Shelf Research **26**(8): 943-958.

Serra, T., J. Colomer, X. P. Cristina, X. Vila, J. B. Arellano, and X. Casamitjana. (2001). Evaluation of laser in-situ scattering instrument for measuring the concentration of phytoplankton, purpule sulfur bacteria, and suspended inorganic sediments in lakes. J. Envir. Eng. Nov.:1023-1030.

In-situ optical observations of particulates in Lake Tahoe

S. Andrews*, D.M. Nover, S.G. Schladow, J.E. Reuter

Tahoe Environmental Research Group, University of California, Davis, One Shields Ave. Davis, CA, USA 95616

**Corresponding author, e-mail swandrews@ucdavis.edu*

KEYWORDS
Backscatter; index of refraction; Lake Tahoe; Mie theory; particle size distribution.

EXTENDED ABSTRACT

INTRODUCTION
Suspended particles in Lake Tahoe (California-Nevada, USA), a very clear oligotrophic mountain lake, vary greatly in size and composition, from small bacteria and inorganic mineral grains to midsize diatoms to large, heterogeneous flocs. The dominant particle composition is known to shift between inorganic mineral particles during the spring snowmelt season to organic phytoplankton cells and detritus during autumn and winter (Swift et al. 2006), but is currently monitored using time consuming and expensive laboratory instruments and techniques. Since accurate determination of the suspended particle size distribution and bulk composition is essential for understanding ecosystem function and for organizing monitoring and management programs for lake clarity, in-situ optical techniques for assessing particle characteristics are explored here. Because of their low cost and relative ease of use, these techniques have great potential for increasing the spatial and temporal resolution of particle monitoring and thus our understanding of in-lake particle dynamics.

METHODS
Data on forward light scattering, spectral backscattering, light attenuation, and fluorescence, and lake physiochemical variables were measured using a winched package at the Lake Tahoe Index station, located off the lake's west shore in approximately 150 m of water, on 18 September 2009 and again on 16 November 2009. The particle size distribution between 1.25 and 250 μm was obtained using forward scattering measurements made with the Laser In-situ Scanning and Transmissometry (LISST) 100X series instrument. Backscatter was measured at two wavelengths using a HydroScat instrument, a FluoroProbe multichannel fluorometer was used to measure fluorescence at six wavelengths, and a Seabird SBE25 CTD recorded temperature, dissolved oxygen, light attenuation at 488 nm, and solar insolation in the photosynthetically active range. Particle size distributions were used to predict the expected backscatter ratio as a function of bulk particle index of refraction using Mie theory. At each depth predicted backscatter ratios were compared to the observed backscatter ratio in order to infer a bulk index of refraction. This method is similar to that introduced by Twardowski et al. (2001), although concentrations in 32 individual particle size bins are used in place of an assumed power law size distribution.

RESULTS AND CONCLUSIONS

Results from the September sampling date are shown in Fig. 1. The calculated index of refraction for the majority of the upper water column was 1.10, similar to backscattering results obtained for phytoplankton cells by Vaillancourt et al. (2004). This was consistent with a general dominance by organic particles known to be typical of this time of year. More inorganic indexes of refraction beginning below the photic depth may be indicative of flocs of heterogeneous composition or phytoplankton detritus. The suspended particle maximum was found 10 m above the chlorophyll maximum, indicating photo-acclimation of cells and typical of case I waters (Kitchen and Zaneveld, 1990). Scattering in the upper water column was largely due to a single diatom genus, *Cyclotella*. Since recent research has shown a shift toward smaller diatom cell sizes in response to climate change (Winder et al. 2009), the effect on lake clarity may be significant.

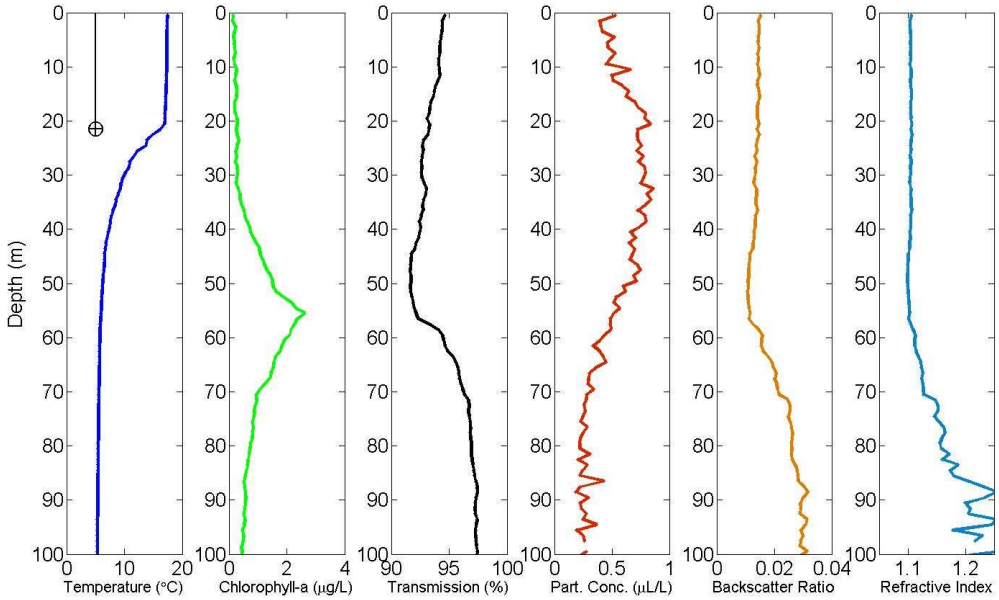

Figure 1. Measured physiochemical and optical properties of Lake Tahoe on 18 September 2009.

REFERENCES

Kitchen J.C. and Zaneveld J.R. (1990). On the noncorrelation of the vertical structure of light scattering and chlorophyll *a* in case I waters. *J. Geophys. Res.*, **95**(C11), 20237-20246.

Swift T.J., Perez-Losada J., Schladow S.G., Reuter J.E., Jassby A.D., and Goldman, C.R. (2006). Water clarity modeling in Lake Tahoe: linking suspended matter characteristics to Secchi depth. *Aquat. Sci.*, **68**, 1-15.

Twardowski M.S., Boss E., Macdonald J.B., Pegau W.S., Barnard A.H., and Zaneveld J.R.V. (2001). A model for estimating bulk refractive index from the optical backscattering ratio and the implications for understanding particle composition in case I and case II waters. *J. Geophys. Res.*, **106**(C7), 14129-14142.

Vaillancourt R.D., Brown C.W., Guillard R.R.L., and Balch W.M. Light backscattering properties of marine phytoplankton: relationships to cell size, chemical composition and taxonomy. *J. Plank. Res.*, **26**(2), 191-212.

Winder M., Reuter J., and Schladow S.G. (2009). Lake warming favours small-sized planktonic diatom species. *Proc. R. Soc. B*, **276**, 427-435.